Cranfield University

Marco Osvaldo VIGUERAS ZUÑIGA

ANALYSIS OF GAS TURBINE COMPRESSOR FOULING AND WASHING ON LINE

School of Engineering

PhD

Cranfield University

SCHOOL OF ENGINEERING

PhD Thesis

2007

Marco Osvaldo VIGUERAS ZUÑIGA

ANALYSIS OF GAS TURBINE COMPRESSOR FOULING AND WASHING ON LINE

Supervisor: Professor Pericles Pilidis

Academic Year 2007 to 2008

ABSTRACT

This work presents a model of the fouling mechanism and the evaluation of compressor washing on line. The results of this research were obtained from experimental and computational models.

The experimental model analyzed the localization of the particle deposition on the blade surface and the change of the surface roughness condition. The design of the test rig was based on the cascade blade arrangement and blade aerodynamics. The results of the experiment demonstrated that fouling occurred on both surfaces of the blade. This mechanism mainly affected the leading edge region of the blade. The increment of the surface roughness on this region was 1.0 μm. This result was used to create the CFD model (FLUENT). According to the results of the CFD, fouling reduced the thickness of the boundary layer region and increased the drag force of the blade.

The model of fouling was created based on the experiment and CFD results and was used to calculate the engine performance in the simulation code (TURBOMATCH). The engine performance results demonstrated that in five days fouling can affect the overall efficiency by 3.5%. The evaluation of the compressor washing on line was based on the experimental tests and simulation of the engine performance. This system demonstrated that it could recover 99% of the original blade surface. In addition, this system was evaluated in a study case of a Power Plant, where it proved itself to be a techno-economic way to recover the power of the engine due to fouling.

The model of the fouling mechanism presented in this work was validated by experimental tests, CFD models and information from real engines. However, for further applications of the model, it would be necessary to consider the specific conditions of fouling in each new environment.

Keywords:
Techno-economic, cascade blade, experiment, roughness, CFD

ACKNOWLEDGEMENTS

Thank you GOD for the opportunity to do this postgraduate degree and for the friendship of my family, professors and friends.

I would like to express my sincere thanks to The National Council for Science and Technology of Mexico (CONACYT) for supporting my tuition and fees during this Doctorate study and to the sponsors funding of this project: the Gas Turbine Performance Engineering Group of Cranfield University and the company Recovery Power Ltd.

TABLE OF CONTENTS

TABLE OF FIGURES

TABLE OF TABLES

TABLE OF EQUATIONS

1 GENERAL INTRODUCTION

1.1 Overview

The gas turbine is a machine based on the thermodynamic cycle of Brayton. The function of this engine is to exchange the heat energy product of the combustion to mechanical work. This transformation of energy is through the working fluid (air) that includes three basic sections of the gas turbine.

1. Compression; the pressure of the air is increased by the compressor section.
2. Combustion; the air is mixed with the fuel and the process of combustion takes place in the combustion chamber. In this mechanism, the energy from the fuel increases the enthalpy energy of the air and also the air temperature.
3. Expansion; the enthalpy of the combustion gases exhaust is transformed into mechanical work by the turbine section. The expansion of the gases is used to move the turbine blades connected to rotors and engine shaft.

The mechanical work is extracted from the shaft and is used to drive the compressor and the external equipment.

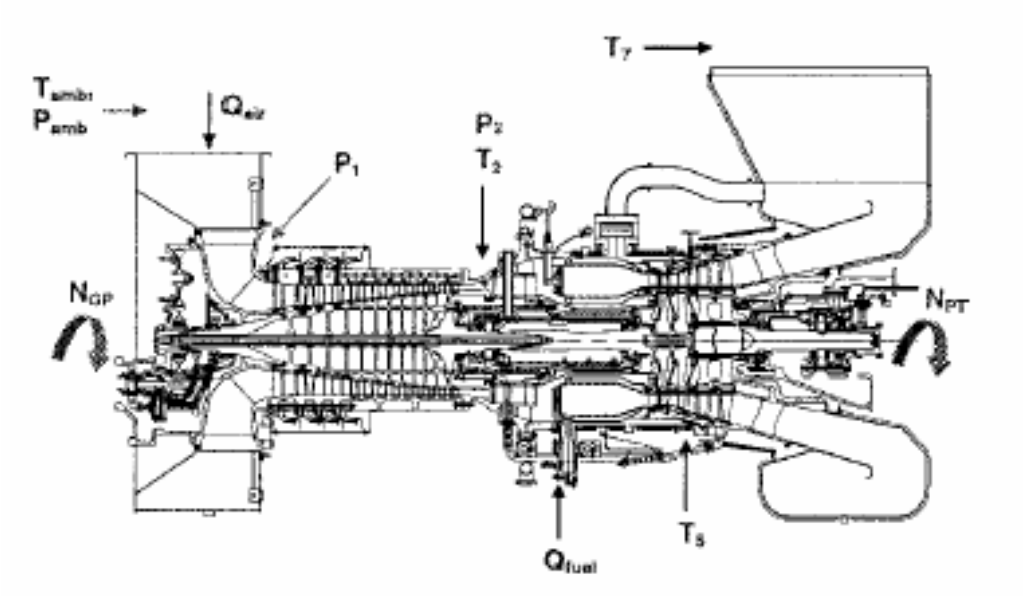

Figure 1-1 Industrial Gas turbine cross section (Kurz and Brun, (2001))

Many applications are possible in a gas turbine. For industrial applications, the shaft is connected to mechanical equipments such as electrical generators, propellers,

pumps, etc. For aero engine applications, the exhaust of the gases is used to produce the thrust of the plane.

Industrial gas turbines are in operation around the world in many unfavourable environments. So, it has been necessary to develop technologies to monitor the engine performance in order to reduce the costs of operation and maintenance.

The problem of compressor fouling is considered as one of the most important and common mechanism of degradation that affects the compressor performance. For that reason auxiliary systems have been developed to eliminate this problem. This is the case of compressor washing on line used frequently in industrial gas turbines.

The investigation presented in this thesis was focused on the fouling mechanism based on experimental and computational results. In addition, the power recovery by the compressor washing on line system was analyzed for the gas turbine application in a Power Plant.

1.2 Thesis Structure

According to the nature of this project, it was decided to separate the thesis into two main sections. The first section (Chapter 3, 4 and 5) presents a study of the fouling mechanism and the blade aerodynamics. The second section (Chapter 6) presents the application of this result in a real case to evaluate the engine performance and the effectiveness of compressor washing on line.

Chapter 2 presents the theoretical bases of this research. An extensive search of information from previous investigations has been summarized in this chapter.

Chapter 3 presents the design of the test rig based on real operational conditions. In this chapter the details of the rig construction and the instrumentation specifications is included.

Chapter 4 presents the validation of the experimental results based on a CFD model. In this chapter, the configuration from the test rig is analyzed by a three dimensional CFD model.

Chapter 5 presents the most important contribution of this research that is the experimental results of the fouling mechanism. The mathematical model was created based on the localization of particle deposition on the blade surface and the changes produced in the surface roughness. In addition, this model was used to study the changes of the blade aerodynamics.

Chapter 6 presents a techno-economic study of the engine operation affected by the fouling mechanism and the effectiveness of compressor washing on line.

1.3 Importance of this study

According to the literature review, the effect of fouling has been associated in previous studies with arbitrary factors from the output power of the engines. However, the mechanism of fouling should be associated with the real physical problems (modification of blade surfaces and blade aerodynamics).

The importance of this problem is illustrated in the following techno economic example. The annual production in a gas turbine of 240MW/h (Power Plant) is 2,120,000 MWh per year[1], this value represents 106 million USD of electricity sale per year. If fouling affects 1% the compressor pressure ratio during a period of 4 years (normal period of the engine overall maintenance), the engine has not produced 520,000MWh. This value represents 26 million USD of electricity that was not sold.

For that reason, companies and governments are interested in studying the deterioration mechanism in industrial gas turbines to be competitive in the energy market. A combination of this effort is this research sponsored by the Mexican Government (CONACYT), Cranfield University (institution leader in gas turbine

[1] Price Retail of 1MWh =50 USD

development) and the company Recovery Power Ltd (leader in technology of compressor washing on line).

1.4 Previous Works

1.4.1 Gas turbine compressor fouling and washing on line

Fouling is commonly found in compressor blades, but the information about this topic is very limited in the literature. According to the literature review, fouling has been studied since 1980 with simple arbitrary factors linked with the output power of the engine. However, this mechanism of degradation involves some other important and relevant changes in the blade aerodynamics.

This thesis has settled its basis from the work produced by the Gas Turbine Performance Engineering Group (GTPE) in Cranfield University in the last ten years. In particular the topic of compressor washing on line has been studied by this group with the participation of the company Recovery Power Ltd. Two previous PhD investigations were presented about numerical CFD analysis of compressor washing on-line (Mund (2006) and Mustafa (2006)). The water droplets distribution in the inlet bell mouth was analyzed by Mund (2006), while the droplets trajectory was analyzed by Mustafa (2006). In both projects the necessity to validate the results with experimental models was mentioned.

The experimental study is the new area explored in this investigation of the Gas Turbine Performance Engineering Group under the supervision and help of Professor Pilidis (director of the project). The experimental work was done with the participation and help of Angel Hernandez (MSc-candidate) and Dimitrios Foulfias (PhD-candidate) and with the technical support of Paul Lambart, Ross Gordon and Andy Lewis from the company Recovery Power Ltd. The writing work of this thesis was done with the help of Miss Ruth Joy.

1.4.2 Software description

The improvements in the computational technology offer the opportunity to solve a complex numerical model. Today, it is possible to solve “n” number of equation systems with “n” number of variables in a reasonable computational time. This is the case of the Computational Fluid Dynamics (CFD) algorithms. The CFD produces a numerical solution from the Navier-Stokes equations. This computational application was used to analyze the flow in this research by the program FLUENT.

FLUENT is a powerful state of the art code that solves computational fluid dynamics models (fluid flow or heat transfer). The program was written in C program language and it has the capacity to process complex geometries with structured and unstructured meshes in two or three dimensional models. In this research, the geometry was created by AUTOCAD (Computational Aided Design package) and the mesh was created by GAMBIT.

The engine performance was studied from results obtained in the simulation program of TURBOMATCH. This program was written in FORTRAN in Cranfield University and it was designed to handle the thermodynamic gas turbine performance (Mund (2006)). This code can include new subroutines to simulate different engine configurations. The library of the program includes nine compressor maps and nine turbines maps to calculate design or off design point of the engine operation. With the use of pre-programmed routines called “codewords” and “bricks” it is possible to calculate the engine performance degradation. The result from the engine performance is presented by the internal parameters of output power, fuel consumption, overall efficiency, etc.

The parameters that change the engine performance in the simulation code were calculated with the computational tool of gas path analysis (GPA). The codes of GPA link the physical fault of the engine with the internal parameters. The solution is generated based on a matrix that includes independent and dependent parameters. In general, there are two basic algorithms involved in the solution (fault tree and fault matrix). The fault tree algorithm is a mechanical decision based on the output value that converges in a possible fault. The fault matrix algorithm compares the values

from two variables (inputs and outputs values). In addition, the deviation of these parameters from the failure can predict the quantity of the damage.

The code selected for the gas path analysis was the program GOTRESS. This software was programmed in FORTRAN (Cranfield University) to predict the internal engine parameters from faults implanted in the engine components. The program is based on the matrix method in order to load multiple faults (input values). An important characteristic of this program is the non linear application that it decreases the errors produced by the numerical solution. The dependent parameters have to be known and the number of independent parameters has to be equal or less than the dependent parameters.

1.5 Thesis Objectives

The objective of this thesis was created based on the following conclusions based on the literature review:

i. The mechanism of fouling in gas turbine compressors has not been studied in detail.
ii. The cascade blade application offers a possibility to study the effect of the blade aerodynamics and the mechanism of fouling.
iii. Experimental information of compressor washing on line is required to validate previous theoretical studies.

Therefore, this PhD research has as its objective ***to obtain a model to predict the fouling in gas turbine compressor blades***.

To achieve with this objective, it is necessary to establish the following particular objectives.

i. Specification of operation conditions from industrial gas turbine.
ii. Design of the test rig based on the blade aerodynamics.
iii. Analysis of blade aerodynamics due to modifications on the blade surface roughness (fouling).

iv. Validation of experimental results with CFD models and information from the real engine.

v. Analysis of gas turbine performance based on compressor fouling.

vi. Techno economic study of compressor washing on line in a Power Plant.

1.6 Contribution

The result of this research will show for the first time experimental information about the fouling mechanism. The results from the CFD will present the effects of the blade aerodynamics due to changes on the surface roughness. The performance of the gas turbine will demonstrate the importance of fouling and compressor washing on line by a techno economic analysis for industrial gas turbine application.

2 LITERATURE REVIEW

2.1 Introduction

In this chapter is summarized the relevant information published in the literature linked with the topic of this research. Divided in four topics, the information is presented with the following order. First section presents a general background of the gas turbine and the common deterioration mechanisms that affect the engine performance. The second section includes the previous studies of the mechanism of fouling in the compressor. It will be important to note that information published at the end of the seventies has been used to represent the problem of fouling for many years linked only to the output power of the engine. The third section comments the process of compressor washing online that it is used to eliminate the problem of fouling in gas turbines. The final section describes previous experimental works of cascade blades.

2.2 Industrial Gas Turbines Performance Deterioration

The deterioration of industrial gas turbines has been studied since 1914 when the ideal cycle of Brayton was modified to represent the real conditions ((Horlock, 1992)). At the end of the forties was observed that the gas turbine deterioration affected the power production and increased the fuel consumption ((Zwebek, 2002)). During the sixties the improvements in different sections of the gas turbine increased the engine efficiency by 17% with pressure ratio of 7:1 and temperatures of 815ºC ((Boyce and Gonzalez, 2005)). The increment of the fuel price in the seventies obligated to the gas turbine users to study new ways to reduce the costs of operation. During this period the deterioration mechanisms that affect the engine performance were classified ((Williams, 1981)). The boom of industrial gas turbines was in the eighties with the installation of Combined Cycles in power plants. The results of new technologies at the end of this decade increased the engine efficiency to 42% ((Zwebek, 2003)). Today it is possible to find public documents published by OEM's where the gas turbine operates with efficiency of 45% and temperatures of 1371ºC (Boyce and

Gonzalez (2005)). However, these results are produced in special conditions (ISA* conditions) and when the engine condition is new, because the gas turbine is a machine that presents a quick degradation (Zwebek and Pilidis (2004)).

2.2.1 Influence of the ambient condition in the gas turbine performance

The airflow plays an important role in the gas turbine performance. The high quantity of air required by the engine in a typical compressor is 500kg of air for each unit of horse power produced by the engine (Zwebek and Pilidis (2003)). Previous publications have demonstrated that optimal conditions of the air can produce high levels of power production from the gas turbine with a low fuel consumption (Weisman and Eckart (1985) & Zwebek and Pilidis (2004)).

The different applications of industrial gas turbine involve different conditions of the air due to atmospheric conditions (Mund and Pilidis (2004)). For example, the increment of a centigrade degree from the ambient temperature can produce that the output power decreases 2% (see Figure 2-1) (Mund (2006)). The altitude also plays an important factor in the engine performance. The pressure in the inlet of the compressor is reduced in engines located at high altitudes (see Figure 2-2). In general, industrial gas turbines for power generation operate in low altitudes (below 800m AMSL†). However, there are cases where these engines are in operation at high altitudes. For example this is the case of: mines facilities, gas & oil pump stations and power plants located at high altitudes (Giampolo (1997) & Mund, (2006)).

* ISA International Standard Atmospheric conditions
† AMSL Above Mean Sea Level

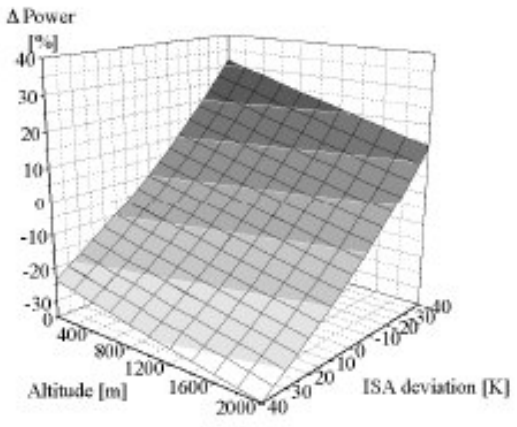

Figure 2-1 Output power of a gas turbine according to altitude and ambient temperature (Mund (2006)).

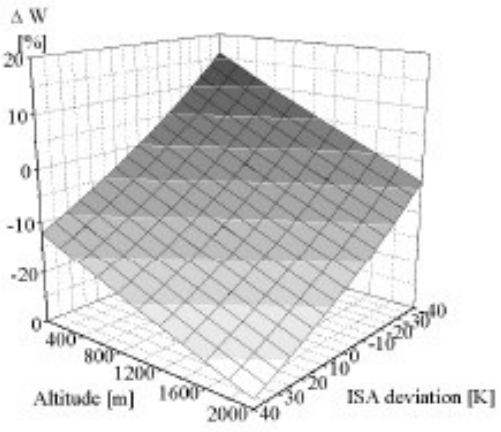

Figure 2-2 Mass flow of a gas turbine according to altitude and ambient temperature (Mund (2006)).

2.2.2 Types of deterioration in gas turbines

The gas turbine components are affected by the wear over the lifetime of operation. These problems are presented in the blade aerodynamics and internal mechanical properties (Kurz and Brun (2001)). The literature review showed that there is limited information about the deterioration mechanisms in the gas turbines. This is due to the marketing used for the OEM's in the public domain (Mund (2006)). In addition, the high costs and difficulty that involves experimental tests have limited the number of investigations in this topic (Syverud and Bakken (2005)).

The deterioration mechanisms are classified by the gas turbine application and the type of damage caused in the engine (Tabakoff (1986)). The deterioration mechanism of industrial gas turbines can be classified according to the type of the damage in three sections (Zwebek (2002), Zwebek (2003) & Singh (1996)).

i. Recoverable damage involves light maintenance such as cleaning or washing.
ii. Major-Recoverable damage involves maintenance such as welding or coating process.
iii. Non-Recoverable damage requires the replacement of the part.

The non-recoverable damage is attributed when the engine is in operation with some part already damaged. This is also presented when the engine operates at lower efficiency and it produces excess of fuel consumption and increases the temperature in the turbine inlet that can produce internal damage in the components (Morillo De Hart (1994)). For that reason in the last decade, the development of technologies to monitor the engine health has given the opportunity to the engine users to solve the problem before the damage becomes non-recoverable. These preventive actions have demonstrated that reduces the maintenance cost and unexpected shut downs (Zwebek (2002)).

The common deterioration mechanisms presented in gas turbines are divided into six categories (Kurz and Brun (2001)).

- Fouling (it is caused by the particle deposition on the airfoils and annulus surfaces).
- Corrosion and hot-corrosion (it is caused by chemical reactions between the contaminant and the component material).
- High-temperature-oxidation (it is caused by chemical reactions between metal components and oxygen).
- Erosion (it is caused by the result of abrasive components that removes the component material from the surfaces.
- Foreign Object Damage (FOD) (it is caused by the ingestion of large objects into the flow path. They are the results of internal pieces broken or ice formation in the inlet.)
- Abrasion, rubbing and wearing (it is caused by the contact between two surfaces in movement, generally one in rotation and other static).

These problems are difficult to detect when the engine is in operation. In some cases, the effects of the engine degradation can be detected when the engine decreases the output power or increases the fuel consumption (Kurz and Brun (2001)). However, these parameters do not give enough evidence to find the source of the problem. Because this is due to changing from the operation conditions (Caguiat, Zipkin, and Patterson (2002)).

2.2.3 Compressor degradation

Compressor fouling is produced due to the ingestion of dust mixed with the air. This mechanism decreases the compressor isentropic efficiency. Fouling and erosion have been demonstrated to affect the thermal efficiency and output power of the engine (Zwebek (1993)). The deposition of the particles in critical areas can change the geometry of the airfoils and then the flow condition is modified (Lakshminarasimha, Boyce, and Meher-Homji (1994)). In addition, the accumulation of dust reduces the tip clearance and increases the roughness of the surface roughness (Kurz and Brun (2001)). These changes in the blades affect the compressor delivery pressure (CDP) and reduce the mass flow.

Howell and Calvert (1978) & Aker and Saravanamuttoo (1989) calculated the impact of degradation mechanisms in the compressor performance based on the output power of the engine. Gulen, Griffin, and Paolucci (2002) reported that fouling decreased by 5% the output power due to mass flow reduction.

2.2.4 Combustion chamber degradation

The combustion chamber is one of the sections with a low level of degradation. The operation time of the combustion chamber has an irrelevant effect to degrade this section (Diakunchak (1991)). However, small variations in the combustion process such as increment of the fuel ratio can affect the components from the turbine section. For that reason, it is necessary to control the process of combustion. In addition, an incorrect combustion can produce ash that is deposited in the fuel injectors. This problem produces fluctuations in the flame and high local temperatures. The alteration in the temperature profiles increases the possibility of secondary flows, reduces the turbine efficiency and damages the turbine blades (Kurz and Brun (2001)).

2.2.5 Turbine degradation

Erosion is a common problem present in this section that modifies the profile of the blades. Fouling is also present in the turbine blades due to ash adhesion on the surfaces (Zwebek (2002)). It has been demonstrated that fouling on the turbine blades

reduces the turbine isentropic efficiency by 1% and the output by 3.7% (Diakunchak (1991)). As it was mentioned in the previous section, the high temperatures and incomplete fuel burning affect the turbine section due to overheating. This effect is responsible for hot corrosion that modifies the shape of the leading edge from the blades (Kurz and Brun (2001).

2.2.6 Monitoring, simulation and diagnosis of gas turbines degradation

Due to the fuel prices crisis in the last decades, many gas turbine users have introduced the use of technologies for monitoring the engine performance. The data obtained from engine monitoring have estimated the deterioration of the gas turbine. This information is used to schedule the preventive maintenance and to extend the period of the optimal production (Williams (1981), Haq and Saravanamuttoo (1991)). For example Pinelli (2002) reported a gas turbine model AVIO TG20 that reduced in the first month 4.1% of the power production due to degradation. Similar result was reported by Gulen, Griffin, and Paolucci (2002) where two single shaft gas turbines in operation in CCGT reduced 5% the output power in the first month. Mund (2006) mentioned that the single shaft configuration has a high sensitivity in the output power when the aerodynamics of the flow changes. For that reason, it is necessary in power plant applications the periodic maintenance in the engine (Zwebek (2003)). The typical overall maintenance period for industrial engines is approximately between 3000 to 4000 hours of operation. At the end of this period it is possible to find that the engine has lost 20% of the production capacity (Zwebek (2002)).

In the last decade, the development of algorithms based on the engine monitoring has created the possibility of detecting the location of the problem in the engine and predict the failure. Gulen, Griffin, and Paolucci (2002)) presented a model* based on the real time of monitoring the engine performance in order to predict the gas turbine degradation. The model compares the parameters given by the manufacturer and the values represented from deterioration factors.

* Equation that represents the engine at full load condition, for part load condition sees reference.

$$Y_{j,x} = Y_{j,b} \prod_{i=1}^{7} X_{i,j}$$

Equation 2-1

Where:

Y_j is the performance parameter from the manufacturer and j is the gas turbine parameter according to:

1 output power at generator terminals

2 heat rate at generator terminals

3 exhaust gas turbine temperature

4 exhaust gas mass flow rate

x, b are the baseline values respectively.

X_{ij} is the correction factors for specific turbine operation,

where i corresponds to:

1 ambient temperature (or compressor Inlet Temperature)

2 ambient pressure

3 ambient humidity (or compressor Inlet Humidity)

4,5 inlet and exhaust pressure drops

6,7 water/steam injection

Although this model presents an alternative to evaluate the engine deterioration. The criterion to determine the engine deterioration is a difficult process because the components present nonlinear tendency (Syverud, Brekke, and Bakken, (2005)). The instrumentation used in monitoring the engine health can fail to detect the degradation mechanism in some cases such as in the case of fouling (Razak and Dosanjh (2002)).

In the last few years, studies based on the engine simulation have predicted the possible problems in different sections of the gas turbine. For example, the salt formation inside of marine gas turbines have been studied by Caguiat, Zipkin, and Patterson (2002) and it was suggested to simulate the engine performance with data from the compressor inlet, engine vibration, fuel volumetric flow, turbine inlet temperature and generator load. However, according to Sorli, Langes, Laagland, and Hastings (2002) an integrated monitoring study has to select only the exclusive parameters linked with the problem.

2.3 Compressor Fouling Mechanism

The mechanism of fouling presented in the gas turbine is defined as a degradation mechanism produced by the particle deposition on the airfoils surface (Diakunchak (1991)). The problem of fouling has been represented by the reduction of the flow capacity from the compressor and the reduction of the efficiency. However, the real effects of fouling in the compressor are unknown because many arbitrary factors have been associated to this problem (Zwebek, (2002)). For example, Diakunchak (1991) attributed 1% of fouling and 1% of erosion in losses for the total engine efficiency (see Figure 2-3). This factors have been used to develop computational codes in the diagnosis of the engine (Escher (1995)).

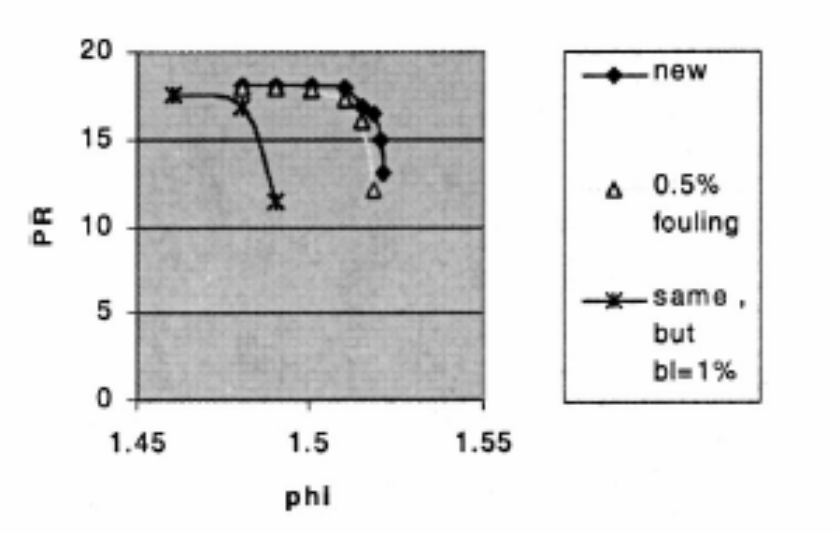

Figure 2-3 Representation of axial compressor performance map in three different conditions: new, fouling and fouling with 1% of blockage factor (Kurz and Brun (2001)).

2.3.1 Fouling background

The gas turbine operators have identified the presence of fouling in the engine since 1936 (Zaba (1984)). However, since the sixties the problem of fouling in industrial gas turbines has been considered an important cause to degrade the compressors performance and to be an evil inherent product of the operation (Upton (1974) & McDermott (1991)). The Middle East crisis in the seventies produced that the fuel prices increased 70%. The high cost of fuel produced the sufficient incentive to gas

turbine operators to look for new technologies to abate the mechanism of degradation to obtain optimal efficiencies for long periods (McDermott (1991)).

The studies in this area have demonstrated that the fouling mechanism represents approximately 80% of the compressor losses. A reduction of 5% from the mass flow can reduce 13% the output power and increase 5.5% the heat rate (Hoeft (1993) & Mustafa (2006)). These losses represent millions of USD in power and fuel consumption (Diakunchak (1991) & Mustafa (2006)).

Fouling is found in all engines due to the big quantities of air ingested. A typical gas turbine in operation in a residential location ingests 1.5 kg of solid contaminants per day (Zaba (1984)). For example, an engine of 7.5MW in an environment with particles concentration of 1 ppm can ingest 5 kg of dust in a single day (Tabakoff (1986)). This problem could turn worse if the engine operates in a very polluted environment such as mining or oil field areas where the ingestion of foreign particles can rise up to 39kg per day (Mustafa (2006)). It is necessary to pay careful attention to the inlet of the engine, because the ingestion of high quantities of particles reduces also the engine life (Osborne (1977)). In general, the industrial gas turbines are installed with inlet filters that stop the pass of particles (Tarabrin, Bodrov, Schurovsky, and Stalder (1996)). The size of particles stopped by the filters can be in the range of μm (Meher-Homji and Cyrus B, (1990)).

The selection of the filtration system has to be made and selected according to the environment conditions (Mustafa (2006)). In modern power plants, the filtration system involves different stages of filtration that consist in cylindrical and conical arrangements of synthetic media filters (Huff & Puff[*] systems). For example, filtration for industrial engines require efficiency of 99.5% for particle retention in the range of 1-3µm (Boyce and Gonzalez (2005)). In the case of marine or off shore applications, the filtration system has to stop the ingestion of chemical vapours and salt[†] (Orsach, Kazcprzynski, Roemer, Scharschan, Caguiat, and McGroarty (2002)).

[*] Huff & Puff is a gas turbine filtration configuration to operate in positive or negative conditions of the flow. Source Donaldson Company GTS-102 rev6/05.

[†] The typical salt-air concentration in a marine gas turbine after filtration is approximately of 0.01 ppm (Caguiat (2003)).

2.3.2 Filtration systems

The configuration of the filtration system for industrial applications is divided into Pre-filter and Main filter stages (Brumbaugh (2002)). They are selected based on the flow velocity (low or high velocities). The filters for low velocity are cheaper and with longer life than filters of high velocity (Mund (2006)). However, according to Gulen, Griffin, and Paolucci (2002), the filters for low velocity produce bigger pressure losses than filters of high velocity

The typical characteristics of the filter are efficiency, pressure losses and useful life.

1) The efficiency of the filter is measured by the quantity and size of particles stopped by the filter media (see Figure 2-4) (Levine and Angello (2005)).

2) The pressure losses are the consequence of the flow passing through the filter media. This property is typically measured in mm or inches of water (Vigueras Zuniga (2003a)).

3) The useful life of the filters is represented by the period between filter replacements (Vigueras Zuniga (2003a)).

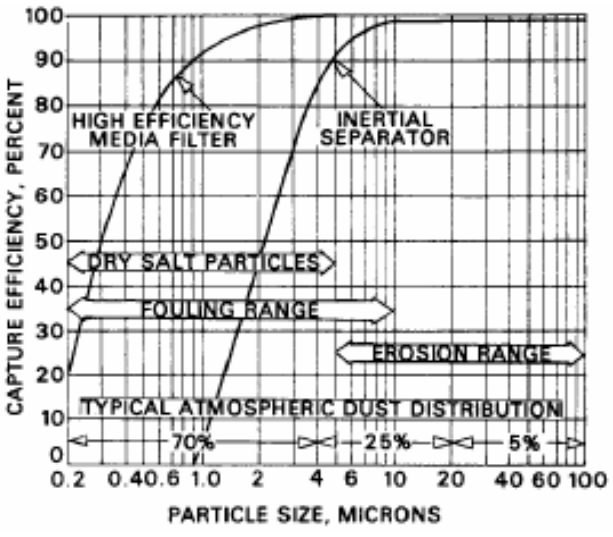

Figure 2-4 Filter efficiency chart (Levine and Angello (2005)).

The filter systems used in industrial applications are pulse-clean or static filters. The pulse-clean system (self-cleaning filter) retains the particles on the filter surface. The maintenance is automatic and consists of changing the filter orientation and passing a secondary air stream through the filter. The particles are removed from the surface and deposited outside of the inlet (Donaldson Company (2005)). Pulse-clean systems have demonstrated 98% efficiency of retention in the particle size range of 3µm with pressure losses of 4 inH2O (1000Pa) (Brumbaugh (2002)). The static filters are fixed in static panels and the maintenance is manual. The advantage of these filters is the long period of the useful life (Vigueras Zuniga (2003a)).

The Pre-filters stage consists of hoods, wraps and filters. Their job is to extend the life of the main filters. The retention in this stage includes large foreign particles (birds, seeds, leaves, airbone fibers, etc). The function of the inlet hoods is to avoid the ingestion of rain or snow. The wraps is a plastic net with large spaces from the grill to reduce the pressure losses at the same time that stop the inlet of big objects. The filters located in this stage are static and with low efficiencies of filtration. The filter media is an arrangement of polyester fibers randomly orientated to create an artificial web (Vigueras Zuniga (2003a)).

The main stage of the filtration system provides a high efficiency of filtration: retention of 95% in the arrange of 2µm particle size (Brumbaugh (2002)). They can be pulse clean filter systems or static filter systems. The filter packing technique combines different materials and properties. Special fibers are added to the filter packing to retain corrosive particles such as salt or chemical vapours. In hardness environments it is necessary to install a third filtration stage as a barrier to the salt immigration from the main filters (Vigueras Zuniga (2003a) & Donaldson Company (2005)). In naval applications, the third stage of filtration is used to stop the salt migration with particle size filters of 13µm (Caguiat (2003)). The use of new fibers have reduced the size of particle retention with acceptable pressure losses (Gahr, Benson, Graham, Gogins, and Brown (2005) & Meher-Homji and Cyrus B (1990)).

The problems of filters in gas turbine applications are summarized as follows.

- There is not any system of filtration that can guarantee to stop compressor fouling (Lakshminarasimha, Boyce, and Meher-Homji (1994), Tabakoff (1986) & Caguiat, Zipkin, and Patterson (2002)). This is because only filters with effectiveness of 99% and particle size retention of 3µm could solve this problem. But this condition is not possible to use in gas turbines due to the quantity and velocity of the mass flow driven by the compressor (Osborne (1977) & Diakunchak (1991)).
- The pressure losses increases as the particles are accumulated in the filter media passages (Zwebek (2002) & Mund (2006)).
- In many industrial applications (marine and offshore) the location of the inlet is at ground level due to the limitation of space and this accelerates the ingestion of ground dust (Mund (2006)).
- Low power levels of operation from the engine decrease the efficiency of the filters (Fielder (2003)).

Hence, the filters application in gas turbine can not guarantee to stop the 100% of the particles mixed in the air. However, they can reduce the presence and quantity of foreign objects inside of the engine (Mustafa (2006), Vigueras Zuniga (2003a)).

2.3.3 Fouling contaminant source

The atmospheric air ingested by the gas turbine contains certain amounts of contaminants. These contaminants are the product of soft aerosols formed by small particles of dirt, dust, pollen, insects, oil vapour, sea water salt, water vapour, sticky industrial chemicals, un-burnt hydrocarbons, soot particles, etc. (Upton (1974) & Brooks, (2000)). The performance deterioration of the compressor is due to these particles that can cause in the blades a temporary problem (fouling) or a permanent problem (erosion) (Tabakoff, Lakshminarasimha, and Pasin (1990)).

The main source of the fouling problem in the compressor has the origin from the particles mixed with the atmospheric air. The fouling layer on the blade surface is formed with 80% of the dust that is found in the filters (Diakunchak (1991)). The layer of fouling presents in many cases a combination of contaminants with residues

of oil or water mist (Kurz and Brun (2001)). The concentration of particles increases under unfavourable conditions such as sand storms or chemical polluted clouds and the mechanism of fouling is accelerated (Mustafa (2006)). For that reason, it is important to consider the environment conditions, layout of the plant and maintenance schedule in order to reduce the probability of compressor fouling (Stalder and Sire (2001)).

The particle that are deposited on the compressor blade surface are in the range of micrometers (Kurz and Brun (2001), Zwebek (2002) & Osborne (1977)). The x-ray analysis for a fouling sample demonstrated that the layer of fouling is a mix of different components (see Figure 2-5) (Kolkman (1993)). Two groups of components were identified from this analysis. The first group was water-insoluble solids represented by the presence of silicon, and the organic materials were represented by the presence of carbon and oxygen. The second group was water soluble substances that cause corrosion. They were hydroscopic and contained chlorides to promote corrosion.

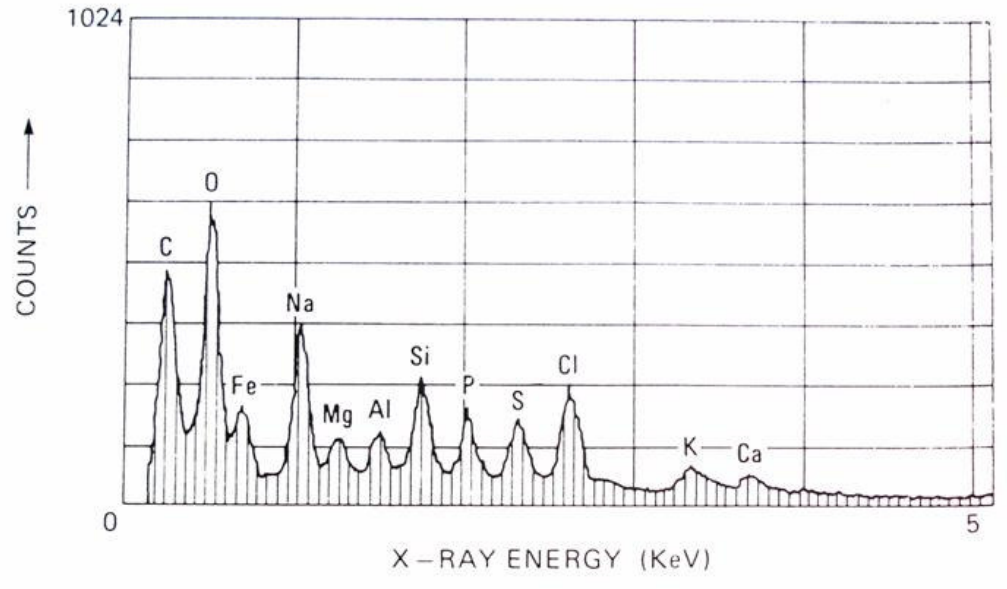

Figure 2-5 EDX spectrum of layer deposit on the surface of compressor blades (Kolkman (1993)).

2.3.3.1 Sources of external contaminants

Table 2-1 proposes a general classification from the contaminants according to geographical location of the engine (Mund and Pilidis (2004)). For marine applications, it has been demonstrated that salt is the main source of compressor fouling (Mund and Pilidis (2004), Syverud, Brekke, and Bakken (2005) & Caguiat, Zipkin, and Patterson (2002)).

LOCATION	MAIN CONTAMINANT
Industrial	Dust and hydrocarbon aerosols
Rural	Pollen
Costal	Salt

Table 2-1 Gas turbine location and typical contaminants (Mund and Pilidis (2004)).

New technologies of filtration have demonstrated to stop the particles from the air stream. However, their effectiveness is random due to changes from the environment conditions. The common particles retained from the filters are summarized in Table 2-2 . These particles are found mixed between them and seldom were found isolated in the filters (Brumbaugh (2002) & Giampolo (1997)).

TYPE	TYPE OF PARTICLE	SIZE (μM)
F1	Sand	20 ~ 2,000
F2	Ground-Dust	1 ~ 300
F3	Oil Smokes (oil & gas plants)	0.02 ~ 1
F4	Fly Ash	1 ~ 200
F5	Salt Particles in Mist	Less than 10
F6	Salt Particles on Spray	More than 10
F7	Insects Swarms	More than1,000
F8	Smog*	Less than 2
F9	Clouds & Fog	2 ~ 60
F10	Rain	More than 60
F11	Fume*	Less than 1
F12	Clay	Less than 2

F13	Rosin smoke	0.01 ~ 1
F14	Fertilizer	10 ~ 1,000
F15	Coal Dust	1 ~ 100
F16	Metallurgical Dusts and Fumes (welding smoke)	0.001 ~ 100
F17	Ammonium	0.1 ~ 3
F18	Cement Dust	3 ~ 100
F19	Carbon Black	0.01 ~ 0.3
F20	Contact Sulphuric Mist	0.3 ~ 3
F21	Pulverized Coal	3 ~ 600
F22	Paint Pigments	0.1 ~ 5
F23	Plant Spores	10 ~ 30
F24	Pollens	10 ~ 100
F25	Snow & Hail	More than$1x10^4$

Table 2-2 Common particle size and concentration in atmospheric air (Brumbaugh (2002) & Giampolo (1997)).

The ambient conditions such as temperature, pressure and humidity play an important role in the engine performance and they have to be considered in the study of fouling. The ambient temperature is considered into three ranges: Hot (50 to 30ºC), Warm (29 to 15ºC) and Cold (15 to -20ºC). The humidity is considered into three ranges: Dry (less 10%), Medium (around 50%), and Wet (more than 75%) (Mathioudakis and Tsalavoutas T. (2002)). The combination of the possible environmental scenarios between the temperature and humidity result in nine cases (see Table 2-3).

CASE	CONDITION	LOCATION EXAMPLES:	FOULING EXAMPLES:
1	Hot+Dry	Desert locations	F1,F2,F3
2	Hot+Medium	Jungle and Marshes locations	F7, F9, F10, F14, F23, F24
3	Hot+Wet	Coast & offshore locations	F1, F3, F4, F5, F6, F7, F9, F10, F14,
4	Warm+Dry	Barred locations	F2, F3, F4, F11, F15, F16, F18
5	Warm+Medium	Central locations	F2, F3, F4, F7, F8, F14, F15, F23, F24
6	Warm+Wet	Raining or Coast locations	F1, F3, F4, F9, F10, F12
7	Cold+Dry	Central Artic Locations	F3, F4, F17, F25
8	Cold+Medium	High Sea Level locations	F2, F3, F4, F5, F8, F9, F12,

			F25
9	Cold+Wet	Artic Coasts locations	F1,F2, F3, F5, F6, F16, F25

Table 2-3General environment scenarios of industrial gas turbines in operation.

The type of fouling can change due to the season time in the same location. This is influenced by the ambient temperature and the concentration of particles. For example, the ambient temperature in the northern hemisphere can change dramatically between one season and another. The altitude is an ambient parameter that also modifies the engine performance. However, the influence of this parameter in the mechanism of fouling is nil.

2.3.3.2 Sources of internal contaminants

The internal causes that produces compressor fouling are due to non-maintenance or incorrect operation from auxiliary equipments (Vigueras Zuniga (2003b)). For example, the presence of oil residues due to lakes seals is commonly found in the compressor. The cooling system by fog in the inlet of the engine can carry salt or water impurities into the compressor (Lakshminarasimha, Boyce, and Meher-Homji (1994) & Zwebek (2002)). The filter panels are affected by erosion and corrosion and this increases the presence of FOD inside of the engine (Zwebek (2002)). In a sample of fouling the presence of steel and aluminium particles was found due to the components rubbings from the brush seals and bearings (Langford (1977)). The wear of graphite bushing from the compressor guide vanes has been demonstrated to be also a source of compressor fouling (Yee and Myers (2003)).

2.3.3.3 Steam and vapours as source of fouling

The presence of oil and vapours inside of the compressor increases the adherence of particles on the blade surface (Thames, Stegmaier, and Ford (1989)). The oil vapours are produced by oil lakes from internal components of the engine (Lakshminarasimha, Boyce, and Meher-Homji (1994)). The deposition of oil and particles on the rear compressor blades formed a hard layer due to the temperature.

This layer is only possible to remove by hand in the overall engine maintenance (Fielder (2003)).

The chemical vapours mixed in the air are the product of polluted environments. For example, in marine applications the diesel vapour is produced by the auxiliary engines localized close to the engine inlet (Fielder (2003)). The natural ambient agents accelerate the adhesion process as such as heavy fog, rain and excessive humidity (Bagshaw (1974)).

2.3.4 Fouling in axial compressors

The presence of fouling in the different compressor stages have demonstrated to be higher in the first stages than the rear stages (Lakshminarasimha, Boyce, and Meher-Homji (1994), Seddigh and Saravanamuttoo (1990) & Mezheritsky and Sudarev (1990)). The IGV's and first stage of the compressor represent between 40 to 50% of the total compressor fouling (Upton (1974) & Tarabrin, Bodrov, Schurovsky, and Stalder (1996)). This result was similar in a study of salt formation in a multistage compressors by Syverud, Brekke, and Bakken (2005)). According to Wilkinson and Shark (2004) the IGV can represent 70% of the total fouling.

The presence of fouling decreases in the rear stages in a multistage compressor (Aker and Saravanamuttoo (1989)). This has been demonstrated in a previous study where the quantity of dust accumulated was measured in blades from different stages (see Table 2-4) ((Tarabrin, Schurovsky, Bodrov, Stalder, and Bodrov (1998)). This result coincided with results from the salt accumulation in marine engines obtained by Syverud, Brekke, and Bakken (2005)).

STAGE	ROTOR CONCAVE [g] (PRESSURE SURFACE)	ROTOR CONVEX [g] (SUCTION SURFACE)	STATOR CONCAVE [g] (PRESSURE SURFACE)	STATOR CONVEX [g] (SUCTION SURFACE)
0 (IGV)	N/A	N/A	0.90	1.35
1	0.50	0.70	0.78	1.00
2	0.40	0.28	0.40	0.27

3	0.12	0.12	0.10	0.10
4	~ 0	~ 0	~ 0	~ 0

Table 2-4 Fouling distribution in a gas turbine compressor Frame-5 (Tarabrin, Schurovsky, Bodrov, Stalder, and Bodrov (1998))

However, the location of the particles deposition on the blade surface can differ. For example, a study suggest that on the blade tip the deposition of particle is null due to the centrifugal effect (Ingistov (2002)). In contrast with this, Levine and Angello (2005) reported that fine particles were adhered on the rotating blades under high centrifugal forces.

The visual inspection from the IGVS was reported in a marine engine at 2000 hrs with the following results (Syverud, Brekke, and Bakken (2005)).

i. The salt deposition was found on the leading edge region for the first four stages.
ii. The heaviest deposition was along the first stage annulus.
iii. The thickness of the salt layer on the first stator was at the hub of 500μm and at the annulus of 25μm.

2.3.5 Gas turbine performance deterioration by fouling

Visual inspections, endoscopies or internal cameras have been used to detect fouling when the engine is shut down. An example of this is the automatic real condition monitoring to detect ice and fouling in industrial engines with the use of endoscopies, camera and digital image process (Wilkinson and Shark (2004)). Although this system could detect the presence of fouling in the IGVs, the only way to know certainly the cause of fouling is analyzing the contaminants in the laboratory (Kolkman (1993)). The real applications of these tests are expensive and limited to shut down the engine.

The use of indirect parameters is used to make an estimation of the fouling level. However, this method is based on many arbitrary assumptions that induce uncertainty

in the results, because, in the real application, the turbine entry temperature (TET) is estimated from the turbine output power (Saravanamuttoo and Lakshminarasimha (1985)). According to Haq and Saravanamuttoo (1991) small engines can present a fast degradation because fouling reduces the compressor performance and is represented by increases the TET. However, according to Kurz and Brun (2001) this condition does not represent the average value of TET and represents the temperature of a local flame. The engine size is a topic of discussion because some reports agree that small engines are more susceptible to degradation as (Tarabrin, Schurovsky, Bodrov, Stalder, and Bodrov (1998)) and another argue exactly the opposite as (Aker and Saravanamuttoo (1989) & Haq and Saravanamuttoo (1991)).

The output power of the engine is used for many gas turbine users to predict the fouling. However, this method does not always represent the real situation due that the automatic control of the engine adjusts the internal components. This problem is illustrate in the study of an engine that was re-adjusted after several hours of operation (Kurz and Brun (2001)). After the engine was re-adjusted, the TET recovered the original value but the power decreased 2.5%. It was then necessary to adjust the engine by increasing the heat rate to 1.2% to obtain the original power. In this case, the deterioration was evident and non-recoverable. This demonstrates that the engine configuration plays an important role in the deterioration of the performance.

In the case of the compressor configuration, fouling has a higher impact in axial compressors than in centrifugal compressors (Meher-Homji and Cyrus B (1990) & Seddigh and Saravanamuttoo (1990)). The map of the axial compressor shows the reduction of the surge margin due to fouling (Diakunchak (1991) & Seddigh and Saravanamuttoo (1990)). The speed of the engine also could hide the fouling effect in gas turbines. This is because the movement from the design point represented in the compressor map could be easy confused with a different compressor line of operation (Seddigh and Saravanamuttoo (1990)). The case is illustrated when the design point of the compressor is located in a higher shaft speed point and lower efficiency. When compressor fouling occurs, the compressor efficiency increases due to the reduction of the shaft speed and then effect of fouling is difficult to detect (Kurz and Brun (2001)).

The importance of the engine configuration to evaluate the influence of fouling was analyzed by Caguiat, Zipkin, and Patterson (2002). The first case is an engine configuration of two shafts* (see Figure 2-6). The normal operation condition was linked to a specific value of the compressor delivery pressure (CDP) and the gas generator turbine (GGT) was linked to a specific value of the shaft power speed (SPS). When the CDP was reduced due to fouling, the turbine entry pressure (TEP) was also reduced. This affected the GGT and then the SPS was also reduced. The automatic control had to increase the fuel consumption to increase the power from the GGT and to obtain the correct SPS. In this case, it is possible to detect the problem in the compressor based on the speed and fuel consumption of the engine. The second case was the operation of a single shaft† engine (see Figure 2-6). The CDP was decreased due to fouling and then the SPS also decreased. The automatic control increased the SFC and hence the turbine entry temperature (TET) increased to obtain the correct SHP. In this case, it is difficult to detect the problem directly because it requires to check the engine performance with two different loads. However, in the real application, it is not possible to change the load.

The detection of fouling in a multiple axial compressor is also a difficult, because the early stage modifies the rear stages. The analysis in this case is a complex study based on the blade aerodynamics to detect the stage affected (Ramsden (2002)). For that reason detecting fouling inside of the compressor is a difficult work and is generally based on the operation experience (Scott (1979), Mund (2006) & Mustafa (2006)).

* LM2500 Industrial Gas Turbine manufactured by General Electric, more information www.ge.com

† Allison 501K Industrial Gas Turbine manufactured by Rolls Royce, more information www.rolls0royce.com.

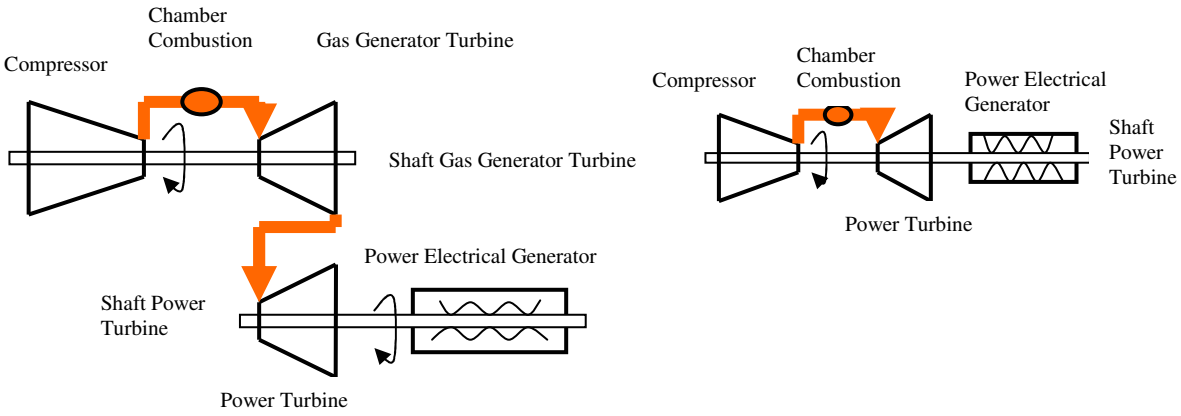

Figure 2-6 Gas turbine configuration: two-shafts configuration (left), single-shaft configuration (right).

2.3.6 Surface roughness change and aerodynamic consequences in blades

The major contribution of fouling to decrease the efficiency and pressure ratio in axial compressor is due to changes from the blade geometry (roughness and thickness of the surface) (Mezheritsky and Sudarev, (1990) & Upton (1974)). The changes on the surface roughness increase the friction with the air and affect the compression process (Zwebek (2002)). The particle deposition reduces the cross-area section and the mass flow is reduced by this effect. This modifies the pressure ratio and compressor efficiency (Tabakoff, Lakshminarasimha, and Pasin (1990)). The increment of roughness increases the friction losses that produces an early transition in the boundary layer (laminar to turbulent) that is transmitted in the compressor performance as losses (Kurz and Brun (2001)). Also, the particles tend to adhere easily on rougher surfaces due to the frictional forces (Caguiat, Zipkin, and Patterson (2002)).

The change of the surface roughness due to blade erosion has demonstrated that affects the engine performance and increases the fuel consumption. According to Lakshminarasimha, Boyce, and Meher-Homji (1994) if the surface roughness increases from 55 to 120µm the fuel consumption also increased in 0.13%. Kurz and Brun (2001) reported an increment of the surface roughness after a long time of operation, the rotor blades increased from 4µm to 6.0µm and the stator blades to

8.0µm . Gbadebo, Hynes, and Cumpsty (2004) reported in a Rolls Royce stator blade the change of the surface roughness from 1.53 to 2.03µm . The value of the surface roughness can change due to the blade coating (see Table 2-5) (Caguiat, Zipkin, and Patterson (2002)).

Type of Surface	Roughness value
non-coating	1µm
solid-coating	60-70 µm
fluid-coating	14 µm

Table 2-5 Blades from the gas turbine Allison 501K.

The difficulty to observe the changes on the surface roughness in a compressor is due to the space limitation. An empirical technique to measure the roughness in the laboratory is comparing with a microscope the contaminant size with standard sand paper grain. This technique was used to measure the salt accumulation in the first stator blade in a marine engine (Syverud, Brekke, and Bakken (2005)). The result of the salt accumulation was on the pressure surface of 25 µm and on the suction surface of 10µm.

The results from the experiment of Gbadebo, Hynes, and Cumpsty (2004) demonstrated that minimum increments on the surface roughness can degrade fast the aerodynamic performance. The experiment consisted of changing the condition of the surface roughness in a stator blade with a sand emery paper adhered to the surface (ASTM150). The sand emery paper increased the surface roughness from 25µm to 150µm. and it increased the thickness of the blade by 0.3mm. The results are summarized as follows.

- The suction surface on the leading edge region was the localization of the highest blade aerodynamics changes. The thickness of the boundary layer in this region was modified.

- The major effect for three-dimensional separation was due to the increment of the surface roughness in the hub of the stator blade. This effect was observed on the suction surface close to the leading region.
- The numerical analysis demonstrated that the skin-friction coefficient produced turbulent flows.

Similar to this result, Levine and Angello (2005) demonstrated in a numerical study that increasing the surface roughness changed the thickness of the boundary layer around the blade.

2.3.6.1 Boundary layer

The early separation from the boundary layer produces changes in the exit angle of the blade and consequently affects the following stage (Ramsden (2002)). Small changes from the airfoil shape produces changes in the inlet and incident angles from the blades and reduces the airfoil throat opening (Diakunchak (1991)). According to Caguiat, Zipkin, and Patterson (2002), the deposition of the particle can change the effective angle of attack in each blade and produce the compressor stall. However, Syverud, Brekke, and Bakken (2005) mentioned that the increment of the surface roughness does not produce a significant change in the inlet angle or outlet angle.

The drag and thickness of the boundary layer are functions of the Reynolds number. If the boundary layer tends to be laminar the drag and energy are reduced and opposite to this result, it is when the boundary layer tends to be turbulent (Barlow, Rae, and Pope (1999)). The transition point is produced when the boundary layer changes from laminar to turbulence. This is a three dimensional phenomenon which occurs where the laminar and turbulent flows coexist and it can be produced by natural process, for a bypass or flow separation (Mayle (1991)). However, the two dimensional study for the transition point in turbomachinery application is used in theoretical investigations (Gbadebo, Hynes, and Cumpsty (2004) & Mayle (1991)). The effect of flow separation transition can be consulted in the following reference Hobson, Hansen, Schnorenberg, and Grove (2001).

The transition between laminar to turbulent can occur with any disturbance in the flow around the blade (Mayle (1991)). For example, an imperfection from the smooth surface can generate fluctuations in the flow that when it is amplified can produce:

- Turbulence due to formation of spots
- Bubbles on surfaces, when the flow is separated and reattached to the surface

The smooth surface of the blade produces forces that send backward the transition point. This condition is produced when the surface roughness increases and then the transition point is moved forward. In this case, the thickness of the boundary layer is modified and produces two effects (Meher-Homji and Bromley (2004)).

i. The blade drag increases.
ii. The skin friction increases.

The study of Zaba (1984) demonstrated that due to blade coating the thickness of it increases in 0.1mm. This can reduce the mass flow by 10% and the compressor efficiency by 5%.

2.3.6.2 Surge margin

Fouling affects the airflow conditions due to the change of the velocity angle that decreases the efficiency and the stall region margin from the compressor (Saravanamuttoo and Lakshminarasimha (1985), Langford (1977) & Ramsden (2002)). This reduction is due to the increment of the surface roughness that changes the boundary layer thickness and reduces the aerodynamic properties from the blade (Kurz and Brun (2001)). This change is represented in a compressor map when the operation point is moving close to the surge line (Zwebek (1993), Saravanamuttoo and Lakshminarasimha (1985), Olhovsky (1985) & Meher-Homji and Cyrus B (1990)). According to Mustafa (2006) the condition of operation close to the surge line is a dangerous situation for the compressor.

2.3.6.3 Compressor performance

The numerical study of Lakshminarasimha, Boyce, and Meher-Homji (1994) assumed that fouling reduces: the mass flow by 5%, the compressor efficiency by 2.5% and the output power of the engine by 10%. According to Zwebek (2002) the mass flow is reduced by 5% due to fouling and it increased the fuel consumption of the engine by 2.5%. Meher-Homji and Bromley (2004) suggested that the losses due to fouling could affect the total output power by 20%. This agreed with the study of Leusden, Sorgenfrey, and Dummel (2003) where 85% of the compressor losses were attributed to fouling. Caguiat (2003) found in an experimental salt was injected of 30g; that the compressor delivery pressure was reduced by 7% and the fuel consumption increased by 3%.

The turbine power is a function of the temperatures and pressure from the engine represented in the following isentropic equation.

$$TurbinePower = mC_pT_3\left[1-\frac{1}{\left(\frac{P_3}{P_4}\right)^{\frac{\gamma-1}{\gamma}}}\right]$$

Equation 2-2

where: P_3 pressure delivery by the compressor

P_4 pressure delivery at the outlet of the turbine

m mass flow

T_3 temperature in the combustion chamber

γ air constant

C_p specific heat

The output power decreases when P_3 is affected by the reduction of mass flow. For power generation applications these changes are immediately corrected by the automatic engine control that increases the fuel consmption when the output power decreases. However, the turbine entry temperature (TET) is increased by this

corrective action and it affects the hot section due to the high temperatures produced for the rich fuel ratio in the combustion.

The use of compressor pressure ratio was used as a criterion of fouling in some previous studies (Scheper, Mayoral, and Hipp E.J. (1978) & Haq and Saravanamuttoo (1991), Kulle (1974)). However, the compressor pressure ratio is also affected by the inlet losses and it has to be considered because it can represent an increment of the fuel consumption of 1% (Walsh and Fletcher (1999)).

Zwebek (2002) and Seddigh and Saravanamuttoo (1990) reported that in real applications 1% of reduction in the compressor efficiency increased the heat rate by 1.5% to produce the same output power (see Figure 2-7). However, Scott (1979) and Diakunchak (1991) suggested to use the mass flow as a parameter of compressor degradation due to fouling. The study of Diakunchak (1991) demonstrated that reducing the mass flow by 5% represented a reduction in the output power by 4.9% and in the overall engine efficiency by 3.3%. These studies were based on arbitrary assumptions with the objective to know the sensibility from the engine performance due to compressor degradation. Then in order to avoid the use of arbitrary factors Diakunchak (1991) suggested to monitor the compressor efficiency based on non-dimensional parameters to estimate the fouling. However, it is common to find that gas turbines operators in power plants are still using the output power reduction as criterion of compressor degradation (Jeffs (1992) & Jeffs (2000)).

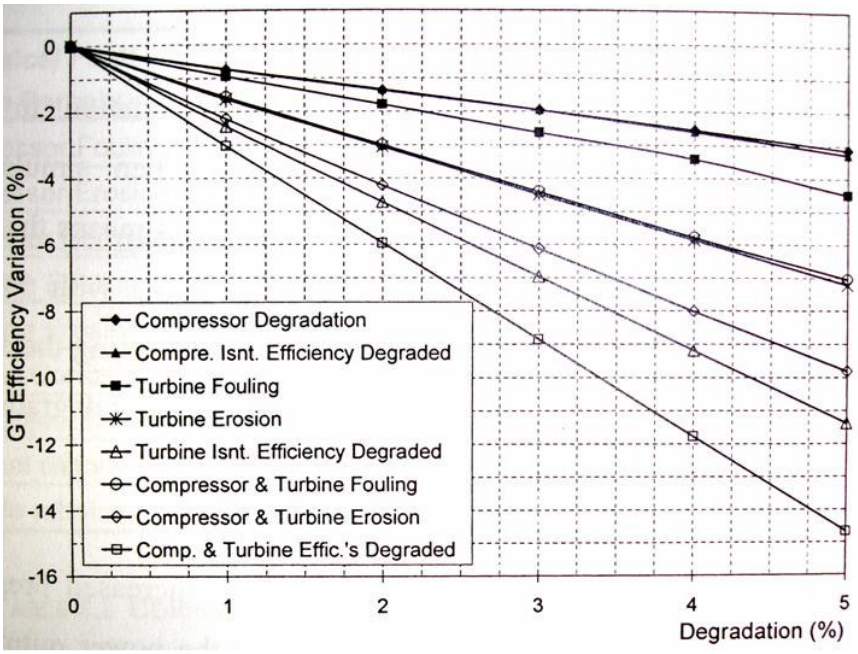

Figure 2-7 Gas turbine efficiency based on deterioration in specific sections (Zwebek (2002))

2.3.6.4 Emissions

The environmental regulations ensure that the emission of gasses has to be controlled. In this case fouling has an influence in the increment of the fuel consumption that produces rich mixes* ((Boyce and Gonzalez, 2005)). This condition of excess of fuel in the mix causes the production of NOx due to the high local temperatures produced during the combustion ((Singh (2002)).

2.3.6.5 Mechanical problems

According to Zwebek (2002) fouling can produce separation of the boundary layer that results in unexpected pressures on the blade surface. These conditions can produce vibration and noise. Also, the changes of the exit blade angles due to fouling can produce vibration Ramsden (2002). An excessive deposition of particles on the airfoil surfaces reduces the cross section of the flow passage and it is possible to have conditions of flow choke. Orsach, Kazcprzynski, Roemer, Scharschan, Caguiat, and McGroarty (2002) suggested that compressor fouling evidently increases the

* Rich mixes in the combustion process are produced when the fuel ratio increased respect the quantity of air (Singh (2002)).

vibrations, but it is difficult to identify the source of the problem based only in the engine vibration. Sorli, Langes, Laagland, and Hastings (2002) commented that the deposition of particles can produce imbalance in the blade at high velocities of rotation.

Although the mechanical properties of the blade material have been studied, the relation between they and the aerodynamic properties has not been explored. Scala Sinclaire, Konrad, and Mason (2003) suggested that compressor deterioration due to fouling could be detected by sensors used into the vibration monitoring. Mathioudakis, Stamatis, Tsalavoutas, and Aretakis (2001) suggested developing a numerical algorithm to estimate the engine health based on the noise produced by the engine.

2.3.7 Previous fouling studies

Studies about fouling in the public literature are generally based on the engine power production. These theoretical investigations have used arbitrary factors to modify the mass flow, the compressor pressure ratio and efficiency. For example, the factors suggested by Saravanamuttoo and Lakshminarasimha (1985) were used in the following studies such as the study of Lakshminarasimha, Boyce, and Meher-Homji (1994). In this study the degradation of the engine was estimated based on the output power produced by the engine. However, all of these studies recognized the necessity to demonstrate the results with experimental tests (Saravanamuttoo and Lakshminarasimha (1985)). Schlichting (1979) suggested a complete study of fouling based on aerodynamic problems and recognized the difficulty of this task due to the micro-scale involved in the study of the boundary layer.

The first studies assumed a linear degradation of the output power due to fouling (Zaba (1984)). Later on, Saravanamuttoo and Lakshminarasimha (1985) estimated the compressor degradation with the reduction of the mass flow and efficiency (see Figure 2-8). One of the first deterioration studies that included the factor of fouling to estimate the engine deterioration was presented by Lakshminarasimha and Saravanamutto (1986). The use of the stage stacking technique proposed by Aker and

Saravanamuttoo (1989) resulted that the compressor fouling was linear. A decade later, Tarabrin, Schurovsky, Bodrov, Stalder, and Bodrov (1998) suggested the compressor fouling with an exponential tendency behaviour over the time until the thickness formed by the particle deposition was stabilized.

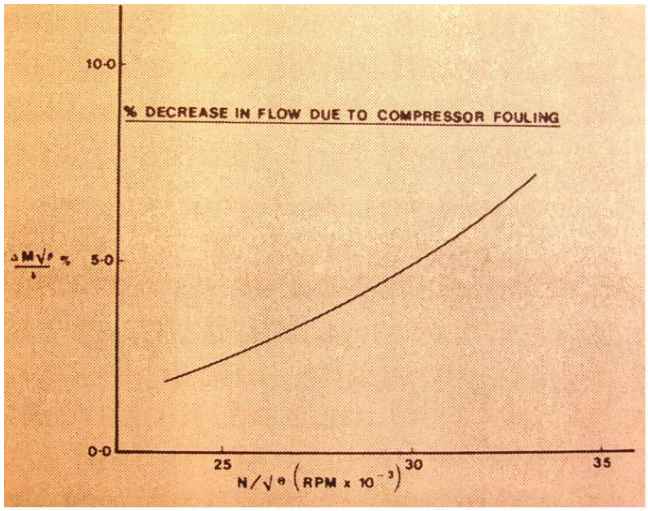

Figure 2-8 Mass flow reduction due to Fouling. (Saravanamuttoo and Lakshminarasimha (1985))

Kurz and Brun (2001) demonstrated that fouling decreased the clearances between the blade and the casing and it caused secondary flows. According to Bouris, Kubo, Hirata, and Nakata (2002) the highest deposition occurs on the leading edge region of the blade due to the inertial impaction of the particle. Similar to this conclusion, Mustafa (2006) suggested that the deposition of water droplets by the inertial impaction is due to the laminar flow presented in this region. This condition of the flow causes the inability from the water droplets to follow exactly the curve of the air streamlines in the blade passages. Bouris, Kubo, Hirata, and Nakata (2002) demonstrated by a numerical study that the leading edges region and the stator pressure surfaces are the regions affected by deposition of large particles. It was observed in this study that the profile thickness and roughness surface increased; for the rest of the blade surface the deposition was due to turbulent diffusion. However, all of these studies were based on numerical studies and included many arbitrary assumptions and for that reason they concluded that their results have to be validated with experimental tests.

2.4 Compressor Washing

The maintenance of a gas turbine plays an important role for optimal performance. For many years, compressor washing operated when the gas turbine was shut down for overall maintenance (inspection, replacement of components and cleaning service) (Vigueras Zuniga (2003b)). The first abrasive materials used for cleaning the compressor were nutshells, rice and synthetic resin particles introduced at high velocities into the compressor working off line. This method of compressor washing resulted quick and effective, however this produced erosion in the blade (Mund and Pilidis (2004)).

The method of cleaning by soft erosion was replaced by the use of water injection. The injection of water from the inlet followed the same technique used to boost the power in aero-engines with the use of water injection into the compressor (Mund (2006)). Water injection includes characteristics as injection of fluid, droplet impact on blades, fluid radial displacement, droplet size, re-ingestion and heat transfer (Murthy, Ehresman, and Haykin (1986) & Mund and Pilidis (2004)). The first patents of water injection into the compressor were presented in the seventies. The patent by Freid and Tapparo (1971) included a spray system of four nozzles injecting parallel to the air stream. A few years later Mansson (1975) patented a system to spray water with low speeds in order to penetrate until the rear stages (Mund (2006)).

During the eighties the improvements in the aerodynamic airfoil geometry obligated to reduce the level of erosion allowed in the blades (Brittain (1983)). For that reason, during this decade the first studies of automatic and controlled systems of compressor washing were tested in power plants (Mund (2006)). The use of demineralised water to wash the compressor demonstrated non erosion on the blades and was adopted for compressor washing with a combination of clean liquids (water-detergent or water-petroleum solvent) (Boyce, Bowman, Meher-Homji, and Focke (1985)). In 1986 a patent to clean the gas turbine at full speed was presented, this result was considerable improved in the engine performance (McDermott (1991) and Mund (2006)). The results from the study of Thames, Stegmaier, and Ford (1989) demonstrated the possibility to wash the compressor during normal operation, and this process was called compressor washing on line. Improvements in the compressor washing on line

continued during the nineties. During this decade the gas turbine users found interest in this technology to improve the engine performance (McDermott (1991)). The compressor washing on line has become a priority preventive maintenance in industrial gas turbines (Margolis (1991)). The new injection systems included advances in the injection system, such as the cone nozzle patent (see Figure 2-9) and the flat nozzles (McDermott (1991)). According to Mund (2006) at the end of the nineties the compressor washing on line has been used for commercial and military aero engines.

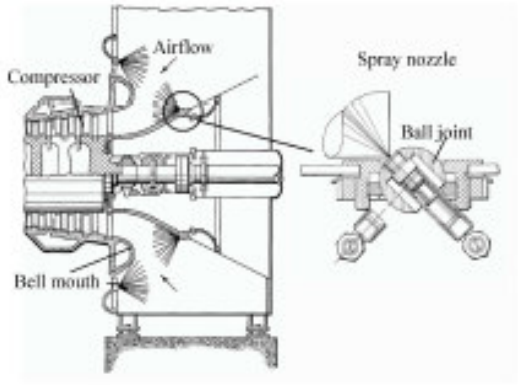

Figure 2-9 Washing system and cone nozzle (Kolev and Robben (1993)).

Valenti (1998) demonstrated that improvements in compressor washing on line represented a considerable reduction in the maintenance costs. In recent investigations have been focused to develop systems that combine the ingestion of the detergent-fluid with air in order to atomize the droplet size in the nozzles (Mund (2006) & Syverud and Bakken (2005)).

A report from General Electric (2001) mentioned that the technology of compressor washing on line does not represent a problem of erosion on blades. Nowadays, the compressor washing on line and detergent suppliers present this cleaning technology as a tool to improve the output power, reduce fuel consumption, and increase the reliability and longevity of the equipment (Lambart, Gordon, and Burnett (2003)). This technology has been developed based on the experience and empirical design philosophies of the suppliers and operators accumulated during this time (Mund (2006)). Currently one of the problem presented for compressor washing on line is the

spray nozzle angles that due to vibration and corrosion has demonstrated to affect the effectiveness of this technology (Mund (2006)).

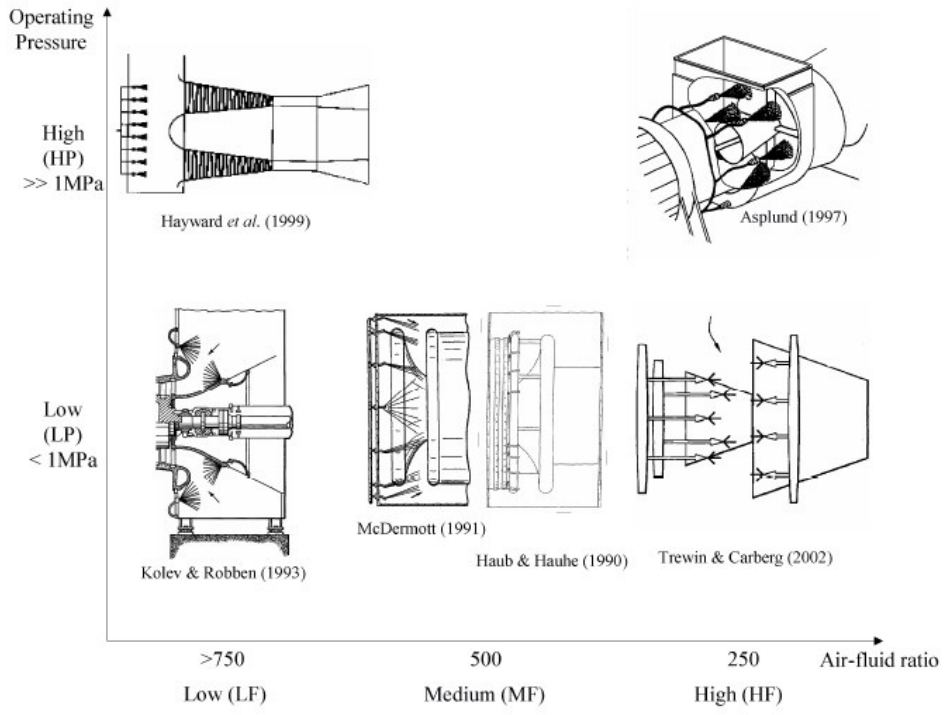

Figure 2-10 Commercial systems of on line washing systems (Mund (2006)).

2.4.1 Classification of compressor washing

There are four typical techniques of compressor washing. The basic technique involves a manual cleaning using brushes and washing detergents. This method is very effective to recover the losses due to fouling. However, this technique requires shutting down the engine, time and human work. The second is by the ingestion of solid particles such as nutshells, rice, or synthetic particles. This is a fast way for washing but also requires shutting down the engine and unfortunately produces erosion in the blades (Mustafa (2006) & Mund (2006)).

The compressor washing off line (crank washing) is another possibility. This technique is very effective to wash the compressor and can recover almost 100% of the losses produced by fouling (Meher-Homji and Bromley (2004)). The off line operates in a low speed shaft and the injection includes high quantities of water with a low risk of erosion (Leusden, Sorgenfrey, and Dummel (2003)). The typical procedure for this method is to use the starter motor of the engine and to inject the

cleaning detergent into the inlet. In this process the cleaning fluid passes through all the compressor stages and the wash is drained away (Fielder (2003)).

The disadvantage of washing off line is that only it is possible to operate when the engine is shutting down (Meher-Homji and Bromley (2004)). In addition, running the shaft at a low speed reduces the starter motor life of the engine and then increases the washing costs. This last problem is important in places where the space is limited or where it is necessary to produce the water as such as ships and offshore rigs (Fielder (2003)).

The new technique is compressor washing on line (fired washing) that operates at full load of engine operation. This maintenance extends the intervals between compressor washings off-line and corrects automatically the fouling losses produced in the compressor. The system of compressor washing on line is based on the state of the art and involves the following characteristics: droplet size, speed and angles of injection (nozzle location) (Raykowski, Hader, Maragno, and Spelt (2001) & Mund and Pilidis (2004)). Compressor washing off line and on line are different in three principal characteristics: number and location of nozzles (more nozzles are required in on line), quantity of fluid (more liquid is required in off line) and washing effectiveness (better results in off line) (Stalder and Sire (2001)). Kolkman (1993) commented that compressor washing on line cleans partial the fouled deposits on the compressor blade. This last result was recognized in previous studies, but it gives a good alternative to abate the compressor fouling (Stalder and Van Oosten (1994), Mustafa (2006) & Mund (2006)).

2.4.2 Cleaning fluids

During the eighties the use of demineralised water, water-detergent mixtures and water-petroleum solvent were used as cleaning fluid (Mund (2006)). The chemical formula for the cleaning fluid patented by Woodson, Cooper, White, and Fischer (1989) increased the boiling point of the water. Later on, the use of anti freezer as additive in the cleaning fluid allowed the compressor washing under low temperatures. In the nineties, the improvements of the cleaning fluid resulted to be

fully combustible and biodegradable (Kaes (1991)). The use of corrosion inhibitors mixed with the cleaning fluid increased the effectiveness of compressor washing (Kolkman (1993)). For example, a marine engine study resulted that the use of anti-fouling inhibitors gave a smooth finished protection on the surface and un-reactive dirt or salt deposition (Caguiat (2003)).

The environmental law have limited the use of some chemical products and regulated the disposition of the cleaning fluid. For example, soil pollution that contains mineral oils adhered to the airfoils can not be thrown into the drainage. The same case applies to aromatic-hydrocarbons mixed with the compressor washing cleaner that are considered harmful to peoples health by skin contact or inhalation (Kolkman (1993)). However, the improvements on the solvent cleaners have been developed for the use against the organic pollution (hydrocarbon particles) (Leusden, Sorgenfrey, and Dummel (2003)). Today three types of fluids are commercially available: demineralised water, solvents-based and aqueous-based cleaning fluids, but in some places due to environment regulations the use of solvents is limited (Fielder (2003)).

Information about the chemical formula of the cleaning fluid is not available due to the policy of the companies (Vigueras Zuniga (2003b)). However, the supplier guarantee that the cleaning fluid is a water-based formulation, non-toxic, non-flammable, non-corrosive, readily biodegradable, no harmful effects for the engine and broad spectrum cleaning of fouled compressor blades (Lambart, Gordon, and Burnett (2003)). The result of different commercial cleaning fluids can be found in Harris and Calabrese (1994) publication.

The detergent concentration plays an important part in cleaning the compressor (Thames, Stegmaier, and Ford (1989)). This because the wet time that the fluid is on the blades depends on the surface tension and viscosity of the cleaning fluid (Mezheritsky and Sudarev (1990)). It is important that the cleaning fluid properties remain liquid (no steam) in the early stages of the compressor. Because, the fouling deposition is highly dominant in the first four stages and it is almost zero in the rear stages (Tarabrin, Schurovsky, Bodrov, Stalder, and Bodrov (1998), Fielder (2003) & Syverud, Brekke, and Bakken (2005)). However, the gas turbine operators and cleaning fluid suppliers have reported that a hard layer was adhered to the airfoils

from the rear stages due to high temperatures that bakes the deposits (Mund and Pilidis (2004)). For that reason, it is important that the cleaning fluid remain in a liquid state until the last stages. The chemical composition for the cleaning fluid have resulted to have solid states of the droplets until 400ºC (sixth stage for typical industrial axial compressors) (Lambart, Gordon, and Burnett (2003), Asplund (1998) & Stalder and Sire (2001)). The chemical treatment to improve the evaporation point can be consulted by Jeffs (1992). The conventional washing fluid can operate in temperatures around of -10ºC but with the use of anti-cooling mixed with the fluid the temperature could be lower than -15ºC (Leusden, Sorgenfrey, and Dummel (2003)).

2.4.3 Cleaning fluid injection

The cleaning fluid injection is an essential characteristic of compressor washing on line. The objective of compressor washing is to wet the more possible region from the blade surfaces (Meher-Homji and Bromley (2004)). Also, a wet region reduces the possibility of evaporation of the cleaning fluid and increase the effectiveness of the washing (Scheper, Mayoral, and Hipp E.J. (1978)). However, the water droplets tend to follow the air stream and not all the blade surface is wet (Tsuchiya (1982)). For that reason, the number of nozzles and angles of injection are very important in the installation of compressor washing on line (Meher-Homji and Bromley (2004) & Mustafa, (2006)).

The speed and size of the droplet from the injection of compressor washing on line play an important role to clean the blades surfaces. The numerical study by Mustafa (2006) demonstrated that that the velocity between the washing liquid and the air is the parameter that regulates the droplets impact on the blade surface. In this study was demonstrated that the air stream velocity has a low impact in changing the droplet size. The selection of the injection angle is a difficult task and involves the centrifugal and coriolisis effects in the droplet trajectories (see Figure 2-11) (Tsuchiya (1982)). Mustafa (2006) demonstrated that the angle of injection between 0 to 90 degrees relative to the air stream direction can reduce the size of the droplet.

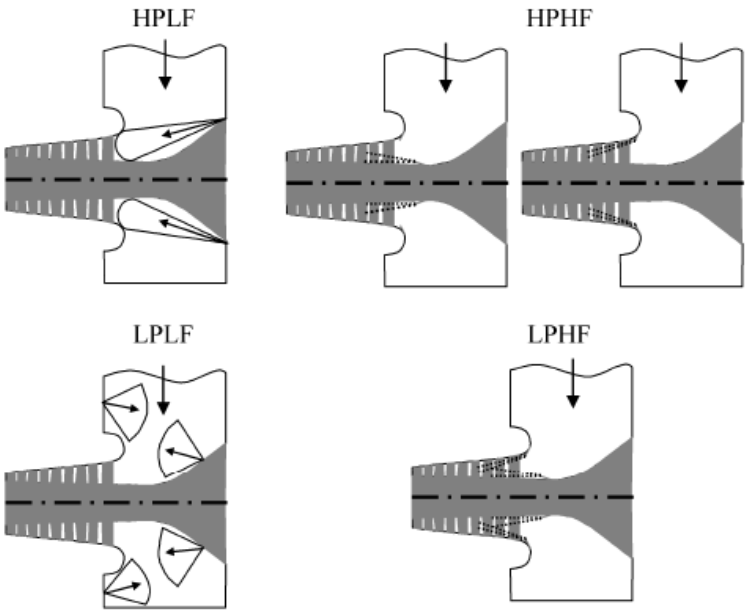

Figure 2-11 Typical nozzle locations and for online washing systems (Mund (2006)).

2.4.4 Cleaning fluid droplets

The effectiveness of washing as was mentioned before depends from the droplet size, velocity and temperature on the air stream (Murthy, Ehresman, and Haykin (1986)). These characteristics modify the momentum (mass and velocity) resulting in some droplet trajectory (Tsuchiya (1982) & Caguiat (2003)). Hence, the droplet is produced by the nozzle and can follow the trajectory of the flow stream, rebound on the blade surface or stay on the surface and build a wet film.

The size of the droplet depends on the pressure injection of the nozzle and it is divided into three categories:

i. Low pressure systems: 1MPa (10 bar) and droplet size of 100 to 150 µm (Syverud and Bakken (2005)).

ii. High pressure systems: 5MPa (50bar) and droplet size of 150µm (Syverud and Bakken (2005)).

iii. Nozzle assisted by air: It produces small droplets size at high pressure systems (Mund (2006)).

The problem of erosion on the airfoils surfaces by water injection has been linked to impacts from big droplets (Zwebek (2002) & Mustafa (2006)). The different sized droplets produced from the compressor washing system have been studied in order to avoid erosion problems*. The results have demonstrated that droplets with a small size (less 80µm) do not cause erosion (General Electric (2001) & Mustafa (2006)). Meher-Homji and Bromley (2004) demonstrated that droplets used for the fogging systems with size between 30 to 40 µm produced non-erosion in the blades. However, the small droplet size follows the air stream and they do not touch the blade surface (Mustafa (2006)). Large droplet sizes are more suitable to be in contact with the blade surfaces and in a short periods they do not represent a problem of erosion (Mustafa (2006), Lambart, Gordon, and Burnett (2003) & General Electric (2001)).

The phenomenon of rebounding and non-rebounding from the droplet in the compressor has been studied in different applications. For example, Farrel and Vittal (1996) demonstrated that small droplets between 18 to 24 µm are non-rebounding in the inlet of helicopters. However, in the case of industrial application the small droplet size (less than of 40µm) evaporates due to the ambient temperature (Mustafa (2006)).

Hayward (1999) suggested an optimal range of droplet size between 80 to 120µm to clean the first stages and 130 to 170µm to clean the rear stages. The numerical study from Mustafa (2006) suggested droplets from 50 to 300 µm in a multistage axial compressor (16 stages). The results are summarized as follows:

- Only large size droplets arrived to the rear stages in the liquid stage

- For engine applications without the presence of salt formation the range of droplet size suggested is 80 to 160µm (compressor washing on line).

* The erosion mechanism can be consulted the following literature (Tabakoff, Lakshminarasimha, and Pasin (1990), Tabakoff and Balan (1983) & Kurz and Brun (2001)).

- For engines with presence of salt formation (offshore or ships) the range of droplet size suggested is 80 to 800 µm (compressor washing on line)

2.4.5 Engine performance

The engine can recover the losses due to fouling when the compressor washing on line combines the correct frequency of washing and cleaning fluid (Meher-Homji and Bromley (2004)). In addition, the engine operation conditions have to be considered to guarantee an effectiven compressor washing. For example, the ambient temperature modifies the stage temperature and it affects: the mass flow, the momentum balance and the evaporation point from the droplet (Mund and Pilidis (2004)). Mustafa (2006) presented a schematic graphic (see Figure 2-12) to explain the evaporation point of the droplets according to the compressor stages.

Haub and Hauhe (1990) and Flashberg (1992) agree that compressor washing on line reduces the total power losses by 3%. Compressor washing on line have demonstrated to reduce significantly the costs of maintenance (Peltier and Swanekamp (1995), Leusden, Sorgenfrey, and Dummel (2003) & Stalder and Sire (2001)). Boyce and Gonzalez (2005) suggested that the theoretical representation of compressor washing on line recovers the original compressor polytrophic efficiency. According to Orsach, Kazcprzynski, Roemer, Scharschan, Caguiat, and McGroarty (2002) compressor washing on line delayed the overall degradation in a rate of 0.2%, but without washing the degradation increases by 1%. Gulen, Griffin, and Paolucci (2002) reported a case where compressor washing on line reduced 50% the engine losses produced by fouling in a period of two months. A successful result of compressor washing on line involves a study of the system configuration, the level of degradation and the inlet configuration (Mund (2006)).

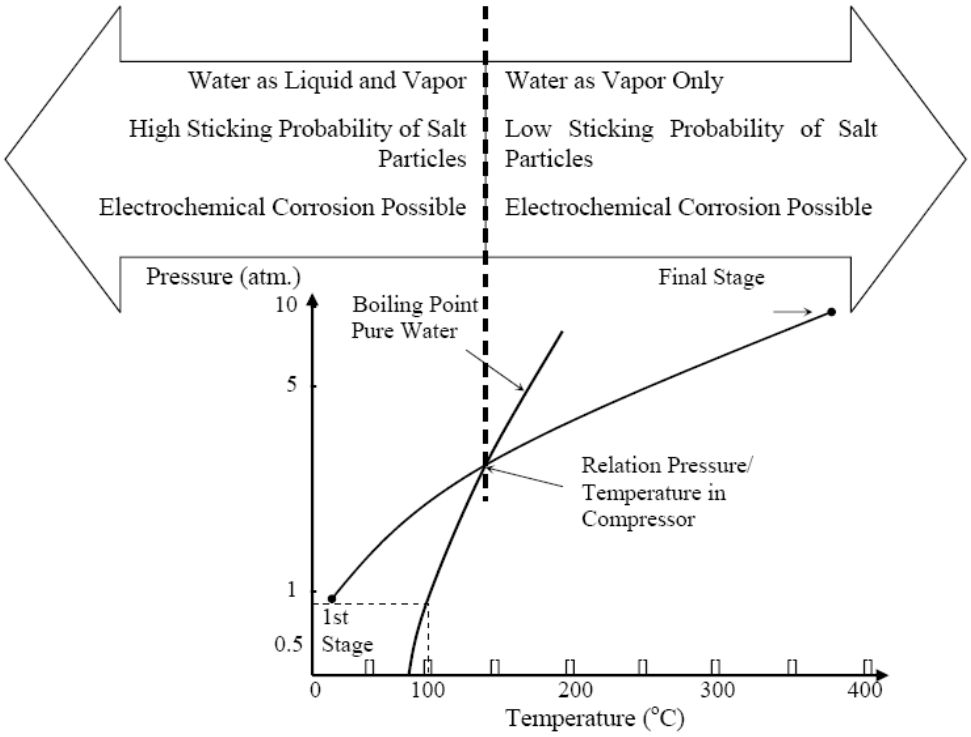

Figure 2-12 Result of the washing-fluid state due to temperature and pressure condition (Mustafa (2006)).

2.4.6 Technical problems

Water injection presents some technical problems. For example, the droplet evaporation absorbs part of the work from the compressor, also the water film on the casing reduces the tip clearance and the wet blades require more power to move (Tsuchiya (1982) & Mund (2006)). However, the time of compressor washing injection is short (between 5 to 10 minutes) and in this case it does not represent a compressor performance problem (Lambart, Gordon, and Burnett (2003)).

If the compressor washing on line operates incorrect, some problems can result. For example, Sorli, Langes, Laagland, and Hastings (2002) observed erosion in the first stage due to compressor washing on line. According to McDermott (1991) the water evaporated in the rear stages of the compressor produces a mixture of air and cleaning vapour that can produce corrosion in the rear stages.

There are reports that the results of compressor washing on line were not successful. Abdelrazik and Cheney (1991) mentioned that compressor washing on line used in a marine engine did not present any improvement in correcting the engine performance. According to Gulen, Griffin, and Paolucci (2002) compressor washing on line produced re-deposition of contaminants from the front to the rear in a multistage industrial compressor. Yee and Myers (2003) detected that water used for compressor washing on line in some marine applications contains salts particles that in contact with the bushings produced corrosion. Thames, Stegmaier, and Ford (1989) concluded that compressor washing on line is not always the solution to recover the power from the compressor losses.

2.4.7 Compressor washing frequencies

The compressor washing frequencies has resulted from trials, engine inspections and operators experience (Fielder (2003)). Information from the literature suggests some parameters to select the correct compressor washing frequency.

- Mezheritsky and Sudarev (1990) and Diakunchak (1991) suggested the use of the airflow as a parameter of compressor washing on line (reduction of the air flow by 2 to 3%).
- Scott (1979) and Syverud, Bakken, Langnes, and Bjornas (2003) suggested to wash the compressor when the pressure at the inlet of the compressor drops to 3%.
- Caguiat (2003) suggested the compressor washing on line for marine engine each 48 to 96 hrs of operation and compressor washing off line each 500 hrs of operation.
- Boyce and Gonzalez (2005) and Lambart, Gordon, and Burnett (2003) suggested compressor washing on line for power plants with a frequency of two times per week.

According to Leusden, Sorgenfrey, and Dummel (2003) the correct frequency of compressor washing on line can extend the washing off line interval for more than 12 months. Long intervals between compressor washing on line can increase the

possibility to remove larger insoluble pieces to the rear stages (Stalder and Van Oosten (1994) and Stalder and Sire (2001)). However, the best parameter to select the frequency of compressor washing on line should be based on the fouling level, the rate deposition and the type of particle adhered, however this information is very difficult to obtain during the engine operation (Fielder (2003)).

The costs for the cleaning fluid and demineralised water can represent an economical problem (Mund (2006)). For example, in marine applications the production of clean water is an extra cost, however in an optimal frequency this system can reduce the cost of operation by 50% (Fielder (2003)). The study of Syverud, Bakken, Langnes, and Bjornas (2003) demonstrated that compressor washing on line was economic rentable and benefit for the operation for an offshore application..

According to Mund (2006) the operation benefits for compressor washing on line are:

- Reduction of engine performance degradation (almost eliminated in some instances)
- Increments in power production (more kilowatts available to sell)
- Optimal compressor efficiency (operation point stay near of design point)
- Reduction of fuel consumption
- Reduction of the number of shutdowns
- Reduction of time and costs of the maintenance

2.5 Experimental Cascade Rig Tests

The principle of turbomachinery operation is based on diverts the flow from the blades. In the case of compressors, the flow (air) is compressed and it involves the change of the physical properties of the air. The use of experimental cascade has been used for aerodynamic studies in axial compressors. The compressor cascade is defined as “an infinite row of equidistant similar bodies, these bodies, or blades, are usually airfoil-shaped” (Gostelow (1984)). A typical configuration of a cascade includes the arrangement of blades settled inside of an air stream. Depending on the application, the air stream is produced by external equipment, typically a fan or compressor. The

air stream can be produced by positive pressures (blow) or negative pressures (suction) (Barlow, Rae, and Pope (1999), Gostelow (1984) & Hobson, Hansen, Schnorenberg, and Grove (2001)).

The experimental cascades are connected to a wind tunnel based on the consideration that the flow around the body is a relative motion to the body. Hence, the same result should be obtained if the body is moving or not in a relative uniform velocity flow (Pankhurts (1952)). It is important to reproduce the similar conditions of viscosity and density in the experimental cascade according to information from the real situation (Gostelow (1984) & Pankhurts (1952)).

The wind tunnels are classified into two categories based on the flow velocity (Dixon (1998)).

i. Low speed wind tunnel is defined by the air stream speeds in the range of 9 to 60 m/s at ISA. In this application, the viscosity forces from the flow are small and in the practice they are not considered (Hobson, Hansen, Schnorenberg, and Grove (2001)).

ii. High speed wind tunnel is defined by the air stream speed in the range of more than 60 m/s at ISA conditions. In this case, the viscosity forces affect the behaviour of the flow and they have to be considered in the interaction between surface body and flow (Hobson, Hansen, Schnorenberg, and Grove (2001)).

The number of blades used in the cascade row is a topic of discussion. Different criterions have been adopted from previous experiments. The ideal case includes an infinite number of blades, that in practical situation it is impossible. According to Dixon (1998) seven blades is the minimum number of blades in the row. However, the periodicity of the flow from one passage to another passage is the most important characteristic (Gostelow (1984)). This last characteristic was confirmed by Hobson, Hansen, Schnorenberg, and Grove (2001) and suggested using the middle passage from the cascade row blades due to the uniformity and periodicity presented from the flow. The best approach with real situations is the use of original dimensions for

building the cascade. However, the power required for the external equipment to create the flow condition will be bigger than the original power generated from the engine ((Dixon (1998) and Pankhurts (1952)). For that reason, small scales from the blades are used in cascade blade test rigs.

The effect of the floor and ceiling can affect the blade region close to these surfaces. This problem has been identified due to the boundary layer separation and the three dimensional effects produced on these surfaces. According with the literature, some authors have suggested different empirical philosophies to solve this problem. For example, Gostelow (1984) suggested setting the row blades at one chord distance from the inlet of the cascade to guarantee that the variation from the pitchwise angle will be small. Dixon (1998) suggested using blades with a height of aspect ratio* of three to avoid the effect of the boundary layer separation from the top and bottom walls.

According to Pankhurts (1952) the benefits of working with wind tunnels give an opportunity to validate theoretical models. The use of test rigs is safe and relatively cheap. The results obtained from the experimental cascade represents invaluable information that due to the complexity are not possible to obtain by theoretical ways (Gostelow (1984)).

2.5.1 Flow Visualisation

There are many methods to study the flow behaviour in the wind tunnel. One of them is the technique of visualization in order to describe the flow trajectory. The particle path technique is commonly used for this application and it consists to describe the air streamline by the instantaneous position of the particle. This method includes small particles (liquid drops or solid materials) with fluorescent properties that are delivered into the air stream. The flow is illuminated and the particles are visible showing the path of the air stream (Pankhurts (1952)).

* Value obtained from the blade height and chord distance division.

The smoke technique is also often used in low speed of the flow (see Figure 2-13). The technique consists of injecting small solid particles in suspension (smog) into the air stream. The smog is produced by organic-compounds combustion or vaporization of liquids such as stannic tetrachloride that reacts with water and it produces a dense white fume. However, the disadvantage of this technique is the possible chemical reaction with the airfoil surfaces (Pankhurts (1952)).

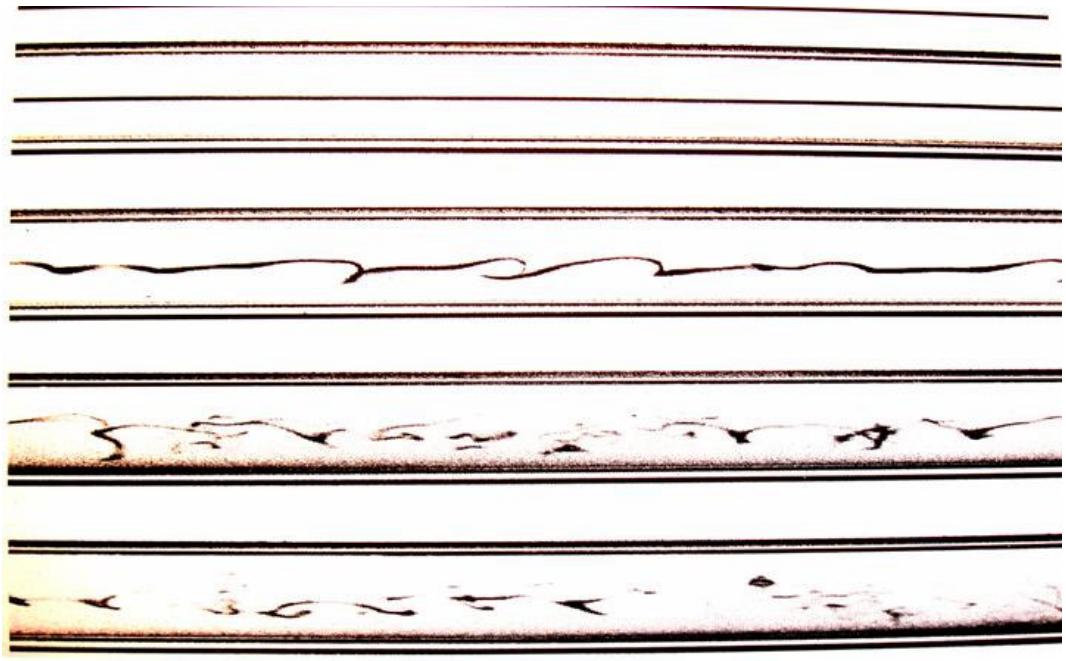

Figure 2-13 Representation of the flow visualization by smoke technique (Rubini (2006)).

The experiment of Hobson, Hansen, Schnorenberg, and Grove (2001) studied the flow trajectories in a cascade blade with the particle path technique of oil mist injection. The results were recorded by a laser-droplet-velocimeter (LDV) in order to calculate the flow velocity at different locations. The LDV processes information from volumes in the range of 0.1 x 0.1 x 0.3 mm, however it was not possible to detect with this instrument the boundary layer separation (Britchford, Manners, McGuirk, and Stevens (1994)).

2.5.2 Turbulence

Turbulence is a physical phenomenon presented in many engineering flow applications. The complexity of turbulence involves the solution of the Reynolds Averaged Navier Stokes (RANS) equations. Turbulence affects the aerodynamic performance of the airfoils due to movement of the transition point Mayle (1991). The difficulty to obtain information from the compressor cascade depends on the turbulence level to know the uniformity of the flow (Hobson, Hansen, Schnorenberg, and Grove, 2001). The hot wire is an instrument used to calculate the turbulence from the flow stream in wind tunnels. This device consists of a thin wire resistance made from platinum connected to voltmeter terminals and located in the air stream. The estimation of turbulence is made by the change of the electrical current in the resistance due to the air flow stream.

2.5.3 Boundary layer visualization

The difficulty of visualizing and calculating the boundary layer is due to the micro scale involved in this phenomenon. In real aerodynamic application it is almost impossible to measure the velocity profile of the boundary layer (Pankhurts (1952)). However, the liquid film technique detects on the surface the separation of the boundary layer or some recirculation. This method consists of the application of a layer of oil on the surface. The oil evaporation is higher in the turbulence region than in the laminar region, and then the oil total evaporates after the transition point (Pankhurts (1952)). The disadvantage of this method is that the oil layer changes the properties of the surface. However, in many applications the changes are minimum and these changes can be omitted (Barlow, Rae, and Pope (1999)).

2.5.4 Pressures

The total pressure (stagnation) and static pressure are properties of the flow that can be measured in wind tunnels to determinate the condition of flow in specific locations (Pankhurts (1952)). The typical instrument to measure the dynamic pressure is the

Pitot tube. In the case of incompressible flow the total pressure is the same that dynamic pressure and is defined as follows.

$$P_0 = P + \frac{\rho V^2}{2}$$

Equation 2-3

Where P = static pressure

ρ = air density

V^2 = air velocity

If the flow becomes compressible, the effects of viscosity and density affect the measurements and the difference between the dynamic pressure and total pressure is presented. Saravanamuttoo, Cohen, and Rogers (1996) demonstrated a total difference of 11% between the total pressure and the Pitot tube pressure at Mach number of 1. However, it is possible to consider that at lower velocities such as Ma < 0.3 the pressure measure from the Pitot tube can be considered the same as the total pressure (Gostelow (1984)).

The Pitot tube is an instrument with an open-mouthed tube that it is parallel to the flow and facing upstream (same direction of the axis stream line). The open-mouth has to be a circular section (typical 1.6mm) to avoid hydraulics factors (Gostelow (1984)). The shape of the head should be flat to find easy the stream lines (Pankhurts (1952) & Barlow, Rae, and Pope (1999)).

The static pressure for the airfoils surfaces in low speed wind tunnels is measured with a series of holes located on the surface in an uninterrupted motion zone and connected to a barometer or to a pressure transducer that display the pressure. It is important to check that the holes do not affect the area in study. The static tube is another option to measure the static pressure. The tube is built with a solid nose and a collar of holes in the pipe-body (see Figure 2-14).

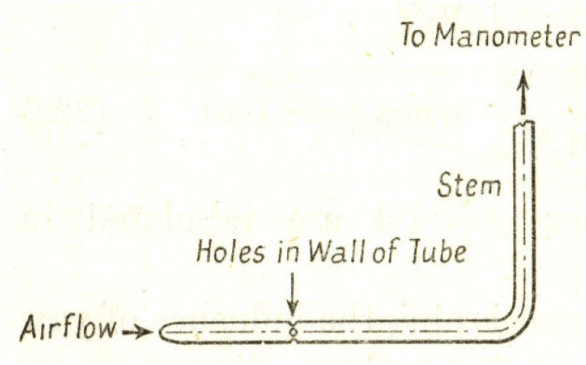

Figure 2-14 Schematic of static tube ((Pankhurts, 1952)).

2.5.5 Previous studies based on cascade blades

Gostelow (1984) mentioned that the axial velocity distribution in experimental cascades could affect the flow uniformity and in the worst situation could present secondary flows. For low flow speeds, it is possible to observe vortices at the leading corners of the blade. According to Ramson (2004) the pressure distribution on the blade surface twists the boundary layer, and vortices can be observed downstream. When the flow speed is high, the bottom and top walls of the cascade section can produce vortexes (see Figure 2-15) (Saravanamuttoo, Cohen, and Rogers (1996), Gbadebo, Hynes, and Cumpsty (2004) & Britchford, Manners, McGuirk, and Stevens (1994)).

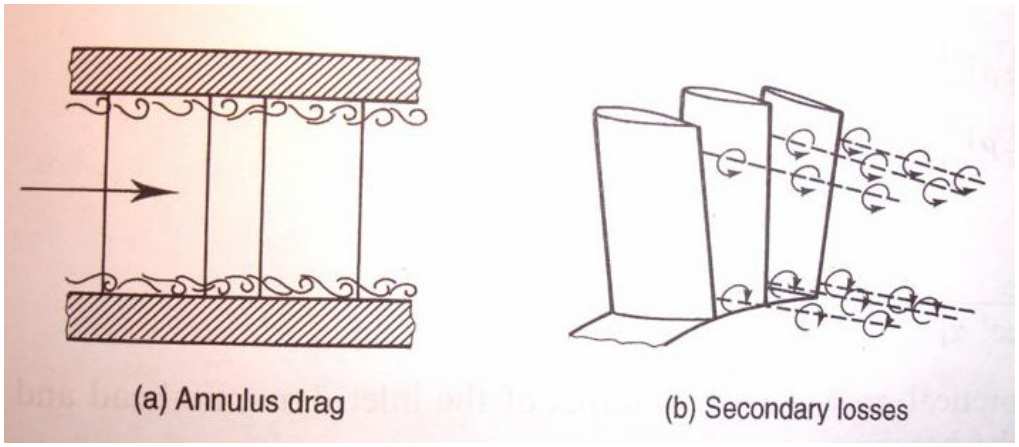

Figure 2-15 Three-dimensional flow effects (Saravanamuttoo, Cohen, and Rogers (1996)).

The study of Hobson, Hansen, Schnorenberg, and Grove (2001) was based on an experimental cascade rig. Three different conditions of the flow were studied based on the Reynolds number (2.1, 3.8 and 6.4×10^5). The study involved only two-

dimensional effects at the middle section of the blade. The study of the boundary layer separation and re-attachment (bubbles) around the blade was the objective of study. The static pressures were estimated from the walls of the cascade and with a blade-instrument prototype (see Figure 2-16). The visualization of the flow on the surface was with a mixture of oxide of titanium and kerosene. The results of this experiment are summarized as follows.

- $Re=6.4x10^5$. According to the pressures recorded on the suction surface, the flow was not separated in this region. However, the flow presented three-dimensional effects (no-uniformity) from the trailing edge region; it produced vortices near to the cascade end-walls.
- $Re=3.8x10^5$. According to the pressures recorded on the suction surface a flow separation at 50-60% chord. The flow was two-dimensional along most of the midspan section with a periodicity between the passages. In the spanwise (46-77% chord) an intermittent separation was identified (transition point of the boundary layer).
- $Re=2.1x10^5$. According to the pressures recorded on the suction surface was observed a separation and reattachment of the flow to the surface at 45-70% chord. The flow was two-dimensional along most of the midspan section.

The inlet flow angle increased when the Reynolds number was reduced. The same result was observed from the inlet angle standard deviation, inlet turbulence deviation and inlet turbulence standard deviation. The blade wake was longer as the Reynolds number increased. The same case was with the exit angle that increased as the Reynolds number increased. The exit turbulence and reverse flow due to three-dimensional effects were presented only in the case of $Re=6.4x10^5$. In the case of $Re=3.8x10^5$ only in the leading edge region presented turbulence. Finally, in the case of $Re=2.1x10^5$ turbulence was only detected close to the boundary layer separation.

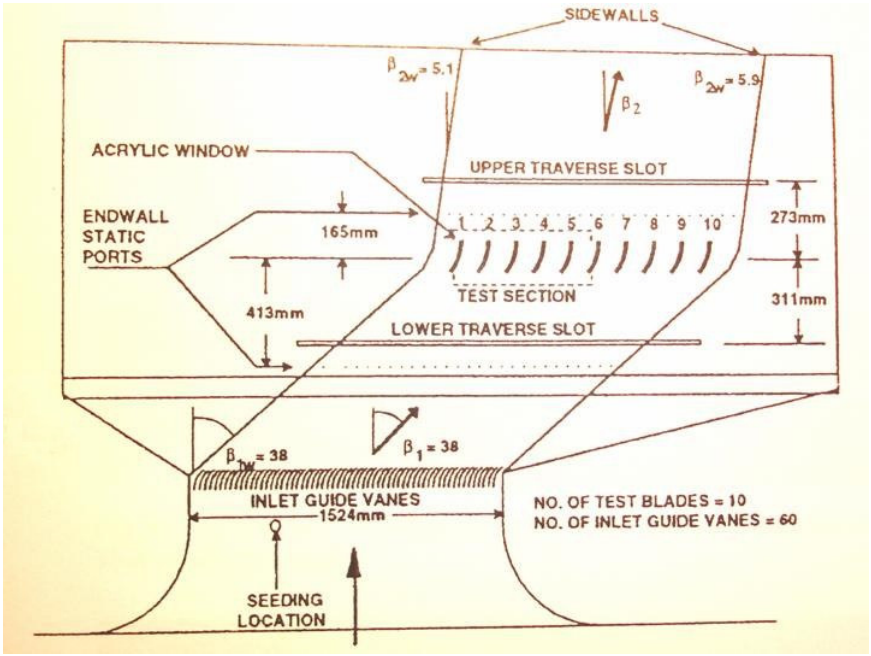

Figure 2-16 Low Reynolds cascade blade rig (Hobson, Hansen, Schnorenberg, and Grove (2001)).

2.5.6 Previous experimental studies of compressor fouling and washing

Very few experiments have been reported in the open literature about fouling. The study of Wilkinson and Shark (2004) presented a technique to analyze digital colour information to evaluate the state from the IGVs and first stage of the engine in operation (Alstom GT13E*). This study included the use of monochromatic images for ice detection and colour images for fouling detection. The results concluded that the leading edges were more affected than the rest of the surfaces. The separation between two peaks of dust or ice accumulating increased the deposits build in that region. However, fouling tended to darken the images recorded and was not possible to process the images automatically. In addition, the salt deposition was confused with ice formation in some cases. In the case of compressor washing, Kolkman (1993) studied the effectiveness of eight washing detergents with an experimental rig. The blades were artificial fouled by carbon deposits (see Figure 2-17) and later removed by the injection of the cleaning fluids. The results consisted in measuring the difference of weight from the blade clean, the blade dirty and the blade washed.

* Industrial Gas Turbine manufactured by ALSTOM, more information www.alstom.com.

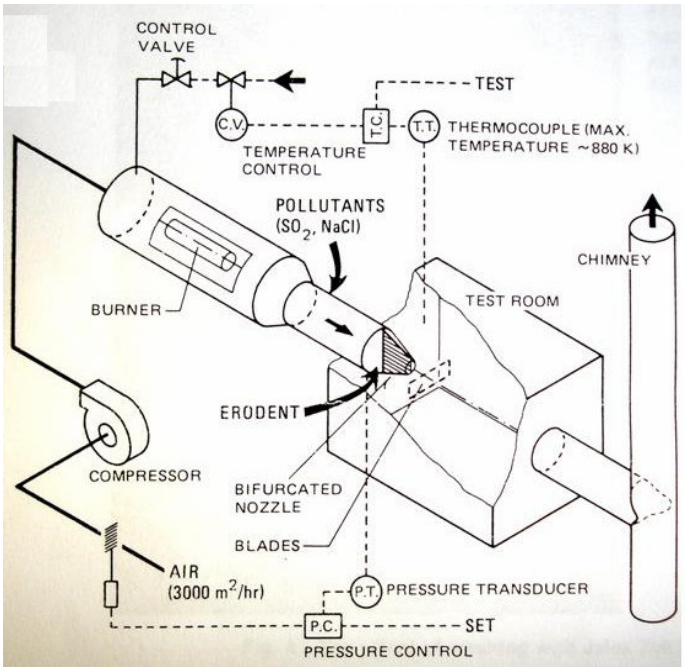

Figure 2-17 Configuration of the NLR compressor rig test. Results from particles removed by the washing process in the rig test (Kolkman (1993)).

Syverud, Brekke, and Bakken (2005) and Syverud and Bakken (2005) presented an experimental study of compressor washing on line for marine applications. The engine was artificially deteriorated by water injection mixed with high concentrations of salt. The deposition of salt was detected by visual inspection and the thickness of the layer was measured. Due to the difficulties in measuring the roughness from the engine, an indirect method of image analysis was used. This consisted in comparing the surface with a standard profile (in this case a standard sand paper grain). The results demonstrated that the IGV surface the salt accumulation formed a layer in the hub of 500µm and in the annulus of 25µm. The first stator rotor blade the layer resulted on the pressure surface by 25 µm and on the suction surface by 10µm.

A similar experiment was reported by Levine and Angello (2005), however the sand roughness Ks was used to estimate the hydraulic smoothness condition. The results demonstrated that when Re is less than 90, it is possible to consider that there are no effects of the roughness parameter that affects the flow.

$$\text{In this case: } \mathrm{Re} = \frac{VxKsx\rho}{\mu} \leq 90$$

Equation 2-4

The study of a degradation mechanism as fouling implies complex and expensive rig tests (Mustafa (2006)). In addition, the possibility to study this phenomenon in the real application is very limited due to space and conditions of operation (Fielder, 2003). For that reason, many studies have been based on theoretical results as numerical analysis and engine performance simulations. Saravanamuttoo and Lakshminarasimha (1985), Lakshminarasimha and Saravanamutto (1986), Haub and Hauhe (1990), Flashberg (1992), Tabakoff, Lakshminarasimha, and Pasin (1990), Mustafa (2006), Mund (2006), etc, agree with the necessity to validate the results with experimental tests.

3 TEST RIG

3.1 Introduction

The information presented in the previous chapter showed that compressor fouling and washing on line are topics that have not been investigated. Much of the current information available on this topic was based on theoretical results. Therefore the use of assumptions and arbitrary factors were inevitable. This has produced uncertainties from the real effect that fouling represents in the engine operation. The complexity of isolating the problem inside the engine has limited the studies about engine degradation mechanisms. For that reason, it is necessary to demonstrate and validate the theoretical results of previous investigations with experimental studies.

The author and sponsors of this research have decided to make an effort to describe with a preliminary model the fouling phenomenon in the compressor blades. This work has used for first time an experimental cascade blade (test rig) to study the problem of fouling. The description of the test rig design includes the aerodynamic conditions of the flow, the selection and description of the instrumentation and the manufacturing process. The aerodynamic conditions of the flow are represented in a scaled section (cascade) of the first compressor stage. With the information recorded from the experiment, the phenomenon of compressor fouling will be studied.

3.2 Experimental cascade blade

The test rig design was based on previous experimental studies reported in the literature. Many of these studies concentrated on salt deposition on blades. In addition, they were limited to studying the phenomenon outside of the engine due to the space limitation and operation conditions of the engine. However, in this experimental investigation the problem of fouling and the process of compressor washing on line are studied directly from the blade aerodynamics.

3.2.1 Particular Objective

The particular objective of this chapter is to design and build the experimental rig. The study parameters were the inlet conditions of the first compressor stage as follows.

- Original size of the blade
- Aerodynamic conditions of the first compressor stage at the inlet of the blade
- Data acquisition of the fouling mechanism in real time
- Control of flow conditions in the test rig
- Analysis of costs for the test rig construction and operation

The design was based on turbomachinery theory, previous experiments and interviews of specialists in the area. The methodology used to achieve the previous characteristics of the design was divided into five steps.

1. Specify the flow aerodynamic condition in the test rig.
2. Design a test rig according to the flow condition required.
3. Selection and installation of auxiliary equipment and instrumentation.
4. Specify the process of manufacturing and building of the test rig.
5. Calibrate and validate the operation condition of the test rig with a CFD model.

3.2.2 Background and source of information

The test rig was designed according to the conditions of operation of an industrial gas turbine (1.2 MW and mass flow of 6.4kg/s)[*]. The compressor configuration of this engine was considered axial-annulus and the original blade size of the first stage was selected for the design. There is a particular interest from the sponsors of this project to evaluate the compressor fouling in Combined Cycle Gas Turbines (CCGT) used in Power Plants. The engine selected to cover this task was a single shaft turbine of

[*] Similar to this engine is the commercial gas turbine model Saturn-20 of 1.2 MW manufactured by Solar Turbines. This engine is used to drive electrical generators, compressors and pumps in the industry. See Appendix A for further information.

240MW and mass flow of 640 kg/s[*]. The performance characteristics of this particular industrial engine were taken from the data-base available[†]. This information includes the compressor and turbine maps. The atmospheric conditions were taken from an industrial engine monitored and recorded in 2001[‡].

3.3 Test Rig Design

The dimensions and characteristics of the air flow were calculated to design the cascade section (blades row). The study region was focused on the blade passages. In this region the effect of fouling was evaluated according to the blade aerodynamics. However, the design corresponded to a static rig and only some specific condition (inlet) of the blade was reproduced. The public information was very limited due to company polices. For that reason, the information available from the public information of a typical gas turbine (Saturn20) was taken and the rest of the parameters were calculated.

External dimension	Gas Turbine model Saturn 20
Compressor configuration	Axial annulus compressor
Compressor Pressure Ratio	6.2:1
Operation conditions	ISA conditions at maximum speed shaft
Stage of study	First stage

Table 3-1. **Information from the compressor section of the gas turbine model Saturn 20**

3.3.1 Axial compressor design (First stage)

The design of an axial compressor involves the physical laws of turbo-machinery, fluid mechanics and gas turbine performance. The methodology used in the design of

[*] Similar to this engine is the commercial gas turbine SIEMENS model V94.3A of 260MW. See Appendix A for further information.
[†] Engine Library for the Data-Base of the Gas Turbine Performance Engineering Group (Cranfield University).
[‡] Information provided by the company Recovery Power Ltd for the gas turbine model Frame 6B manufactured by General Electric. See Appendix A for further information.

this compressor in this study was based on the methodology described in Ramsden (2002) and from the public information published by Caterpillar (2005). The outside diameter was considered constant to facilitate the calculus and to specify the size of the annulus configuration. The International System Unit was used in this research and the air properties were calculated from ideal compressible air flow tables (Ramsden (2002)). The following values were used to specify the compressor characteristics.

Overall Pressure Ratio*	Rc	6.2
Target Efficiency Polytropic**	np	0.88
Mass Flow*	W	6.4
Inlet Pressure*	P1	101000
Inlet Temperature*	T1	288
Ratio of Specific Heat**	γ	1.4
Blockage factor**	kb1	0.99
Shaft Speed [rpm]*	N	22850
Diameter Tip 1st rotor**	Dt	0.281
Blade Height 1st rotor*	B1	0.07
Blockage factor Stage1**	Kb	0.99

Table 3-2 Characteristics of the compressor. *(Caterpillar (2005)) **(Ramsden (2002).

The initial variables for the design were considered as follows.

Number Stages*	Stages	8
Mean Blade Speed 1st rotor inlet**	Umr1	252.28
Mean Absolute Air Angle at Inlet to 1st Stage IGV*	alfa0	30
Mean Axial absolute Velocity [m/s]**	Vo1	140
Inlet Hub/Tip Ratio**	Dhr1/Dt	0.50
Stage Temperature Rise Distribution**	ΔT	Constant
Annulus Configuration*	AC	cte. Diam

Table 3-3. Initial Chosen Variables. Source *(Caterpillar (2005), **(Ramsden (2002).

The inlet conditions for the first stage were calculated according to the following procedure.

$$Va = \cos\alpha_0 \times V_0 = 121.24 \text{ m/s}$$

$$\frac{V_0}{\sqrt{T}} = 7.14145 \qquad \text{from tables } Q_0 = 0.02328$$

$$A = \frac{W\sqrt{T}}{kb \times P \times Q_0} = 0.046649 \text{m}^2$$

Equation 3-1

Summary Compressor Inlet Annulus Dimensions

Annulus area	m^2	0.046649
Tip diameter	m	0.281
Mean diameter	m	0.21087
Hub diameter	m	0.14074
Annulus blade height	m	0.071

Table 3-4 Inlet annulus dimensions for axial compressor design.

Compressor Overall Efficiency

$$\eta_c = \frac{Rc^{\frac{\gamma-1}{\gamma}} - 1}{Rc^{\frac{\gamma-1}{\gamma\eta_p}} - 1} = 0.8465$$

Equation 3-2

$$\Delta T = \frac{T_{in}}{\eta_c}(Rc^{\frac{\gamma-1}{\gamma}} - 1) = 232.78\text{K}$$

Equation 3-3

$$\Delta T_{stage} = \frac{\Delta T}{8} = 29.09\text{K}$$

Equation 3-4

Outlet Annulus Geometry

$$R_{stage} = \left[\eta_c \frac{\Delta T_{stage}}{T_1} + 1\right]^{\frac{\gamma}{\gamma-1}} = 1.3473$$

Equation 3-5

$$P_{out} = R_{stage} \times P_{in} = 136080 \text{ Pa}$$

Equation 3-6

$$T_{out} = T_{in} + \Delta T_{stage} = 317.1 \text{K}$$

Equation 3-7

If $Va_{out} = Va_{in}$, then:

$$\frac{Va_{out}}{\sqrt{T_{out}}} = 6.8088 \text{ from tables } Q_0 = 0.02245$$

$$A = \frac{W\sqrt{T}}{kb \times P \times Q_0} = 0.03926 \text{m}^2$$

Summary Compressor Outlet Annulus Dimensions

Annulus area	m^2	0.03926
Tip diameter	m	0.281
Mean diameter	m	0.225
Hub diameter	m	0.170
Annulus blade height	m	0.063

Table 3-5 Results of outlet annulus dimensions for an axial compressor design

Assuming axial lengths are equal for rotor and stator without axial space between blade rows the first stage configuration is as follows.

Annulus area at first stage exit	m^2	0.046
Diameter hub stator	m	0.170
Diameter Medium exit stator (Dm 2nd rotor)	m	0.225
Diameter Medium at inlet stator (Dm at exit 1st rotor)	m	0.218
Annulus blade height inlet	m	0.071
Annulus blade height outlet	m	0.063

Table 3-6 Results of the 1st stage annulus dimension for an axial compressor design

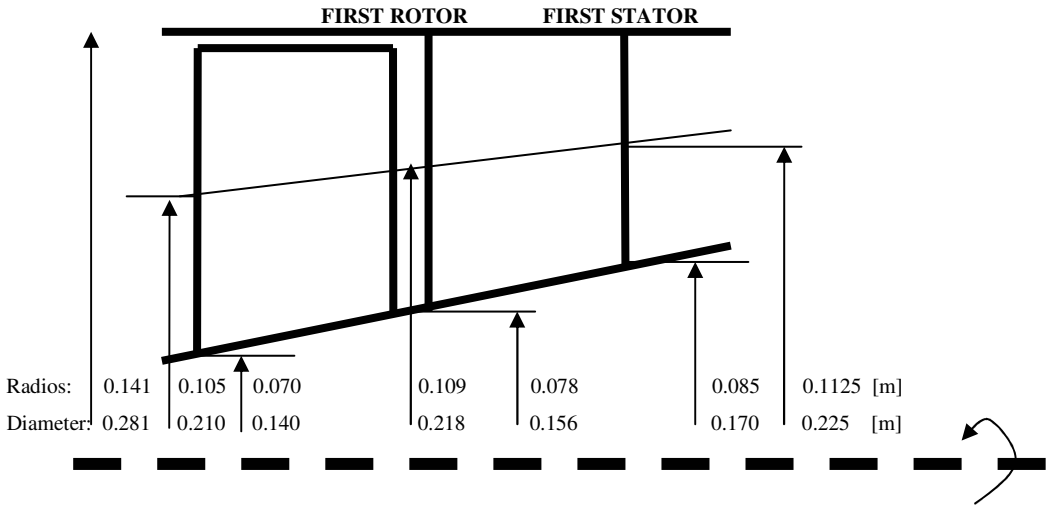

Figure 3-1 First stage result of annulus diagram in the compressor design.

Results of blade velocities through the first stage at mean radius.

At Rotor Inlet

V_0 =140m/s

α_0 =30

Va =121 m/s

U_1 =252 m/s

$\tan\alpha_1 = \frac{U_1}{Va}$, α_1 =64.33

$V_1 = \frac{Va}{\cos\alpha_1}$ =279 m/s

At Rotor Outlet

a) Rotor Exit Blade Speed

$$U_2 = \frac{\pi \times D_2 \times N}{60} = 261.37 \text{ m/s}$$

but since $Cp \times \Delta T_{satge} = U_2 \times V_{w3} - U_1 \times V_{w0}$

Equation 3-8

$$V_{w0} = \frac{V_0}{\cos\alpha_0} = 69.99 \text{ m/s}$$

$$Cp = \frac{\gamma \times R}{\gamma - 1} = 1004.5$$

$$V_{w3} = \frac{Cp\Delta T_{satge} + U_1 V_{w0}}{U_2} = 111.88 \text{ m/s}$$

b) Rotor Exit Axial Velocity. The absolute velocity from the rotor exit has to be equal to the inlet velocity ($Va_2\ V_{w3}$). In order to use the axial velocity as variable the $Va_2 = Va_1$. Approaching this condition with different values of Va_2, the result converged in the sixth iteration (see Table 3-7).

Tangential Velocity	U1	252.28
Axial Absolute Velocity [m/s]	Vo1	140
Absolute Air Angle at Inlet to 1st Stage IGV	alfa0	30
Axial Velocity [m/s]	Va1	121.24
Mach Number of Axial Velocity (Va1)	Ma1	0.36
Tangential projection of Va1 [m/s]	Vw0	69.99
Incidence Velocity [m/s]	V1	218.93
Mach Number of V1	M1	0.71
Alfa 1	alfa1	56.37

Table 3-7 Triangle of velocities for inlet medium 1st rotor

Tangential Velocity	U2	261.37
Tangential projection of V3	Vw3	111.82
Incidence velocity stator1 [m/s]	V3	159.77
Mach Number of Incidence Velocity	M3	0.46
Alfa 3	alfa3	46.27
Axial Velocity [m/s]	Va2	106.97
Alfa 2	alfa2	54.42
Mach Number Axial Velocity (Va2)	Ma2	0.305
Incidence Velocity [m/s]	V2	183.87
Mach Incidence Velocity	M2	0.53

Table 3-8 Triangle of velocities for outlet medium 1st rotor

Mean Radius Stage Loading Parameters

The following calculations are based on the rotor outlet blade speed

$$\Delta H = Cp\Delta T = U_2 \times V_{w3}$$

$$\frac{\Delta H}{U_2^2} = 0.4278$$

Stage coefficient $\frac{Va_2}{U_2} = 0.4092$

Then De Haller Number for the rotor results

$$D_{hr} = \frac{V_2}{V_1} = \frac{Va_2}{\cos\alpha_2} \times \frac{\cos\alpha_1}{Va_1} = 0.68$$

Equation 3-9

and De Haller Number for the stator results

$$D_{hs} = \frac{V_4}{V_3} = \frac{Va_1}{\cos\alpha_4} \times \frac{\cos\alpha_3}{Va_2} = 0.78$$

Equation 3-10

The De Haller Number is a common parameter used to predict the limits of the compressor according to the results of the geometry configuration. This method consists of estimating the excessive losses based on the compression specification results from the De Haller Number with a value lower than 0.72.

$$D_h = V_2 / V_1 \geq 0.72$$

Equation 3-11

In the rotor blade the De Haller Number was lower than 0.72. This indicated that some arbitrary parameters as the angle α_0, shaft speed or dimensions were wrong. However, these modifications did not take place as they would have resulted in a change of the original engine size. The result of the preliminary design from the first stage compressor was considered in the building of the test rig. A final compressor design should include the following procedure.

- Calculations of all the compressor stages following the same procedure of the first stage.

- Modification of the inlet angles until they obtain the correct De Haller numbers.
- Inclusion of the real blade profile and use of the diffusion factor parameter to calculate the compressor losses instead of the De Haller number is suggested by Saravanamuttoo, Cohen, and Rogers, 1996.

The final compressor design is outside of the limits of this study and further information can be obtained in the following references: (Ramsden, 2002), and (Saravanamuttoo, Cohen, and Rogers, 1996).

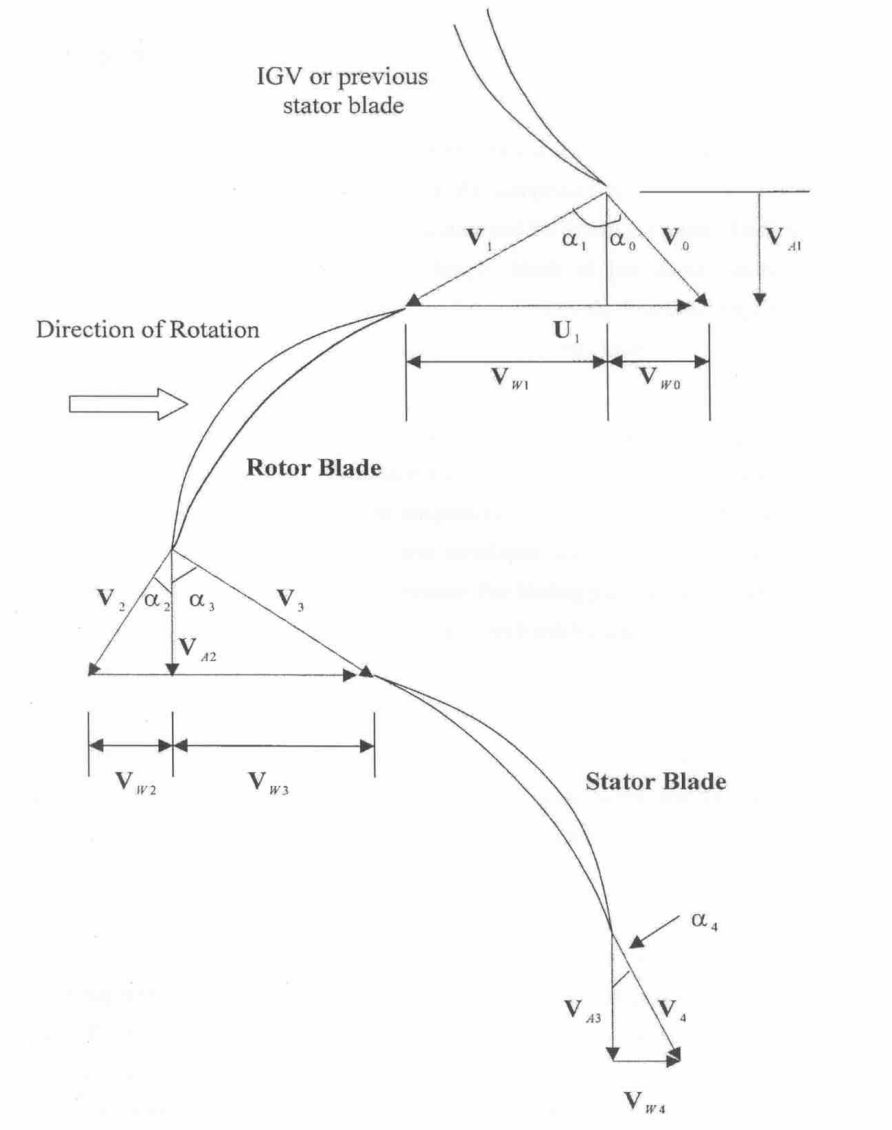

Figure 3-2 Triangle of velocities in a cascade representation (Ramsden (2002)).

3.3.2 Cascade Blade Design

The cascade configuration was designed based on the experiment of Hobson, Hansen, Schnorenberg, and Grove (2001). However, the conditions of operation and geometry were adapted to the requirements of this investigation and equipment available. The cascade blade consisted of a static blade row settled into an air stream according to the following physical effect: The blade and flow are in a relative movement and the same aerodynamic result is obtained if the air is moving and the blade is static. The compression effect is due to blade profile, cross section reduction and the rotation effect (see Figure 3-3). However, the rotation effect was not possible to reproduce in this static condition of the cascade. For that reason, only a particular region of the blade is selected from the real operation. According to previous reports the highest blade area affected by compressor fouling is the leading region. Therefore, the aerodynamic conditions selected to be reproduced in the cascade were the inlet blade conditions (velocity V_1 and angle α_1).

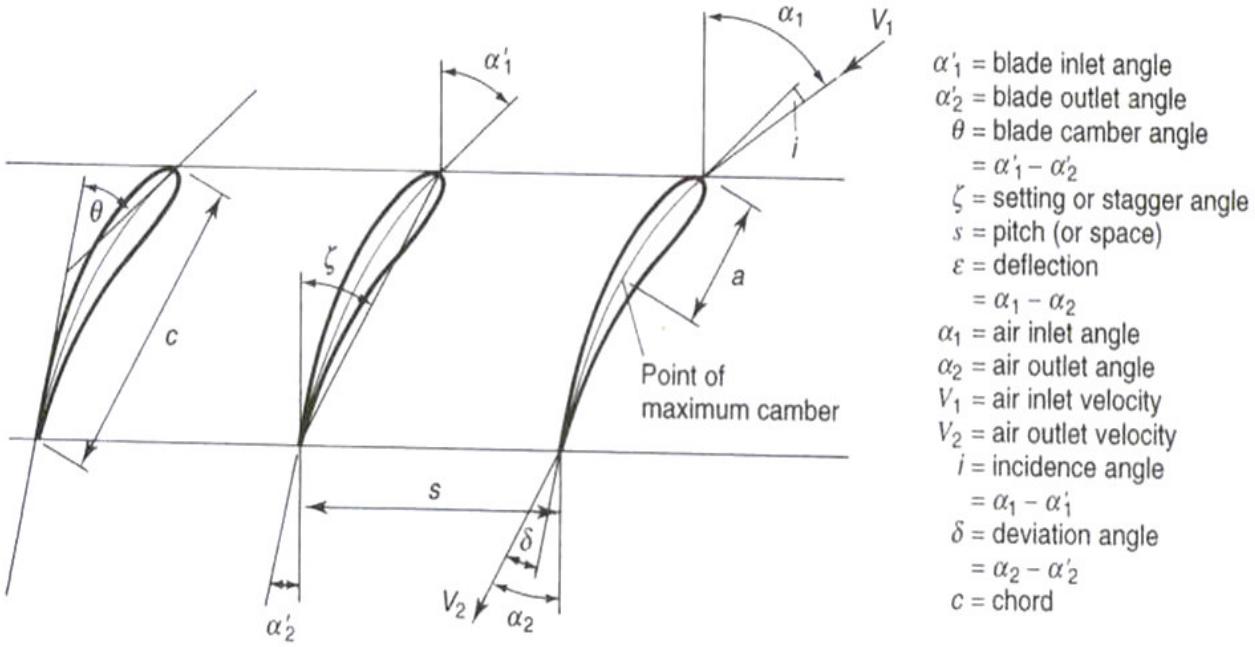

Figure 3-3 Cascade blade row representation (velocities and angles), (Saravanamuttoo, Cohen, and Rogers (1996)).

The inlet conditions can be represented in compressible flows with non-dimensional numbers. The non-dimensional numbers keep the relation with the air properties

(density, viscosity, pressure and temperature) and dynamic conditions of the flow (velocities). The non-dimensional number selected in this research to specify the flow conditions in the cascade was the Mach number.

The cascade blade was designed for two dimensional studies and the region selected was the middle section of the blade (see Figure 3-4). The geometrical size corresponded to the results of the previous first stage design. It was assumed that the air flow in the cascade passages was affected only by the blade profile and that the inlet velocity magnitude was equal to the outlet velocity.

Mach number of v1	m1	0.71
Incidence Velocity [m/s]	V1	218.93
Alfa 1	alfa1	56.37
Mach Incidence Velocity	M2	0.53
Incidence Velocity [m/s]	V2	183.87
Alfa 2	alfa2	54.42

Table 3-9 Summary of the inlet parameters of the axial design section 3.2.2.

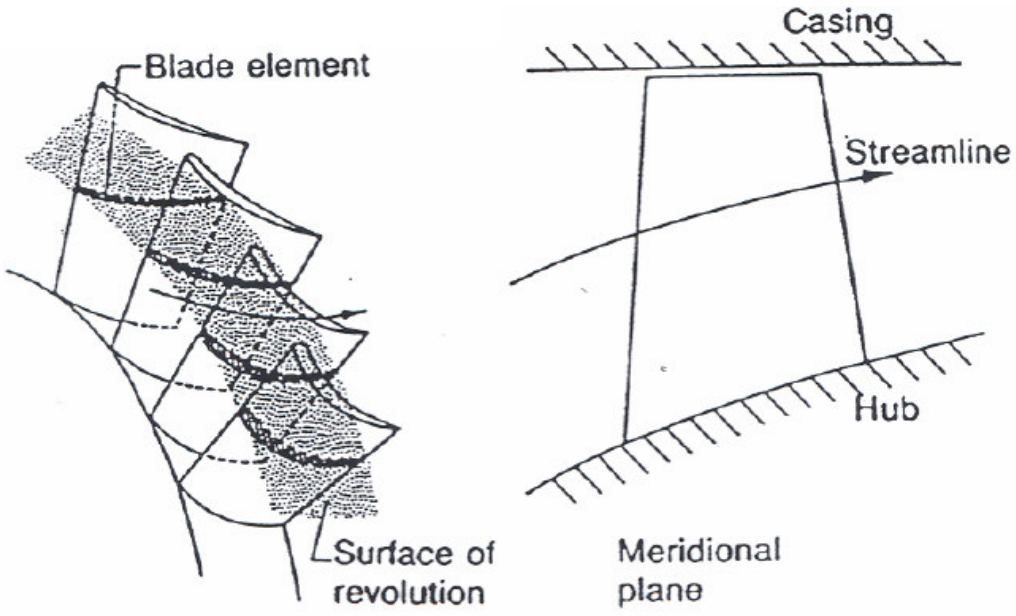

Figure 3-4 Middle section of cascade rotor (left). Annulus configuration and flow streamline at middle section of first rotor (right) (Howell and Calvert (1978)).

The blades available for this project were taken from a previous project in Cranfield University. The blade profile was generated by the use of Digital Image Technique*. The profile of this blade was close to the standard C4 (see Figure 3-5).

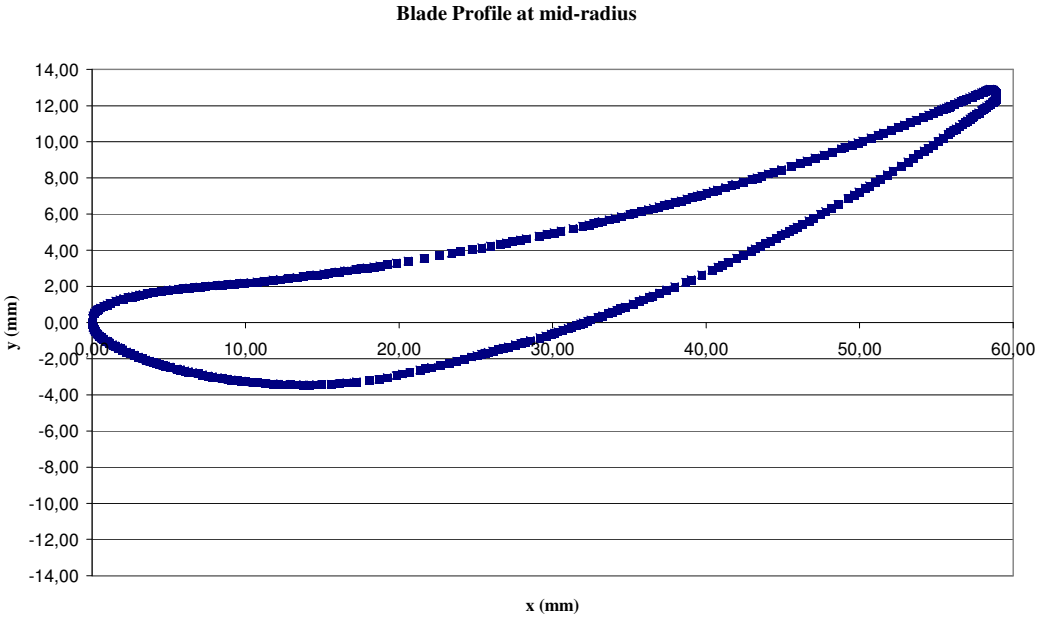

Figure 3-5 Results from the digital Image Technique (blade profile).

According to the compressor design, the blade height of the first rotor stage was at the inlet of 71 mm and outlet of 63 mm. To guarantee the two dimensional and planar region of the flow, the blade height was constant from inlet to outlet. This characteristic of the design was used to avoid the three dimensional flow effect produced by the reduction of the cross section. Also, the floor and ceiling of the cascade could produce three dimensional flow effects that affects the middle section. Hence, a safe margin was added in the blade height to isolate the middle region as much as possible. The final result of the blade height was 80 mm and included a safe margin of 5mm in each extreme (see Figure 2-15).

3.3.2.1 Cascade geometry

A rectangular configuration was designed for the cascade section. The cascade length was six times the chord blade distance. According to Gostelow (1984) this distance

* Digital Image Technique consists of analyzing digital images from real objects in order to scale the real dimensions, Picture Gear 4.5 (commercial software).

helps to obtain equal velocities at inlet and outlet $V_1 = V_2$ (Hobson, Hansen, Schnorenberg, and Grove (2001)). The blade row has to be settled one chord distance from the inlet of the cascade for a uniform flow in the blade passages. The distance between each passage was calculated with the dimensions of the middle-section and resulted in a distance of 40mm.

The inlet velocity of the cascade was the incidence blade velocity (V_1). The blades were settled according to the air inlet angle (α_1) and the incidence blade angle (j)* . The outlet angles were defined by the blade profile.

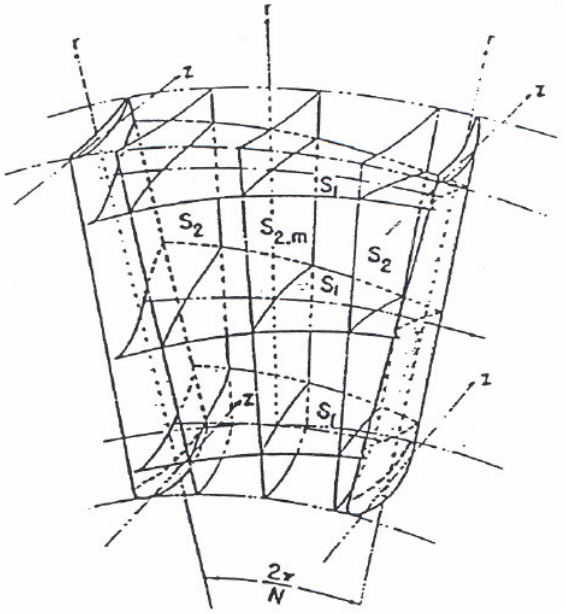

Figure 3-6 Middle section plane representation in a real blade row (Gostelow (1984)).

The Cartesian coordinates system was adopted in this research due to the absence of rotation. The axis configuration was as follows.

+X in the direction of V_1

+Y in the direction of the passages

+Z in the direction of the height

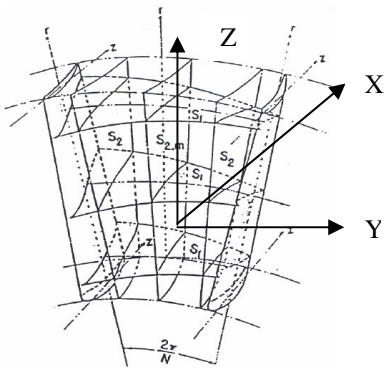

* The blade angle (j) and outlet angle were defined according to the blade profile.

3.3.3 Wind tunnel design (compressor)

This section describes the calculations used to reproduce the Mach number of 0.7 at the inlet of the cascade. To produce the air stream it was necessary to use the auxiliary equipment. The use of compressors or fans is usually installed to reproduce an air stream through the cascade. When the studies are focused on the of the outlet conditions, the fan is used to blow the air inside of the cascade. However, in this study the region selected was the inlet of the blade. Hence, the suction section of the fan was used to create a vacuum difference and move the airflow into the cascade section. The advantages and reasons to use this configuration are summarized as follows.

- The flow can be controlled easily because the initial velocity is 0 m/s (atmospheric conditions)

- The equipment of compressor washing on line operates in this condition.

The external equipment available was a centrifugal fan model HD77L manufactured by Carten Howden (see Figure 3-7).

Maximum mass flow	5 Kg/s @ 3410 rpm
Configuration	1 centrifugal stage
Pressure ratio	1:1.5
Cross inlet section	0.1134 m^2
Electrical Motor	Three-phase Alpak induction motor

Table 3-10 Characteristics of the centrifugal fan model HD77L manufactured by Carten Howden.

Size: D225M	Nº A2318-12051
Power : 45 kW	Phases: 3
RPM: 2955	Frequency: 50 Hz
Volts: 414	Current: 81 Amp
Connection: Δ	Ins class: B

Table 3-11 Characteristics of the three-phases electrical motor Alpak manufactured by GEC Machines.

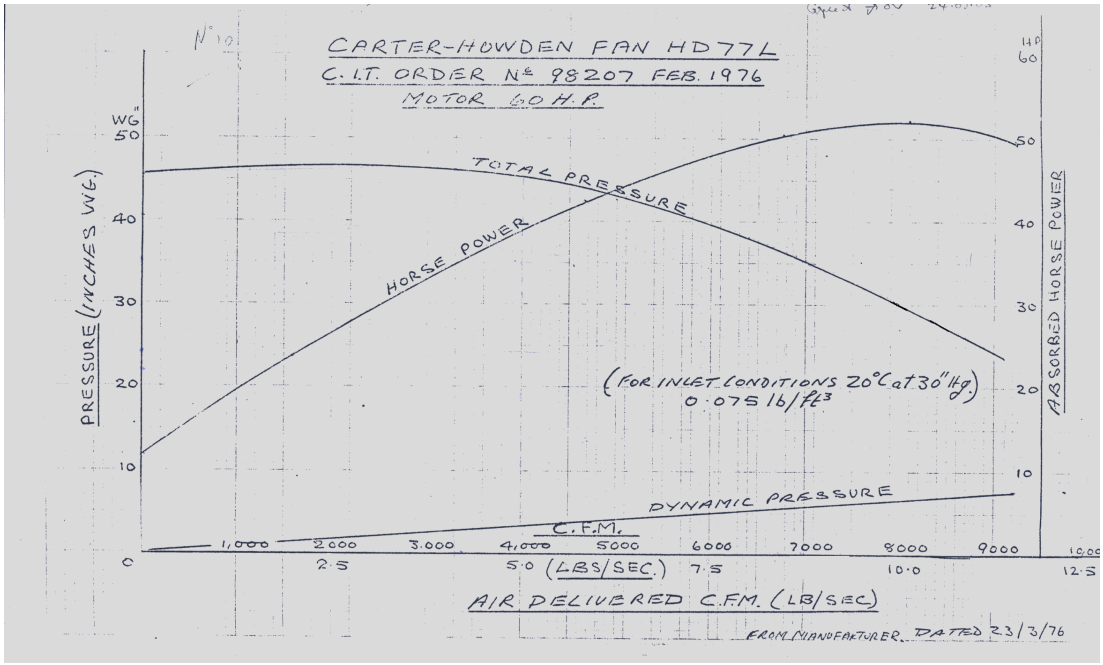

Figure 3-7 Power and load curve for the Carter Howden centrifugal fan model HD77L.

The design of the rig was based on the fan power curve with the following considerations.

- Design a section to produce the Mach number of 0.7 in the cascade inlet.
- Design a section to stop the induced vortex produced from the inlet of the fan.
- Design a section to install the fouling and washing systems.

The design was to calculate a venturi wind tunnel that produced a flow conditions of Mach=0.7. The inlet conditions of the fan were used as the wind tunnel outlet conditions (see Table 3-12).

Inlet cross section	m^2	0.08698
Maximum Delivery Pressure @ 2.26Kg/s	Pa	112442
Maximum mass flow @ Delivery Pressure 108645 Pa	Kg/s	4.54

Table 3-12 Fan inlet conditions (see figure 3-7).

The following assumptions were used to complete the general configuration.

- The cross area section from the fan inlet was used to define the cross area at the inlet and outlet of the wind tunnel.

- The outlet section of the wind tunnel was circular to joint with the fan inlet.
- The inlet section of the wind tunnel was rectangular to joint with the rectangular section from the cascade (see Figure 3-8).

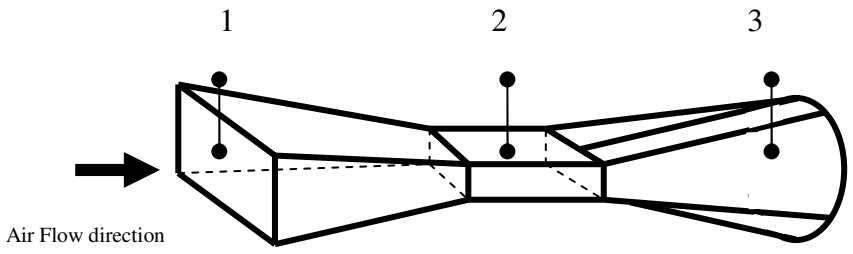

Figure 3-8 Sketching of test rig: (1) Wind tunnel-inlet open to atmospheric conditions, (2) Cascade Blade, (3) Wind tunnel-outlet connected to fan.

The cascade dimensions were calculated based on the inlet and power of the fan. The cross area of the cascade represented 3/7 of the total area of the first stage (section 3.2.2). With this value it was possible to calculate the following dimensions.

$A_{cascade}$ =0.046 x 3/7=0.0197 m^2

if $A_{cascade} = Height_{blade} \times Width_{cascade}$, then $Width_{cascade}$ = 0.223 m

The cascade inlet was 0.081 (blade height) x 0.223 m ($Width_{cascade}$). A similar procedure was followed for the inlet of the wind tunnel. The area was assumed equal to the outlet area of 0.08698 m^2 and the height was scaled 3 times bigger than the blade height.

$$A_{inletwindtunnel} = (3 \times Height_{blade}) \times Width_{windtunnel}$$

Then, the $Width_{windtunnel}$ = 0.3722 m,

The rectangular cross section was 0.2337 x 0.3722 m.

The next step was to calculate the operation condition of the fan in order to reproduce the Mach number in the cascade inlet. The mass flow was calculated with an algorithm based on the wind tunnel dimensions to obtain the Mach number of 0.7 (see Table 3-13).

Ideal constant gas	R	Data	287	
Gama	g	Data	1.4	
mass flow	W	**variable to give**	**4.3**	**Kg/s**
cross area inlet	A1	condition (0.3722 x 0.2337)	0.086983	m^2
total ambient pressure inlet	P1	condition	101000	Pa
total ambient temperature inlet	T1	condition	288	K
static pressure inlet	p1	P1=p1	101000	Pa
static temperature inlet	t1	T1=t1	288	K
density inlet	r1	P1/R*t1	1.228338	Kg/m^3
velocity inlet	V1	W/r1*A1	40.86	m/s
sound velocity	a1	(g*R*t1)^0.5	340.17	m/s
mach inlet	M1	Vi/ai	0.12	
loss converge	L2%	Pressure Losses (from experiment)	0.00%	
total pressure outlet	P2	P2=P1-Loss%	101000	Pa
total temperature outlet	T2	T2=T1 (assumption)	288	K
cross area outlet (bed test)	A2	0.223 x 0.0881	0.019646	m^2
	C2	1/[(((T2*R)/g)^0.5*W)/(P2*A2)]	1.880352	
equation to solve mach outlet		(1+0.2*M^2)^3=C1*M		
mach outlet	M2	SOLVE EQUATION HP	**0.71**	
static temperature outlet	t2	T2/(1+(g-1)/2*M2^2)	262.29	K
static pressure real outlet	p2	P2/(1+(g-1)/2*M2^2)^(g/1.4-g)	72092	Pa
Density	r2	p2/Rt2	0.957679	Kg/m^3
Sound speed2	a2	(g*R*t2)^0.5	324.63	m/s
Velocity outlet	V2	M2*a2	227.68	m/s
Velocity outlet	V2	W/(r2*A2)	228	m/s

Table 3-13 Summary of results for fan operating point (see Appendix-B)

According to these results, the wind tunnel was designed in four modules:

i. Bell mouth
ii. Inlet-section
iii. Cascade Blade
iv. Outlet-section

i. Bell mouth

The bell mouth was designed to drive the air inside the wind tunnel in a manner which avoided turbulence. The configuration of the shape was calculated according to industrial bell mouths and experience from Cranfield Staff. The semicircular ring from the inlet was calculated with the hydraulic diameter* according to the following equation† (see Figure 3-9).

$$D_{Mouth} = \frac{1}{2} D_{hydrahukic}$$

Equation 3-12

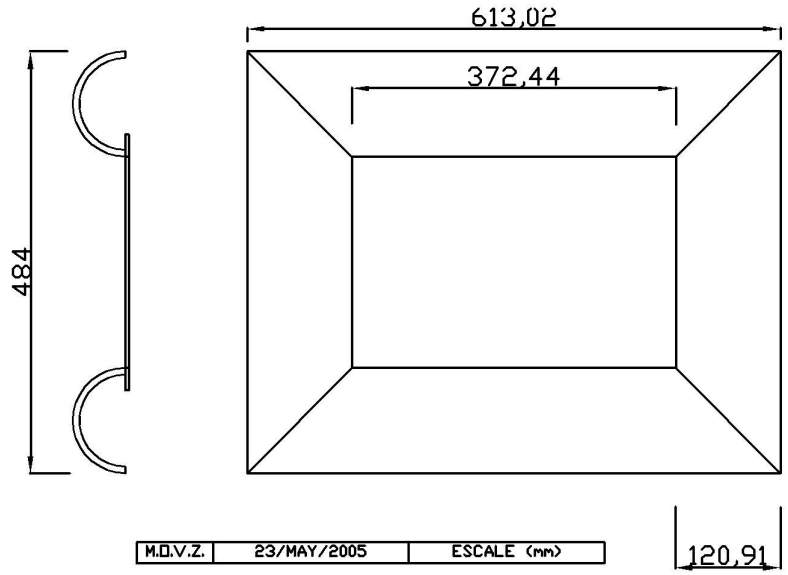

Figure 3-9 Diagram of the bell-mouth section design. Lateral View (left figure), Front View (right figure).

A filter section was added in the bell mouth to avoid the ingestion of the external objects. According to the environment conditions from the laboratory a single filter stage was selected (see Table 3-14).

* For further information Pankhurts (1952) and Gostelow (1984).
† Empirical equation used for the intake of wind tunnels in Cranfield University.

Particle size retain	µM	10
Mass flow work	Kg/s	0.1~5
Pressure ratio	bar	0.05
Temperature of operation	ºC	-5~25
Relative humidity of operation	%	+80

Table 3-14 Filter media properties.

ii. Inlet section

The inlet section of the wind tunnel was designed to accelerate the flow from the bell mouth to the inlet of the cascade (Mach 0.7). The design reduced the cross section and utilized the pressure difference produced by the fan. The cross section was gradually reduced using an angle of 9^{o} from the lateral wall to avoid the boundary layer separation (see Figure 3-10). The length of this section was the result from the angle projection of the cascade height and the bell mouth height. The last section of the inlet had a constant area of one chord length to guarantee the uniformity of the flow in the cascade.

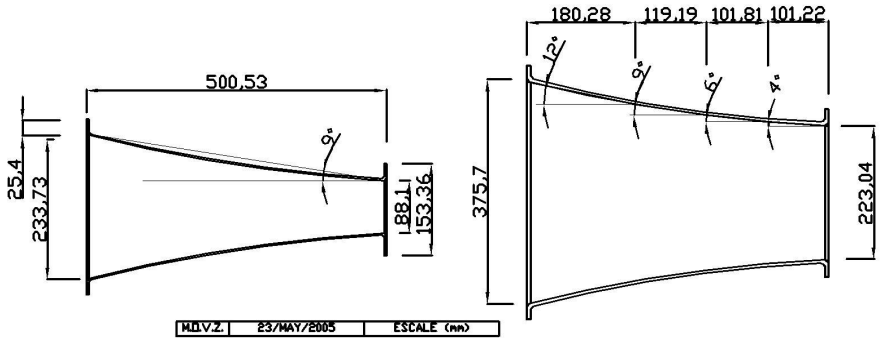

Figure 3-10 Diagram of inlet section from the wind tunnel. Lateral View (left figure), Plan View (right figure).

iii. Cascade Blade

With the previous values calculated it was possible to complete the cascade dimensions. The cross section was 8 x 228 mm that could hold 6 blades. The blade incidence angle was adjusted with a bolt-lock from the blade root. The lateral walls were designed with an angle of 11º following the projection of the middle blade chord line (see Figure 3-11).

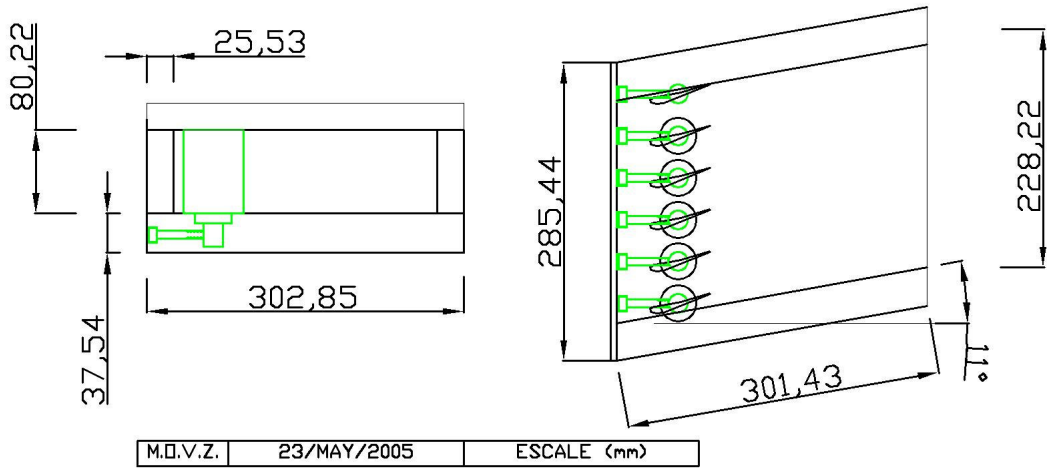

Figure 3-11 Diagram of cascade blade section. Lateral View (left figure), Plan View (right figure).

iv. Outlet section

The configuration of the outlet-section was based on the industrial configuration "diffuser dumper". The cross area of this section configuration increased gradually until it reached a step that produced a fast expansion. The expansion stopped the induced vortex from the fan. Also, this section modified the cross section from rectangular (cascade outlet) to circular (fan inlet). The aperture was made with an angle of 9º (see Figure 3-12).

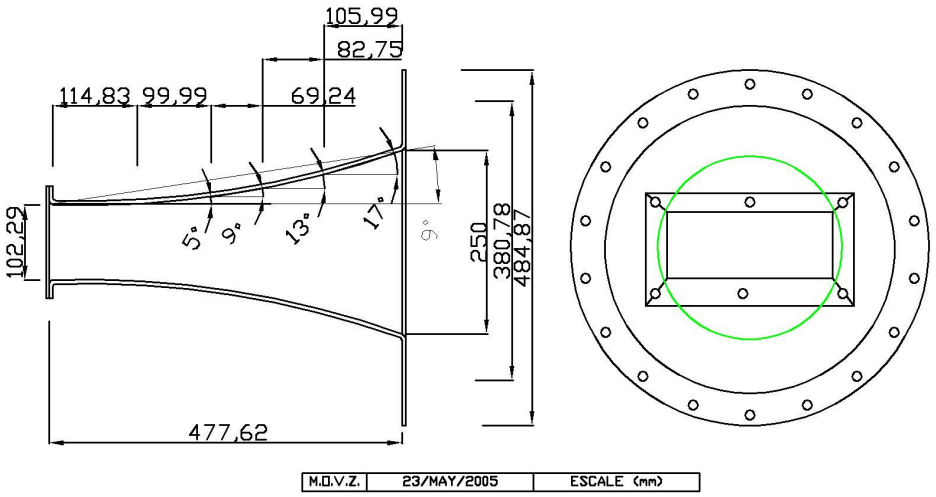

Figure 3-12 Sketch diagram of the cascade blade section design. Lateral View (left figure), Plan View (right figure).

The four modules can be disconnected and removed individually. A butterfly valve between the fan-inlet and outlet-section was added to control the flow. The four modules were settled in a steel frame with wheels to allow the whole rig to be moved from the laboratory.

3.4 Test rig construction and installation

The construction of the rig was authorized by the sponsors after they were presented with the preliminary risk analysis of the project. The process of manufacture, selection of materials, instrumentation selection and operation of the test rig are presented in this section*.

3.4.1 Industrial Fan

The industrial centrifugal fan was electromechanical installed in the Test House 12 (Cranfield University Laboratories). The mechanical installation consisted in a steel

* The test rig was built in the workshop of Cranfield University and installed in the Test House-12.

frame clamped to the floor to hold the electrical motor and centrifugal fan (see Figure 3-13). The electrical installation included the 3-phases power line and the electrical control panel.

Figure 3-13 Electro-mechanical installation of the centrifugal fan model Carten Howden LTD in Test House 12.

3.4.2 Bell Mouth

The bell mouth was manufactured from stainless-steel sheet (A286) with a thickness of 1.68 mm (1/16") which was welding using the process of TIG*. The filter (see Figure 3-14) and a steel-grill (20 x 10 mm) were installed between the bell-mouth and inlet-section of the wind tunnel to avoid the ingestion of objects. The joints between each component were stainless steel bolts & nuts and the test rig was hermetically sealed with neoprene.

* Gas tungsten arc welding (GTAW), also known as tungsten inert gas (TIG) welding, is an arc welding process that uses a non-consumable tungsten electrode to produce the weld. The welding area is protected from the atmospheric contamination by a shielding gas (usually an inert gas such as argon), and a filler metal is normally used, though some welds, known as autogenous welds, do not require it. GTAW is most commonly used to weld thin sections of stainless steel and light metals such as aluminium, magnesium, and copper alloys.

Figure 3-14 Sample of the cloth-filter: efficiency of 90% for particles retention of 10µm, synthetic fiber media thickness of 10mm and pressure drop of 1% at low speeds (static filter).

3.4.3 Inlet and Outlet sections

The inlet and outlet sections of the wind tunnel were manufactured out of stainless-steel sheet (A286) of 1.68 mm (1/16") thickness. The TIG welding process was used to manufacture the internal sections to avoid erosion and corrosion produced during the tests of fouling and washing (see Figure 3-15). The thickness of the sections provided the necessary stiffness to prevent the rig collapse due to the force produced by the internal pressure. The joint between the outlet-section and the valve was made from hard plastic and double neoprene seals to absorb the vibration produced from the fan.

Figure 3-15 Manufacture of inlet-section (left) and outlet section (right) by the TIG welding process.

3.4.4 Cascade

The cross section of the cascade was a constant rectangle of 0.01964 m^2 (223 x 88.1 mm). The lateral and ceiling walls were made from acrylic to observe the

phenomenon of fouling on the blade surfaces. The base of the cascade was made with aluminium (RR58) to make it easy to manufacture and to provide the stiffness required for this section (see Figure 3-16). The blades were held using a locked bolt from the blade root to remove the blade and adjust the incidence angle. The whole cascade can be removed from the wind tunnel without uninstalling any other section.

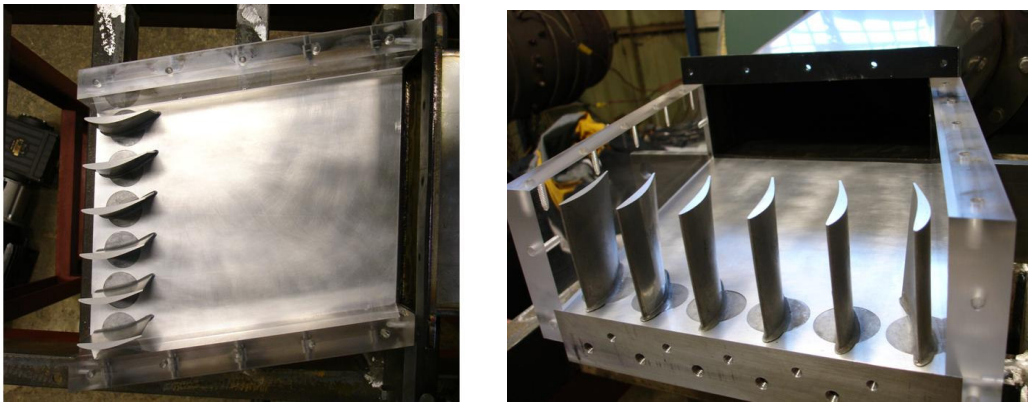

Figure 3-16 Plane view of the cascade blade section (left), Isometric view of the cascade blade section (right).

The blades used in the cascade section were manufactured in Cranfield University (see Figure 3-17).

Height	80 mm
Chord	59.98 mm
Material	cast aluminum-alloy 4227SC AMS Al-300, Mg-100: 0.6%, Mn-200: 0.5%, Cu-400: 0.8%, Ni: 0.5%)
Density	0.101

Table 3-15 Characteristics of compressor axial blades used in the cacade blade.

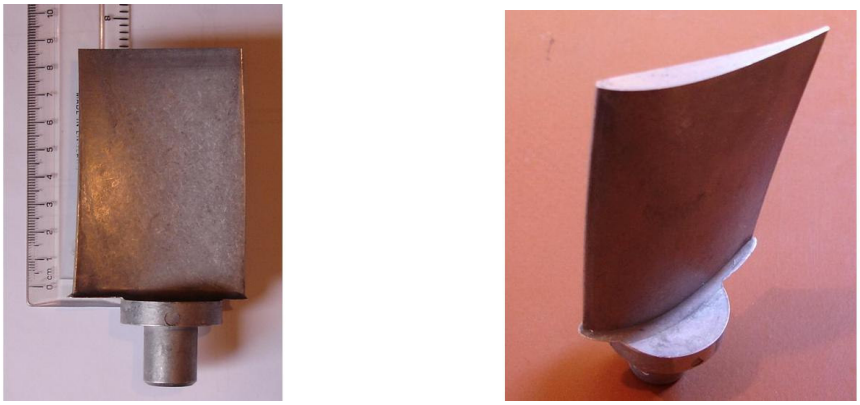

Figure 3-17 Lateral view of the blade pressure surface (left), Isometric view of the blade (right).

3.4.5 Frame

The Frame was manufactured in steel with a "L" cross section (angle) of 6 mm and welding by conventional electrical deposition. The wind tunnel was held on the top of the frame. The low level section of the frame was left free to install the compressor washing system[*].

3.4.6 Instrumentation

The effect of the fouling mechanism was evaluated with the change of the blade aerodynamics. Hence, the instrumentation was selected according to the following aerodynamic parameters that were measured from the test rig.

- Static Pressure
- Total Pressure
- Temperature
- Humidity
- Surface roughness[†]

The flow uniformity inside the cascade was estimated with the static pressure distribution. A ring of taping holes was installed around the inlet and outlet of the cascade. The dynamic pressure was measured with a conventional Pitot tube instrument that traverses inside the cascade. This instrument measured the pressure profile in the cascade, estimated the internal flow uniformity and located the geometrical position of the weak blade (parameter used later on for the CFD model, Chapter 4).

The static and dynamic pressures were recorded by electronic transducer (see Figure 3-18). The electronic transducer converted the pressure from the Pitot or taping tubing into an electrical signal. The signal was transmitted by mili-volts into a pressure display. The electronic transducer used in this experiment was connected with the

[*] The washing system description and installation will be discussed in Chapter 6.
[†] This instrument is described in Chapter 5.

electronic display model DPI 145 DRUCK (see Figure 3-18). The total channels used to monitor the flow in the cascade were 21 (20 for the static pressure and 1 for the dynamic pressure). The calibration of the instrumentation was done by Cranfield technicians.

Figure 3-18 Pressure transducer and electronic display (left). Screen from the DRUCK electronic display (left). The electronic display had pressure ranges of up to 700 bar with a precision of 0.15 mbar.

3.4.6.1 Temperature

The total temperature was measured in different points of the test rig with digital thermometers (see Table 3-16).

MEASURING RANGE	-50℃ TO 150 ℃
DISPLAY ACCURACY	±1℃
DISPLAY RESOLUTION	0.1°
PROBE SIZE	3.5(DIA)* 120(L)MM
CABLE LENGTH	1 METER

Table 3-16 Compact Digital Thermometer specifications

3.4.6.2 Humidity

The digital barometer model Sea-Pathfinder SPF-70T CASIO was used to measure the ambient conditions (pressure, temperature and humidity). The instrument was calibrated with information provided from the Cranfield Airfield Control Tower.

3.4.7 Test Rig Operation Instructions

SAFETY REQUIREMENTS

- Ear defenders and safety glasses
- People and objects must stay away from the wind tunnel inlet and fan outlet
- The wind tunnel should only operate with the protective grill in the wind tunnel inlet
- To protect the electrical equipment and avoid internal damages due to internal pressures the valve has to be opened/closed slowly
- Only authorized personnel can operate the equipment and make modifications

OPERATION INSTRUCTIONS

(1) The butterfly valve must be closed before the electrical motor is turned-on (see Figure 3-20).
(2) Turn-on the energy with the general switch located in control-1 (see Figure 3-13).
(3) Turned-on the electrical motor with the green button in control-2 and wait until the 3 phases of the compressor are working at full load which is indicated by the green light (see Figure 3-13).
(4) Open the valve slowly to achieve operation conditions (se Figure 3-20).
(5) Close the valve slowly to turn off the system (see Figure 3-20).
(6) Turn off the electric motor with the red button in control-2 (see Figure 3-13).
(7) Turn off the energy with the general switch located in control-1 (see Figure 3-13).

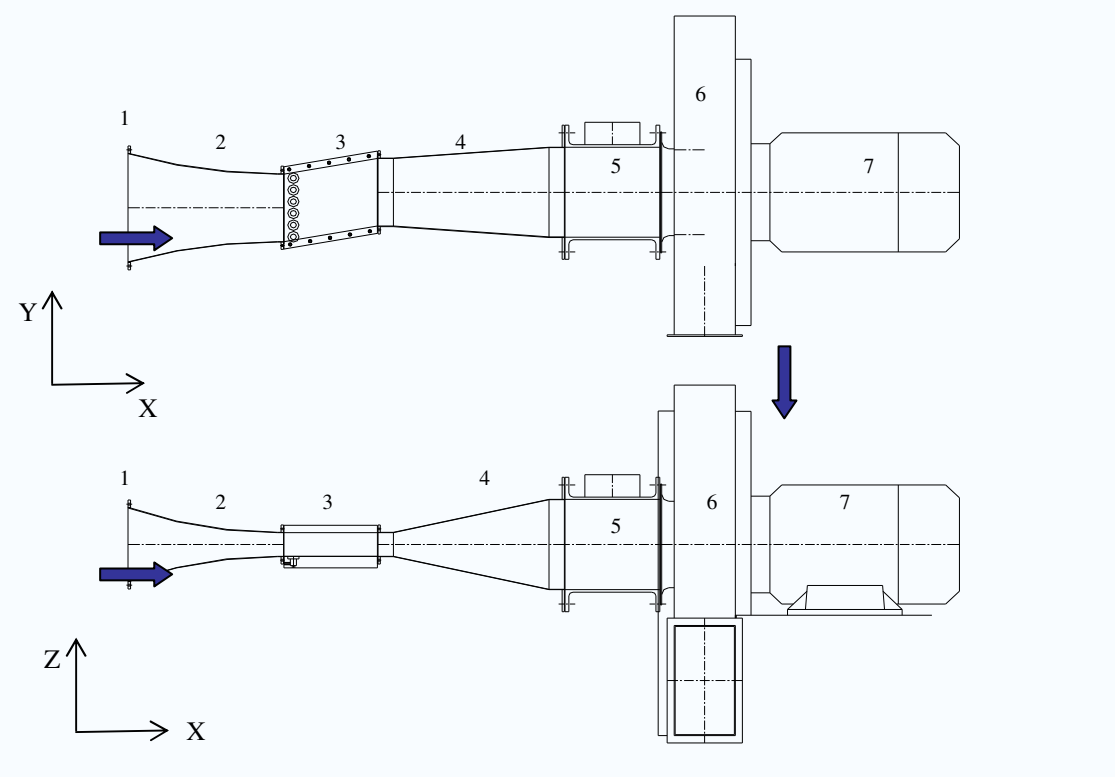

1.- Bell mouth and filters
2.- Inlet-section
3.- Cascade blade (test section)
4.- Outlet-section
5.- Butterfly valve
6.- Fan
7.- Electric motor

Figure 3-19 Schematic representation of test rig and fan. Plan View (top), Lateral View (bottom)

Figure 3-20 Photo from the Test Rig (Cranfield University Laboratory).

4 EVALUATION OF CASCADE PERFORMANCE

4.1 Introduction

This chapter presents the contribution of the CFD to validate the experimental information. The information recorded from the experiment was obtained from the instrumentation selected. However, this instrumentation was limited to measure only the aerodynamic condition of the flow in the macro-scale. The chapter is divided into three sections. The first section, discusses the flow uniformity based on the experimental and CFD results. The second section presents the experimental validation of the two dimensional condition for the flow. This implied experimental techniques of flow visualization to study the behaviour of the flow in the blade passage. The last section of this chapter presents the aerodynamic study of the cascade section using a three dimensional CFD model. The three dimensional effects of the flow inside the cascade were analysed to complete the information that was not possible to measure with the instrumentation.

4.2 The CFD study

The aerodynamic conditions of the flow can be calculated using the computational numerical simulation. In this section of the research this tool was used to adjust the CFD model with the experimental results. The model of the CFD was adapted to the same conditions for the experiment. This means that the geometry and boundary conditions of the test rig were exactly reproduced in the CFD model.

The first objective of the CFD application was the evaluation of the cascade performance. The results from the CFD were used to validate the information recorded from the cascade (pressure distribution). The aerodynamic parameters such as velocity, Mach number and turbulence were calculated by the CFD. The second application and main contribution of the CFD in this research was the analysis of the boundary layer. The boundary layer as was mentioned in Chapter 2 corresponds to a

micro-scale study. This region was impossible to measure with the instrumentation available in the experiment.

The CFD model was created with the use of the following computational tools.

- AUTOCAD is an engineering drawing software that was used in this work to draw the two and three dimensional geometry.
- GAMBIT is an engineering post processing geometry software that was used in this work to create the mesh (grid), volume in study and boundary conditions region for two and three geometry.
- FLUENT is computational fluid dynamic software that was used in this work to calculate the flow aerodynamics. The aerodynamic parameters and boundary layer was studied from the numerical solution of Navier Stokes equations.

The CFD study was divided into three particular objectives.

i. Study of cascade configuration in a two dimensional model.
ii. Study of cascade configuration in a three dimensional model.
iii. Study of fouling effect in the boundary layer region of the blades.

The first two particular objectives are presented in this chapter and the third objective is presented in Chapter 5.

The two dimensional region was the real dimensions at the middle blade section of the cascade. The sections represented in this model were from the inlet to the outlet of the wind tunnel. To simplify the geometry, the bell-mouth and filter were omitted in the CFD model. The effects from the valve and vortex induced by the fan were also omitted. The aerodynamic parameters in study were: flow velocity, static and total pressure distribution, Mach number and Reynolds number.

4.2.1 Geometry

The geometry was created in AUTOCAD and exported to GAMBIT to generate the mesh to be computed in FLUENT. The blade profile was created in GAMBIT using

Nurb-curves*. The total blade profile was divided in 24 regions (12 regions for pressure surface and 12 for suction surface). This division on the blade surface allows each region to be modified according to the particles deposition.

4.2.2 Boundary conditions

In FLUENT it is necessary to specify two types of regions (continuous and boundaries). The continuous region was considered the inner of the flow (wind tunnel internal region). The boundary region corresponded to inlet and outlet of the wind tunnel and the walls (blades and side walls). These conditions were defined based on the following parameters.

1. Inlet condition. The inlet condition was the total pressure (Inlet Pressure) from the ambient pressure. The pressure losses due to the bell-mouth and filter were omitted.
2. Outlet condition. The outlet condition was the static pressure in the outlet of the wind tunnel (Outlet Pressure). The experimental condition was unknown, then this parameter was automatically adjusted by the program to force convergence in the results when the backflow occurred during the iterations.
3. Wall conditions. The flow was limited by the walls (duct walls, cascade walls and blades). They were defined in FLUENT as solid regions according to the type of material (stanley steel, acrylic and aluminium). The non-slip condition was activated in FLUENT and the surface roughness value was the default included in the program.

4.2.3 Mesh

FLUENT, as was mentioned before, solves the Navier-Stokes equations in a finite volume by the iteration of numerical algorithms. This arrangement of equations is created by the equations defined from the elements (mesh), each element represent a particular position and time. In FLUENT the mesh can be created by structured or unstructured meshes. The use of structure-mesh (squares) increases the accuracy of the results but also increases the number of elements and the computational process time. The study of the boundary layer separation requires a fine and precise mesh near

* Nurb-curve, is a polynomial function of FLUENT used to create curves from single points.

to the blade surfaces and for that reason the structured-mesh was selected in this region. The regions that did not require necessary precision the unstructured-mesh was selected. The use of unstructured-mesh reduced the number of cells and decreased the number of iterations (computational time). GAMBIT program limits the number of cells to 11 million; hence the unstructured-mesh was used for the ducts and some sections from the cascade.

The structured-mesh can be manipulated automatically in FLUENT to reduce or increase the scale. However, it was found in the creation of the mesh that if the number of cells is higher than 1 million this function was not working correct. To avoid this problem the mesh of the boundary layer was created manually. The number and spacing of the nodes were created according to the type of region (boundary or continuous). For example, the sharpness of the blade was an essential condition for the aerodynamic study and the blade profile consisted of 1000 points. The result of this was a dense mesh around this region used to calculate the flow conditions near to the blade wall (see Figure 4-1).

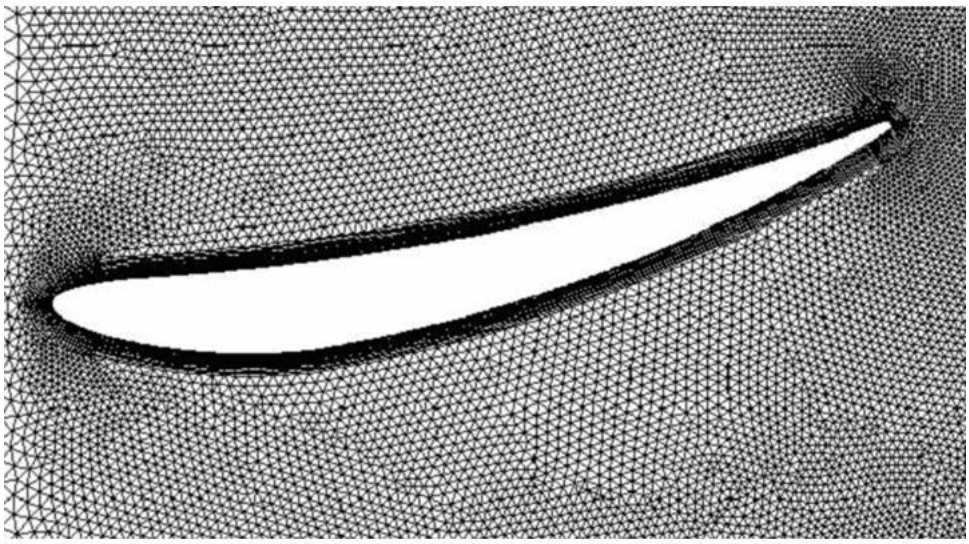

Figure 4-1 Unstructured mesh around the structured mesh in a compressor blade.

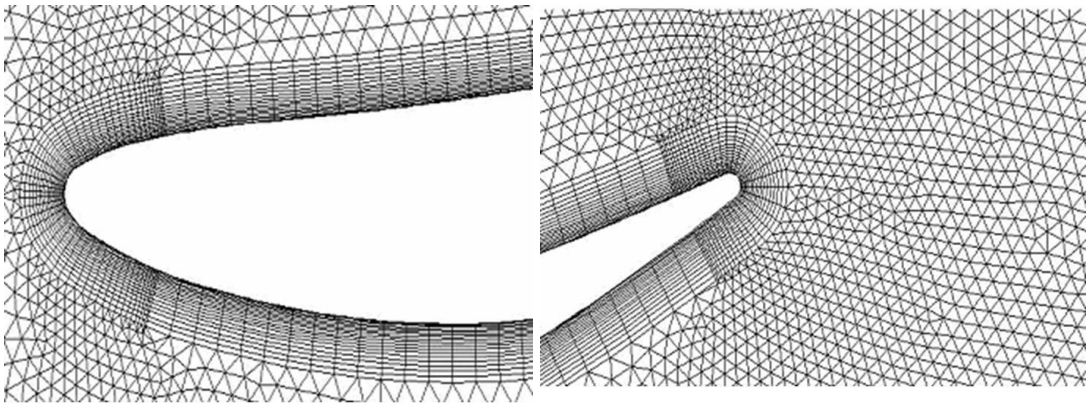

Figure 4-2 Mesh at leading edge of the blade (left). Mesh at trailing edge of the blade (right).

The flow around the blade near to the surface is laminar and hence the viscous shear stresses dominate the flow behaviour. But, when the boundary layer starts to separate the turbulent stresses are presented. The interaction between these two regions has to be studied carefully in order to determine the transition point. Outside of this region, the flow can be considered turbulent and it is dominated by the turbulence effect (see Figure 4-3).

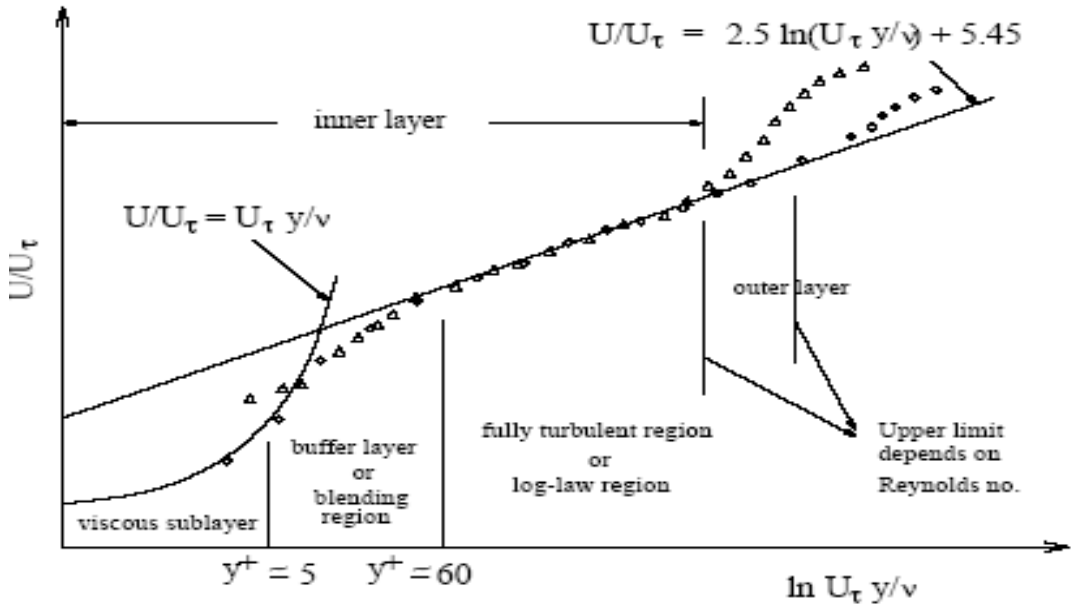

Figure 4-3 Layer treatment near to the wall region (Fluent 2005)

The infinity-velocity U and the wall-shear velocity U_t are scaled by the term u^+ as:

$$u^+ = \frac{U}{U_t}$$

Equation 4-1

a non dimensional parameter y^+ is defined in the near-wall region as:

$$y^+ = \frac{y\rho U_t}{\mu}$$

Equation 4-2

where: γ =gama (compressible gasses)

ρ =density

μ =viscosity

y=dimensional parameter

Then, the wall layer is defined by:

Viscous sub-layer: $0<y^+<5$ and buffer layer: $5<y^+<35$

To approach the real phenomenon near the surfaces it was necessary to consider a mesh with y^+ and the value in the first level of the mesh of 1 (Fluent (2005)). The following table presents the characteristics of the mesh created in the two dimensional model.

Edge	Type of mesh	Number of elements
Inlet	Unstructured (Triangular)	30
Inlet Duct	Unstructured (Triangular)	60
Cascade test section walls	Unstructured (Triangular)	250
Outlet Duct	Unstructured (Triangular)	60
Outlet	Unstructured (Triangular)	25
Boundary Layer around the blades	Structured (Rectangular)	96
Total Nodes		**802151**
Total Cells		**1196718**
Total Faces		**1998872**

Table 4-1 Mesh summary created in GAMBIT to be processed in FLUENT.

4.2.4 Model

The turbulent model in FLUENT can be selected from wall layer (viscosity) or outer layer (convection). In this study the wall layer was the concern due to the modification of the blade surface. When large gradients from the flow velocity are present near to the blade surface, the kinetic energy increases and flow fluctuations can result. This effect is possible to simulate in FLUENT by turning off the turbulence model and viscosity. Then, the program code modifies the original Navier-Stokes by applying time-average equations.

FLUENT offers complex models to calculate the conditions of the flow. In this case due to the static and two dimensional conditions of the blades the k-ω turbulence model was selected. The k-ω model is suggested to predict the free shear flows and mixing layers presented in the phenomenon of fouling. This model incorporates the Wilcox k-ω model that includes the effects from the low Reynolds number with the use of the transport equation of turbulence kinetic energy (k) and specific dissipation (ω) (Fluent (2005)). In this study, the model was activated with the solution of viscous-model due to the nature of the phenomenon (boundary layer study).

4.2.5 Solver

FLUENT provides two tools to process the information according to the application: segregated and coupled. Both solvers require the same discretization process for a finite volume and linearization of the equations. The difference between these two solvers is the discrete equation solution used. For segregated solver the momentum, continuity and energy equations are sequentially solved. For couple solver the equations are solved simultaneously, however the computational time and number of iteration increase. In this study, the segregated solver was selected due to the high number of cells and low flow speed involved.

4.2.6 Boundary conditions

The boundary condition at the inlet corresponded to atmospheric conditions. The walls were considered solid and with constant characteristics. The outlet boundary condition was the parameter used to modify and adjust the results from the CFD

simulation with the experimental results. The following values were used to stabilize the numerical.

- The inlet velocity at the wind tunnel was different from zero to avoid the solution diverging in the first iteration.
- The total stagnation temperature at the inlet was 288K (ambient temperature).
- The turbulence was calculated according to the turbulence percentage equation produced by the grid protection (Osborne (1997)).

$$Tu = 1.12\left(\frac{x}{d}\right)^{(-5/7)} = 2.57\%$$

Equation 4-3

where:

x: is the distance between the grid and blades (0.55 m)

d: is the diameter of the grid bars (0.0028 m)

4.2.7 Parameters of convergence

The parameters of convergence considered in a numerical solution are based on the experience and judgment of the user. Residual monitors were used as a numerical parameter of convergence in this study. This included checking the mass flow continuity according to the limit of difference between inlet and outlet of 1% (Fluent (2005)). It is also possible to use the drag coefficient as a percentage of error when the residual monitors do not converge and the result looks stable. The drag coefficient is useful when the computational time is limited. However in this investigation it was not necessary to use because the Cranfield network and equipment used in this project were available to process the information as long as the solution required to converge from the residual monitors.

The successful procedure to analyze the CFD model is described as follows.

(1) Run the model assuming incompressible flow, constant density and laminar condition (approximately 10,000 iterations).

(2) Run the model assuming incompressible flow at ideal gas (approximately 9,500 iterations).

(3) Run the model with energy equation, ideal gas and k-ω at first order (approximately 12,500 iterations).

(4) Run the model with energy equation, ideal gas and k-ω at second order (approximately 30,000 iterations).

The number of iterations necessary to process the model and obtain a solution that converges in k-ω was approximately 60,000 iterations. The real time corresponded approximately to six days of continuous computational process.

4.3 Performance evaluation of the test rig

This section presents the first experimental results and the application of the CFD to know the flow performance in the cascade. The conventional Pitot tube presented problems to measure the pressure of the flow in conditions of Mach=0.7 due to the difficulty to find a single streamline. Although the rig was designed for this condition, it was necessary to change the air flow conditions of the rig to reduce the Mach number. The following section describes the new conditions of operation.

4.3.1 Conditions of operation of test rig

The new values used in the test rig are presented in the following table. When the flow results in Mach numbers lower than 0.3, the accuracy of conventional Pitote tubes is higher. Because, in this condition of the flow the Pitot tube can localize the air stream line and measured the dynamic pressure. Also, it was possible to assume that the flow was incompressible in some sections of the wind tunnel in order to simplify the calculations.

TEST RIG		**THEORETICAL CALCULATION**	
mass flow	W	Variable to give	1.4
cross area inlet	Ai	condition (0.3722 x 0.2337)	0.086983
total ambient pressure inlet	Pi	condition	98600
total ambient temperature inlet	Ti	condition	290
static pressure inlet	pi	P1=p1	98600
static temperature inlet	ti	T1=t1	290
density inlet	ri	P1/R*t1	1.18
velocity inlet	Vi	W/r1*A1	16.67
sound velocity	ai	(g*R*t1)^0.5	341.35
mach inlet	Mi	Vi/ai	0.04
INLET CASCADE			
loss converge	L2%	Pressure Losses (from experiment)	0.52%
total pressure	P	P2=P1-Loss%	98085
total temperature	T	T2=T1 (assumption)	290
cross area	A	0.223 x 0.0881	0.019646
	C	1/[(((T2*R)/g)^0.5*W)/(P2*A2)]	1.880352
equation to solve mach outlet		(1+0.2*M^2)^3=C1*M	
Mach	M=M1	SOLVE EQUATION HP	**0.28**
static pressure real	p	Experiment	92900
static temperature	t	T2/(1+(g-1)/2*M2^2)	285.53
Density	r	p2/Rt2	1.1336
Sound speed	a	(g*R*t2)^0.5	338.71
Velocity	V=V1	M2*a2	**94.71**
Reynolds number	Re	V*r*Core/mi; mi=1.7894x10^-5, core blade core=0.058	3.48E-05

Table 4-2 Wind Tunnel operation conditions.

The pressures were measured in specific locations of the wind tunnel inlet (see Figure 4-4). The monitoring for the ambient condition (pressure and temperature) was recorded continuously. This information was used in the two dimensional CFD model in FLUENT to study the performance of the flow inside of the cascade.

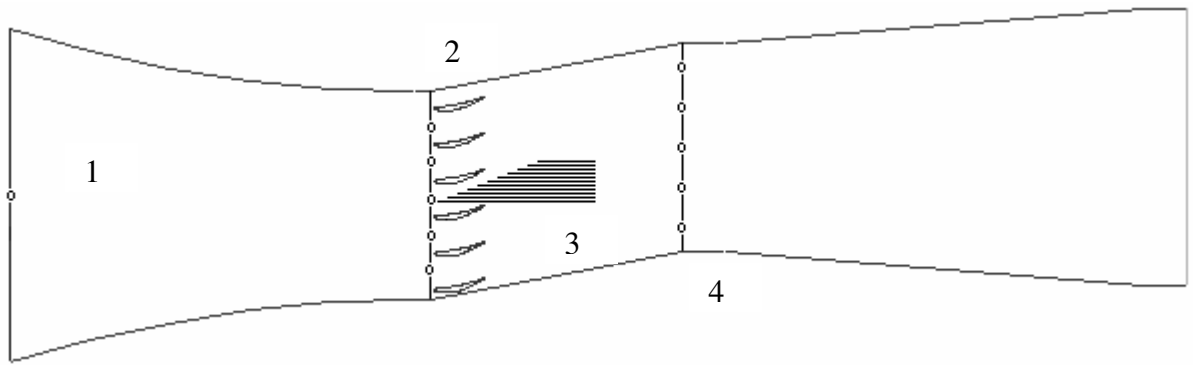

Number	Station	Parameters
1	Inlet wind tunnel	Ambient pressure and ambient temperature
2	Inlet cascade	Static Pressure (taps)
3	Cascade passages	Dynamic Pressure (Pitot tubes)
4	Outlet cascade	Static Pressure (static taps)

Figure 4-4 Schematic representation of test rig.

The dynamic pressure was measured with the Pitot tube with three grades of movement (see Figure 4-5).

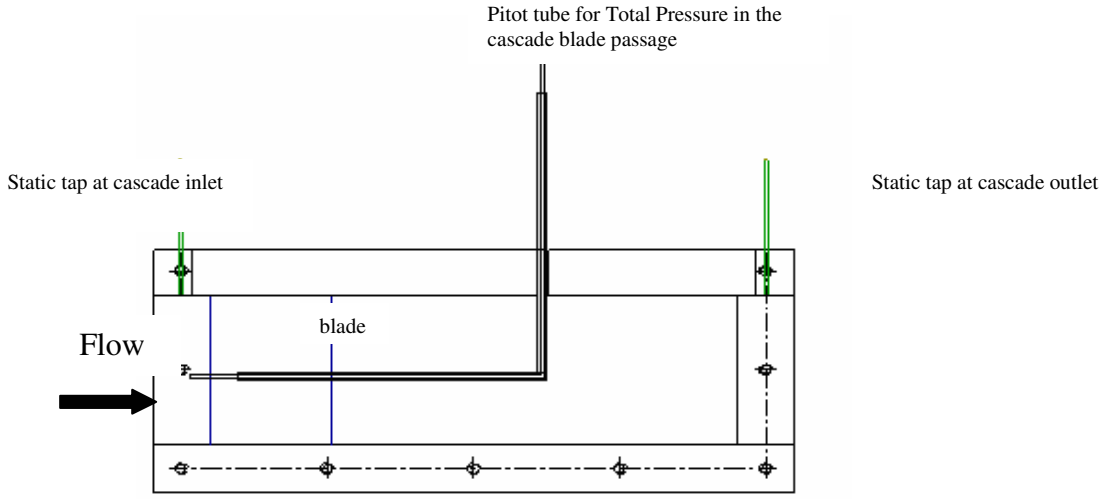

Figure 4-5 Cascade Side view for total and static pressure measurements locations

The static pressure was measured with static taps that were connected to the pressure transducer by silicon tubes of 2mm diameter (see Figure 4-6).

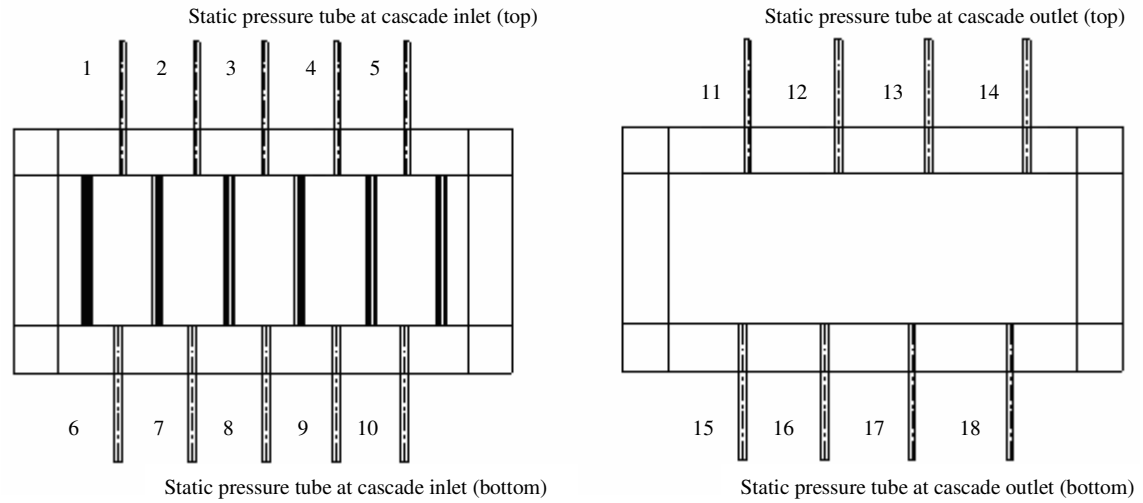

Figure 4-6 Location of static pressure points in the inlet and outlet of the cascade.

The pressure losses produced by the wind tunnel were measured with the difference of the total ambient pressure and the dynamic pressure at different mass flows. The different mass flows were produced with different apertures of the butterfly valve.

Valve % open	T_{02} [K]	P_2 [Pa]	P_{02} [Pa]	P_2 [Pa]	P_{02}/P_2	M_2	T_2 [K]	V2 [m/s]	P_2 [Pa]	m [kg/s]
1/4	288	-483	101484	101117	1004	0.07	287.90	24.47	1224	0.59
1/2	288	-5500	100990	96100	1051	0.27	284.14	90.29	1178	2.10
2/3	288	-8400	100680	93200	1080	0.33	281.91	112.39	1152	2.55
3/4	288	-13200	100270	88400	1134	0.43	278.01	143.08	1108	3.12

Table 4-3 Measurements and calculation at different openings valve from the test rig.

The flow velocity at the cascade inlet is calculated under incompressible flow. With the information from the experimental static pressure in position 2 the velocity results as follows (energy equation for incompressible flows).

$$V_2 = \sqrt{\frac{2(P_1 - P_2)}{\rho}}$$

Equation 4-4

If the flow velocity increased, the static pressure decreased (see Figure 4-7).

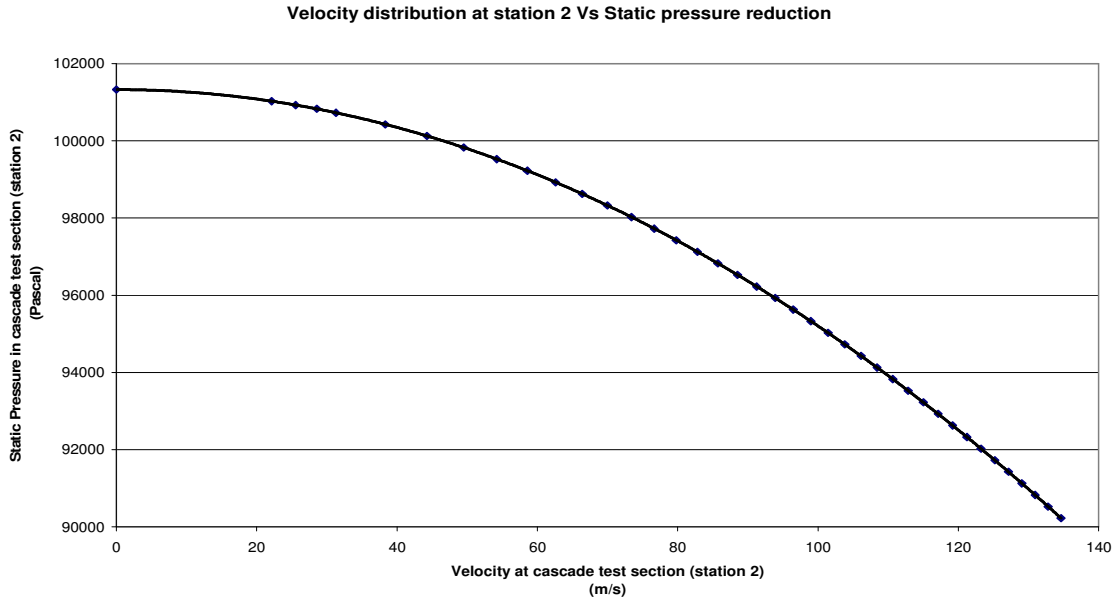

Figure 4-7 Variation of static Pressure at cascade inlet and different cascade velocities

4.3.2 First configuration (6 blades)

4.3.2.1 Geometry

The first cascade configuration was the direct result of the manufacturing process (see Figure 4-8). The distance between the lateral walls and blades was smaller than the original drawing design. This was due to problems with the manufacture of the acrylic. The thickness of the acrylic wall was increased from the original specification to increase the stiffness to screw the bolts and support the internal pressures (see Figure 4-9).

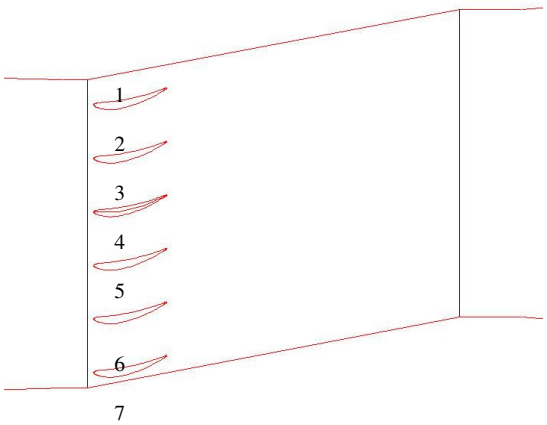

Figure 4-8 Sketch of cascade blade first configuration.

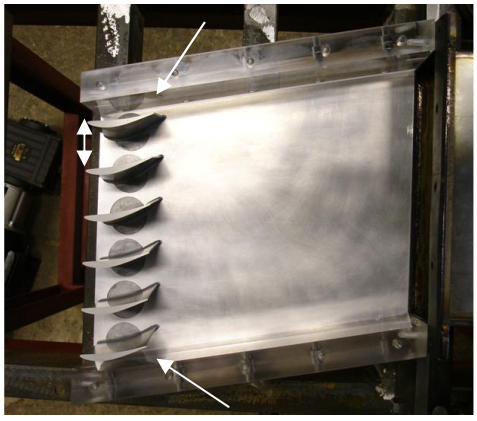

Figure 4-9Manufacturing process of cascade blade first configuration.

4.3.2.2 Experimental Results

The parameter chose to evaluate the experimental uniformity of the flow was the static pressure distribution inside the cascade, because was possible to measure from the test rig. The result demonstrated a high difference of pressure between each extreme of the cascade (See Figure 4-10). The Mach number was calculated with the static and dynamic pressure in position-3 and it was 0.27.

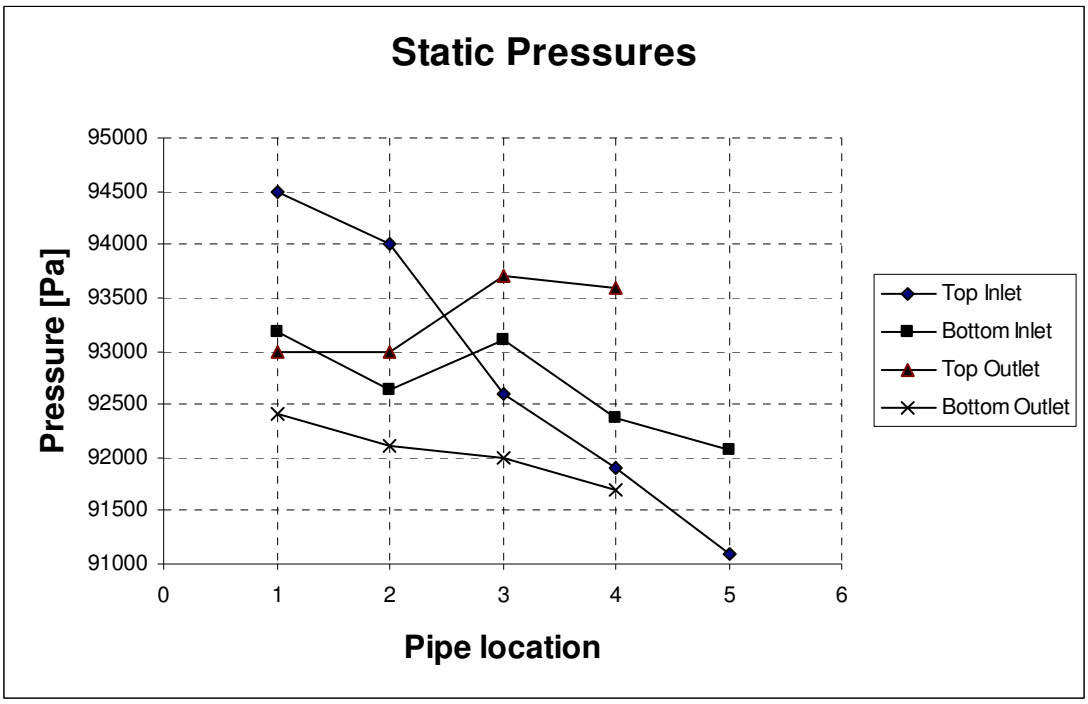

Figure 4-10 Static pressure distribution at cascade inlet and outlet (6 blades configuration)

4.3.2.3 CFD Results

The experimental results were used to adjust the CFD model. The boundary conditions of the CFD were settled according to the real geometry and inlet conditions of the wind tunnel. The static pressure profile in the inlet of the cascade was used as a reference to adjust the CFD model with the experiment. A similar result from the experimental flow was obtained in the CFD model. The non-uniform of the flow through the cross section was also obtained in the CFD. With the application of the CFD was possible to calculate the whole flow distribution in the cascade regions that were not possible to be measured in the experiment.

The static pressure at the inlet of the passage was from the CFD result with a variation from the 1st passage of 96500Pa to the 6th passage of 85000Pa. The static distribution was different in each passage and demonstrated the non-uniformity of the flow. In addition, the CFD showed that in the space between the 6th blade and the wall the static pressure was 54200Pa.

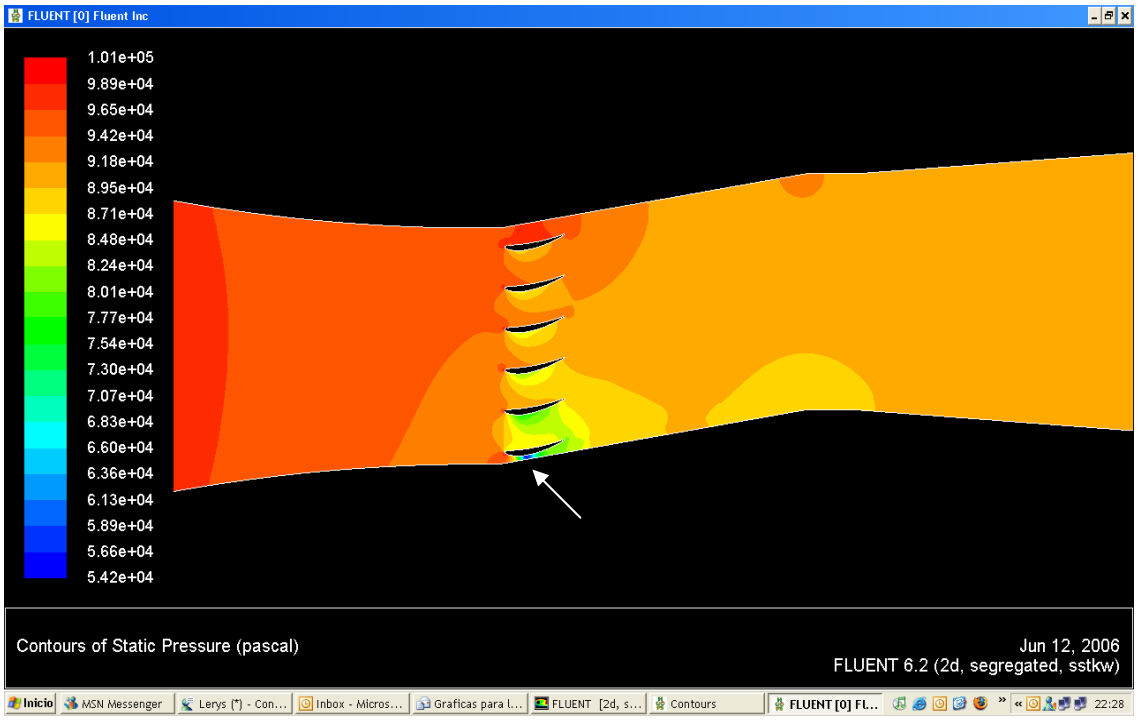

Figure 4-11 Results of CFD study for static pressure distribution (6 blades configuration).

The influence of the pressure in the 6th passage into the cascade was calculated by the CFD process. This result demonstrated a high Mach number (Ma=0.954) produced in this region (see Figure 4-12). The suction surface of blade-6 and the lateral wall configured a small ventury. This result was observed also in the flow velocity distribution (see Figure 4-13). The high velocity produced in this location created flow fluctuations in the whole cascade.

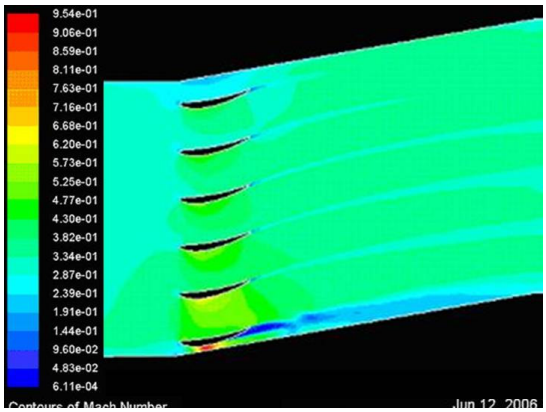

Figure 4-12 Contours of Mach Number by the CFD analysis (6 blades configuration).

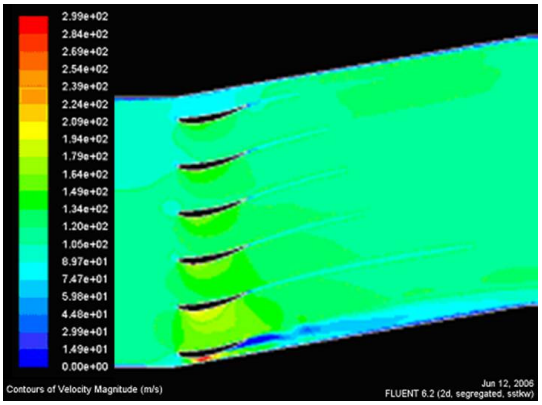

Figure 4-13 Contours of Velocity Magnitudes by the CFD analysis (6 blades configuration).

4.3.2.4 Discussion

The conclusion of these results was that the geometry modifications due to the process of manufacturing considerably affected the internal flow. So, a new configuration was designed to improve the cascade performance as follow.

4.3.3 Second configuration (5 blades)

4.3.3.1 Geometry

The new configuration included only 5 blades and the 6th blade was eliminated (see Figure 4-14). The idea of this change was to avoid the gap formed between the blade and wall. This modification was looked for an easy and fast solution (to avoid lost time in the manufacturing process).

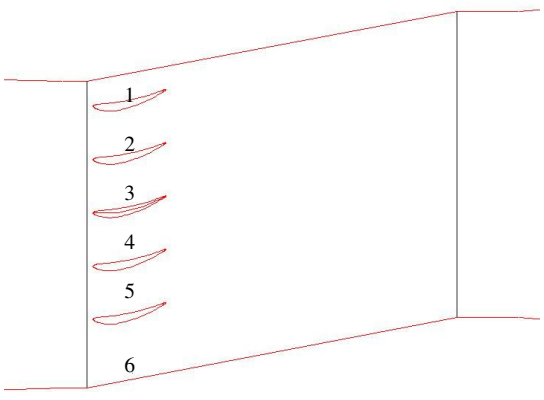

Figure 4-14 Sketch of cascade blade second configuration.

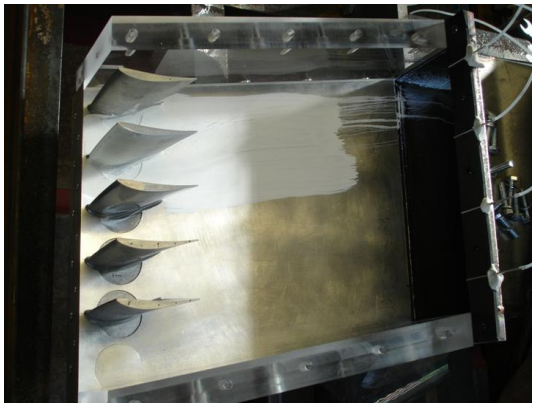

Figure 4-15 Manufacturing process of cascade blade second configuration.

4.3.3.2 Experimental Results

The experimental results demonstrated that the static pressure distribution was improved from the previous configuration (see Figure 4-16). However, the difference of the pressure in the cross section was still considerable enough to affect the flow. The difference of 2000 Pa was between the first static pipe and the last static pipe at the cascade inlet. It was not possible to detect the influence of the pressure difference in the flow from the experiment.

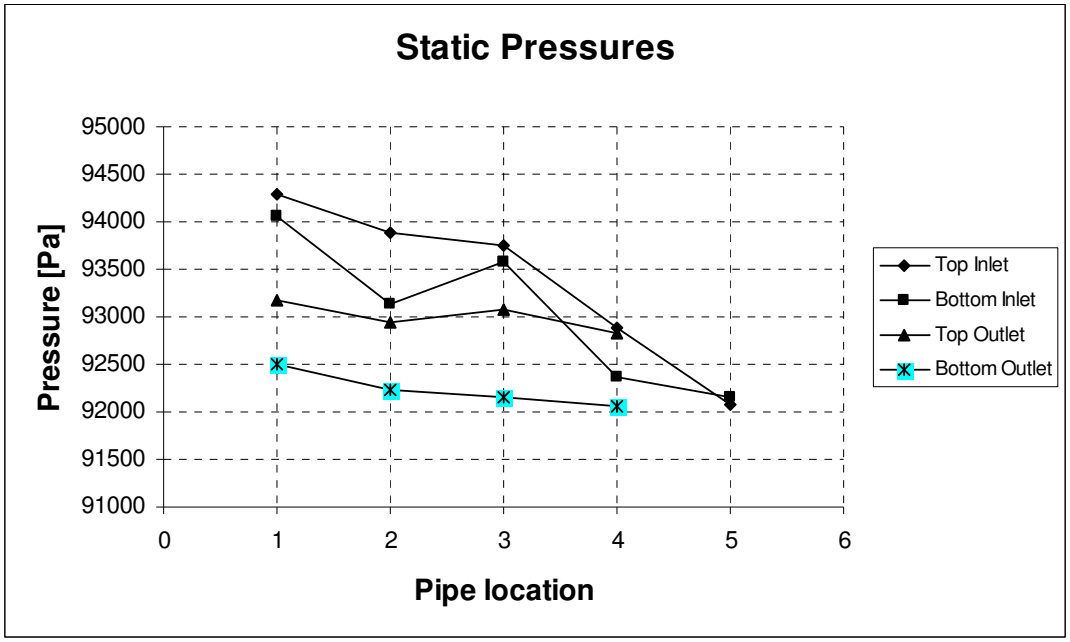

Figure 4-16 Static pressure distribution at cascade inlet and outlet (5 blades configuration)

4.3.3.3 CFD Results

The result was imported to the CFD model to evaluate the flow distribution similar to the previous case. This result demonstrated that the static pressure distribution was non-uniform in the whole cascade. However, the flow uniformity was improved in the 2nd, 3rd and 4th passages (see Figure 4-17).

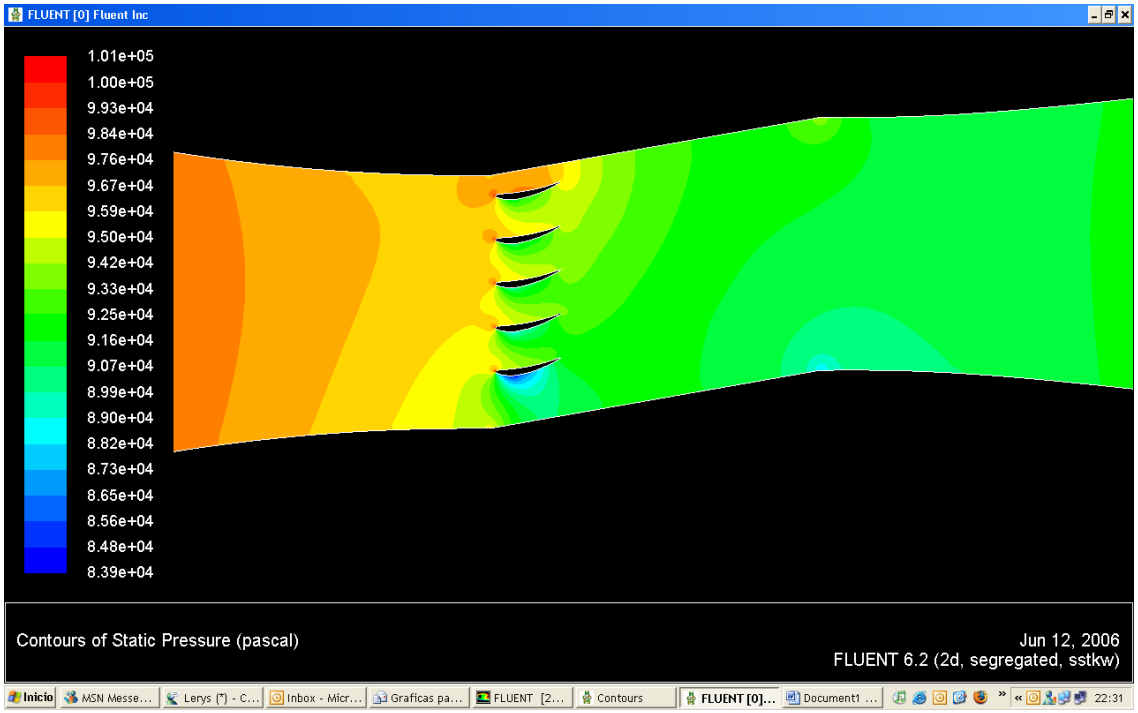

Figure 4-17 Results of CFD analysis for the static pressure distribution (6 blades configuration).

In order to make a correct judgment of this new configuration it was necessary to calculate other parameters. The resulting Mach number was similar in all passages with the exception of the 6th passage. The distribution of the Mach number and the flow velocity between the 2nd and 4th passage was improved than the previous case. However, the flow velocity next to the 6th passage was bigger from the central passages in approximately 15%.

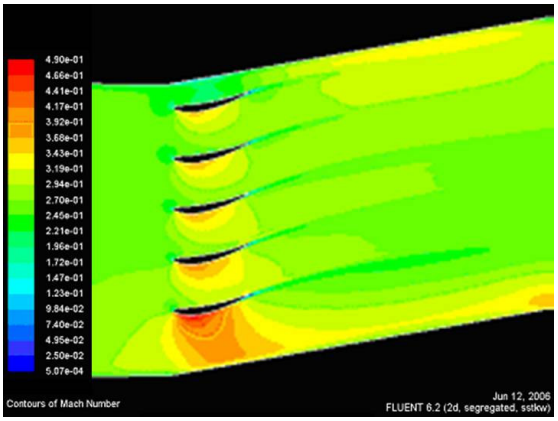

Figure 4-18 Contours of Mach Number by the CFD analysis (5 blades configuration).

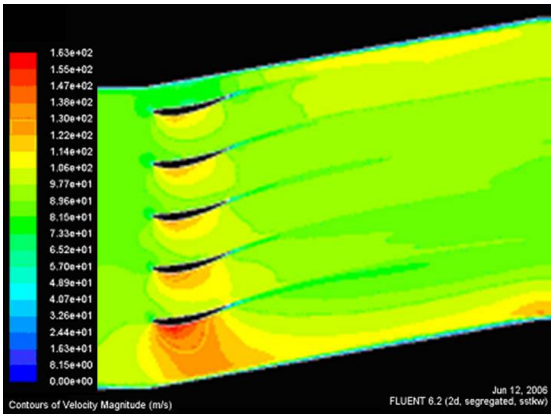

Figure 4-19 Contours of Velocity Magnitudes by the CFD analysis (5 blades configuration).

4.3.3.4 Discussion

Effectively the new configuration improved the flow uniformity inside the cascade. The velocity periodicity was observed between the 2nd and 5th passages. If this study was focused purely on the aerodynamic condition of the flow at clean conditions, this configuration could be enough to continue with the post-processing study of the flow (boundary layer region, drag, etc.). However, the fouling experiment involves the injection of dust from the inlet of the wind tunnel. The dust injection is linked with the flow distribution and this characteristic is essential to obtain correct results. The gap between the 1st passage and the 6th induced a factor of incorrect distribution. Also, in the 6th passage the flow was accelerated and this meant that the mass flow could tend to travel through this passage.

4.3.4 Third configuration (4 blades and lateral walls)

4.3.4.1 Geometry

The third configuration was designed to solve the problem of the flow distribution. This configuration included lateral walls with aerodynamic shapes based on the blade exit angle. The new walls were manufactured with aluminium and attached to the acrylic walls (Figure 4-20). The result implied that it was necessary to have equal distances between the passages, but also it reduced the number of blades from 5 to 4.

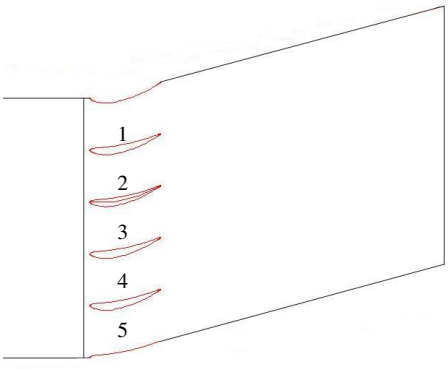

Figure 4-20 Sketch of cascade blade third configuration

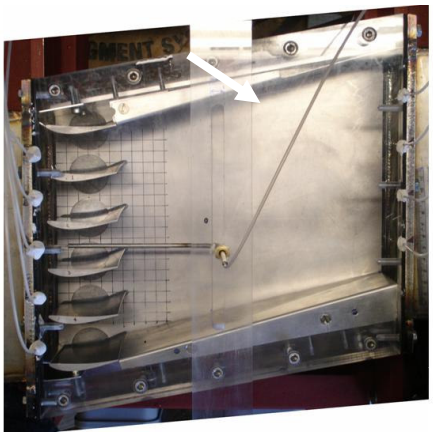

Figure 4-21 Manufacturing process of cascade blade third configuration.

4.3.4.2 Experimental Results

The static pressure distribution at the inlet and outlet of the cascade was considerably improved (See Figure 4-22). The inlet condition presented a variation between 600 Pa and the outlet variation was 350 Pa this demonstrated that the walls had a big influence on the flow.

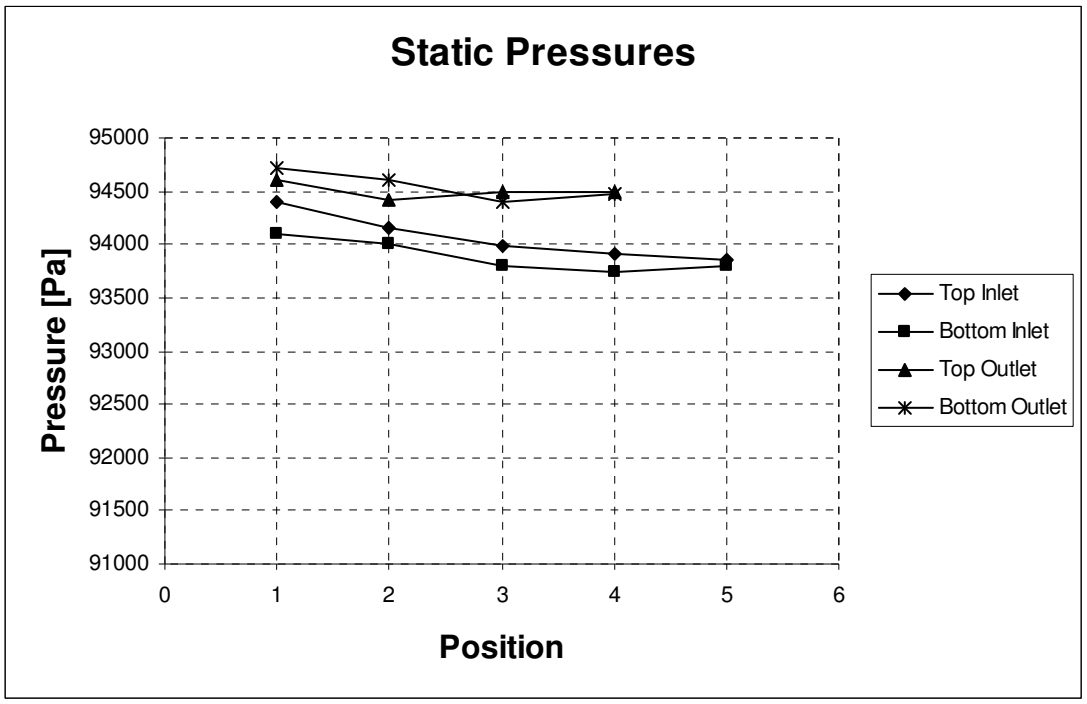

Figure 4-22 Static pressure distribution at cascade inlet and outlet (4 blades configuration).

4.3.4.3 CFD Results

The CFD results for this new configuration showed a uniform flow in the cascade and with acceptable flow periodicity between the passages (see Figure 4-23).

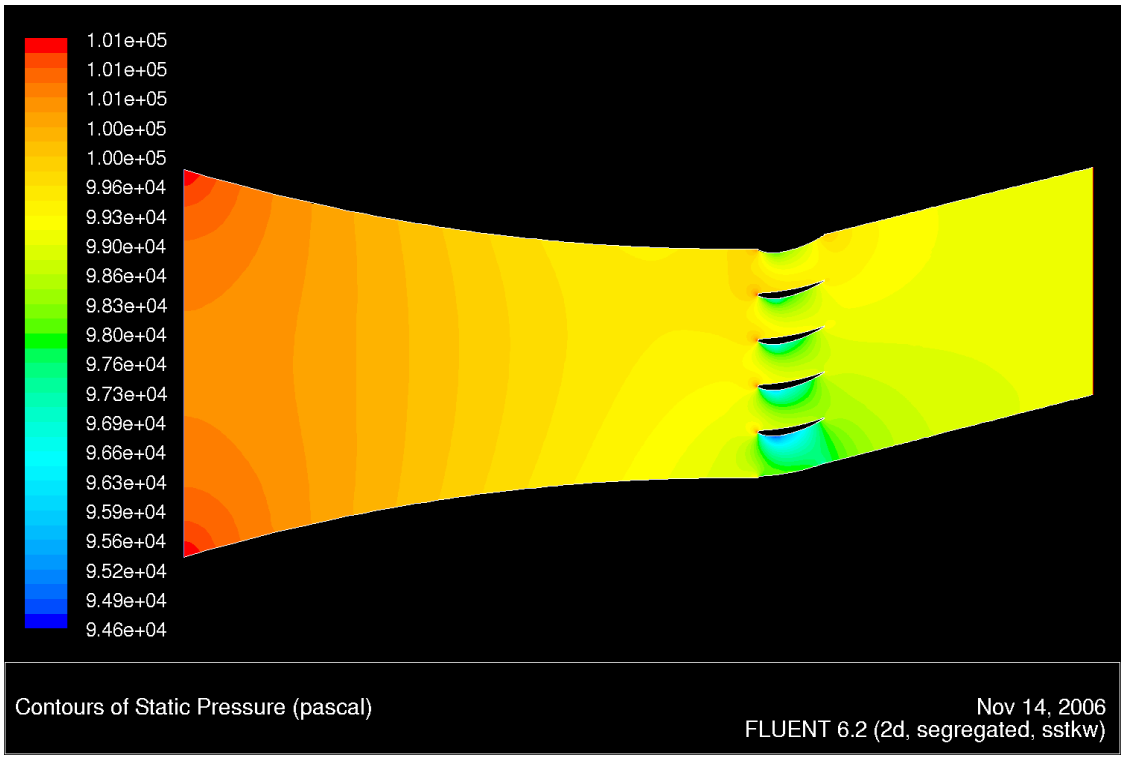

Figure 4-23 Results of CFD analysis for the static pressure distribution (4 blades configuration).

The Mach number in the inlet of the passage was 0.29 (see Figure 4-24). The 5th passage of the flow was lightly accelerated due to the change of the flow direction; however the influence of this in the velocity distribution was not significant (see Figure 4-25).

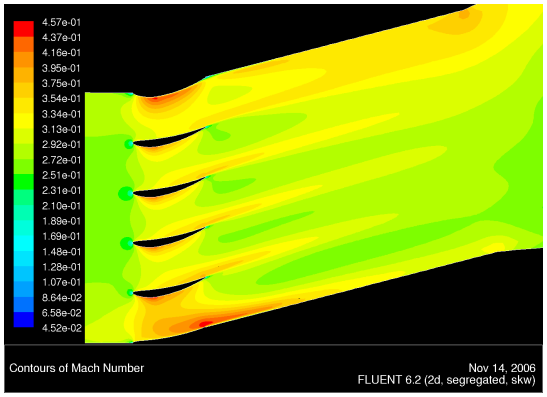

Figure 4-24 Contours of Mach Number by the CFD analysis (4 blades configuration).

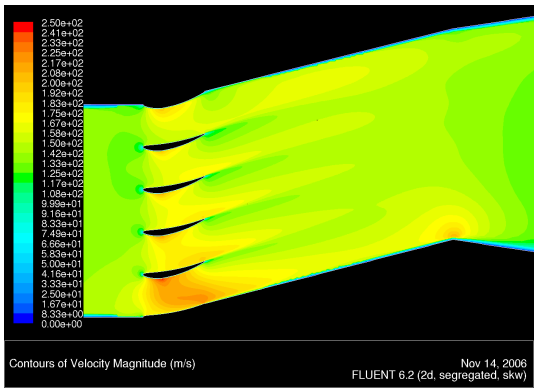

Figure 4-25 Contours of Velocity Magnitudes by the CFD analysis (4 blades configuration).

4.3.4.4 Discussion

One of the reasons to have a big number of passages is the gradual elimination of the lateral wall effect in the flow. However, the space limitation in the laboratory

obligated to scale the cascade size. According to the previous results, the uniformity and distribution of the flow in passages 2, 3 & 4 was acceptable. The central passage (3^{rd}) was selected as the study region for the experimental tests and for the CFD study, the inlet velocity in this passage was 99 m/s with a Mach number of 0.29.

4.4 Experimental validation of two dimensional flow

The configuration of 4 blades and the aerodynamic walls produced a uniform flow distribution in the cascade. The result from the CFD was based on two dimensional conditions of the flow. However, it was important to assure that the flow in the cascade was not affected by three dimensional effects. The three dimensional effects could be produced by the presence of recirculation and vortex in the cascade region. The assumption of two dimensional flow conditions is demonstrated based on experimental tests of flow visualization.

As was mentioned in Chapter 2 there are many visual techniques of flow visualization. The most common is the "smog visualization" used to describe the tracking of the stream lines. This technique is used for slow flow velocity (10 m/s) to assure that the smog is not dissipated at the moment it comes in contact with the flow. The velocity inlet in the cascade was approximately 100 m/s and for that reason the smog visualization was not selected. Another visualization technique is the use of TiO (oxide of titanium) that is used to find out the flow behaviour on the surface of the blade.

The TiO technique consists of mixing the titanium powder oxide with kerosene. The final mixture is applied to the surface in a thick layer. The study surface is in contact with the air stream and the kerosene is evaporated leaving on the surface the TiO particles that are used to track the flow path. The advantage to use this technique is that the blade surface is not damaged by corrosion or erosion and the airfoil can be used for the further studies. This technique does not require any special equipment and offers a cheap solution. With this technique it is possible to detect turbulence and bubbling formation region on the blade surface.

The objective of this technique in this research was to identify if the blade surface is affected by three dimensional effects produced by the blade surface. The correct proportion between titanium powder oxide with kerosene was calculated empirically. Because, if the mixture is extremely dry or wet incorrect results can be interpreted by this technique.

4.4.1 Results for the 1st test of flow visualization test by oxide of titanium

The application of the mixture on the blade surface was made with a brush in the axial direction to help to easily localize the tangential path of the flow (see Figure 4-26). The first test consisted of mixing 5g of titanium powder oxide with 50 ml of kerosene.

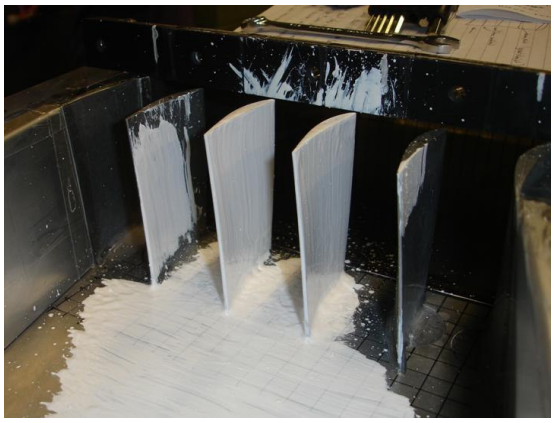

Figure 4-26 Application of mixture of TiO and Kerosene on blades to visualize the flow path (pressure surfaces).

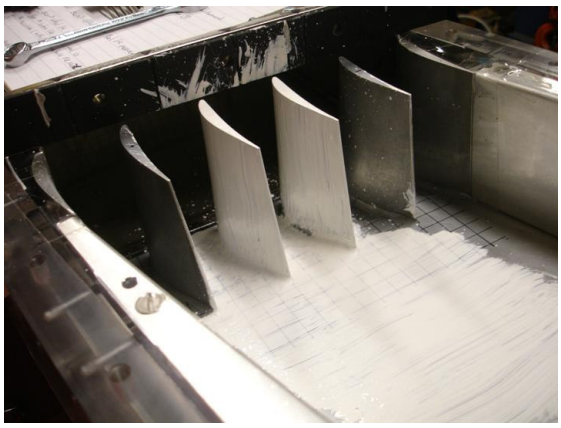

Figure 4-27 Application of mixture of TiO and Kerosene on blades to visualize the flow path (suction surfaces).

The results showed that on the leading edge region the track of the flow was not tangential. This result could be evidence of a early flow separation due to boundary layer separation and bubbles formation (see Figure 4-28 and see section 2.5.5).

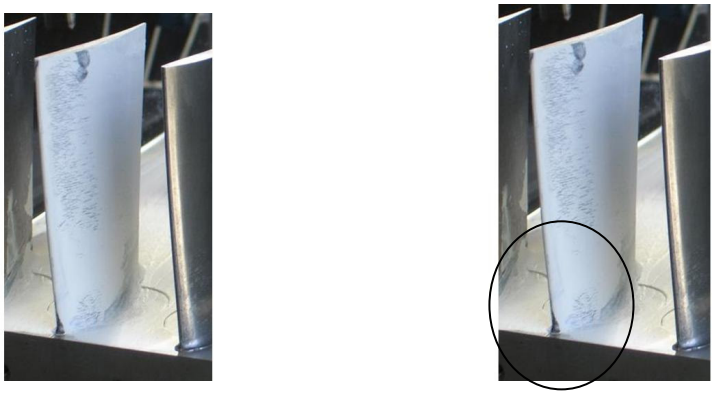

Figure 4-28 1st test result of TiO flow visualization. The circle indicates the region that was not modified by the flow path.

4.4.2 Results of flow visualization by wool trajectories

According to the study by Hobson, Hansen, Schnorenberg, and Grove (2001) the bubbles were usually generated after the half chord of the blade and not at the leading edge. A second different technique was used to check these results from the TiO visualization technique. This consisted of attaching small pieces of wool to the blade surface in order to visualize the possible boundary layer separation (see Figure 4-29). The result of this technique demonstrated that the wool was attached all the time to the surface. This result demonstrated that maybe the mixture of TiO and kerosene was dried before to be in contact with the air stream.

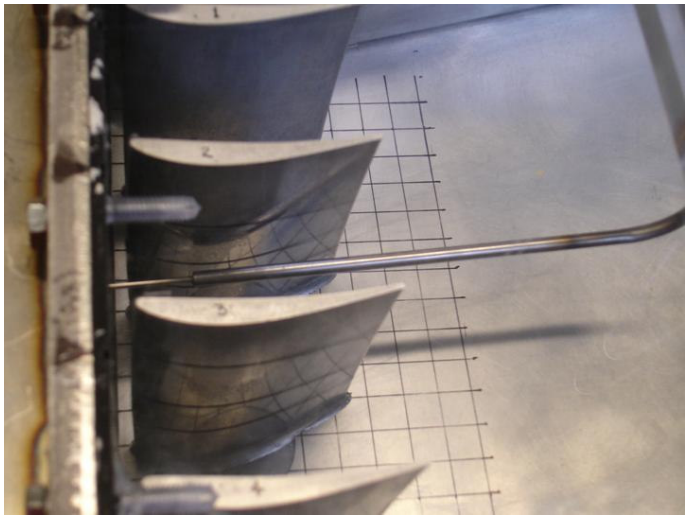

Figure 4-29 Results of attaching pieces of wool to the blade surface in order to visualize boundary separation.

4.4.3 Second test of flow visualization by oxide of titanium

The tests showed that to be successful the mixture must be made up of 5g of TiO and 100 ml of kerosene. This empirical result allowed for enough time (5 min) to apply the mixture on the blade surface and to operate the test rig. The results demonstrated that the flow path was completely horizontal and parallel to the blade surfaces (see Figure 4-30). It can be assumed from this result that the flow is two dimensional in this particular region of the cascade (blade surface). The head shape the blade incidence angle did not reproduce any three dimensional effect of consideration (see Figure 4-31). In addition, this characteristic demonstrated that the flow arrived to the

cascade inlet uniform in the three axes. The flow trajectory after the passage is driven by the direction of the walls.

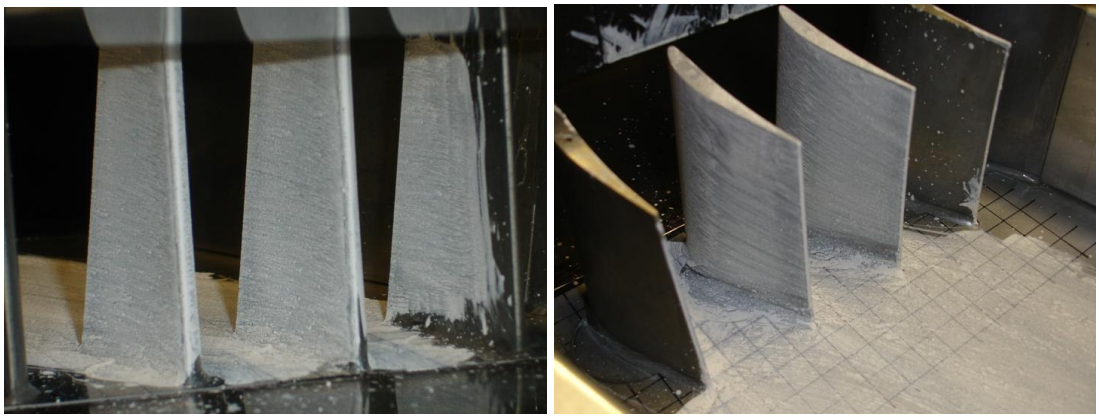

Figure 4-30 Flow trajectory visualization on pressure surface (left) and suction surface (right) by TiO visualization.

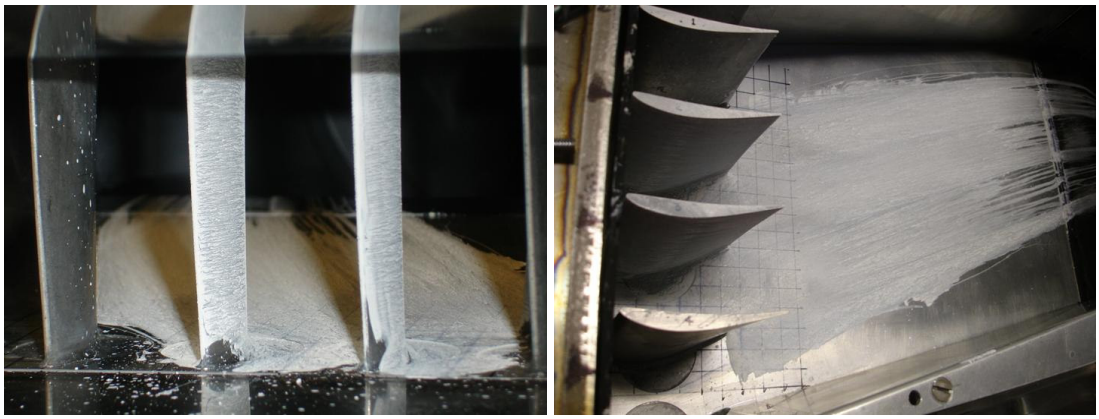

Figure 4-31 Flow trajectory visualization on the front leading edge (left) and outlet passages (right) by TiO visualization.

4.5 Study of three dimensional flow effects in the cascade

The three dimensional CFD model was created to study the internal effects of the flow in the cascade. Models of this type are complex and laborious studies that involve long periods of computational time. In the case of FLUENT the number of cells is limited and then it was necessary to reduce the precision for the three dimensional model. This was one of the reasons that are not suggested to study the boundary layer region in three dimensional CFD models. However, the advantages of three dimensional models are the macro-results of the flow and the possibility to estimate some aerodynamic parameters from the blade surface.

The three dimensional model only included the inlet of the wind tunnel and the cascade section. The boundary conditions were adjusted according to the ambient conditions at the inlet of the test rig and cascade outlet (experimental static pressures values). The mesh included 3.5 million nodes distributed in a structured mesh around the blades and an unstructured mesh for the rest of the section. The model selected was the k-ω with the wall function active to estimate the three dimensional effects near to the walls. The walls were considered as non-slip walls with the default turbulence factor from FLUENT.

4.5.1 Three dimensional results of velocity and vortex

Following the same procedure from the two dimensional study, the solution converged after 15,000 iterations. The results of the velocity distribution in the passages were acceptable with a velocity difference between the 1st and 5th passage of 10 m/s (see figure Figure 4-32). This result was similar to the two dimensional analysis (Figure 4-32). There was no evidence of three dimensional effects due to vortices or walls that affected the middle section of the blade (see Figure 4-33).

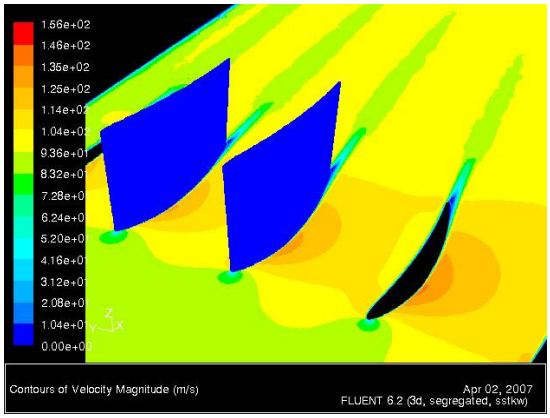

Figure 4-32 Three dimensional Velocity Distribution

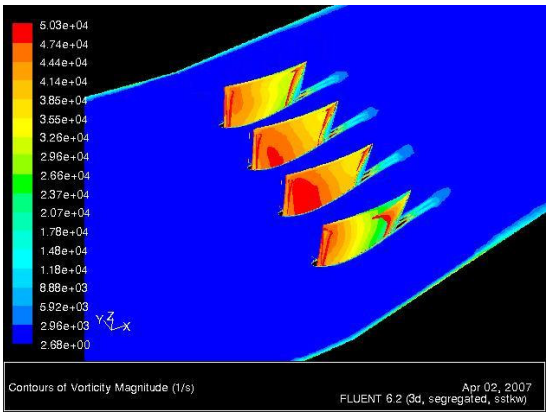

Figure 4-33 Three dimensional Vorticity Distribution and blade wake location.

4.5.2 Three dimensional results of pressure surfaces

The parameter of the surface pressure is an important indicator of the flow distribution. This parameter was not possible to measure with the instrumentation

available in the laboratory, so the three dimensional results from the CFD model were used to calculate this parameter. The distribution of the static pressure on the blade surface was uniform (see Figure 4-34). This parameter demonstrated that the two dimensional result was similar to the three dimensional model (see Figure 4-35).

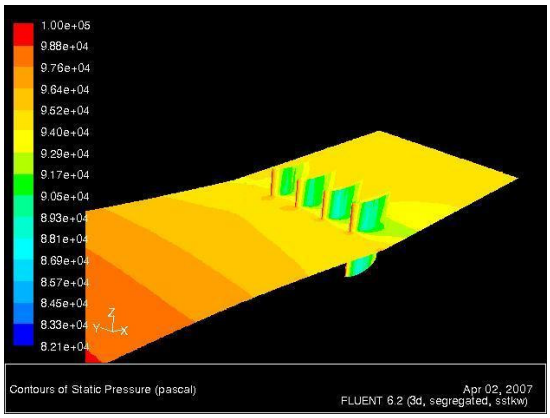

Figure 4-34 Static Pressure Distribution in the middle section of the blade section in study.

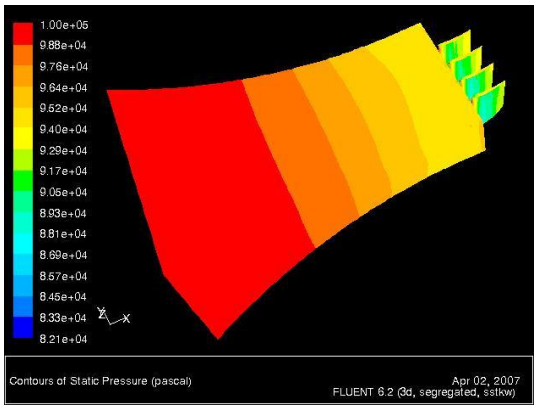

Figure 4-35 Three dimensional distribution of the static pressure in the inlet section of the wind tunnel.

The leading edge of the suction surface showed the highest values of the static pressure due to the normal-impact of the air stream on this region of the blade. The static pressure distribution on this surface was progressively decreased to 33% of the chord (maximum velocity due to blade profile, see previous Figure 4-35). After this point the static pressure was gradually increased until the trailing edge region. The evidence of recirculation or bubble formation on the surface was nil (see Figure 4-36). In the case of the pressure surface, the static pressure was progressively decreased from the leading to the trailing edge (see Figure 4-38).

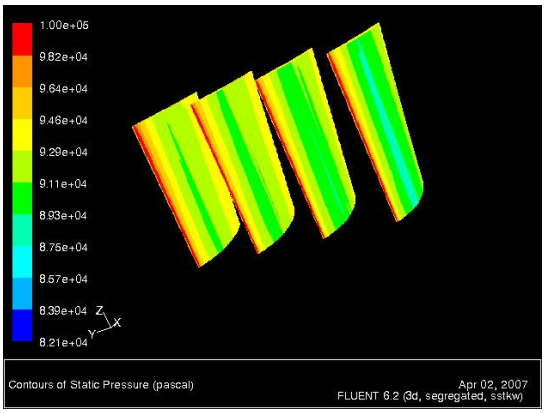

Figure 4-36 Static Pressure Distribution on suction surface in three dimensional.

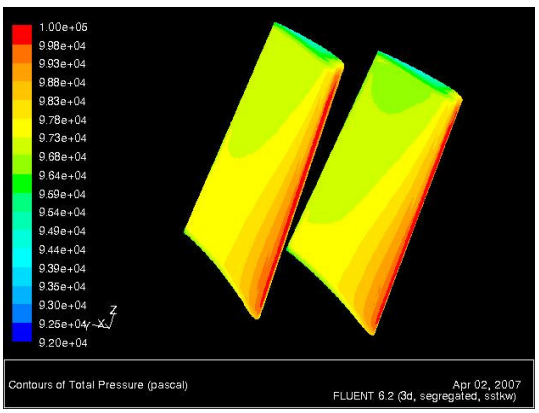

Figure 4-37 Static Pressure Distribution on pressure surface in three dimensional.

The total pressure distribution on the blade surfaces was calculated by the CFD model. In both surfaces of the blade the total pressure was gradually decreased from the leading to the trailing edge.

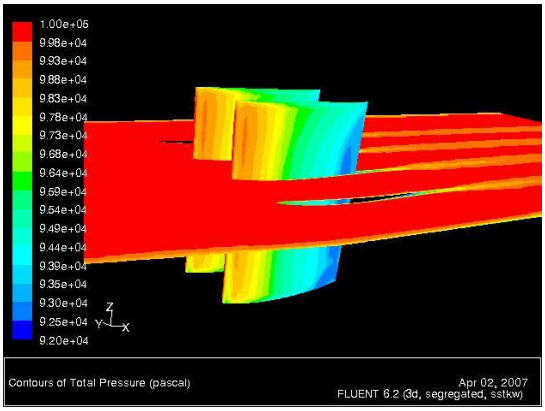

Figure 4-38Total Pressure Distribution suction surface three dimensional.

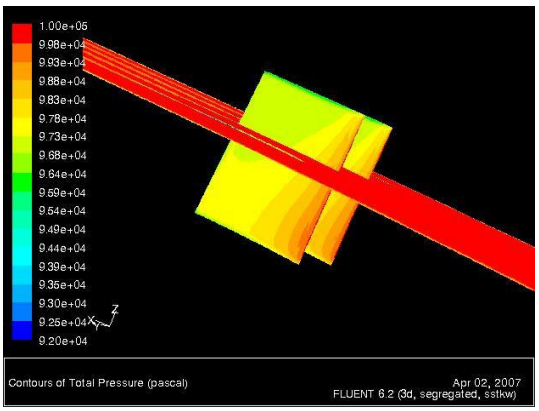

Figure 4-39 Total Pressure Distribution pressure surface three dimensional

These results illustrate the combination of information between the experiment and the CFD. Although, the three dimensional study was not highly precise and accurate the results demonstrated an acceptable flow distribution in the macro-scale.

4.6 Experimental validation of aerodynamic parameters with the CFD model

This section compares the experimental results and the CFD results. The two dimensional model was used to post-process the information and study the boundary layer region. Transversal study lines were added into the CFD model to calculate the transverse velocity profile of the flow (see Figure 4-41).

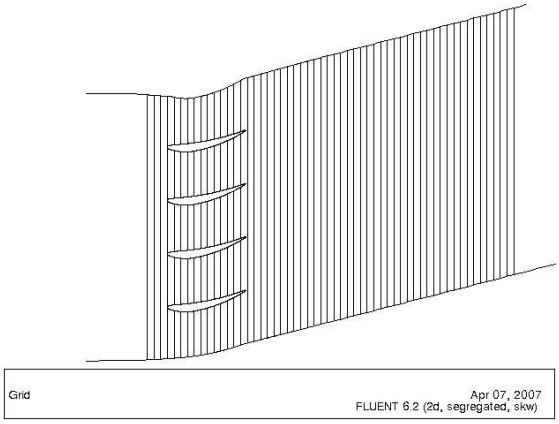

Figure 4-40 Representation of the cascade section in the CFD model and Lines of study (30 lines).

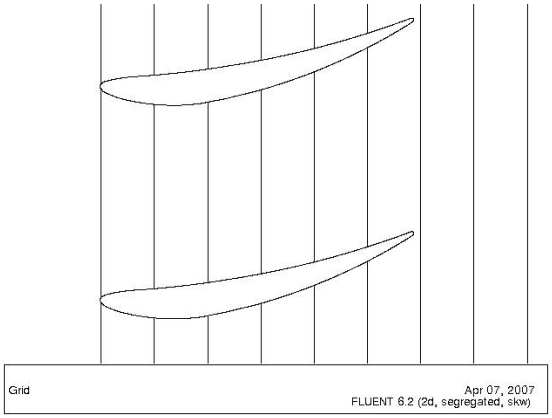

Figure 4-41 Representation of blade passage in the CFD mode (lines: 111, 113, 115, 117, 119, 121, 123, 125, 127, distance between each line 5mm).

4.6.1 Total Pressure Profiles and localization of wake

In the case of the experiment, the Pitot tube was introduced in the 3rd passage to measure the total pressure distribution of the flow. This instrument was used to locate the blade wake when the pressure in the Pitot tube dropped. The geometrical location of the wake was used to adjust and compare the CFD model.

The total pressure profiles presented in the following charts corresponded with the final results*. The experimental results demonstrated that the total pressure profile at Line-111 (passage inlet) presented some fluctuations in the inlet (see Figure 4-42) and the same case was observed in the CFD close to the surfaces (Figure 4-43).

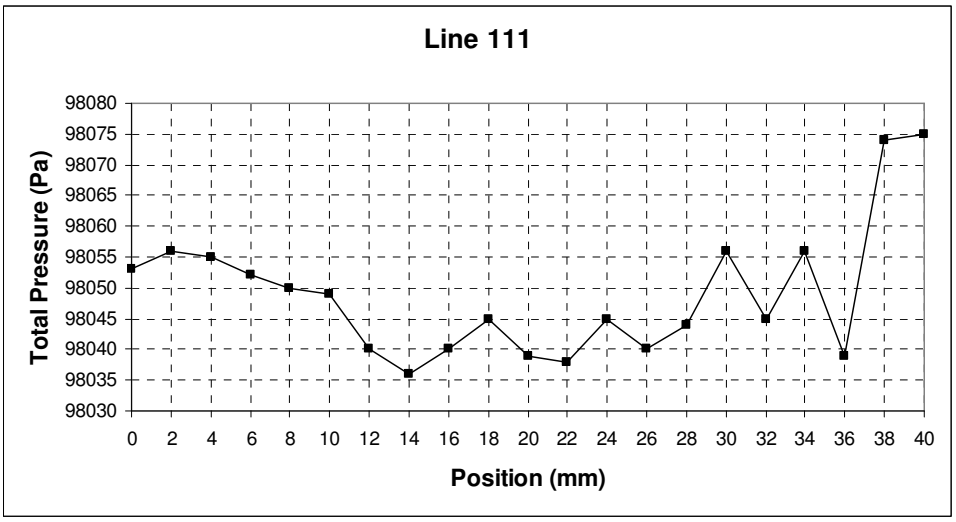

Figure 4-42 Test rig result of the total pressure distribution in Line 111 (inlet passage).

* In the case of the experiment, the origin was located at the suction surface of blade-3 (passage) and in the case of the CFD the origin was located on the right side wall. However, the absolute distance was in both cases the same (40mm).

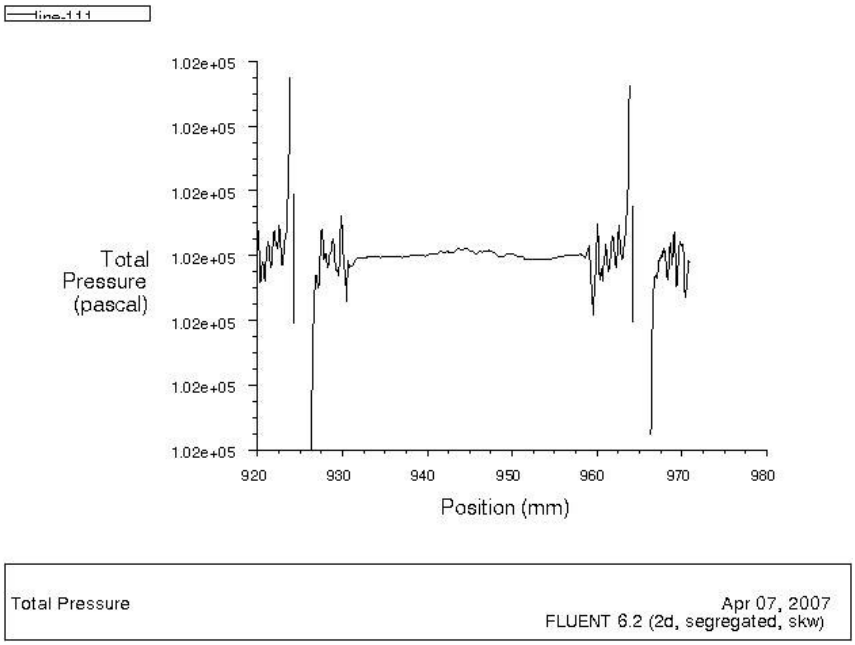

Figure 4-43 CFD result of the total pressure distribution in Line 111 (inlet passage).

The total pressure distribution from the experimental results was constant between Line-112 to Line-122. The same effect was obtained from the CFD model (see Figure 4-44).

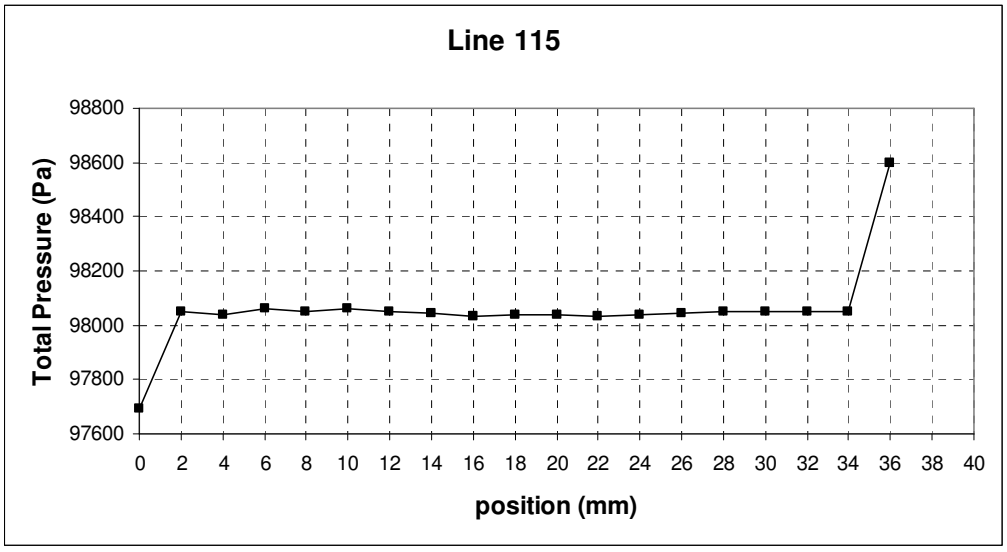

Figure 4-44 Test rig result of the total pressure distribution in Line 115 (inlet passage).

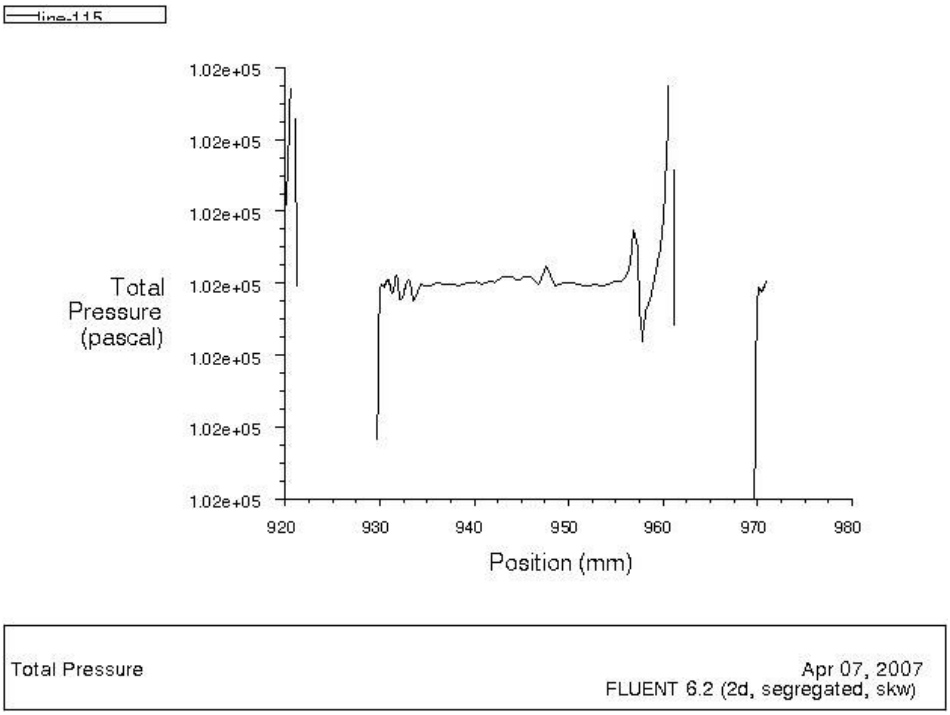

Figure 4-45 CFD result of the total pressure distribution in Line 115 (inlet passage).

The Line-122 represents the end of the blade surface, after this point the blade wake was localized by the following lines (123 to 131. The shape and localization of the wake was the same that the CFD result (see Figure 4-47). It is possible to observe in both figures the width of the blade and the direction tendency.

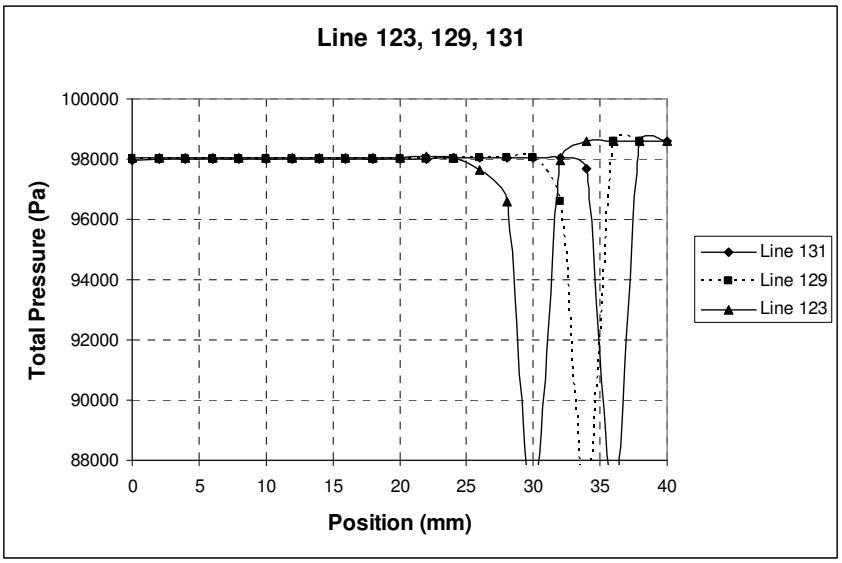

Figure 4-46 Test rig result of the total pressure distribution in Lines 123,129,131

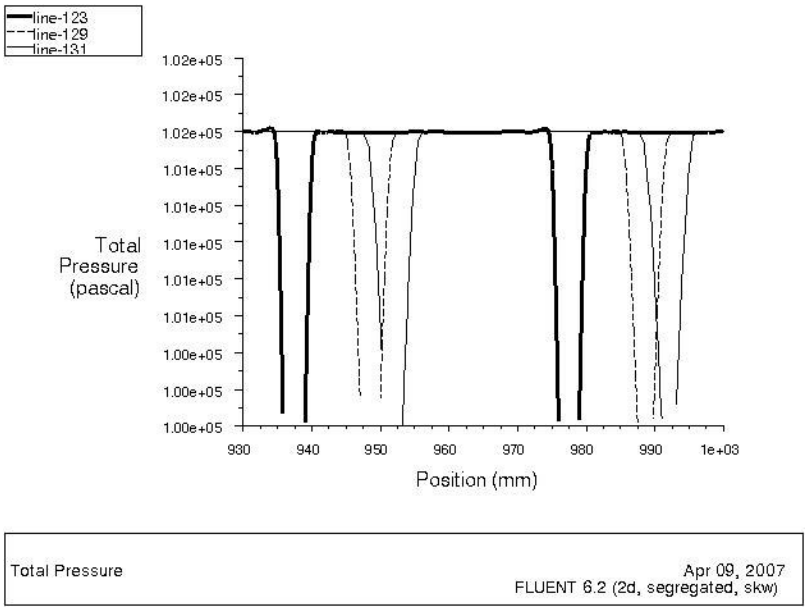

Figure 4-47 CFD result of the total pressure distribution in Lines 123,129,131

The CFD results calculated the total-pressure distribution from the passage in study (see Figure 4-48). The velocity (see Figure 4-49) and Reynolds Number distribution (see Figure 4-50) in the passage were calculated by the CFD model.

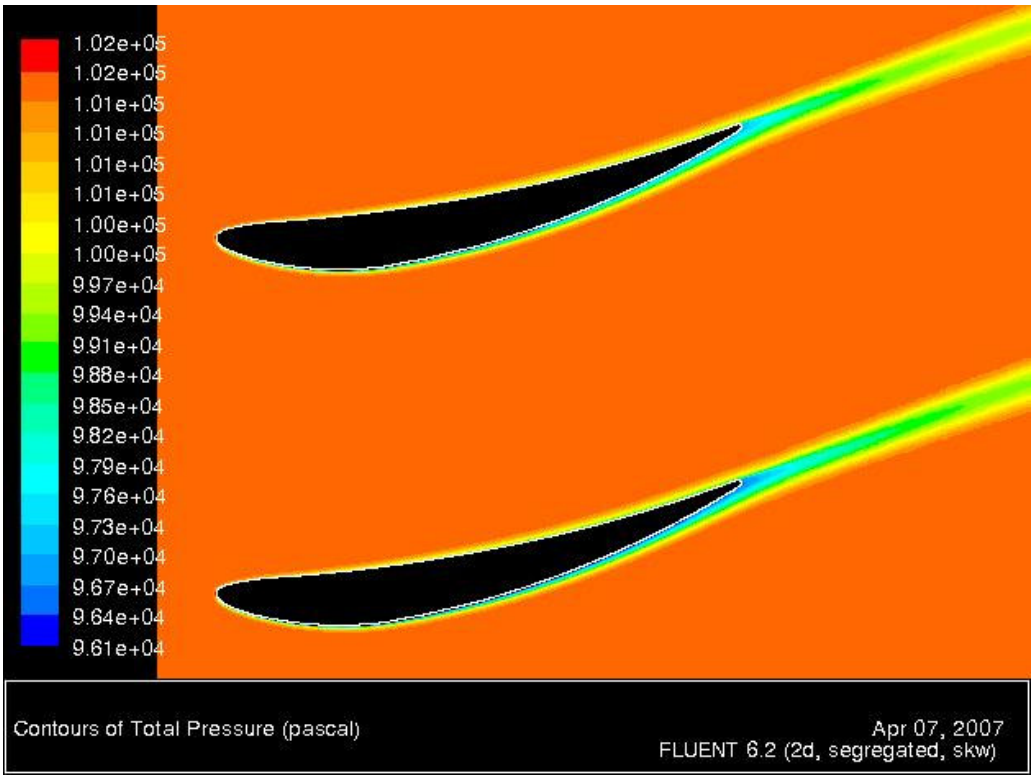

Figure 4-48 CFD result of the total pressure distribution in the 3rd passage.

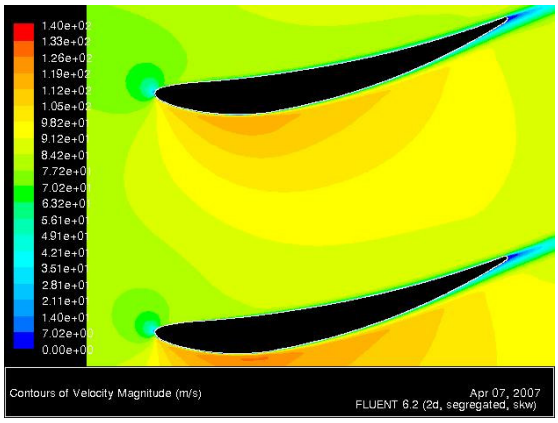

Figure 4-49 CFD result of the Velocity distribution in the 3rd passage.

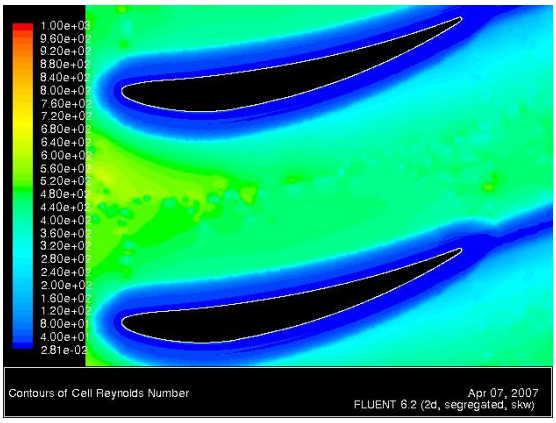

Figure 4-50 CFD result of the Reynolds Number distribution in the 3rd passage.

4.6.2 Boundary Layer analysis

The boundary layer region is localized near the blade surface. The phenomenon involves a micro-scale study. In this study the boundary layer region was represented by the velocity profile close to the blade surface. The velocity of the flow in this region was gradually increased from zero in the surface to the main flow velocity (see Figure 4-51). The effects of viscosity and surface smoothness (roughness) dominate the behaviour of this phenomenon. The aerodynamic of the blade is designed to reduce the losses produced by early separation of the boundary layer from the blade surface. These losses are quantified with the drag of the blade. According to the CFD results (see Figure 4-51), the value of the Reynolds Number in this region was between 0 and $1.6x10^3$. This result means that the viscosity effects can be depreciated and only the surface smoothness controls the physical phenomenon of the boundary layer (Meher-Homji and Cyrus B (1990). The boundary layer was studied on each surface of the blade (suction and pressure surfaces) based on the CFD model. This region was created with a structured mesh ring of 2mm around the blade and with distance nodes of 0.05 mm. The results are represented by the velocity profile in different positions of the blade (see Figure 4-51).

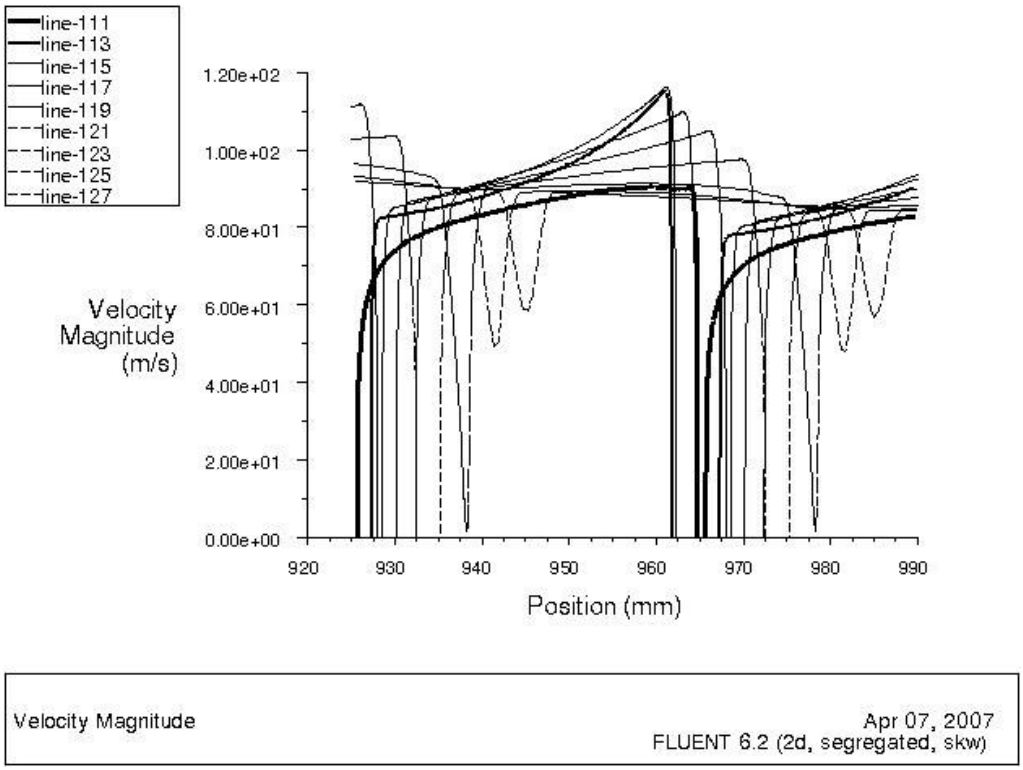

Figure 4-51 Boundary layer region represented by the velocity Profiles in the 3rd passage (CFD result).

The inlet of the passage (Line-111) resulted that in the pressure surface of the boundary layer being laminar. In the velocity profile (see Figure 4-52) the gradual velocity increment was up to 1mm. from the surface. The transition point and separation were presented together.

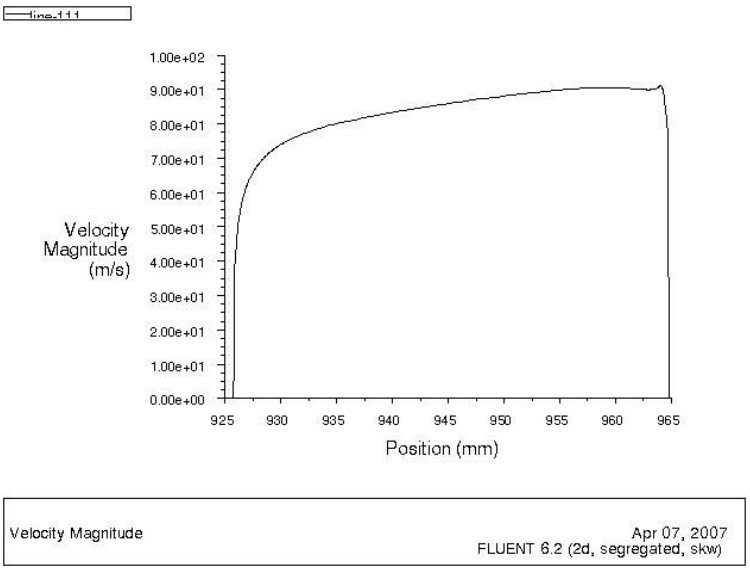

Figure 4-52 Velocity Profile of line-111 (inlet of the passage).

The boundary layer from the suction surface presented a transition point very close to the surface. The thickness of the turbulent boundary layer was approximately 4 mm before the separation (see Figure 4-53).

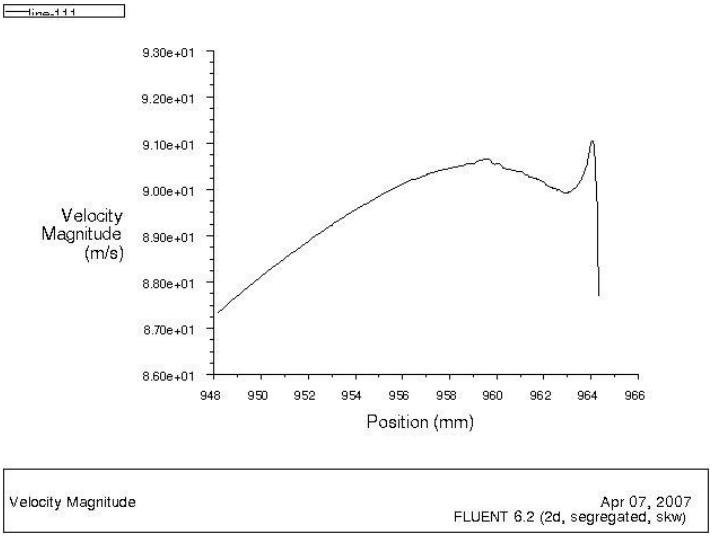

Figure 4-53 Boundary layer region in the suction surface represented by the velocity profile from Line-111.

From the pressure surface it could be observed that the transition point was presented at 1 mm from the surface in Line-112 (see Figure 4-54). In this point, the turbulent layer thickness was approximately 3 mm before it produced the separation.

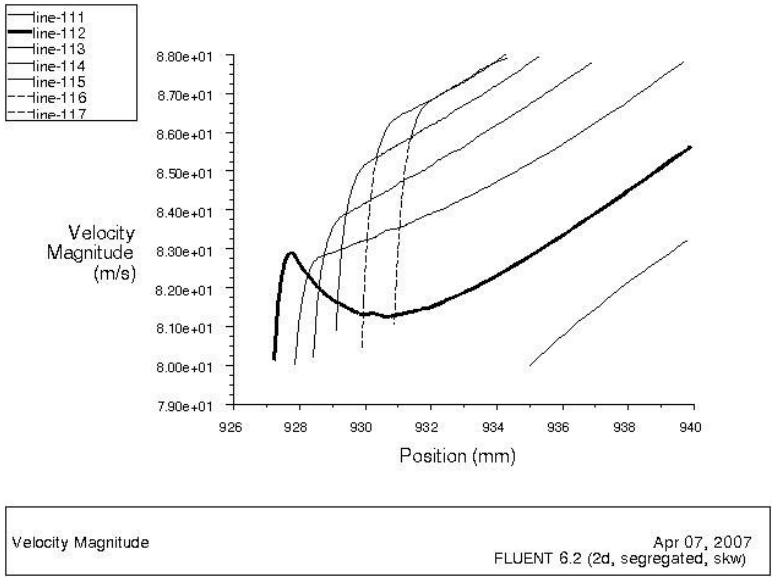

Figure 4-54 Boundary layer represented by flow velocity profiles from 0 to 50% chord of the blade on pressure surface.

The following velocity profiles down stream demonstrated that the boundary layer was laminar until separation (Figure 4-55).

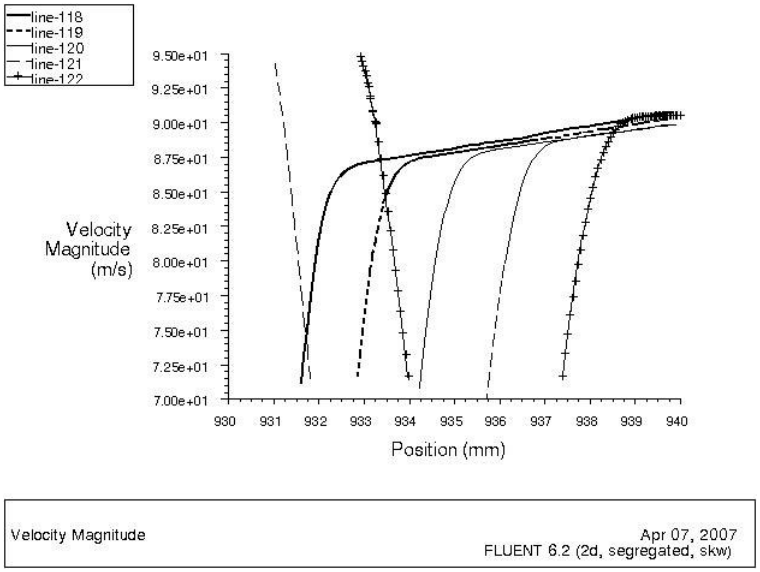

Figure 4-55 Boundary layer represented by flow velocity profile from 50 to 100% chord of the blade on pressure surface

The suction surface resulted in a laminar boundary layer until the separation (see Figure 4-56). The thickness of the boundary layer was reduced down stream to 30% of the chord. The change of the flow direction produced an increased in the thickness of the boundary layer. However, there was no evidence of turbulent region (see Figure 4-57).

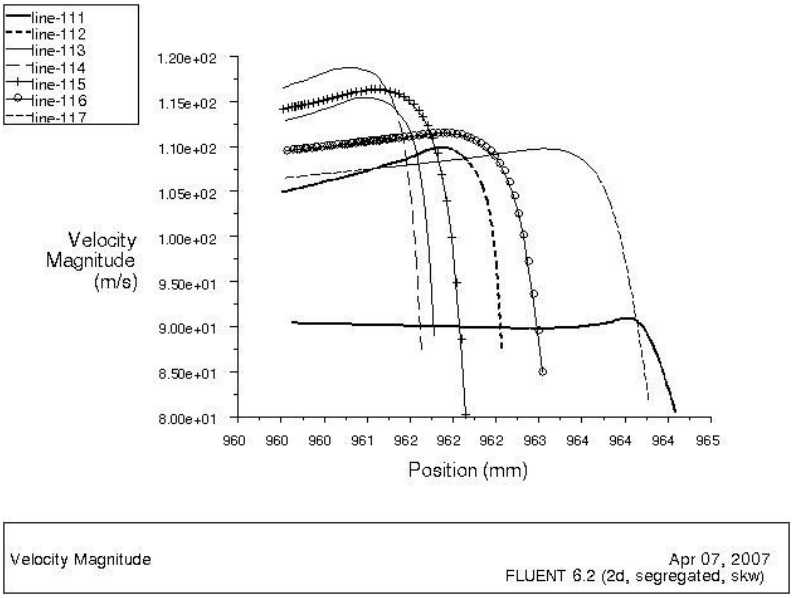

Figure 4-56 Boundary layer represented by the flow velocity profile from 0 to 50% chord of the blade at suction surface.

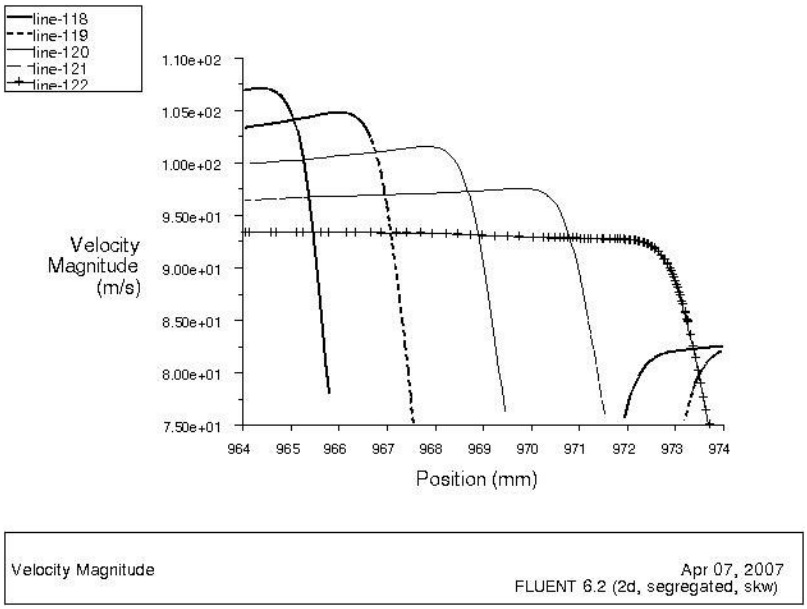

Figure 4-57 Boundary layer represented by the flow velocity profile from 50 to 100% chord of the blade at suction surface.

The results from the pressure surface demonstrated that the laminar regimen in the boundary layer was gradually reduced downstream. However, the effects of the turbulent region were not observed from the velocity profiles. This means that the transition point and the boundary layer separation occurred almost at the same time. The concave shape of the pressure surface decreased the thickness of the boundary layer region until the middle chord and after this it was again increased. The verticality of the line represents the thickness of the laminar region. In the case of the suction surface the boundary layer region tended to increase the thickness at the middle chord. This effect was due to the blade profile that changed the direction of the flow. In the trailing region of this surface the boundary layer was attached close to the surface.

The boundary layer effects under this condition are summarized in the following four points.

i. There was not presented boundary layer separation, recirculation or bubbles.

ii. The velocity profiles from the passage demonstrated uniformity in the flow.

iii. The middle section of the blade on the surface suction presented a change of velocity and boundary layer region due to the aerodynamic shape of the blade and change of direction.

iv. The head of the blade in both surfaces presented changes in the boundary layer region due to the impact of the air in the blade surface.

5 FOULING MODEL

5.1 Introduction

Fouling is one of the most important degradation mechanisms present in gas turbine compressors. Chapter 2 mentioned that the mechanism of fouling on blades has not been studied and many unknowns about this phenomenon remain. In this study, the problem of compressor fouling has been associated with the blade aerodynamics and gas turbine performance. The particular parameter of the surface roughness has been selected to measure the fouling.

The information presented in this chapter includes the most important result of this research. The result of the fouling mechanism was obtained from a preliminary experimental model. The validation of these experimental results was based on two sources of information: the results from the CFD study and the information recorded from industrial engines in operation. As it is going to be presented in this chapter, the mechanism of fouling was evident. The modification of the blade surface changed the blade aerodynamics.

This chapter is divided into four sections. The first section includes information about the real operation of industrial gas turbines in order to know the conditions to reproduce in the test rig. The second section presents the design of the fouling system. The third section shows the experimental results from the fouling process on the blades. The last section summarizes the results in a first approach mathematical model to describe the fouling mechanism. In this last section is presented the study of the boundary layer under fouling conditions.

5.2 Preliminary experimental conditions

The fouling system was designed with the assumption that the flow travels uniform inside the cascade. It was assumed that the dust particles mixed with the air in a uniform manner. However, in the real application this distribution of the dust in the

air stream is a random condition due to different sized particles. The blades used for the test rig were adapted based on new conditions. This condition implies that the surface roughness value was constant over the whole surface.

5.2.1 The blade surface roughness

Information about the blade surface roughness is very limited in the public domain due to the policy of the companies. Few values of the surface roughness in the literature are reported based on arbitrary assumptions. However, this parameter was essential in this study to understand the phenomenon of fouling. It was necessary to obtain this value using a special instrument to measure the surface roughness. The electronic and portable unit model Surtronic-25 manufactured by Taylor Hobson Precision Ltd was used for this propose (see Figure 5-1).

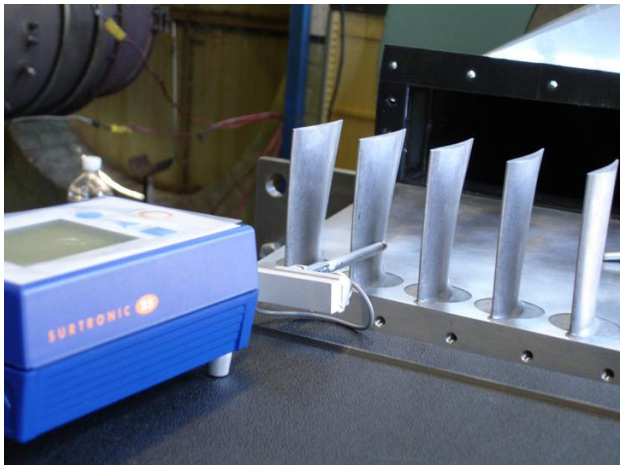

Figure 5-1 Recorded data of the blade surface roughness by the instrument Surtronic-25 Taylor & Hobson.

The instrument reads the surface roughness with a stylus sensor and the information is transmitted into a special program to create the surface roughness profile. The scale selected to analyze the surface roughness was the roughness average (Ra=µm)[*]. The operational characteristics of the instrument are presented in Table 5-1.

[*] For further information about the surface roughness theory see: Leigh Mummery, Surface Texture Analysis - The Handbook, Hommelwerke, 1990.

Power Source	Alkaline Battery 6 volts
Environment operation	Temperature 5~40C Humidity 0-80% non condensing
Traverse Speed	1 mm/s
Traverse distance (cut-off)	0.25, 0.8, 2.5 mm
Display	LCD-matrix 8 lines x 20 characters
Filter	Digital Gauss filter or 2CR filter (ISO)
Parameters	Ra, Rz, Rt, Rp, Rmr, Rsm, Rz1max, Rsk, Rda

Table 5-1 Specifications of Surtronic 25 (Taylor Hobson Ltd, 2001)

The surface roughness result of the experimental blade profile was Ra=0.756 µm (see Figure 5-2).

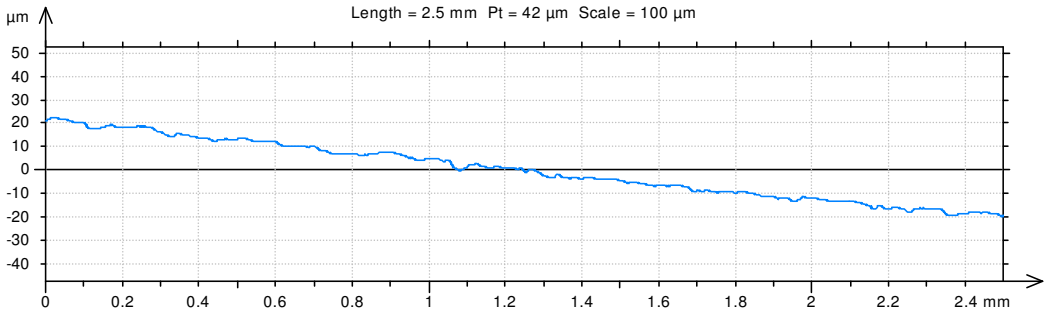

Figure 5-2 Surface roughness result of experimental blades before polishing process (suction surface). The Parameters calculated by mean of all the sampling lengths. A micro roughness filtering is used, with a ratio of 2.5 µm. Roughness Parameters, Gaussian filter, 0.8 mm was Ra=0.756µm[*].

During the literature review no reference was found about the value of the surface roughness of industrial compressor blades. In order to determine a standard value of this surface condition it was necessary to measure real blades. The first blade measured was the Rolls Royce compressor blade from the engine TRENT 900 † (Table 5-2).

High Pressure Compressor Blade GT TRENT 900	Radial direction (Ra µm)	Axial direction (Ra µm)
Rotor Row 1 suction surface	0.31	0.30
Rotor Row 1 pressure surface	0.22	0.27

Table 5-2 Surface roughness of the high pressure compressor blade manufactured by Rolls Royce for the GT Trent 900.

[*] Source, TalyProfile Silver software, (Taylor Hobson Ltd (2001)).
[†] Source: Blade available like a sample in Cranfield University.

The physical state of the Rolls Royce blade was unknown and according to previous reports this blade is generally covered with a coating. Also, this particular blade is for aero engines. Then, it was necessary to analyze a second sample of blades. The blades from the gas turbine Siemens model V94.3A were measured directly.

Compressor blades of GT SIEMENS V94.3A	Radial direction (Ra µm)	Axial direction (Ra µm)
New Stator Row 6 suction surface	0.64	0.52
New Stator Row 6 pressure surface	0.48	0.58
Clean Stator Row 2 suction surface	1.50	2.02
Clean Stator Row 2 pressure surface	1.58	2.32
Coating Blade Row 5 suction surface	1.68	2.18
Coating Blade Row 5 pressure surface	2.40	----
Sand-blasted IGV	3.64	3.2
Coating IGV suction surface	1.76	2.66
Coating IGV pressure surface	1.12	1.62

Table 5-3 Surface roughness of compressor blades manufactured by Siemens for the gas turbine model V94.3A [*].

The information obtained from the previous table was used to determine an average value of the surface roughness Ra=0.60µm (blade in new conditions found in Stator 6). The blades used in the test rig were manufactured by a casting process and it was necessary to polish[†] the surfaces to obtain a uniform value of the roughness on the whole surface (see Table 5-4).

Compressor Blade Prototype (Cranfield University)	Radial direction (Ra µm)	Axial direction (Ra µm)
Rotor Row 1 suction surface	0.61	0.62
Rotor Row 1 pressure surface	0.60	0.61

Table 5-4 Surface roughness of compressor blades prototype manufactured by Cranfield University

[*] Source: Personal visit to Power Plant Didcot in the overall maintenance of the GT unit-2 SIEMENS V94.3A

[†] The blades were polished with steel brass copper manufactured by AUTOSOL to obtain a roughness surface of 0.6µm

5.2.2 Dust Sample Description

Compressor fouling is produced by the particles mixed in the air that travels inside the compressor and they are deposited on the blade surfaces. A real sample of the dust that produces the compressor fouling was collected from the inlet filters of a gas turbine in Inchon Power Plant (South Korea)*.

Type	1Kg Grey Powder sample
Collected on	August 2005
Location	Inchon Power Station, South Korea
Gas Turbine Model	GE Frame 7FA
Type of Filter	Pre filter air inlets in filter housing to GT10
Surrounding description	Farm land, dusty, close to coast, sea aerosols, industrial pollution.
Power Plant description	CCGT 8 gas turbines of 150 MW and 4 steam turbines

Table 5-5 Dust sample collected from the inlet filters of Inchon Power Plant in South Korea.

The type of particles and concentration in the air were considered non-hardness. However, Inchon Power Plant is affected year by year by polluted clouds with a high concentration of carbon produced in China and sand from the coast. With this information, the sample of dust was classified with the following main components: sand (F1), ground-dust (F2), oil smokes (F3), fly ash (F4), insect swarms (F7), clouds & fog (F8&F9), rain (F10), fertilizer(F14) and pollens (F24). The chemical analysis of the dust with the Infra Red Analysis of Solid Particles was outside of the limit of this project.

The weather conditions were arbitrary adopted from the Didcot Power Plant in England due to information available (see Figure 5-3). The carbon source in Didcot Power Plant is produced from a carbon unit that operates in the same facility. The ambient temperature was 15 ºC and humidity was 75%.

* The dust sample was provided by the company Recovery Power Ltd.

Figure 5-3 Inchon Power Plant, South Korea (left), Didcot Power Plant, England UK (right)

5.3 Design of Fouling Injection System

There are many techniques available in the market to mix solid particles into the air stream. The most advanced technologies are used to transport chemical powder products such as detergents, paints, etc. It is common to find powder extractors in the trimmer and metal industries. However, these types of equipment are expensive and destined to transport large quantities of the product. The idea behind the fouling system in this experiment was to find an economic alternative which could be used to transport small quantities of particles. The design of the system was based on the sand-clock function and assisted with the pressure difference produced in the wind tunnel inlet.

5.3.1 Sections of the fouling injection system

The system included three sections:

1. Container to keep the dust powder
2. Hose to transport and deliver the powder into the air stream
3. Bracket to adjust the position of the injection point

The Container was a plastic cylinder graduated according to the dust sample weight in grams. The base of the cylinder was configured with an outlet-cone to control the pass of particles (similar to the sand-clock). The hose was connected to the outlet-cone to

transport the powder into the middle section of the bell mouth (Figure 5-4). The powder was forced to move into the hose due to the gravity and pressure difference from the wind tunnel inlet (house outlet). The dust was delivered to the air stream in a horizontal trajectory in the same direction of the flow. The vibration from this particular section avoided the build up of particles on the cylinder and hose.

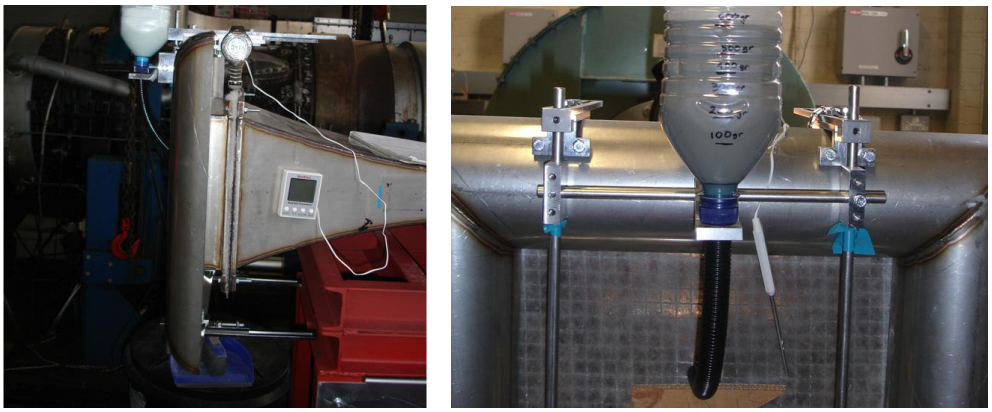

Figure 5-4 Fouling System lateral-view (left) and front-view (right).

5.3.2 Conditions of operation for the fouling system

The aim of this project was to reproduce an artificial deposition of particles on the blades based on real engine operation conditions. For that reason, it was necessary to record information from the real engines to know these operating conditions. The following considerations were taken in to account when was adjusting the fouling system in the test rig.

1. The test rig was configured according to the engine model of 1.2 MW*. Information from the public domain specified that the quantity of air that traveled in the cross area of the first stage is 1.4 kg/s (0.1964 m^2).

2. The concentration of particles from the air surrounding of Didcot Power Plant was arbitrary assumed to be 0.0046 g/m^3 (4.6E-6 kg/m^3) from (Giampolo (1997).

* Gas Turbine model Saturn 20 manufactured by Solar Turbines

3. The engine model of Didcot Power Plant was the engine of 240MW*, according to the public information this engine operates with a mass flow of 640 kg/s.

4. The filtration system was assumed to have an arbitrary efficiency of 90% (middle life).

Under these conditions the rate from the dust injection was calculated as follows.

- For the gas turbine of 240MW

Engine volume flow: $V = \frac{W}{\rho_{air}}$ =528 m^3/s

Equation 5-1

where: V = Volume flow

W = Air Mass Flow (640 kg/s)

ρ_{air} =1.21 kg/m^3

If η_{filter} =90% and the $Concentration1_{foulin/air}$ = 4.6E-6 kg/m^3, then concentration of particles after filtration was:

$Concentration2_{fouling/air} = (1-\eta_{filter}) \times Concentration1_{fouling/air}$ =4.6E-7 kg/m^3

The rate of particles mixed in the air inside the compressor was:

$Rate_{fouling} = V \times Concentration2_{fouling/air}$ =2.433E-4 kg/s = 875.9 g/hr

- For the gas turbine of 1.2MW

The volume flow of this engine was: $V = \frac{W}{\rho_{air}}$ =5.502 m^3/s

where: V = Volume flow

W = Air Mass Flow (6.2 kg/s)

If η_{filter} =90% and the $Concentration1_{foulin/air}$ = 4.6E-6 kg/m^3, then concentration of particles after filtration was:

* Gas Turbine model V94.3A manufactured by SIEMENS

$$Concentration2_{fouling/air} = (1-\eta_{filter}) \times Concentration1_{fouling/air} = 4.6E\text{-}7 \text{ kg/m}^3$$

The rate of dust inside the compressor was:

$$Rate_{fouling} = V \times Concentration2_{fouling/air} = 3.45E\text{-}6 \text{ kg/s} = 12.42 \text{g/hr}$$

The mass flow of the test rig was 1.4 kg/s equivalent to 22.58% of the total mass flow from the gas turbine of 1.2MW. Assuming this factor is correct, the results of the fouling rate are presented in Table 5-6.

Fouling Rate (mass/time)	GT 240MW	GT 1.2MW	Test Rig
g/second	0.2433	0.00345	0.000779
g/minute	14.59	0.207	0.0467406
g/hour	875.9	12.42	2.80
g/day	21,021	298	67.2884
g/week	147,147	2,087	471.24
g/month	4,414,435	9,240	2,086
g/year	52,973,222	110,880	25,036
g/overall maintenance (4years)	211,892,889	443,520	100,146

Table 5-6 Ideal scenarios of fouling rate for the Siemens V94.3A, Saturn 20 and Test Rig.

The quantity of the dust sample available was 700g. According to the results of the fouling rate (2.8g/h) this is equivalent to 10 days of continuous operation from the real engine.

5.4 Experimental results of fouling

The fouling system was tested in the experiment to evaluate the dust deposition according to information from the real compressor fouling. The information used to evaluate and validate the dust deposition was based on the fouling presented in the engine of Didcot Power Plant. Previous experiments were tested in the test rig with an artificial sample (Flour) to specify the operation condition of the fouling system.

i. Injection of artificial sample (flour powder)
ii. Injection of artificial sample (flour powder) with an artificial glue agent-1 (liquid oil UW40)

iii. Injection of artificial sample (flour powder) with an artificial glue agent-2 (liquid grease)

iv. Injection of the real dust sample (Inchon Power Plant).

5.4.1 First test (artificial powder)

The flour powder was selected due to the white colour that was easy to detect on the blade surface by visual inspection. The size and consistence of the flour particles was similar to the real dust sample. The injection rate was adjusted to 100 g/h during 7 hours. Each hour of dust injection was equivalent to 36 hours of operation from the real gas turbine based on the concentration of particles. The results demonstrated that the particle deposition on the blade surfaces was poor. A very light deposition of flour was observed on both surfaces after 3 hours of operating the artificial fouling system (equivalent to 300g of powder injected). After 7 hours of operation the suction surface presented an increment for the particle deposition (see Figure 5-5). On the pressure surface the fouling phenomenon was only observed on the leading region (see Figure 5-6).

Figure 5-5 Artificial powder deposition on suction surface after 7 hours of test rig operation (injection rate of 100g/hr).

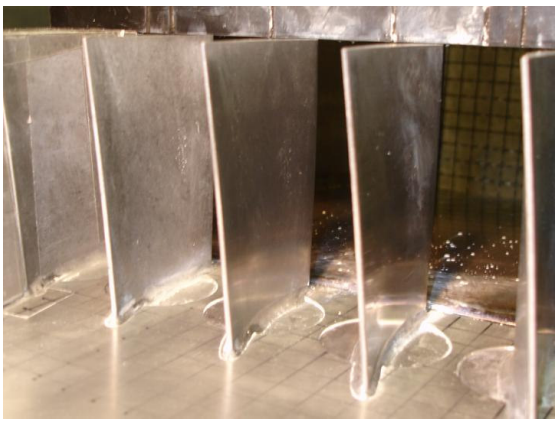

Figure 5-6 Artificial powder deposition on pressure surface after 7 hours of test rig operation (injection rate of 100g/hr).

On both surfaces it was possible to observe deposition from the artificial powder on the leading edge. The pressure surface presented the biggest area of particle deposition on the leading edge region of 4mm^2, however the deposition on the suction surface was only 1mm^2 (see Figure 5-8).

Figure 5-7 Artificial powder deposition on the leading edge (suction surface) after 7 hours of test rig operation (injection rate of 100g/hr).

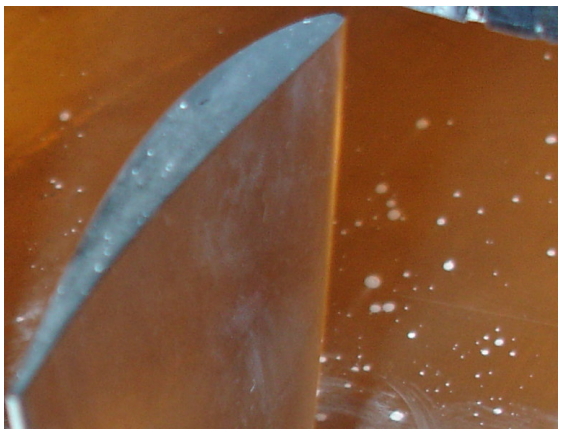

Figure 5-8 Artificial powder deposition on the leading edge (pressure surface) after 7 hours of test rig operation (injection rate of 100g/hr).

5.4.2 Second test (artificial powder and glue agent-1)

Due to the poor particle deposition on the surfaces from the previous test, it was necessary to change the conditions of operation. A second experiment was tested using the same rate of injection but with a glue-agent layer on the blade surfaces. The glue-agent was the commercial UW40 oil. The blades were covered with a thin layer of this oil to increase the particle deposition on the blade surfaces. The flour powder was injected following the same procedure as the first experiment. The results are presented in the following table and the photos illustrate the phenomenon of deposition.

Rate of 100g/h	Artificial flour deposition with a UW40 layer on the blade surfaces
1h =100g (equivalent a 1.5 days of engine in operation)	Pressure: The adhesion of particles was higher than the previous test. For example, on this surface a heavy deposition of particles was found on the leading edge and tip. This deposition was gradually reduced in the direction of the trailing edge and root (see Figure 5-9). Suction: This surface presented a light deposition of particle over the whole surface (see Figure 5-10).
2h =200g (equivalent a 3 days engine in operation)	Pressure: The deposition of particles was gradually increased in this region. The region close to the roof and floor presented higher particle deposition than the middle region (see Figure 5-11). Suction: The deposition of particles increased on the leading region and tip (see Figure 5-12).
3h =300g (equivalent a 4.5 days engine in operation)	Pressure: The deposition of particles formed a symmetrical shape, where the heavy concentration was close to the walls (see Figure 5-13). Suction: The deposition of particles was increased on the leading region and the trailing region (see Figure 5-14).

4h =400g (equivalent a 6 days engine in operation)	Pressure: The rate of particle deposition was reduced on this surface (see Figure 5-15). Suction: The fouling was increased only in the same regions (leading and close to trailing region) (see Figure 5-16).
5h =500g (equivalent a 7.5 days engine in operation)	Pressure: The high accumulation of particles in specific locations formed small peaks that produced increments in the drag (see Figure 5-17). Suction: The rate of particle deposition was reduced on this surface (see Figure 5-18).
6h =600g (equivalent a 9.0 days engine in operation)	Pressure: The rate of particle deposition was considerable reduced on this surface (see Figure 5-19). Suction: On the leading edge region (close to the tip) was found an increment of deposition of particles (see Figure 5-20).
7h =700g (equivalent a 10.5 days engine in operation)	Pressure: The rate particle deposition was almost nil on this surface (see Figure 5-21). Suction: The rate of particle deposition was also nil on this surface (see Figure 5-22).

Table 5-7 Results of artificial fouling from the artificial powder at rate of 100g/h

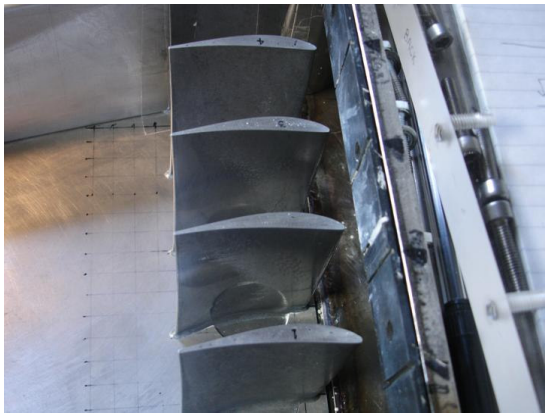

Figure 5-9 Results of pressure surface deposition after 1hr of artificial powder injection at rate of 100g/h.

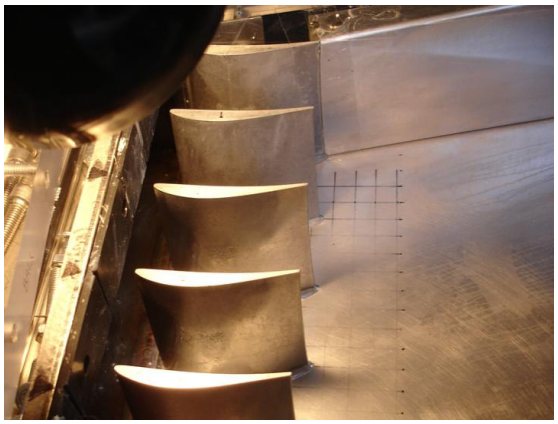

Figure 5-10 Results of suction surface deposition after 1hr of artificial powder injection at rate of 100g/h.

Figure 5-11 Results of pressure surface deposition after 2hr of artificial powder injection at rate of 100g/h.

Figure 5-12 Results of suction surface deposition after 2hr of artificial powder injection at rate of 100g/h.

Figure 5-13 Results of pressure surface deposition after 3hr of artificial powder injection at rate of 100g/h.

Figure 5-14 Results of suction surface deposition after 3hr of artificial powder injection at rate of 100g/h.

Figure 5-15 Results of pressure surface deposition after 4hr of artificial powder injection at rate of 100g/h.

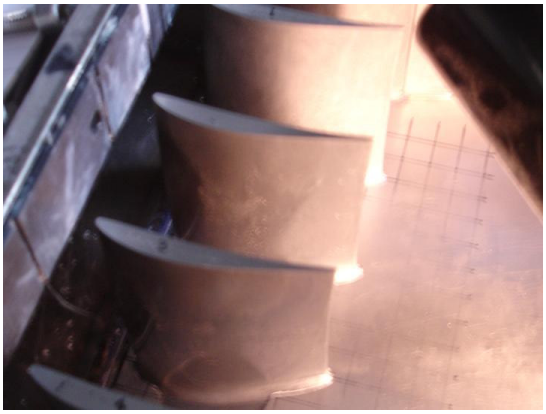

Figure 5-16 Results of suction surface deposition after 4hr of artificial powder injection at rate of 100g/h.

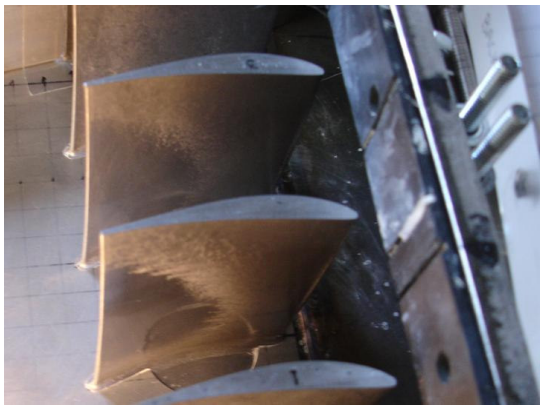

Figure 5-17 Results of pressure surface deposition after 5hr of artificial powder injection at rate of 100g/h.

Figure 5-18 Results of suction surface deposition after 5hr of artificial powder injection at rate of 100g/h.

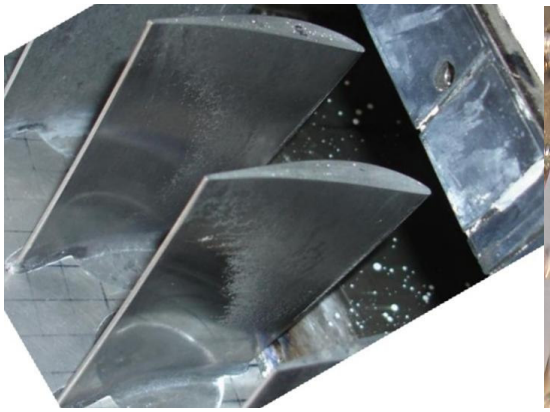

Figure 5-19 Results of pressure surface deposition after 6hr of artificial powder injection at rate of 100g/h.

Figure 5-20 Results of suction surface deposition after 6hr of artificial powder injection at rate of 100g/h.

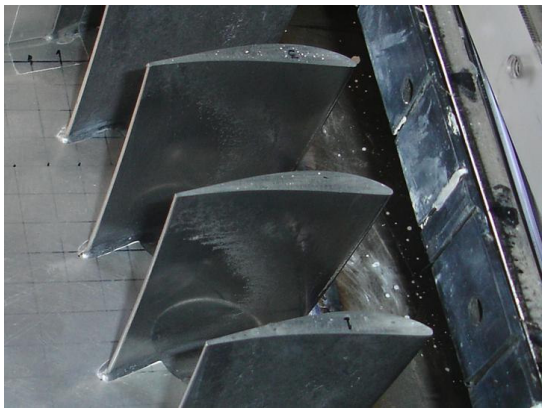

Figure 5-21 Results of pressure surface deposition after 7hr of artificial powder injection at rate of 100g/h.

Figure 5-22 Results of suction surface deposition after 7hr of artificial powder injection at rate of 100g/h.

The use of the glue-agent (UW40 oil) increased the particle deposition. The fouling on the blade surface during the first period of operation (2 hours) was in a constant deposition of particles on the pressure surface. On the suction surface a considerable deposition was built up after 3 hours of operation. The photos are evidence of this gradual deposition of particles. On the leading region the deposition was bigger than other section of the surface. During the last two hours of operation the increment in the deposition of particles was almost cero.

5.4.3 Third test (artificial dust sample and glue agent-2)

The third case involved the use of a liquid-grease. However, the use of this glue-agent was unsuccessful, because the layer that formed on the blade surface was very thick and absorbed the artificial dust (see Figure 5-23).

Figure 5-23 Test of liquid-grass as glue-agent in the deposition of artificial dust.

5.4.4 Fourth test (real dust sample and UW40-liquid oil)

The successful result from the second experiment was used to simulate the artificial blade fouling with the real dust sample. The study of the fouling phenomenon included the location of deposition of particle, the quantity of dust accumulated and the time of operation. The quantity of dust accumulated was estimated using the value from the surface roughness. The information resulting from these tests was exported into the CFD model to study the blade aerodynamics. Following the same procedure of the second test, the blades were impregnated with a thin layer of UW40 oil. The dust sample collected from Inchon Power Plant was injected into the test rig. The results are presented in Table 5-8 followed by photos that illustrated the fouling phenomenon.

Rate of 100g/h	Artificial deposition of real dust sample with a UW40 layer on the blade surfaces
1h =100g (equivalent a 1.5 days of engine in operation)	Pressure: The leading edge region presented the heaviest deposition of particles on this surface (see Figure 5-24). Suction: Particle deposition was only found on the leading edge region (see Figure 5-25).
2h =200g (equivalent a 3 days engine in operation)	Pressure: The fouling was gradually increased on this surface. The leading region was again the location of the heaviest deposition of particles (see Figure 5-26). Suction: The fouling was gradually increased and a considerably increment of particle deposition on the middle chord was observed (see Figure 5-27).
3h =300g (equivalent a 4.5 days engine in operation)	Pressure: A symmetrical shape due to the deposition of particles was formed on this surface. The increment of dust deposition on the leading region at the middle region was considerable reduced (see Figure 5-28). Suction: The deposition of particles was reduced on this surface (see Figure 5-29).
4h =400g (equivalent a 6 days	Pressure: The increment of dust deposition was considerably

engine in operation)	reduced over the whole surface (see Figure 5-30). Suction: The high accumulation of particles formed small peaks that produced increments in the drag (see Figure 5-31).
5h =500g (equivalent a 7.5 days engine in operation)	Pressure: The increment of fouling was null. The region close to the roof and floor was in higher particle deposition than in the middle section. Also the heaviest fouling was found on the leading region (see Figure 5-32). Suction: The increment of fouling was null. The location of heavy fouling produced increment in the drag (see Figure 5-33).
6h =600g (equivalent a 9.0 days engine in operation)	Pressure: Similar to the suction surface, the heavy particle deposition formed peaks that produced increments in the drag (see Figure 5-34). Suction: An increment of fouling was observed close to the leading edge region (see Figure 5-35).
7h =700g (equivalent a 10.5 days engine in operation)	Pressure: Due to the drag produced in the region of heavy particle deposition the peaks were prone from the surface (see Figure 5-36). Suction: The increment of the fouling rate on this surface was null (see Figure 5-37).

Table 5-8 Results of artificial fouling from the real sample powder at rate of 100g/h

Figure 5-24 Results of pressure surface deposition after 1hr of real dust sample injection at rate of 100g/h.

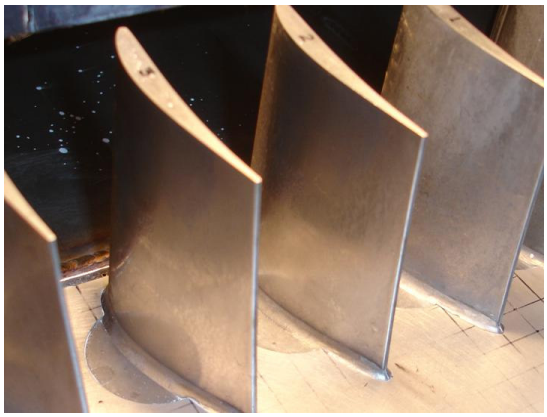

Figure 5-25 Results of suction surface deposition after 1hr of artificial dust injection at rate of 100g/h.

Figure 5-26 Results of pressure surface deposition after 2hr of real dust sample injection at rate of 100g/h.

Figure 5-27 Results of suction surface deposition after 2hr of artificial dust injection at rate of 100g/h.

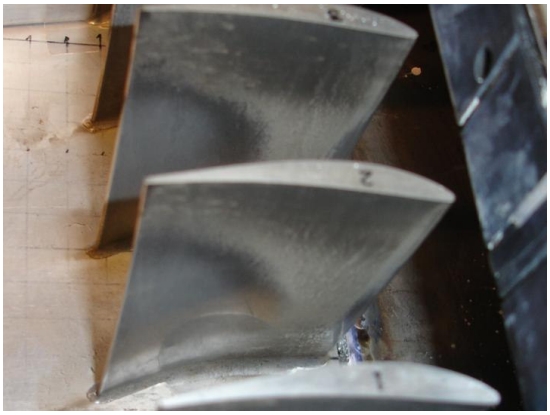

Figure 5-28 Results of pressure surface deposition after 3hr of real dust sample injection at rate of 100g/h.

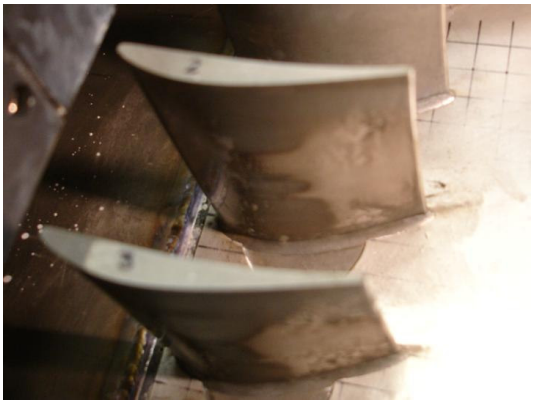

Figure 5-29 Results of suction surface deposition after 3hr of artificial dust injection at rate of 100g/h.

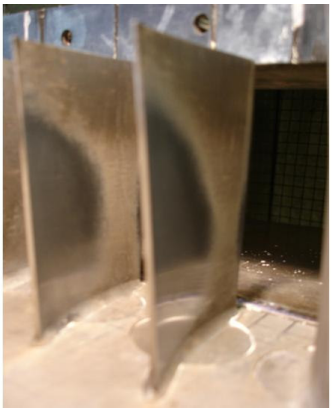

Figure 5-30 Results of pressure surface deposition after 4hr of real dust sample injection at rate of 100g/h.

Figure 5-31 Results of suction surface deposition after 4hr of artificial dust injection at rate of 100g/h.

Figure 5-32 Results of pressure surface deposition after 5hr of real dust sample injection at rate of 100g/h.

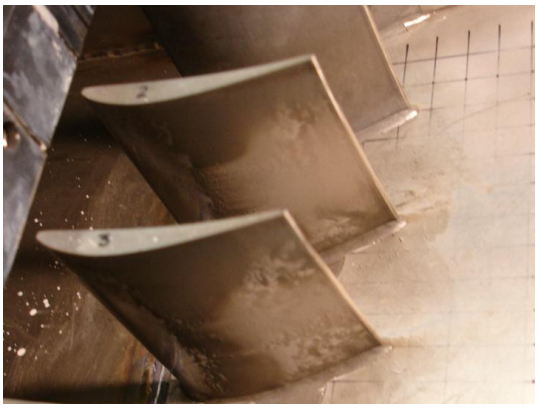

Figure 5-33 Results of suction surface deposition after 5hr of artificial dust injection at rate of 100g/h.

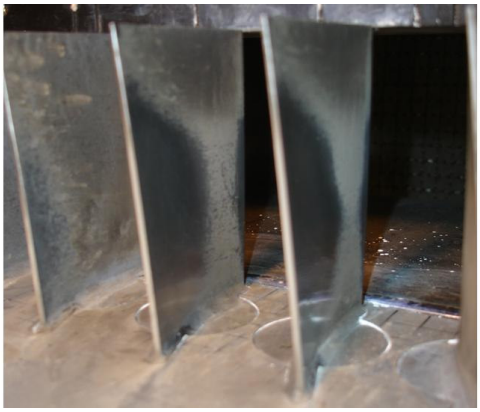

Figure 5-34 Results of pressure surface deposition after 6hr of real dust sample injection at rate of 100g/h.

Figure 5-35 Results of suction surface deposition after 6hr of artificial dust injection at rate of 100g/h.

Figure 5-36 Results of pressure surface deposition after 7hr of real dust sample injection at rate of 100g/h.

Figure 5-37 Results of suction surface deposition after 7hr of artificial dust injection at rate of 100g/h.

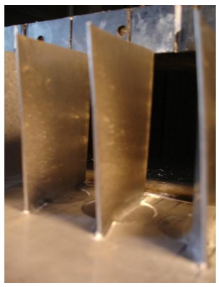

Figure 5-38 Results of pressure surface deposition after 1hr of real dust sample injection at rate of 100g/h.

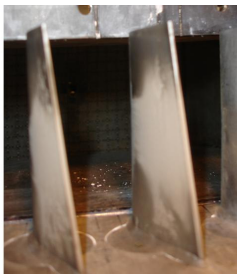

Figure 5-39 Results of pressure surface deposition after 4hr of real dust sample injection at rate of 100g/h.

Figure 5-40. Results of pressure surface deposition after 5hr of real dust sample injection at rate of 100g/h.

5.4.5 Experimental results validation.

In the operation of real gas turbines the compressor fouling can only be studied when the engine is open for overall maintenance. The author had the opportunity to make a

technical visit to Didcot Power Plant when one of the units was opened to overall maintenance. The compressor fouling of that engine was used to validate the experimental results of this research. Information from the engine in the Inchon Power Plant was also recorded (see Table 5-9).

Source	Place	Information
Author personal industrial visit	Didcot Power Plant Oxford, UK	Fouling information from a Unit in overall maintenance after 8000hrs of operation.
Recovery Power Ltd.	Inchon Power Pant, South Korea	Fouling information from the IGVs after 3 days of compressor washing. Dust sample collected from the inlet of the engine.

Table 5-9 Sources of information for real fouling on blades of industrial gas turbine compressor.

The following photos present the evidence of fouling in the real engines. This information is discussed according to the results obtained from the tests of this study. In the case of the Inchon Power Plant (South Korea), the IGV from the engine* presented the highest deposition of particles on the leading edge region. This photo of that engine was taken three 3 days after compressor washing on line (Figure 5-41). The result obtained from this experiment corresponded with the IGV results at one hour of operation from the fouling system (equivalent to 1.5 days of real engine operation) (see Figure 5-42).

Figure 5-41 Fouling on the IGV surface from the gas turbine of Inchon Power Plant, South Korea.

Figure 5-42 Experimental result of fouling on the suction surface after 1hr of artificial dust injection at rate of 100g/h.

The information from the gas turbine† in Didcot Power Plant (UK) was obtained during the main overhaul maintenance after 8000 hours of operation. However, in this

* Industrial Gas Turbina G&E gas turbine model Frame 7E
† Industrial Gas Turbine model SIEMENS V94.3A

engine the last period of compressor washing on line was unknown. The fouling on the IGV surface was located on the leading edge region (see Figure 5-43). This result was also observed from the experiment after two hours of dust injection (see Figure 5-44).

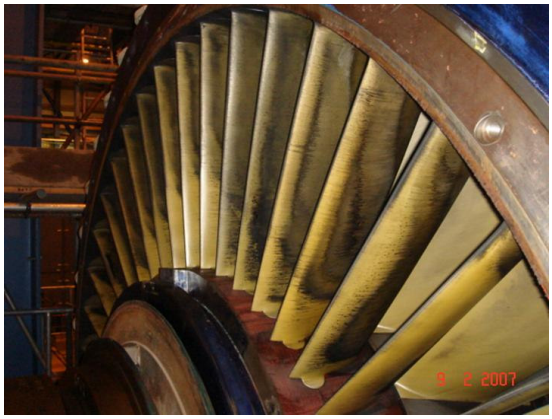

Figure 5-43 Fouling found on the IGV suction surface (Didcot Power Plant, UK).

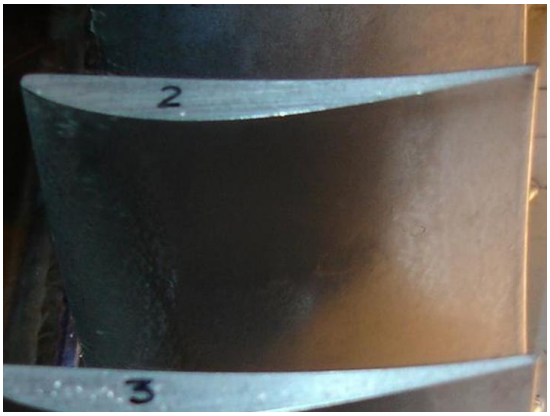

Figure 5-44 Experimental result of fouling on the suction surface after 2hr of dust injection at rate of 100g/h.

Heavy deposition on the leading edge was also found on the pressure surface of the IGV. The deposition of particles was gradually decreased in the direction of the trailing edge (see Figure 5-45). The same fouling location was found on the blades from the test rig at the end of 7 hours of fouling (see Figure 5-46).

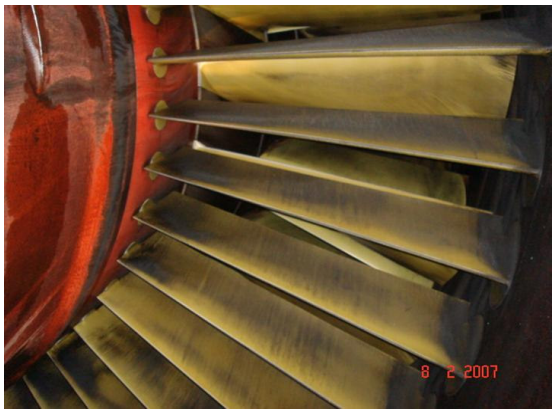

Figure 5-45 Fouling found on the IGV pressure surface (Didcot Power Plant, UK).

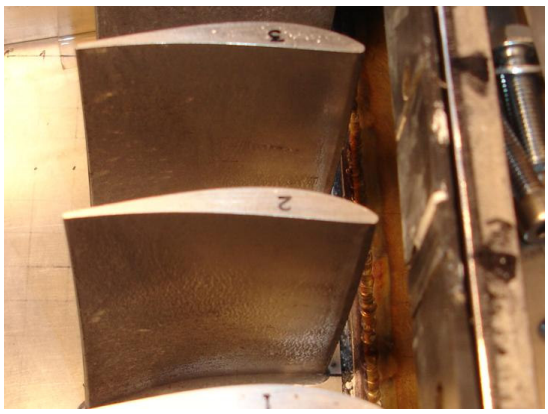

Figure 5-46 Experimental result of fouling on the suction surface after 7hr of dust injection at rate of 100g/h.

Fouling was also observed on the first rotor blade. It was found on the leading edge region of the suction surface (see Figure 5-47). Although, the experimental tests did not include the rotation effect of the blade, a result close to this deposition was observed in the first hour of the artificial fouling (see Figure 5-48).

Figure 5-47 Fouling on the 1st rotor blade suction surface (Didcot Power Plant, UK).

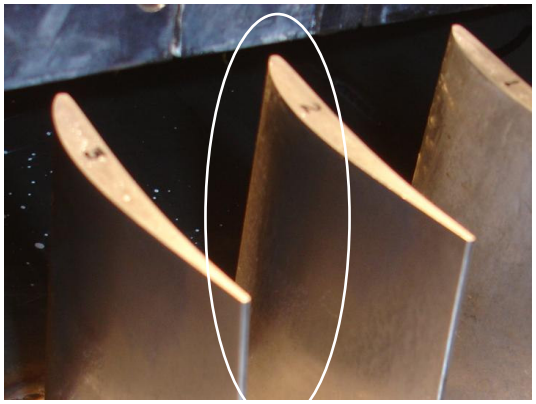

Figure 5-48 Experimental result of fouling on the suction surface after 1hr of dust injection at rate of 100g/h.

The fouling presented on the pressure surface of the rotor blade (Didctot Power Plant) was located on the leading edge and blade tip region. This effect was due to the clearance region and the centrifugal effect (see Figure 5-49.). The centrifugal phenomenon was not reproduced in the experiment, because the cascade was only designed for two dimensional flow effects (static airfoils). However, the results from the fouling on the leading edge region were similar to the results of the experiment one hour after the dust injection (see Figure 5-50).

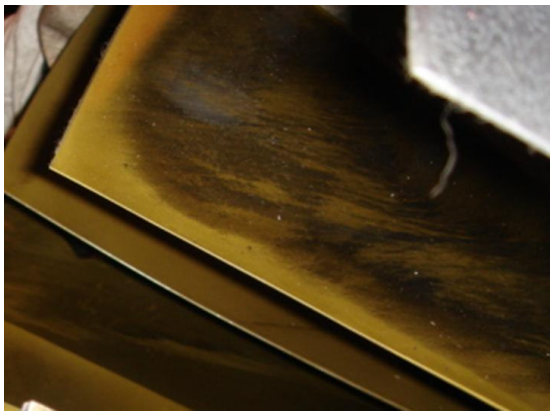

Figure 5-49 Fouling on the 1st rotor blade pressure surface (Didcot Power Plant, UK).

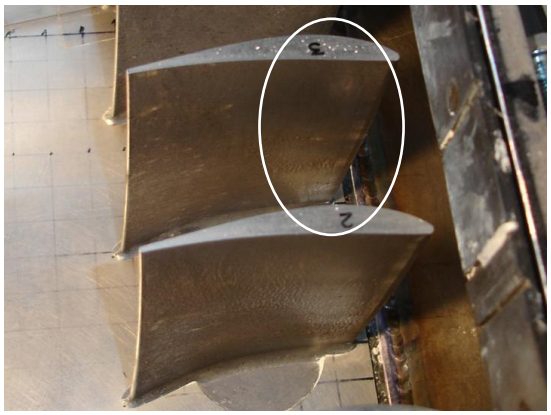

Figure 5-50 Experimental result of fouling on the suction surface after 1hr of dust injection at rate of 100g/h.

The visual inspection of the rear stages (compressor) from the engine in Didcot Power Plant demonstrated that fouling was gradually reduced (see Figure 5-51). The main area affected by fouling on the rear blades was the leading edge region. Fouling was found on the blades from the first and second stage in the root region due to the centrifugal effect.

Figure 5-51 Fouling distribution on blades of the 1st ,2nd, 3rd and 4th stages (Didcot Power Plant, UK).

5.5 Experimental model of the fouling mechanism

The fouling model was generated based on the experimental results from the last test. The study region was the blade profile at the middle height blade. The variables considered in the model were the location of fouling on the surface, the surface roughness value and the time of operation (fouling rate). The next sections include the study of these three variables to create the model that describes the phenomenon of fouling.

5.5.1 Surface roughness changes

The result of fouling in the blade geometry was in the micro-scale region represented by the value of the surface roughness. For that reason, it was necessary to divide the blade profile into 24 study regions (12 for the suction surface and 12 for the pressure surface). The result was recorded with the instrument that measured the surface

roughness (Surtronic-25). The measurements were taken in the direction of the axis x (axial direction) and represented with the scale of Ra=µm.

5.5.1.1 Pressure Surface

The following table includes the results from the surface roughness on the pressure surface.

Pressure Surface	1hr (100g) Ra=µm	2 hr (200g) Ra=µm	3 hr (300g) Ra=µm	4 hr (400g) Ra=µm	5 hr (500g) Ra=µm	6 hr (600g) Ra=µm	7 hr (700g) Ra=µm
1	0.9	1.15	1.3	1.35	1.3	1.35	1.35
2	0.9	1.15	1.25	1.27	1.15	0.82	0.82
3	0.9	1.15	1.3	1.37	1.38	1.4	1.35
4	0.9	1.1	1.3	1.36	1.35	1.35	1.31
5	0.84	1.1	1.3	1.33	1.3	1.34	1.3
6	0.83	1	1.3	1.34	1.29	1.21	1
7	0.8	0.9	0.95	1.02	0.99	0.88	0.83
8	0.75	0.8	0.9	0.93	0.85	0.81	0.8
9	0.72	0.75	0.8	0.82	0.8	0.79	0.81
10	0.72	0.75	0.75	0.8	0.81	0.78	0.77
11	0.72	0.75	0.75	0.77	0.79	0.78	0.75
12	0.72	0.75	0.75	0.75	0.79	0.78	0.79

Table 5-10 Pressure surface roughness results on 12 regions at fouling rate of 100g/h.

The deposition of particles was observed from the first hour of the dust injection. In this period the surface roughness increased on the leading edge region from 0.6 to 0.9 µm and on the trailing region from 0.6 to 0.72 µm. The highest particle deposition was in values of 1.4 µm (see Figure 5-52).

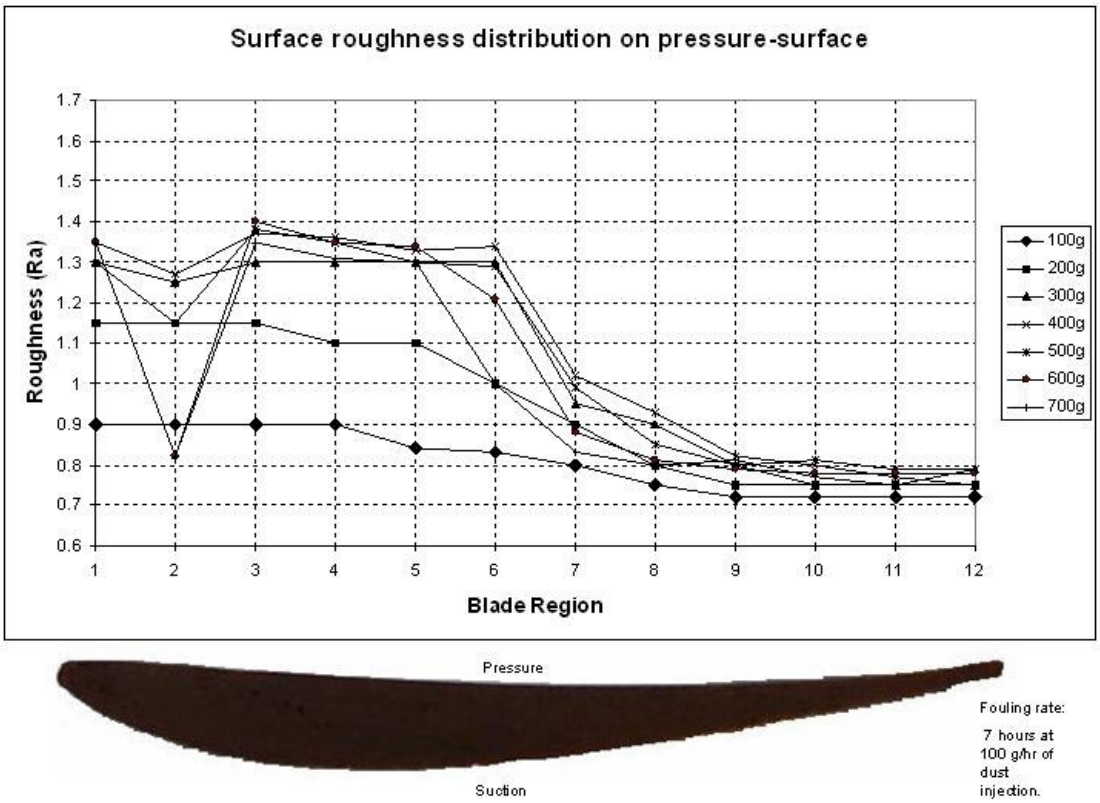

Figure 5-52 Representation of particle deposition by the surface roughness parameter on the pressure surface (µm)

5.5.1.2 Suction Surface

The following table includes the results from the surface roughness parameter on the suction surface.

Suction Surface	1hr (100g) Ra=µm	2 hr (200g) Ra=µm	3 hr (300g) Ra=µm	4 hr (400g) Ra=µm	5 hr (500g) Ra=µm	6 hr (600g) Ra=µm	7 hr (700g) Ra=µm
1	1.15	1.21	1.28	1.22	1.22	1.23	1.26
2	1.11	1.008	0.95	0.95	0.9	0.92	1.007
3	1.03	0.963	0.97	0.94	0.93	0.95	0.96
4	0.97	0.94	0.97	0.93	0.93	0.96	0.96
5	0.95	1.382	1.6	1.57	1.55	1.53	1.52
6	0.92	1.408	1.62	1.55	1.51	1.55	1.6
7	0.9	1.397	1.58	1.55	1.51	1.55	1.55
8	0.85	1.34	1.55	1.43	1.35	1.38	1.4
9	0.8	1.334	1.42	1.4	1.35	1.38	1.43
10	0.74	1.292	1.41	1.4	1.3	1.33	1.37

11	0.72	1.23	1.41	1.32	1.24	1.25	1.3
12	0.73	0.895	0.97	1.01	1	0.99	1.01

Table 5-11 Suction surface roughness results on 12 regions at fouling rate of 100g/h.

After 1 hour of dust injection, the surface roughness increased on the leading edge region from 0.6 to 1.16µm and on the trailing region from 0.6 to 0.78µm (see Figure 5-53). The maximum value obtained from this surface was 1.6 µm in the region-5 (middle core).

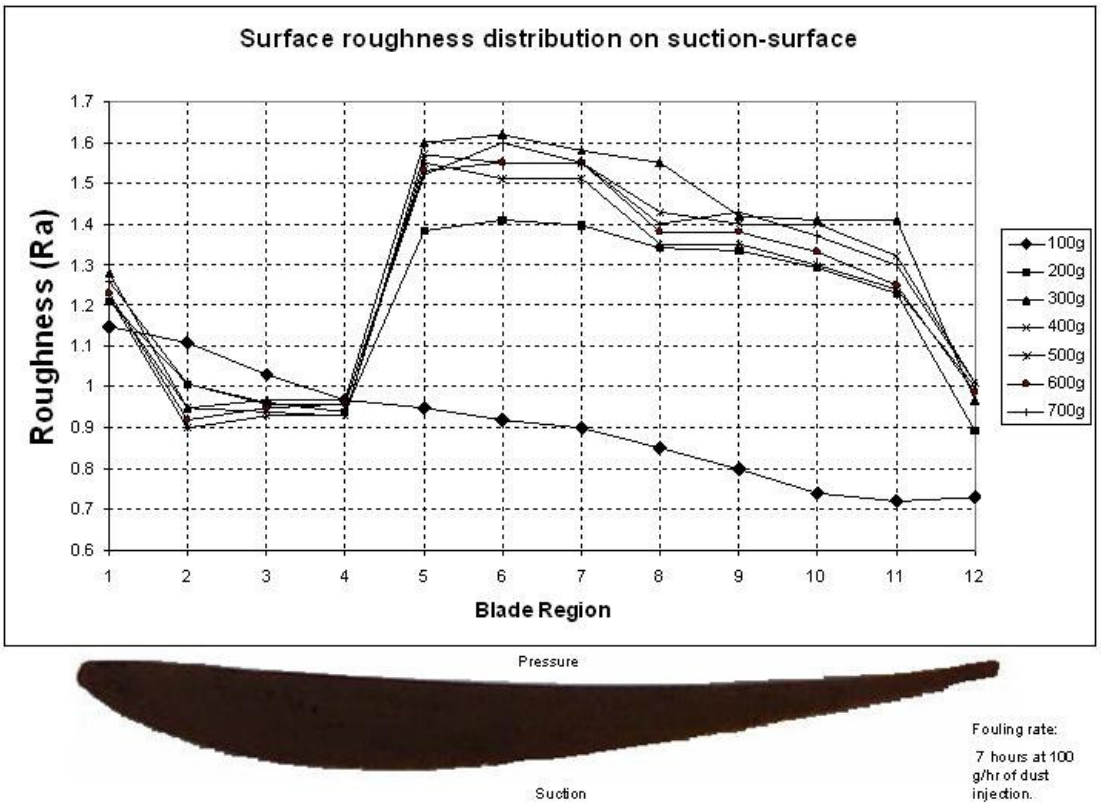

Figure 5-53 Representation of particle deposition by the surface roughness parameter on the suction surface (µm)

The surface roughness on both surfaces was non uniform. This result is shown in the following figures and represents the evolution of fouling in each region based on the surface roughness values.

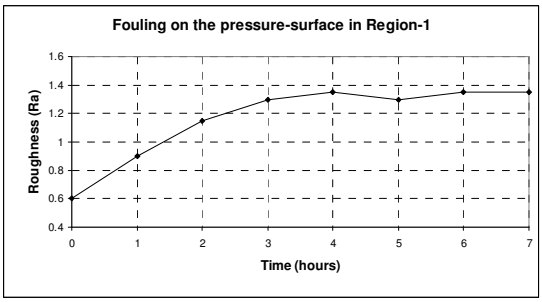

Figure 5-54 Fouling on the pressure surface in Region-1 during 7 hours at rate of 100g/h of dust injection.

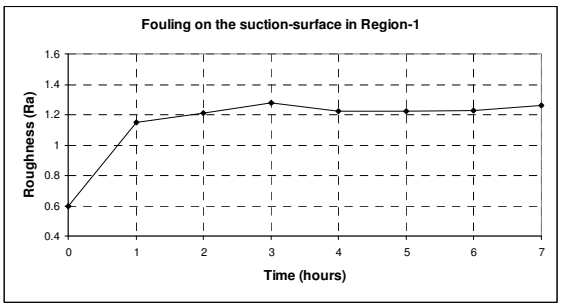

Figure 5-55 Fouling on the suction surface in Region-1 during 7 hours at rate of 100g/h of dust injection.

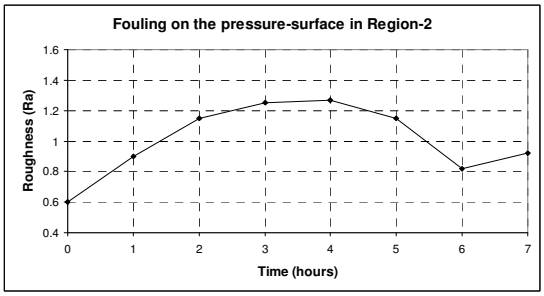

Figure 5-56 Fouling on the pressure surface in Region-2 during 7 hours at rate of 100g/h of dust injection.

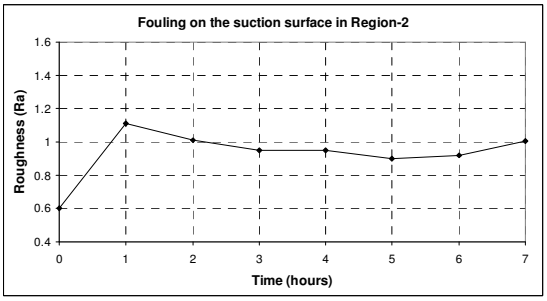

Figure 5-57 Fouling on the suction surface in Region-2 during 7 hours at rate of 100g/h of dust injection.

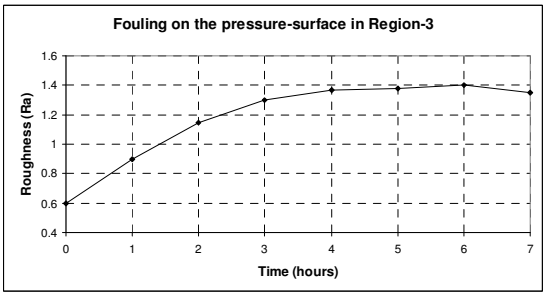

Figure 5-58 Fouling on the pressure surface in Region-3 during 7 hours at rate of 100g/h of dust injection.

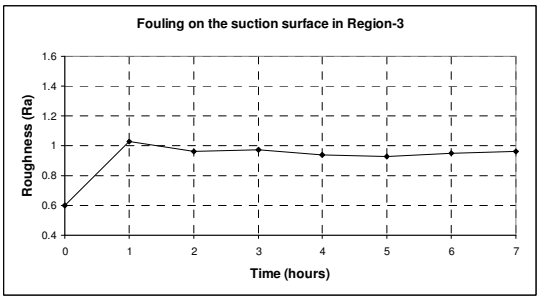

Figure 5-59 Fouling on the suction surface in Region-3 during 7 hours at rate of 100g/h of dust injection.

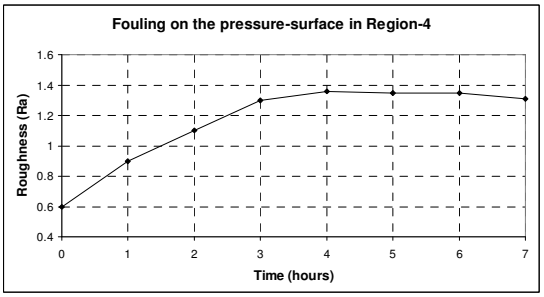

Figure 5-60 Fouling on the pressure surface in Region-4 during 7 hours at rate of 100g/h of dust injection.

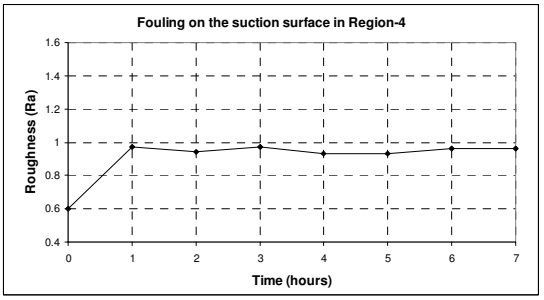

Figure 5-61 Fouling on the suction surface in Region-4 during 7 hours at rate of 100g/h of dust injection.

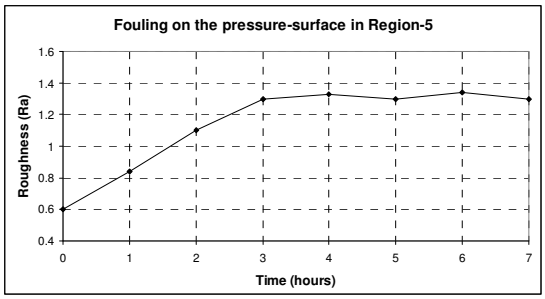

Figure 5-62 Fouling on the pressure surface in Region-5 during 7 hours at rate of 100g/h of dust injection.

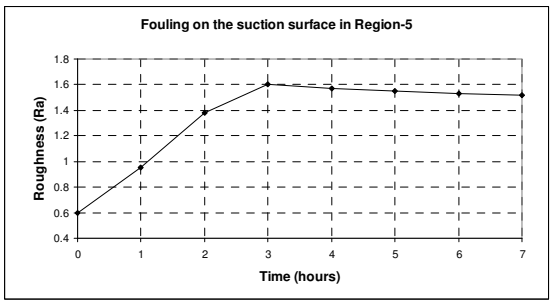

Figure 5-63 Fouling on the suction surface in Region-5 during 7 hours at rate of 100g/h of dust injection.

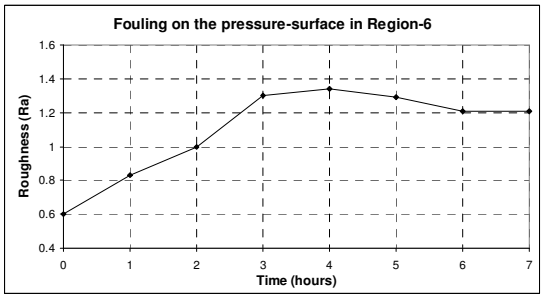

Figure 5-64 Fouling on the pressure surface in Region-6 during 7 hours at rate of 100g/h of dust injection.

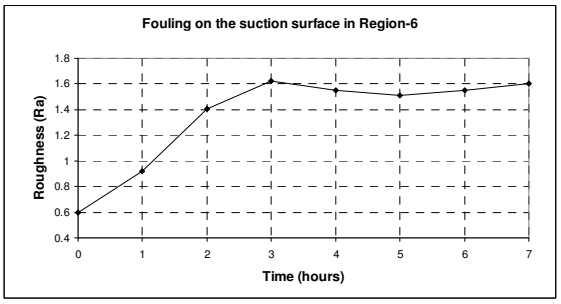

Figure 5-65 Fouling on the suction surface in Region-6 during 7 hours at rate of 100g/h of dust injection.

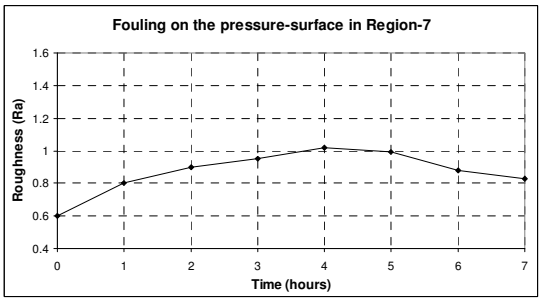

Figure 5-66 Fouling on the pressure surface in Region-7 during 7 hours at rate of 100g/h of dust injection.

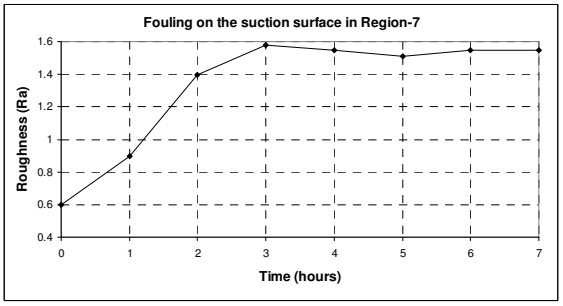

Figure 5-67 Fouling on the suction surface in Region-7 during 7 hours at rate of 100g/h of dust injection.

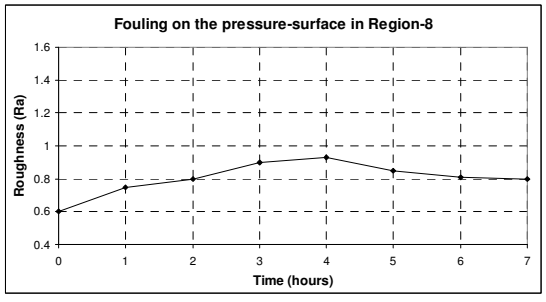

Figure 5-68 Fouling on the pressure surface in Region-8 during 7 hours at rate of 100g/h of dust injection.

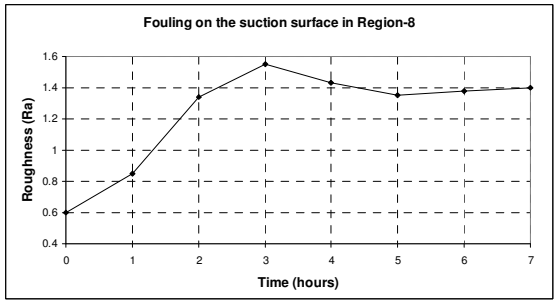

Figure 5-69 Fouling on the suction surface in Region-8 during 7 hours at rate of 100g/h of dust injection.

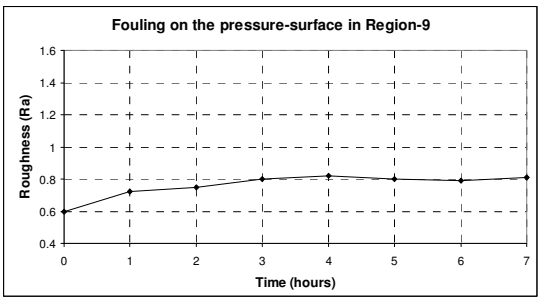

Figure 5-70 Fouling on the pressure surface in Region-9 during 7 hours at rate of 100g/h of dust injection.

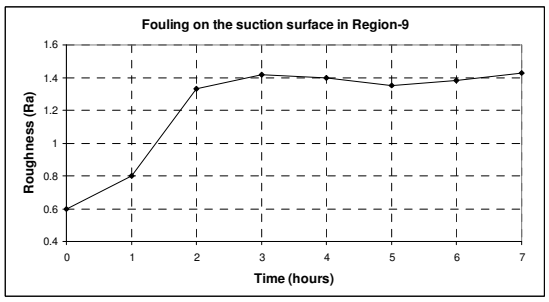

Figure 5-71 Fouling on the suction surface in Region-9 during 7 hours at rate of 100g/h of dust injection.

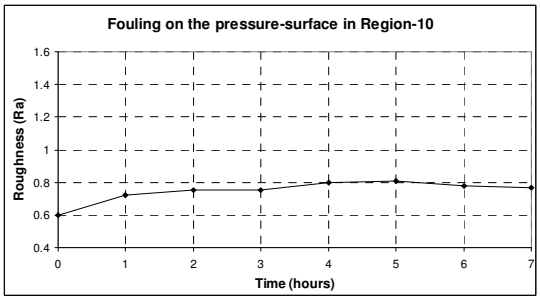

Figure 5-72 Fouling on the pressure surface in Region-10 during 7 hours at rate of 100g/h of dust injection.

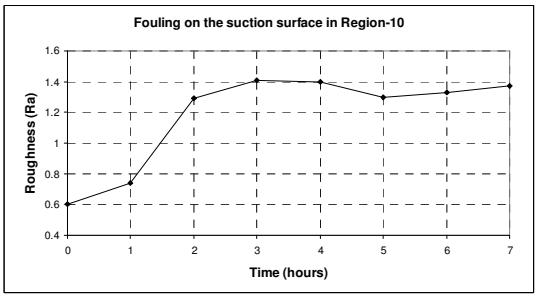

Figure 5-73 Fouling on the suction surface in Region-10 during 7 hours at rate of 100g/h of dust injection.

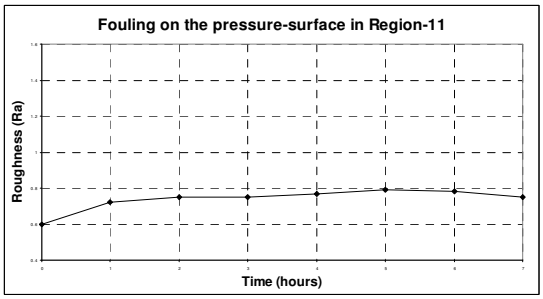

Figure 5-74 Fouling on the pressure surface in Region-11 during 7 hours at rate of 100g/h of dust injection.

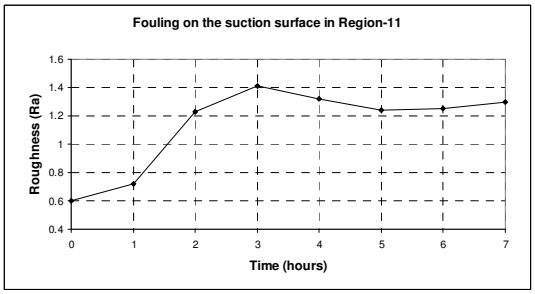

Figure 5-75 Fouling on the suction surface in Region-11 during 7 hours at rate of 100g/h of dust injection.

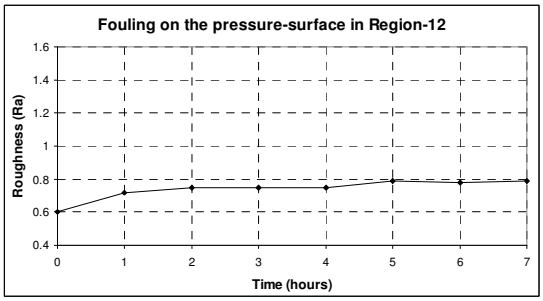

Figure 5-76 Fouling on the pressure surface in Region-12 during 7 hours at rate of 100g/h of dust injection.

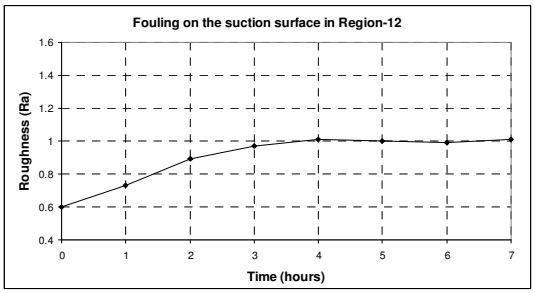

Figure 5-77 Fouling on the suction surface in Region-12 during 7 hours at rate of 100g/h of dust injection.

The roughness of the pressure surface was gradually increased (leading edge region). In regions of heavy particle deposition the drag removed part of the dust accumulation. This was the case in the regions 9 to 11 where a high deposition of particles was found after 4 hours of operation and later this deposition was removed.

5.5.2 Fouling Model

The mathematical model was divided into two (pressure surface and suction surface). The information was generated based on the experimental results (location of fouling on the surface, surface roughness and time).

5.5.2.1 Mathematical model of fouling on the pressure surface of the blade

The result of fouling in this surface is represented in the following three dimensional chart (see Figure 5-78). The mechanism of fouling was non linear and non-uniform on the surface of the blade. Each region represents a different rate of the particle deposition.

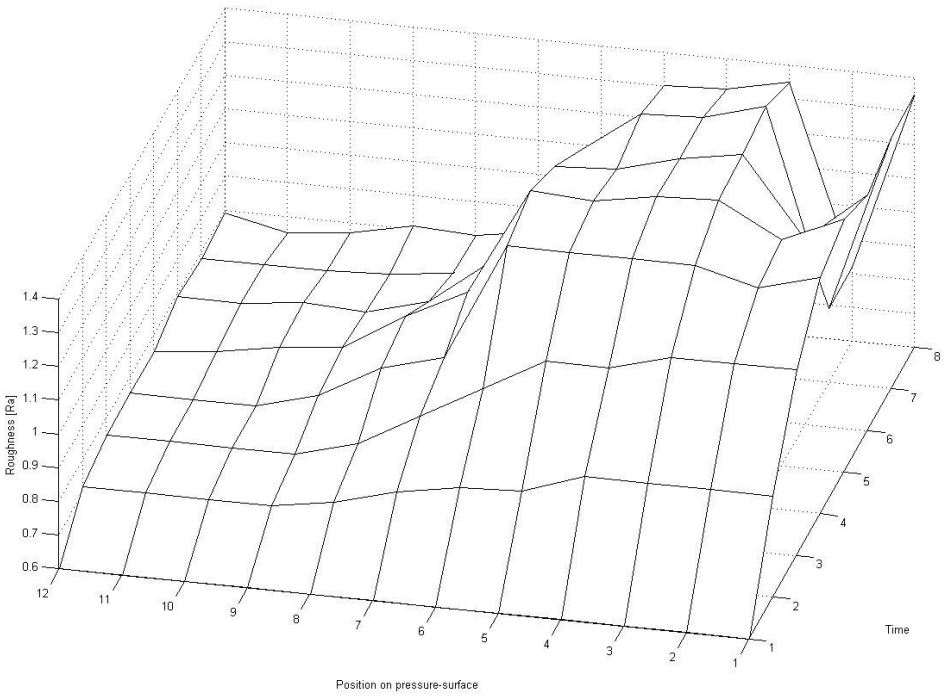

Figure 5-78 Fouling on the pressure surface represented by the change of surface roughness (Ra=µm), location (region) and operation time (hour) at rate of 100g/h dust injection.

The 12 regions were grouped in four sections. These four regions were represented by a trend-line model [*] to adjust the data. The variable selected to create the mathematical model was the operation time (experimental hours and dust injection rate of 100g/h). The first equation is complex and has a high coefficient of determination[†] ($\sqrt{R}$). The second equation is less complex than the previous but the value of the coefficient of determination is low.

Head region (Region 1 or 0-5% chord)

a) Ra= $-2x10^{-13}t^6+1x10^{-10}t^5-3x10^{-8}t^4+3x10^{-6}t^3-0.0002t^2+0.0116t+0.5997$

Equation 5-2

$\sqrt{R}=0.9994$

b) Ra = $-2x10^{-5}t^2+0.0081t+0.6333$

Equation 5-3

$\sqrt{R}=0.9692$

Leading region (Region 2 or 5-15% chord)

a) Ra= $-4x10^{-14}t^6+2x10^{-11}t^5-4x10^{-9}t^4+2x10^{-5}t^3-2x10^{5}t^2+0.0089t+0.5999$

Equation 5-4

$\sqrt{R}=0.9999$

b) Ra = $-2x10^{-5}t^2+0.0086t+0.6187$

Equation 5-5

$\sqrt{R}=0.9928$

Middle-chord region (Region 3-7 or 15-70% chord)

a) Ra= $-4x10^{-13}t^6+3x10^{-10}t^5-8x10^{-8}t^4+1x10^{-5}t^3+0.0005t^2-0.0161t+0.6007$

Equation 5-6

$\sqrt{R}=0.9964$

[*] The trend-line is a graphic representation of trends in data series. Trend lines are used for the study of problems of prediction, also called regression analysis.

[†] The coefficient of determination or R-squared value is an indicator from 0 to 1 that reveals how closely the estimated values for the trend-line correspond to the actual data. A trend-line is most reliable when its R-squared value is at or near 1.

b) Ra (15-90% chord) = $-3x10^{-5}t^2 + 0.0098t + 0.5529$

Equation 5-7

$$\sqrt{R} = 0.9646$$

Trailing region (Region 8-12 or 70-100% chord)

a) Ra = $8x10^{-14}t^6 - 6x10^{-11}t^5 + 1x10^{-8}t^4 - 1x10^{-6}t^3 + 3x10^{-5}t^2 - 0.0035t + 0.6002$

Equation 5-8

$$\sqrt{R} = 0.996$$

b) Ra = $-4x10^{-6}t^2 + 0.0016t + 0.6312$

Equation 5-9

$$\sqrt{R} = 0.8533$$

5.5.2.2 Mathematical model of fouling on the blade suction surface

Similar to the previous analysis the changes of roughness in the suction surface are represented by the following three dimensional chart (see Figure 5-79).

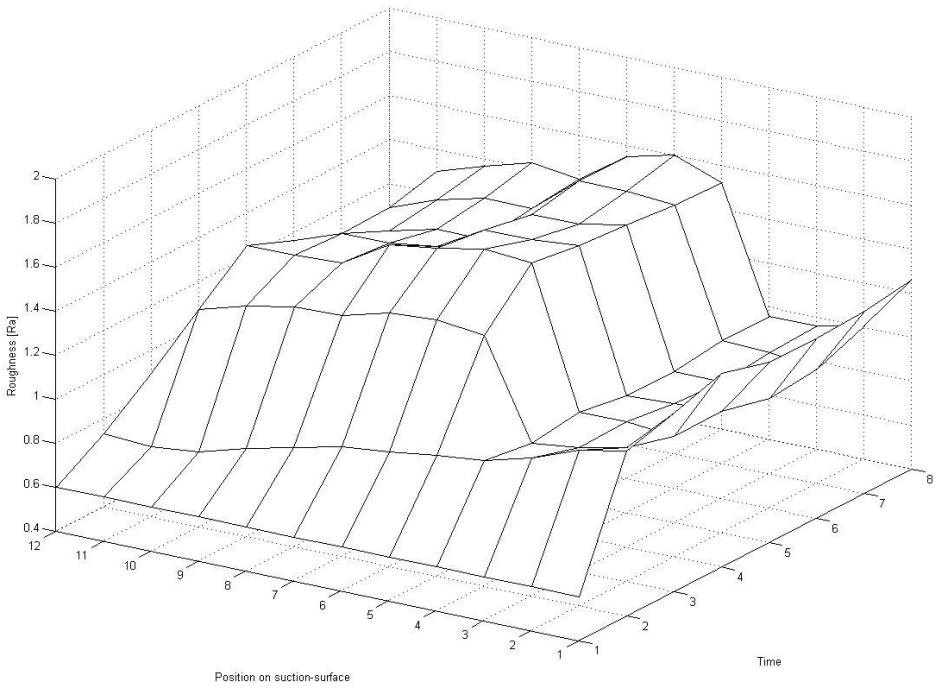

Figure 5-79 Fouling on the suction surface represented by the changes of roughness (Ra), location (region) and operation time (hour) at rate of 100g/h dust injection.

The chord was also divided into 4 sections to describe the fouling phenomenon on the suction surface.

Head region (Region 1 or 0-5% chord)

a) Ra= $-2x10^{-13}t^6+2x10^{-10}t^5-5x10^{-8}t^4+9x10^{-6}t^3-0.0007t^2+0.0321t+0.6007$

Equation 5-10

$$\sqrt{R}=0.9952$$

b) Ra = $-2x10^{-5}t^2+0.0067t+0.7554$

Equation 5-11

$$\sqrt{R}=0.7487$$

Leading region (Region 2-4 or 5-15% chord)

a) Ra= $-3x10^{-13}t^6+2x10^{-10}t^5-7x10^{-8}t^4+1x10^{-5}t^3-0.0009t^2+0.0324t+0.6004$

Equation 5-12

$$\sqrt{R}=0.9961$$

b) Ra = $-1x10^{-5}t^2+0.0034t+0.7379$

Equation 5-13

$$\sqrt{R}=0.4588$$

Middle-chord region (Region 5-11 or 15-90% chord)

a) Ra = $-8x10^{-14}t^6-1x10^{-10}t^5+4x10^{-8}t^4-8x10^{-6}t^3+0.0006t^2-0.0048t+0.6003$

Equation 5-14

$$\sqrt{R}=0.9996$$

b) Ra (15-90% chord) = $-3x10^{-5}t^2+0.0112t+0.6314$

Equation 5-15

$$\sqrt{R}=0.9198$$

Trailing region (Region 12 or 90-100% chord)

a) Ra = $5x10^{-14}t^6-4x10^{-11}t^5+1x10^{-8}t^4-2x10^{-6}t^3+0.0002t^2-0.0004t+0.5998$

Equation 5-16

$$\sqrt{R} = 0.9994$$

b) Ra (90-100% chord) = $-1x10^{-5}t^2 + 0.0045t + 0.604$

Equation 5-17

$$\sqrt{R} = 0.975$$

5.5.3 Boundary Layer Result

The boundary layer phenomenon is localized in a region close to the blade surface (3mm). As was mentioned in the literature review, the study of the boundary layer is in the micro-scale. The instrumentation used in the experiment was not adequate to study the micro-scale region.

The boundary layer was studied exclusively from the CFD model. It was represented by the velocity magnitude of flow. The CFD model was created with a structured micro-scale mesh around the blade. The model was processed with the energy and force equation to include the viscosity and wall treatment effects. The blade profile was divided exactly in the same number of regions from the experiment (24 regions). However, the number of equations resulting from the experiment exceeded the capacity of FLUENT. Therefore, the surface roughness values were inputted manually (see previous Table 5-10and Table 5-11). Also, the range of the surface roughness was limited to values of 0.1 to 1 µm in FLUENT. Since experimental results were bigger than 1µm from the surface roughness, it was necessary to work within the increments of this parameter (ΔRa).

The results presented in this section were based on three periods (1, 4 and 7 hours of fouling system in operation). The results from the boundary layer were analyzed with the velocity profile of the flow.

The velocity profile for the whole passage demonstrated that the higher velocities were presented near to the suction surface (see Figure 5-80). Also, the reduction of the cross section at the middle chord of the blade presented the highest flow velocity (see Lines 112 to 117).

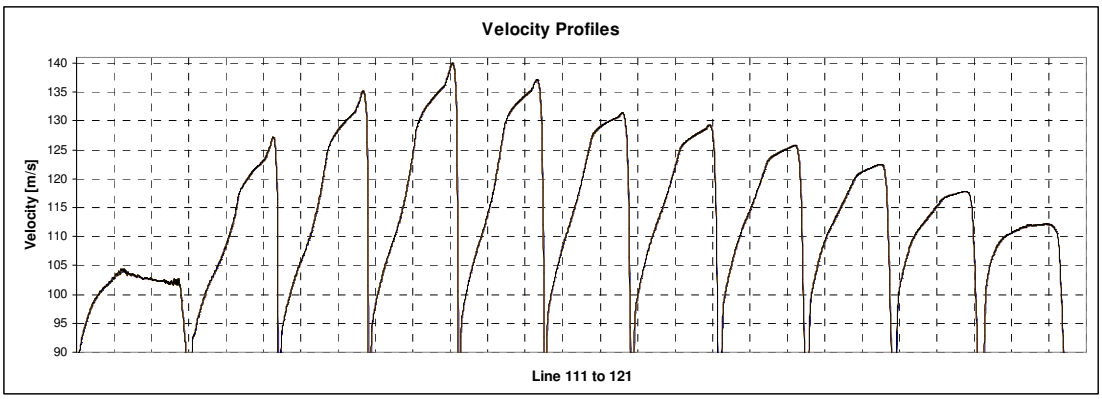

Figure 5-80 Velocity profile in the 3rd passage represented from the Line-111 (transversal line at region 1) to Line-121 (transversal line at region 12).

Due to fouling the boundary layer thickness was reduced close to the pressure surface. For example, the boundary layer thickness of Line-111 (blade head) was reduced in 0.5 mm (see Figure 5-81). The same case was produced in the following study lines (see Figure 5-82). The CFD model did not present a considerable difference in the boundary layer region after the first hour of fouling.

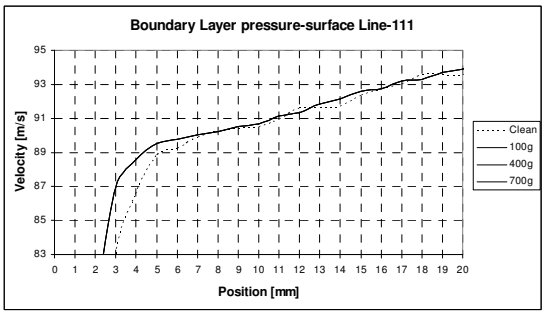

Figure 5-81 Boundary layer region represented by the velocity profile close to the pressure surface in region-1 (Line-111).

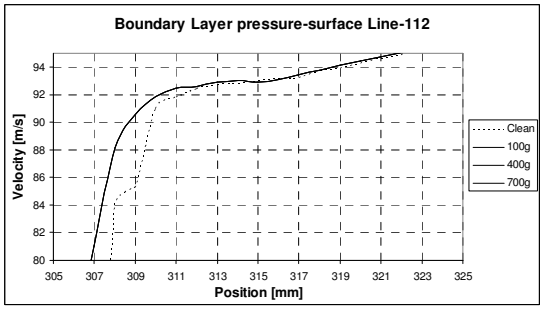

Figure 5-82 Boundary layer region represented by the velocity profile from the pressure surface in region-2 (Line-112).

The suction surface presented similar results to the pressure surface. For example, in the region of the blade head the fouling reduced the boundary layer region by 2 mm (see Figure 5-83). The CFD model did not detect a considerable change in this parameter after the first hour of dust injection.

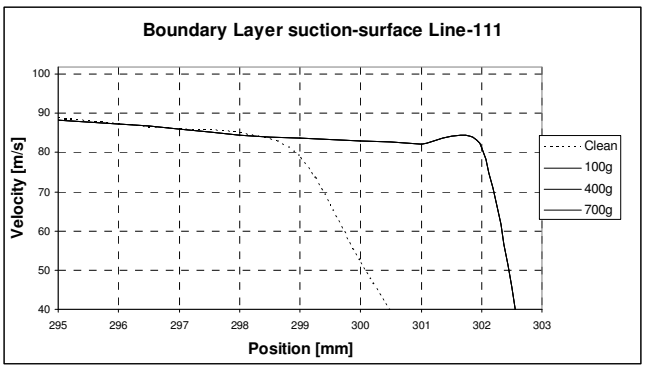

Figure 5-83 Boundary layer region represented by the velocity profile close to the suction surface in region-1 (Line-111).

5.5.4 General discussion of fouling

This section discusses the results from the third fouling test (real sample and UW40 oil) and the information obtained from the engine in Didcot Power Plant. The presence of fouling on the blades demonstrated that the filters can not stop 100% the particles mixed in the air (see Figure 5-43). It was evident that the fouling process occurred on both blade surfaces (pressure and suction surface) but the deposition of particles differs around the blade profile. However, the surface roughness modification due to fouling only reduced the thickness of the boundary layer.

The higher deposition of particles on specific regions produced the formation of peaks on the surfaces. The drag was increased in these regions and removed some areas of the dust. This increment of the drag represents losses in the compression process and this problem is analyzed in the following chapter.

Although the experiment was limited to reproducing some specific conditions from the real case, the results were very similar to the fouling observed from the real gas turbines (Didcot and Inchon Power Plants). The centrifugal effect was omitted in the experiment and for that reason the gradual deposition from the root to the tip was not reproduced in the test rig. This effect is a consequence of three dimensional flow conditions. As it was mentioned before, the test rig was designed for two dimensional studies and for that reason a symmetrical deposition on the blade surface was found (see Figure 5-30).

The non-uniform fouling on the surfaces demonstrated the necessity to divide the blade profile into regions. The complex phenomenon was studied in twelve regions of each surface. However, it was possible to group the results in sections. These results demonstrated the importance of the fouling problem to affect the original blade profile. For that reason, the new blades delivered by the OEM were with a low surface roughness value (0.6 µm) in order to guarantee low losses due to the drag.

6 TECHNO-ECONOMIC STUDY OF COMPRESSOR FOULING AND WASHING ON LINE

6.1 Introduction

The preliminary mathematical model of the fouling mechanism was presented in the previous chapter. This was created based on the experimental particle deposition. The parameters that were chosen to study this phenomenon were: the blade region of particles deposition, the modification of the surface roughness and the time of operation. The results demonstrated that the blade profile played an important role for the mechanism of fouling. This Chapter studies the application of the fouling model in a real study case. The first section of this chapter is focused to study the fouling effect on the blade aerodynamics. The second section analyzes the fouling effect in an industrial gas turbine. The third section presents a techno economic study based on the power produced by the engine in order to evaluate the effectiveness of compressor washing on line.

6.2 Aerodynamics of the blade affected by the fouling mechanism

The results from the experiment and CFD model were studied in this section to calculate the blade aerodynamics. The static pressure distribution, skin coefficient distribution and drag force information were calculated from the two dimensional CFD model.

6.2.1 Static Pressure

The static-pressure distribution in the blade was affected by the increment of the surface roughness. On the pressure surface this parameter did not change (see Figure 6-1). However, on the suction surface was observed that the static pressure increased (see Figure 6-2). The region at the middle chord on this surface presented the maximum static pressure value that coincides with the highest particles deposition

from the experiment. This increment in the static pressure produced that the boundary layer was affected since the first operation hour of the fouling system. After the second hour the results did not show more changes in this parameter.

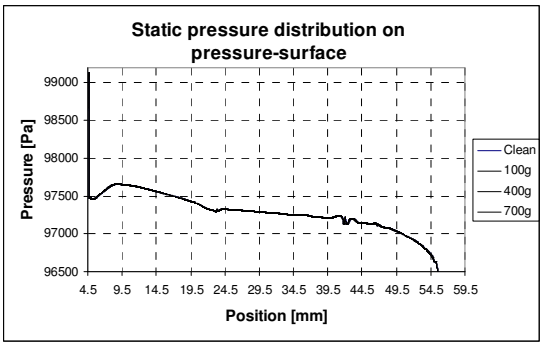

Figure 6-1 Static Pressure distribution on the pressure surface at dust rate injection of 100g/hr.

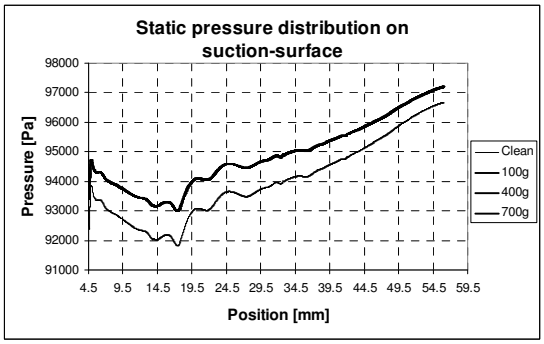

Figure 6-2 Static Pressure distribution on the suction surface at dust rate injection of 100g/hr.

6.2.2 Friction Skin Coefficient

The friction skin coefficient The skin friction coefficient, C_f, is defined by:

$$C_f \equiv \frac{\tau_w}{\frac{1}{2}\rho U_\infty^2}$$

Where τ_w is the local wall shear stress, ρ is the fluid density and U_∞ is the free-stream velocity (usually taken ouside of the boundary layer or at the inlet).The same result was obtained from the skin friction coefficient parameter. On the pressure surface was not found any change in this parameter (see Figure 6-3). However, on the suction surface the friction skin coefficient increased (see Figure 6-4).

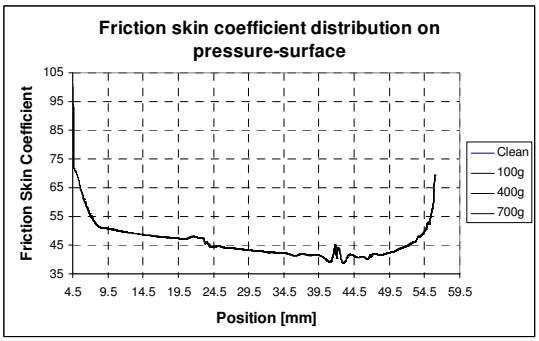

Figure 6-3 Skin Friction Coefficient distribution on the pressure surface at dust rate injection of 100g/hr.

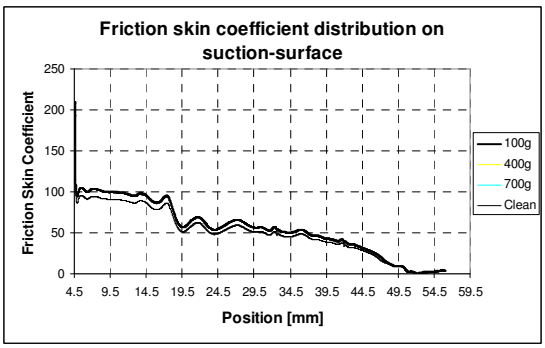

Figure 6-4 Skin Friction Coefficient distribution on the suction surface at dust rate injection of 100g/hr.

6.2.3 Drag force

The parameters of fouling obtained from the previous chapter can not be linked with the engine performance. For that reason, the drag force was calculated by the two dimensional CFD model according to the results of fouling.

The drag force was the parameter to link the blade aerodynamics changes to the engine performance. The relation between the drag force and engine performance was assumed as the difference of the drag force at different levels of fouling. The results demonstrated that the drag force was increased proportional to the change of the surface roughness (see Table 6-1).

Rate of fouling in the air stream: 100g/h	Pressure (N)	Viscous (N)	Total (N)
0h = 0g (clean)	29.2511	3.6228	32.8739
1h =100g (equivalent a 1.5 days engine in operation)	29.2512	3.6228	32.8740
4h =400g (equivalent a 4.5 days engine in operation)	29.2523	3.6229	32.8751
7h =700g (equivalent a 10.5 days engine in operation)	29.2523	3.6229	32.8751

Table 6-1 Drag force force produced in the total surface at of 100g/h of dust injection (fouling).

6.3 Engine performance

The drag force was calculated with information from the CFD model and experimental results (engine model of 1.2MW). To link the drag force with the engine performance it was necessary to consider the following assumptions.

- The difference of the drag force due to fouling was used as compressor losses.
- The result of the two dimensional drag force was scaled to a three dimensional blade using the blade height as scaling factor (80mm).
- The number of blades in the first rotor was 24.

- The flow velocity at the inlet of the first rotor was 80 m/s.
- The results were based on the first compressor stage.

The power from the first rotor was linked to the blade drag force according to the flow velocity and number of blades.

$$\dot{W}_{rotor} = Drag_{2D} \times 8 \times 24 \times v_{flow}$$

Equation 6-1

analysis dimensional:

$$\dot{W}_{rotor} = N \times \frac{m}{s} = \frac{Nm}{s} = \frac{J}{s} = Watts$$

The results are expressed in the following table.

Time (days)	1 Blade (N)	24 blades in 3D effect (N)	Increment of power in the 1.2MW engine due to fouling (kW)
0	32.8739	6311.7888	0
1.5	32.874	6311.8080	5.5296
4.5	32.8751	6312.0192	66.3552
10.5	32.8751	6312.0192	66.3552

Table 6-2 Increment of power due to the drag force.

6.3.1 Deterioration Factors

The evaluation of fouling was based on a gas turbine in a Power Plant. The industrial gas turbine single shaft of 240MW was selected as the engine model. The conditions of operations were calculated according to the design point (See Table 6-3).

Engine Configuration	Industrial Gas Turbine Single shaft
Output power	244.5 MW
Gross efficiency	38.02%
Mass flow	640 kg/s
Engine Configuration	Industrial Gas Turbine Single shaft
Compressor Configuration	16 Stages Pressure Ratio 1: 16

Table 6-3. Specifications of the single shaft industrial gas turbine

The compressor delivery pressure, output power, fuel consumption and overall efficiency were calculated with TURBOMATCH program. The values of these parameters were used for the period of 0 hours as follows.

Shaft Power	W	240000000.00
Equiv. Power	W	244466352.00
Fuel Flow	kg/s	14.6367
S.F.C.	mug/J	60.9861
E.S.F.C.	mug/J	59.8719
Sp. Sh. Power	W	375000.00
Sp. Eq. Power	W	381978.69
Sh. Th. Effy.		0.3802

Table 6-4 Engine performance simulation at design point for the gas turbine

The compressor efficiency and mass flow were the internal parameters that could be modified in TURBOMATCH. The correlation of these parameters with the fouling model was based on the program of gas path analysis GOTRESS. The output power of the engine and the increment of the drag force were processed in GOTRESS to link with these internal parameters (mass flow and compressor efficiency). The dependent parameters were: output power, compressor delivery pressure and compressor delivery temperature. The independent parameters were compressor efficiency and mass flow. The matrix root was created based on the design point and arbitrary modifications from the compressor efficiency and mass flow. The results of the factors from this correlation of parameters were added in the subroutines of TURBOMACH (see Appendix C).

6.3.2 Engine Performance Results

In the real operation, the gas turbine is deteriorated in other sections. However, to simplify this fouling study only the compressor section was deteriorated. The advantage from the simulations is the total control of the engine that in the real case is not possible. The fouling mechanism demonstrated in the simulation that the output power was reduced when the mass flow and the compressor delivery pressure decreased (see Figure 6-5). The output power was proportional to the deposition of particle and the maximum value of reduction was of 4% after 5

days.

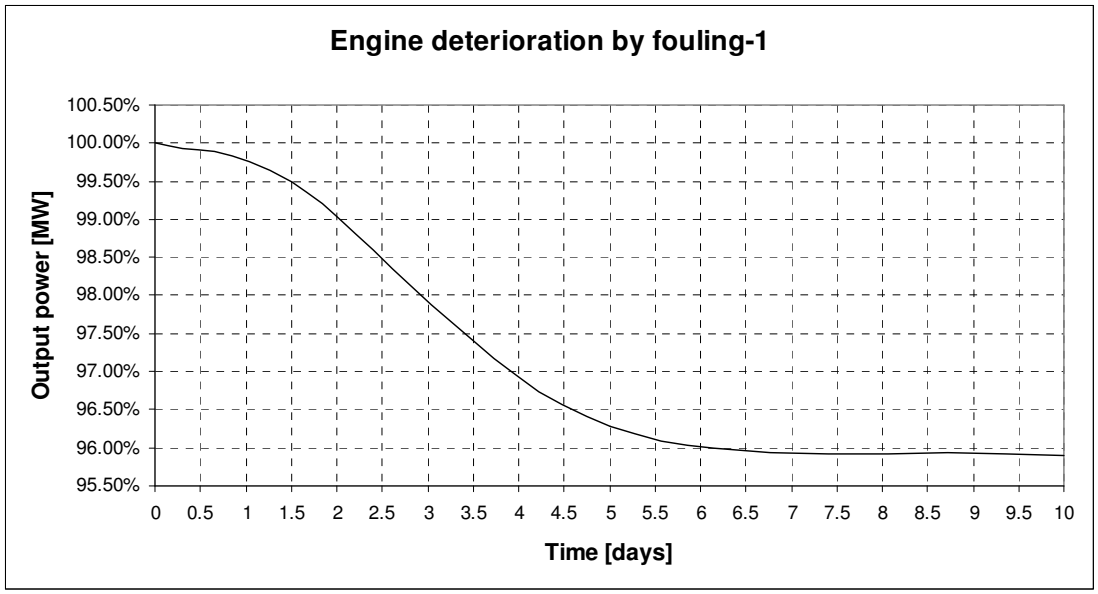

Figure 6-5 Reduction of the output power due to compressor fouling in a single shaft gas turbine according to the fouling rate (experiment 7 hors equivalent to 10 days in real engines).

The compressor delivery pressure and the compressor delivery temperature were mainly affected due to the mass flow reduction. This problem produced that the fuel consumption increased to obtain the turbine entry temperature. Therefore, the fouling effect reduced the overall engine efficiency (see Figure 6-6).

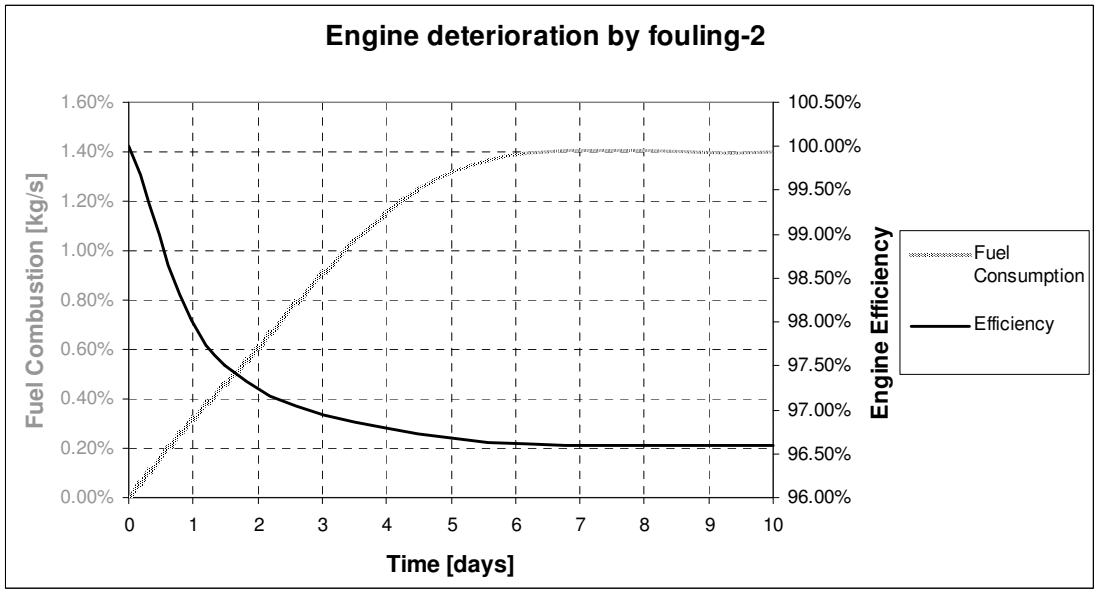

Figure 6-6 Fuel consumption and overall efficiency performance due to compressor fouling in a single shaft gas turbine according to the fouling rate (experiment 7 hors equivalent to 10 days in real engines).

6.3.3 Real case

The results from the engine performance were analyzed in this section with the real information recorded from an industrial engine at full load operation in 2000 (UK). The output power, ambient conditions (temperature and pressure) and time (hour and date) were the parameters in study. The non-dimensional parameters were adopted to avoid the effect of the ambient temperature. $\frac{CDP}{P_i}$, $\frac{UW}{P_i\sqrt{T_i}}$, $\frac{TET}{T_i}$

Where: CDP is the compressor delivery pressure
UW is the output power produced by the engine
TET is the turbine-entry-temperature (1583 K)
P_i & T_i are the ambient pressure and ambient temperature

The period recorded from this engine was 48 hours after compressor washing on line. According to the fouling model the best representation of this time was found between the second and fourth day (see Figure 6-7). The real engine condition was unknown and this could affect other sections that produced a fast reduction in the output power.

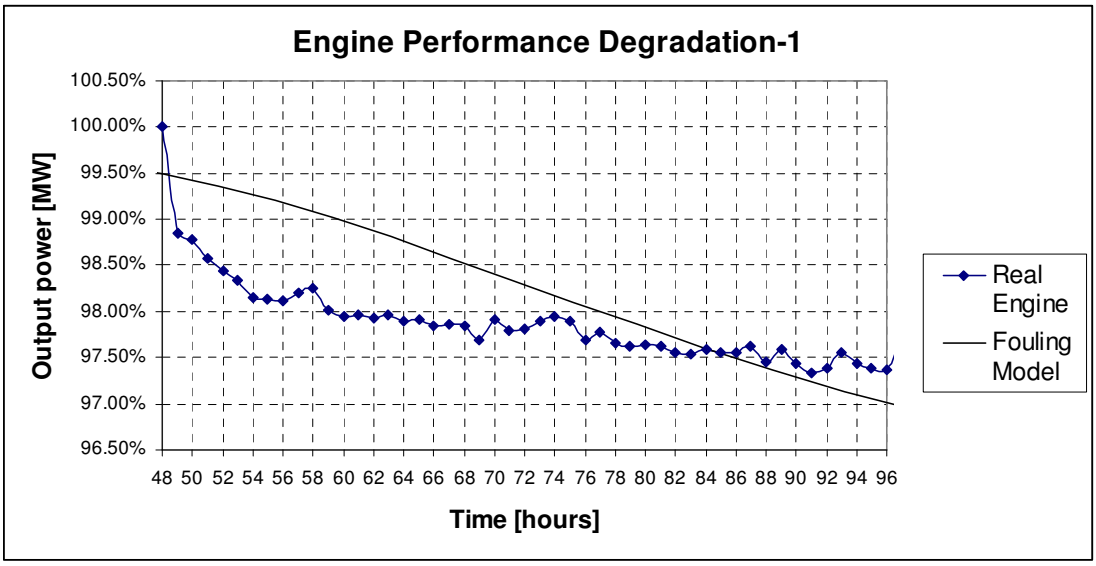

Figure 6-7 Output power from the fouling model and real engine operation (single shaft gas turbine)

The period of the fouling model was scaled to 48 hours with the intention to adjust this to the real engine period. This adjustment was based on the hypothesis that the fouling rate in the real engine was higher than in the model (see Figure 6-8).

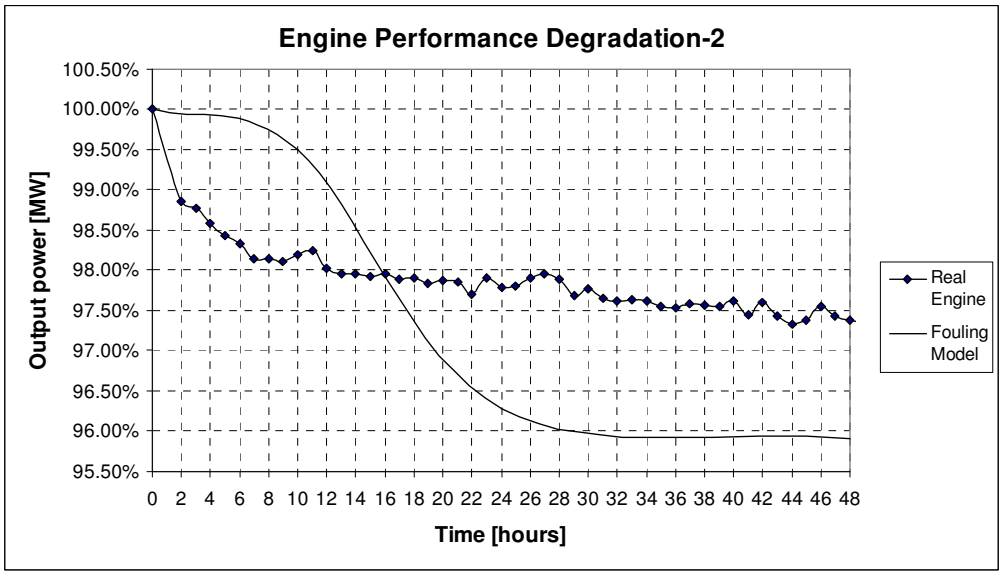

Figure 6-8 Output powers from the real engine and from the fouling model scaled to 48 hours.

A second adjustment in the fouling model was done to approach the model curve to the real engine curve. The model was scaled to the period of 48 hours and scaled to the maximum and minimum values of the real output power (100% and 97.37%) (see Figure 6-9).

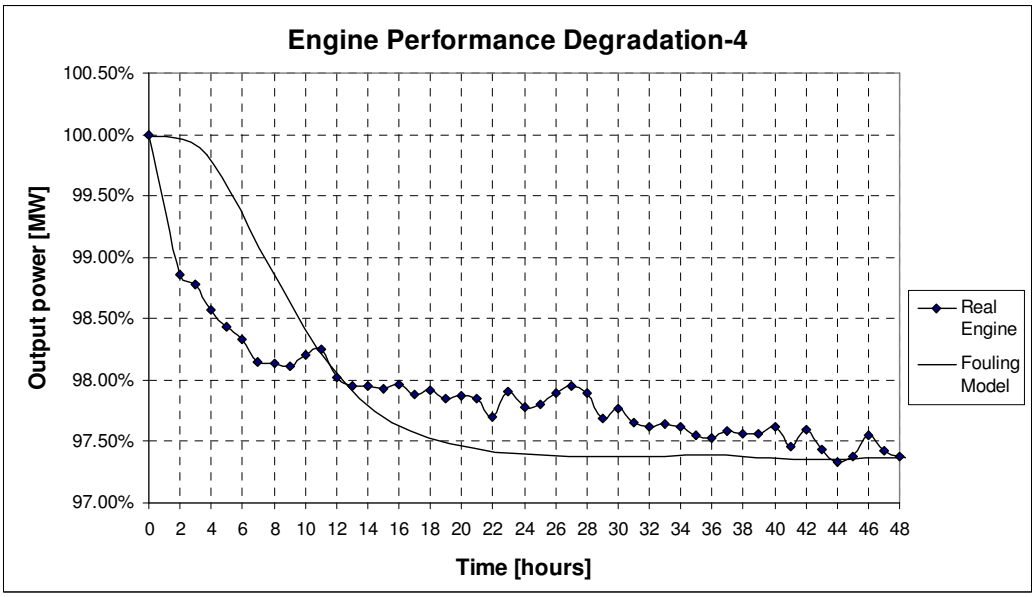

Figure 6-9 Output power from the fouling model and real engine operation with the fouling model period scaled to 48 hours and the output power scaled to the maximum and minimum limits.

6.4 Compressor washing on line

This last section of this work studies the process of compressor washing on line. This technology has been developed during the last years. However, many of the results obtained at the moment have been based on theoretical models that require experimental validation. For example, the literature presented theoretical results of injection angles, droplet size, washing-fluid, operation condition, frequencies of washing, etc. However, this information is waiting the experimental validation. In addition, the incomplete information in this area has created in operators and researchers the uncertainty of the potential of this technology to eliminate the problem of fouling during operation.

A new experimental way to investigate the process of compressor washing on line is presented. The information obtained from this type of experiments can be used to validate many of the theoretical results obtained in this area. The study was limited to adapt a conventional system of compressor washing on line. The results obtained in the tests were used to evaluate the improvements in the gas turbine performance due to this technology.

6.4.1 Experimental results of compressor washing on line

The compressor washing system was adapted and installed in the inlet of the test rig. The system configuration included four sections (see Figure 6-10).

1. Tank to heat the detergent fluid diluted in demineralised water
2. Pump to provide the injection pressure
3. Injection system (single flat nozzle and pressure control valve)
4. Electrical control panel for pump and tank heater
5. Bracket system to adjust the injection angle

Figure 6-10. Compressor washing system installed in the test rig.

The normal operating condition for the compressor washing on line system was used in the test rig (see Chapter 2). The injection of the cleaning fluid diluted in demineralised water was during one minute with the rig in operation (see Figure 6-11). The physical state of the blades was the fouling condition (see Chapter 5).

Figure 6-11 Compressor washing on line operating in the test rig.

Figure 6-12 Top view of the cascade section during the washing on line process (test rig in operation).

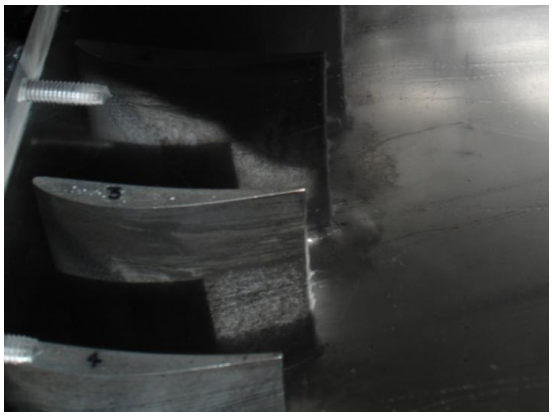

Figure 6-13 Surface of the blade during the process of washing on line (test rig in operation).

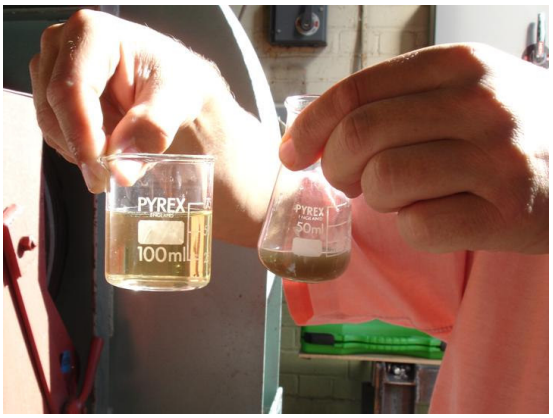

Figure 6-14Washing-fluid before the cleaning process (left). Washing-fluid collected from the cascade (right).

The effectiveness of the washing on line was estimated based on the photos from the fouling tests. The result demonstrated that the fouling was almost removed from the pressure surface of the blade. This can assume that the recovery on this surface was 99% (new condition) (see Figure 6-15).

The result of the washing process on the suction surface was also effective. On the leading region of this surface was found some dust deposition after the washing process. The surface condition result was similar to the result obtained from the fouling blade after 1 hour of the dust injection (see Figure 6-16).

Figure 6-15 Pressure surface of the blades after the washing process (left). Pressure surface of the blades after 1hour of dust injection at rate of 100g/hr equivalent to 1.5 day of engine operation (right).

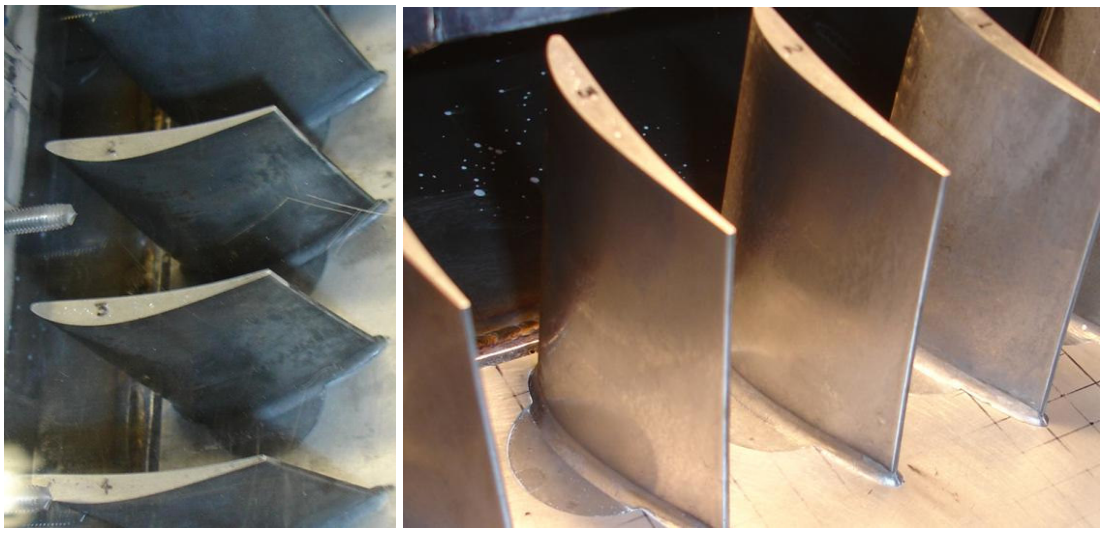

Figure 6-16 Suction surface of the blades after the washing process (left). Suction surface of the blades after 1hour of dust injection at rate of 100g/hr equivalent to 1.5 day of engine operation (right).

With this result is possible to affirm that the washing on line process under this experimental condition of fouling was effective.

6.4.2 Engine performance simulation

The results from the washing process were adapted in the engine of 240MW. The washing process was assumed that recovered the output power until 99.5%.

The total power produced by the engine under this condition was the area below the curve (see Figure 6-17). However, this result of compressor washing can be improved if the compressor is washed before the critical period of degradation observed between the 2 and 5 day. For example, washing the compressor in a frequency of two days, the power is recovered (see Figure 6-18). The result of this frequency demonstrated that the output power was reduced each 48 hours by 0.5%. The engine performance with this washing frequency was more effective 99% than the washing frequency of 10 days.

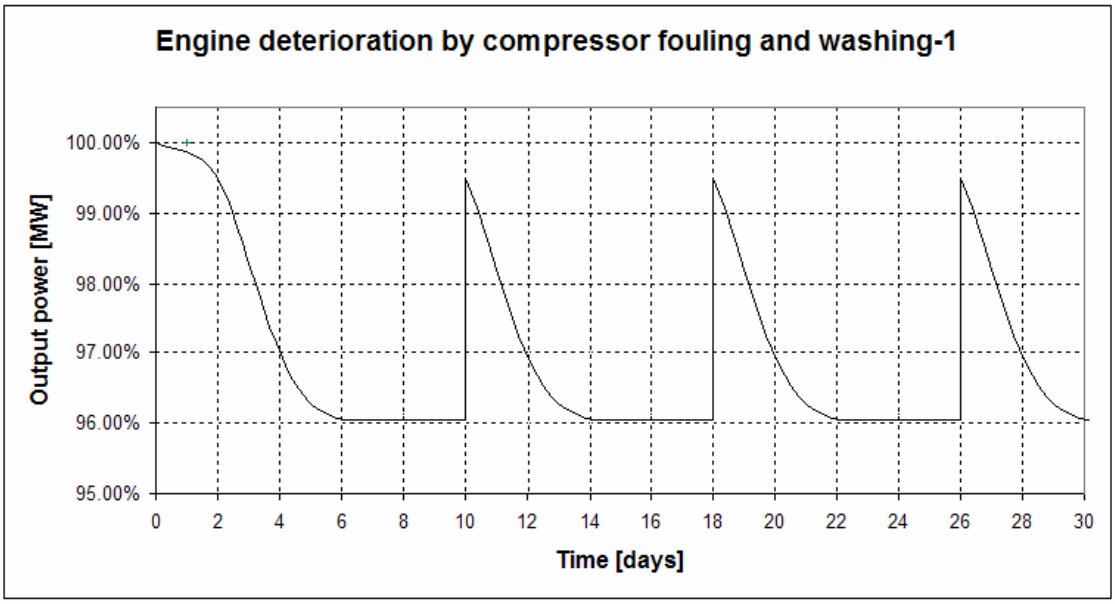

Figure 6-17 Engine performance during fouling deterioration and power recovery by compressor washing each 10 days

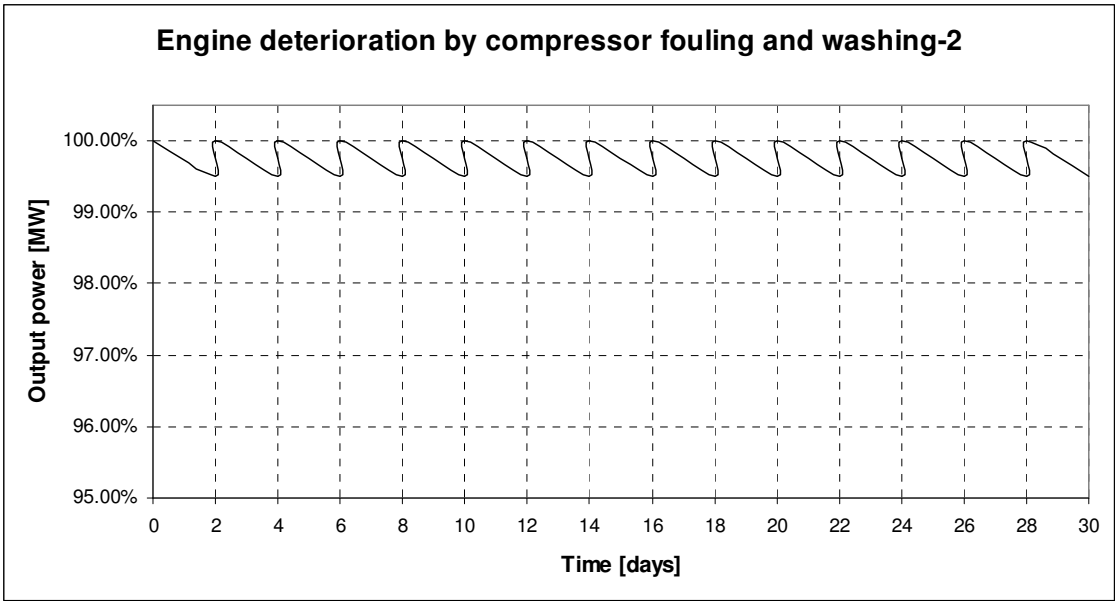

Figure 6-18 Engine performance during fouling deterioration and power recovery by compressor washing each 2 days

6.5 Techno-economic discussion

The power generation plays a fundamental base for the society, industry and economy of the world. However, the production of electricity is a competitive market that requires high levels of production with low cost. This implies that the efficiency of

the engine has to be also high. The advances in this area have produced new systems and equipments that reduce the costs of operation (maintenance and fuel consumption). The environmental laws have obligated to the users of power plants to decrease the emissions and fuel consumption. The use of gas turbines in a combination with a steam turbine in power plants (combined cycles) has been a good alternative to cover these requirements. However, the gas turbine is expensive equipment that requires high quantities of clean fuel for the operation. For this reason, it is necessary a techno economic study of the Power Plant, because the fuel represents the most expensive consumable.

This section was focused on the engine performance simulation to illustrate the importance of compressor washing. The output power of the engine of 240MW was the parameter selected to calculate the costs of operation for the engine in 4 years (overall maintenance period). The prices of the consumables (electricity, gas and compressor washing) were obtained from a data base of the British energy market in 2003. The Present Value and the Future Present Values were calculated in a constant market.

Electricity Price	22.00	£/MWh
Gas Price	6.46	£/MWh
Compressor Washing	20.00	£/Washed

Table 6-5 British market of energy, source INNOGY Ltd 2003.

The costs of production were calculated as follows.

- The fuel consumption was calculated by TURBOMATCH using kerosene as fuel (see Appendix C). However, natural gas is used in the real application to reduce fuel costs. The result of the kerosene was adjusted to the natural gas according to the following equation (Quibel, 1996).

$$W_{nat.gas} = \frac{W_{\ker osene} \bullet CV_{\ker osene}}{CV_{na.gas}}$$

Equation 6-2

Where:

$W_{nat.gas}$ = kg/s

$W_{\text{ker}osene}$ = results from TURBOMATCH in kg/s

$CV_{\text{ker}osene}$ = 42.8 kJ/kgK

$CV_{nat.gas}$ = 46.891 kJ/kgK

- The price of the compressor washing included the cost of washing liquid and equipment.

The two different washing frequencies were analyzed with the consideration of the present value of day 0 and efficiency of 100%. The future values were calculated based on the output power affected by the fouling mechanism. The results demonstrated that the fuel consumption was higher in the frequency of 10 days than in the frequency of 2 days (see Figure 6-19). The frequency of compressor washing each 2 days reduced considerably the costs of the fuel.

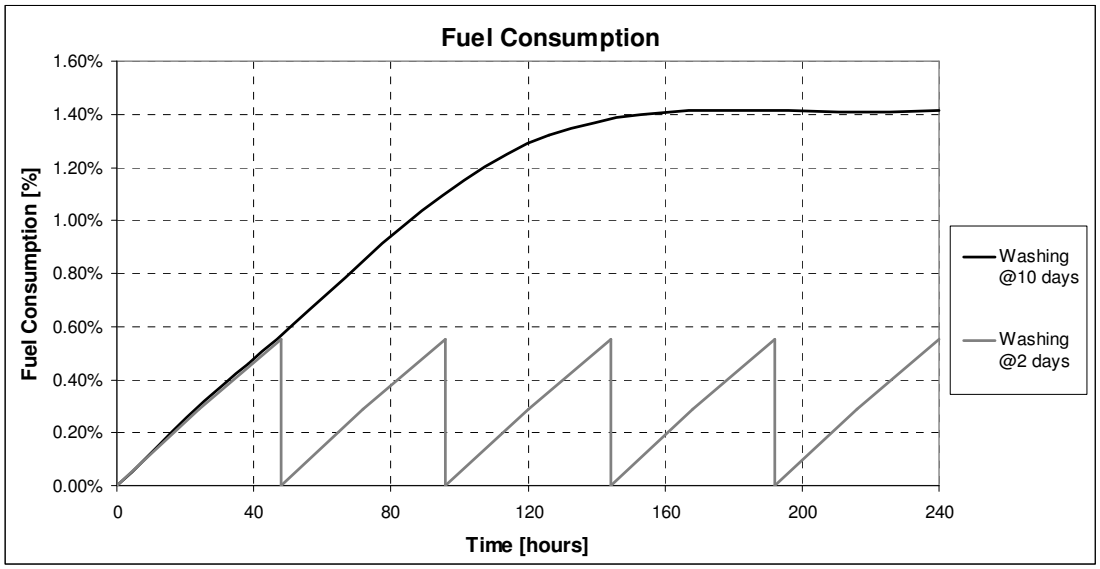

Figure 6-19 Fuel consumption results from the single shaft gas turbine simulation by two different washing frequencies

The economic scenery of the Power Plant was studied with the difference of electricity produced in each washing frequency (see Figure 6-20).

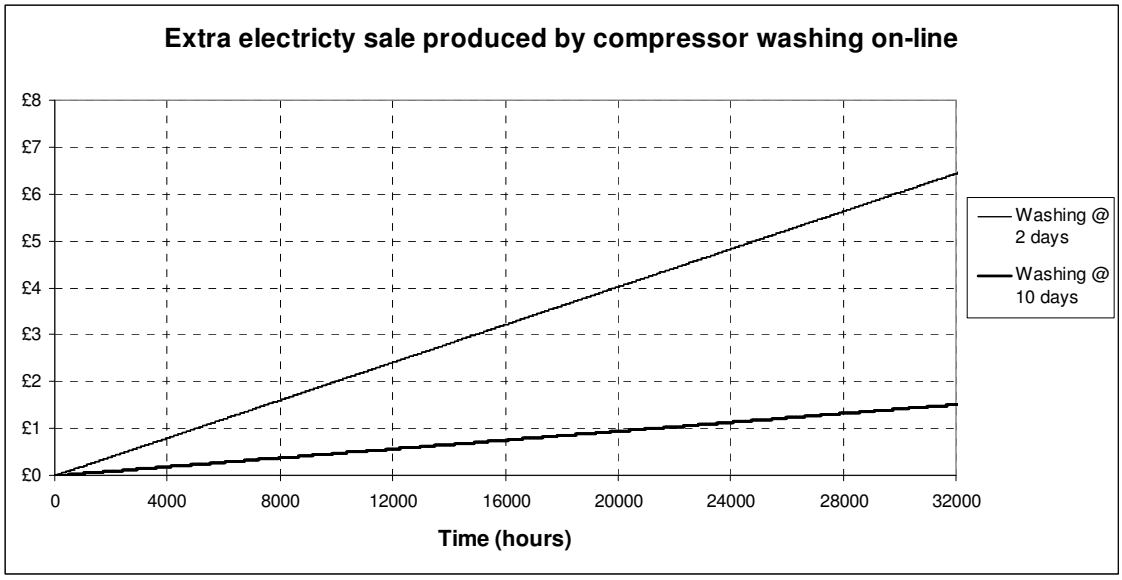

Figure 6-20 Accumulative sale of extra-electricity produced by compressor washing on line in millions of £.

The result demonstrated that in the first year (8000 hours) the washing frequency of 10 days produced £0.402 million more in power production than if the engine was not washed. For the washing frequency of 2 days this difference was £1.733 million. At the end of the four years the washing frequency of 10 days was with accumulative extra production of £1.630 million and in the frequency of 2 days of £6.955 million. The results of compressor washing demonstrated an economic alternative to improve the Power Plant operation.

The production of power for the frequency of 2 days was bigger than the frequency of 10 days. In the first year, the frequency of 2 days produced £1.331 million more than the frequency of 10 days. After the whole period (4 years) this difference was for the frequency of 2 days £5.324 million more than the frequency of 10 days.

The effect of compressor washing in the short period represented in one month was an important fact to save fuel. However, it is necessary to select a correct washing frequency according to operation conditions and level of fouling. It is necessary to adjust the operation condition of the washing system (cleaning fluid temperature, droplet size and washing injection time) to obtain optimal results. The best frequency from the simulation study was the compressor washing of 2 days. This result was

close to the empirical period of washing 3 times per week suggested by the compressor washing manufacturers. However, this value was not definitive, because it was based for an engine in new condition. Then, it is important to evaluate first the engine condition to find the optimal washing frequency. The possibility to combine different frequencies of washing could result an effective technique when the concentration of particles in the air changes.

7 CONCLUSION AND RECOMMENDATIONS

7.1 Conclusion

This last chapter discusses the results obtained by this research based on the experimental study of the fouling mechanism in compressor blades. The model presented in this investigation was created according to the experimental and CFD results. The information obtained from the test rig was validated with the CFD model and with real gas turbines data. The conclusions are presented according to the thesis order.

According to the literature review, the main mechanism of degradation in the compressor is the phenomenon of fouling. This is an evident problem that affects the compressor performance and overall efficiency of the gas turbine. A detailed recompilation of information about the possible sources of fouling was presented in this work. Also, the effect of fouling in a different engine configuration was analyzed. The engine configuration of a single shaft demonstrated to be a complicate job to detect the fouling problem. This is because the engine components in the single shaft are attached to the same shaft and then the problem is hidden by the performance of the components. In Chapter 2 was found that many authors coincided that fouling reduces the overall engine efficiency by 5%. However, this result was created based on arbitrary factors calculated only from the engine output power.

The originality of this work was the use of a test rig to study the effect of fouling in the blade aerodynamics. The complete methodology for the design and building of the test rig and cascade section was presented in this work. The conditions reproduced in the test rig were based on the inlet conditions of a first axial compressor. The geometrical dimension for the real blade size was reproduced in the experiment. The cascade section from the test rig was designed to reproduce uniform flow. The final test rig configuration was the result of three modifications from the original configuration. The condition of the flow was calculated by a CFD model. The application of the CFD was a successful tool to study the physical phenomenon only when the boundary conditions

were known. In this case, the boundary conditions were the atmospheric conditions and the static pressure of the outlet cascade. An internal parameter was used to adjust the model (static pressure of cascade inlet). The use of the real values from the outlet of the cascade in the CFD simulations was not successful. Therefore, the outlet boundary condition was modified from the original values to approach the CFD results to the internal parameter.

The key to reproduce uniform flow inside the cascade was in this case the shape of the side walls. The shape of the walls was designed according to the blade exit angle. This conclusion contrasts with the idea to have several blades in the cascade row mentioned in the literature review. The selection of the materials also played an important role in the design. The use of aluminium was a correct selection to build the test rig. However, the "plexi-glass" selected presented several problems since the machine process and later on in the modifications.

The instrumentation used in the experiment presented two limitations. The first was the collection of information in a high Mach numbers (Ma=0.7). And for that reason, the study was based in a low flow velocities (Ma=0.25). The second limitation was the ability to study the boundary layer. This limitation was mentioned in the literature review because the boundary layer involved the micro scale as was demonstrated in this research. Therefore, the boundary layer region was studied exclusive from the application of the CFD. The thermocouples and surface roughness instruments resulted a correct selection to record the experimental data.

The study region was selected in the central passage of the cascade (between the 2^{nd} and 3^{rd} blade). This was due to present the best flow uniformity in the cascade. The cascade was designed for two dimensional studies. The horizontal plane at the middle blade height was analyzed with the experimental techniques of flow visualization. The oxide of titanium used to visualize the flow path was a successful technique to track the flow path. This result showed the evidence that the flow was travelling in two dimensional trajectories and the three dimensional flow effects was nil. With these two results it was possible to conclude that the flow trajectory was not affected by the top or bottom of the

cascade. In addition, the design of the damper diffusion section at the rig outlet was correct and avoided flow fluctuation produced by the vortex induced in the inlet of the fan.

An important contribution from the CFD in this research was the calculations of parameters that were not possible to measure with the instrumentation available. The two main parameters calculated by the CFD were the static pressure distribution on the blade surface and the boundary layer region. The CFD had to be adjusted and calibrated according to the experimental information from the macro-scale. The parameter used as a criterion to evaluate the CFD model was the geometrical localization of the blade wake. This was a successful result, because the geometrical location of the wake in the test rig coincided with the CFD result. The conclusion was that the results from the CFD are considered reliable in this investigation.

This work is pioneering in the study of fouling and for that reason it was necessary to cover the lack of information missing about this topic. The first problem was to establish the condition of the blade surface. The information regarding the blade surface roughness was limited and it obligated to make a field investigation in real blades. The final result was to adopt the value of Ra =0.6 μm for the roughness surface of the blades. This value was obtained from new blades delivered directly from the OEM. A second problem was the information about the fouling conditions. This information was covered with the data and dust sample provided from the company Recovery Power Ltd. The dust injection rate was calculated with the information and data recorded in the technical visit to Didcot Power Plant. The flow velocity in the cascade was assumed constant and the calculations resulted in a rate of dust injection of 2.8 g/h. The process of fouling was accelerated under two main hypotheses. 1 hour of the experimental dust injection rate was equivalent to 1.5 days of the real operation. The second factor was the use of a glue-agent to increase the particle deposition on the blade surface. These two factors were tested with an artificial powder to evaluate the fouling results in the test rig.

The results from the experimental fouling were close to the fouling observed from the real IGV of the engines. This effect was the result of the static conditions in the cascade.

In this case, the experimental blades represented static airfoils. The most important result from the experiment was the possibility to reproduce and record the progressive formation of fouling. With this information was found that the fouling on the blade was non-uniform. This mechanism is a complex phenomenon that involves the aerodynamic shape of the blade and the rate of fouling. In addition, the blade surface presented regions with roughness increments on the pressure surface of 80μm and on the suction surface of 97μm.

The application of the fouling model resulted in eight sections that represent different regions of the blade surface. However, this model was not practical to evaluate the engine performance and it was necessary to link this with other parameters using the CFD model. The parameters of static pressure and friction skin coefficient were calculated. The fouling effect in these parameters was observed only on the suction surface. Then, a third parameter was calculated to include the whole blade profile. This was the difference of the blade drag when fouling was presented. The result of the drag was used to estimate the fouling effect in the engine performance. The values were scaled to the blade height and processed in GOTRESS to predict the factors that decreased the mass flow and the compressor efficiency. The factors were inserted in the code of TURBOMATCH to calculate the engine performance.

The results of the engine simulation in TURBOMATCH demonstrated that the engine efficiency decreased in a period of 5 days by 3.5%. The engine performance was affected since the first day of operation due to the particles deposition. This was favoured when the smooth surface was presented. According to the results of this simulation, the problem of fouling could affect directly the overall efficiency until 3.5% only. However, in the real application this problem could be transmitted to other section and increases the reduction of the overall efficiency. The results of the engine performance were compared with real data from an engine in operation. The simulation result was adjusted according to the time and output power limits by linear factors. This arbitrary modification in the model was based on the hypothesis that the real engine was affected by higher concentration of particles in the flow. The conclusion of this

adjustment was that that the engine performance of the model resulted almost similar to the performance of the real engine.

The last section of this research was focused to study the compressor washing on line. The experimental results demonstrated that the process of washing removed almost completely the fouling on the blade. The recovery of the engine power was calculated with TURBOMATCH based on an economical scenario of a gas turbine in operation during four years in a Power Plant. The conclusion of this study was that compressor washing on line is an economic and technical solution to recover the power lost due to fouling. In this case of an engine of 240MW the power recovered in four years is equivalent to £6.5 million of electricity sale.

This thesis has covered the objective to create a preliminary model to predict the fouling formation based on experimental tests. The experimental and CFD models resulted a successful way to study the fouling problem and two main conclusions summarize these results. First, the mechanism of fouling is non linear to the time and also is non-uniform on the surface of the blade. The experimental result identified that the critical region of particle deposition is the leading edge of the blade. With this information it was possible to calculate the aerodynamics blade changes and evaluate the effect of fouling in the engine performance. The second conclusion was the effectiveness of the compressor washing on line system to eliminate the fouling problem. Finally, this work has included an overall study of fouling in the study and development of gas turbines.

7.2 Recommendations

In this section is presented the research limitations and the possible recommendations for further investigations in this area. Basically, there are three important considerations that further investigations should be considered before to generalize the application of the fouling model presented in this study. The first one regards the study of the blade profile. Because, the fouling result was based on an exclusive blade profile and the dust deposition could be different from another condition of dust injection rate. The second

regards to the dust type and the third regards to the specific flow condition used (flow velocity).

The use of this particular test rig can be extended for other blades that fix in the cascade the test rig. It is recommended that the blades be located in the centre of the cascade section, so that they are more clearly visible. Also, the use of small blades can increase the number of blades and passages.

For new designs it is essential to consider the characteristics of the power source. The configuration of the fan (blow or suck) depends on the study region selected. In this particular work the blade inlet conditions was selected. Using the fan configuration to (blowing) could give a criterion to decide which configuration is the most appropriate. Another aspect is the material selection for the test rig. It is recommendable to avoid the use of "plexy glass" in sections that requires complex manufacture (aerodynamic shapes) or for main body sections (frames). This material is fragile and difficult for manufacturing process. The use of aluminium is suggested because it is light and easy to manufacture. The test rig is recommendable to be designed in modules. The use of star-bolts and brackets in each section presents a good alternative in the joint of sections.

The CFD was essential in this investigation to calculate the parameters that were not possible to measure in the experiment. However, it is important to have in mind the limitations of the CFD, because each result represents a possible solution that will be judged by the researcher and for that reason it is highly recommended to have a solid criterion of the physical phenomenon based on experimental or real data. This information also will help to adjust the CFD model as it was in this case the macro scale information used to validate and adjust the CFD model. The computational time to process the information is another parameter to consider because this can represent a serious problem when a high precise solution is required. It is suggested to increase gradually the process of the CFD since very basic to complex models. Following this suggestion, it is possible to detect an error during the early stages and avoid long periods of time for incorrect or non-converged solutions.

The results of this research were studied in two dimensional conditions. However, to cover the whole area, it will be necessary to study the rotational effect of the flow. The three dimensional deposition of the dust in the CFD represents a new challenger to investigate. One of the most important applications of the CFD is the possibility of simulating the flow in the whole compressor. So, further investigations could give an important result in studies that includes each particular stage of the compressor. Also, the simulation of the mechanism of fouling by CFD represents a challenge for future investigations. In addition, the compressor washing on line should be analyzed with different fouling samples and this possibility could be studied in the test rig of this investigation.

The results of this investigation can be used as a guide of new projects. The real status of the compressor can only be understood with complete and solid background knowledge of the fouling phenomenon. The future information of compressor washing will result important in the total elimination of fouling.

REFERENCES

Abdelrazik, A. and Cheney, P. (1991), Compressor cleaning effectiveness for marine gas turbines, Conference: International Gas Turbine and Aeroengine Congress and Exposition, Jun 3-6 1991, pp. 6.

Aker, G. and Saravanamuttoo, H. (1989), Predicting gas turbine performance degradation due to compressor fouling using computer simulation techniques, Journal of Engineering for Gas Turbines and Power, Transactions of the ASME, Vol. 111, No. 2, pp. 343-350.

Asplund, P. (1998), Gas turbine cleaning upgrade' (compressor wash), VTT Symposium (Valtion Teknillinen Tutkimuskeskus), Vol. 184, pp. 105.

Bagshaw K.W. (1974), Maintaining Cleanliness in Axial Compressor (National Research Council edition), Canada.

Barlow, H., Rae, W., and Pope, A. (1999), Low speed tunnel testing (3rd edition), New York.

Bouris, D., Kubo, R., Hirata, H., and Nakata, Y. (2002), Numerical comparative study of compressor rotor and stator blade deposition rates, Journal of Engineering for Gas Turbines and Power, Vol. 124, No. 3, pp. 608-616.

Boyce, M. P., Bowman, J. C., Meher-Homji, C., and Focke, A. B. (1985), Energy efficient operation of gas turbine compressor sets, Gas Turbine Conference, USA.

Boyce, M. and Gonzalez, F. (2005), A study of on-line and off-line turbine washing to optimize the operation of a gas turbine, ASME Turbo Expo 2005.*

Britchford, K., Manners, A., McGuirk, J., and Stevens, S. (1994), Measurement and prediction of flow in annular S-shaped ducts, Experimental Thermal and Fluid Science, Vol. 9, No. 2, pp. 197-205.

Brittain, D. (1983), Cleaning gas turbine compressors, Aircraft Engineering.

Brooks, F. J. (2000), GE Gas Turbine Performance Characteristics, GE Report.

Brumbaugh, D. (2002), Inlet air filtration adapts to evolving gas turbine technology, Power Engineering, Vol. 106, No. 10, pp. 51-54.

Caguiat, D., Zipkin, D. M., and Patterson, J. (2002), Compressor fouling testing on Rolls Royce/Allison 501-K17 and general electric LM2500 gas turbine engines, American Society of Mechanical Engineers Turbo Expo 2002, Vol. 2, No. B, pp. 933-942.

Caguiat, D. E. (2003), Rolls Royce/Allison 501-K gas turbine antifouling compressor coatings evaluation, Journal of Turbomachinery, Vol. 125, No. 3, pp. 482-488.

Caterpillar (2005), Power Solar Turbines, available at: www.solarturbines.com

Diakunchak, I. S. (1991), Performance deterioration in industrial gas turbines (International Gas Turbine and Aero-engine Congress and Exposition jun 3-6 edition), New York, USA.

Dixon, S. L. (1998), Fluid Mechanics and Thermodynamics of Turbomachinery (4th edition), Butterworth-Heinemann, USA.

Donaldson Company (2005), TTD Self Cleaning System (GTS -102 rev 6 edition), Donaldson Solution Company.

Escher, P. C. (1995), An Object Oriented Gas Path Analysis Computer Program for General Applications (PhD Thesis), Cranfield University, UK.

Farrel, D. M. and Vittal, B. V. R. (1996), Computer Simulation of Water Ingestion for the T800-LHT-801 Engine Anti-Icing Test Inlet, AIAA.

Fielder, J. (2003), Evaluation of zero compressor wash routine in RN service, 2003 ASME Turbo Expo, Vol. 3, pp. 543-547.

Flashberg, L. S. (1992), Measurement of combustion turbine non-recoverable degradation, International Exhibition & Conference for the Power Generation Industries.

Fluent Inc (2005), User's guide (version 6.2 Manual Edition edition), Fluent.

Freid, W. B. and Tapparo, D. J. (1971), Wash mnifold, USA Patent 3623668, USA.

Gahr, T., Benson, J., Graham, K., Gogins, M., and Brown, M. (2005), Advancements in electrospun nanofiber technology reduce gas turbine compressor fouling, ASME Turbo Expo 2005.*

Gbadebo, S. A., Hynes, T. P., and Cumpsty, N. A. (2004), Influence of surface roughness on three-dimensional separation in axial compressor, Journal of Turbomachinery, Vol. 4, No. 4, pp. 455-463.

General Electric (2001), Compressor rotor R-0 blade erosion, Technical Information Letter, GE Energy Services,

Giampolo, T. (1997), The Gas Turbine Handbook, The Fairmont Press, USA.

Gostelow, J. P. (1984), Cascade Aerodynamics, Pergamon Press Ltd, Australia.

Gulen, S., Griffin, P., and Paolucci, S. (2002), Real-time on-line performance diagnostics of heavy-duty industrial gas turbines, Journal of Engineering for Gas Turbines and Power, Vol. 124, No. 4, pp. 910-921.

Haq, I. and Saravanamuttoo, H. (1991), Detection of axial compressor fouling in high ambient temperature conditions, American Society of Mechanical Engineers , pp. 9.

Harris, H. and Calabrese, M. (1994), On-line detergent fluid evaluation on a TF4OB gas turbine engine, American Society of Mechanical Engineers, 94-GT-452, pp. 1-9.

Haub, G. and Hauhe, W. (1990), Field evaluation of on-line compressor cleaning in heavy duty industrial gas turbines, International Gas Turbine and Aeroengine Congress and Exposition, Jun 11-14 1990, Brussels, Belg, pp. 12.

Hobson, G., Hansen, D., Schnorenberg, D., and Grove, D. (2001), Effect of Reynolds number on separation bubbles on compressor blades in cascade, Journal of Propulsion and Power, Vol. 17, No. 1, pp. 154-162.

Hoeft, R. F. (1993), Heavy Duty Gas Turbine Operating and Maintenance Considerations, GE I&PS.

Howell, A. R. and Calvert, W. J. A. (1978), New Stage Stacking Technique for Axial Flow Compressor Performance Prediction, 100:698-703.

Ingistov, S. (2002), Interstage Injection into Axial Compressor, Gas Turbine Model 7EA, ASME Turbo Expo 2002.*

Jeffs, E. (1992), Compressor washing on line for large turbines, Turbomachinery International.

Jeffs, E. (2000), Siemens Cockpit 2000: Integrated plant management for the IPP, Turbomachinery International, Vol. 41, No. 4, pp. 16-17.

Kaes, G. (1991), Method of a cleaning agent for the cleaning compressors especially gas turbines, US Patent 5076855, USA.

Kolev, S. and Robben, R. (1993), Injection device for the on-line wet cleaning of compressors, US Patent 5193976, USA.

Kolkman, H. (1993), Performance of gas turbine compressor cleaners, : Journal of Engineering for Gas Turbines and Power, Transactions of the ASME, Vol. 115, No. 3, pp. 674-677.

Kulle, V. (1974), Gas turbine blade cleaning at Alberta gas trunk line (AGTL) (Gas Turbine Operation and Maintenance Symposium edition), In N.R.C. of Canada.

Kurz R. and Brun K. (2001), Degradation in gas turbine systems, Journal of Engineering for Gas Turbines and Power, Vol. 123, No. 1, pp. 70-77.

Lakshminarasimha, A., Boyce, M., and Meher-Homji, C. (1994), Modelling and analysis of gas turbine performance deterioration, Journal of Engineering for Gas Turbines and Power, Transactions of the ASME, Vol. 116, No. 1, pp. 46-52.

Lakshminarasimha, A. and Saravanamutto, H. (1986), Prediction of fouled compressor performance using stage stacking techniques, American Society of Mechanical Engineers, Fluids Engineering Division (Publication) FED, Vol. 37, pp. 59-66.

Lambart, P., Gordon, R., and Burnett, M. (2003), Developments in on-line gas turbine cleaning, Institution of Diesel and Gas Turbine Engineers 2nd Gas Turbine Conference, UK.

Langford, J. L. F. (1977), Contamination removal method, Patent 4,065,322, USA.

Leusden, C. P., Sorgenfrey, C., and Dummel, L. (2003), Performance benefits using Siemens advanced compressor cleaning system, Germany (Siemens AG Power Generation), Vol. 1 at Atlanta, Georgia, USA; American Society of Mechanical Engineers, USA, pp. 793-801.

Levine, P. and Angello, L. (2005), Axial Compressor Performance Maintenance, ASME Turbo Expo 2005.*

Mansson, M. Washing apparatus for a compound compressor, USA Patent 4046155, USA.

Margolis, H. (1991), U.S. navy on-line compressor washing of marine gas turbine engines, International Gas Turbine and Aeroengine Congress and Exposition, Jun 3-6 1991, Orlando, FL, USA, pp. 6.

Mathioudakis, K., Stamatis, A., Tsalavoutas, A., and Aretakis, N. (2001), Performance analysis of industrial gas turbines for engine condition monitoring, Journal of Power and Energy, Vol. 215, No. 2, pp. 173-784.

Mathioudakis, K. and Tsalavoutas T. (2002), Uncertainly Reduction in Gas turbine Performance Diagnosis by Accounting for Humidity effects, Journal of Engineering for Gas Turbines and Power, Vol. 124, pp. 801808.

Mayle, R. E. (1991), Role of laminar-turbulent transition in gas turbine engines (Congress and Exposition ASME edition), USA.

McDermott, P. (1991), Gas turbine compressor fouling. The case for on-line cleaning, Turbomachinery International, Vol. 32, No. 1, pp. 34-38.

Meher-Homji and Cyrus B (1990), Gas turbine axial compressor fouling, a unified treatment of its effects, detection, and control, 1990 ASME COGEN-TURBO: 4th International Symposium on Gas Turbines in Cogeneration, Repowering, and Peak-Load Power Generation, Aug 27-29 1990, New Orleans, LA, USA, Vol. 5, pp. 179-190.

Meher-Homji, C. B. and Bromley, A. (2004), Gas Turbine Axial Compressor Fouling and Washing (33rd Turbomachinery Symposium edition), Texas A&M University, USA.

Mezheritsky, A. and Sudarev, A. (1990), Mechanism of fouling and the cleaning technique in application to flow parts of the power generation plant compressors, International Gas Turbine and Aeroengine Congress and Exposition, Jun 11-14 1990, Brussels, Belg , pp. 13.

Morillo De Hart, L. (1994), Performance Diagnostic of RR Avon Engines Using Gas Path Analysis, (MSc Thesis), Cranfield University, UK.

Mund, F. and Pilidis, P. (2004), A review of gas turbine online washing systems, Turbo Expo 2004.*

Mund, F. (2006), Coordinated Application of CFD and Gas Turbine Performance Methods (PhD Thesis), Cranfield University, UK.

Murthy, S. N. B., Ehresman, C. M. N., and Haykin, T. (1986), Direct and system effects of water ingestion into jet engine compressors, American Society of Mechanical Engineering - Fluids Engineering Division,

Mustafa, Z. (2006), Analysis of Droplets in Compressor Gas Turbines (PhD Thesis), Cranfield University, UK.

Olhovsky, G. G. (1985), Power Gas Turbine Unit, Moscow.

Orsach, R., Kazcprzynski, G., Roemer, M., Scharschan, J., Caguiat, D., and McGroarty, J. (2002), Applications of diagnostic algorithms for maintenance optimization of marine gas turbines, ASME TURBO EXPO 2002, Vol. 2, No. B, pp. 1025-1033.

Osborne, R. (1977), Design of an Industrial Gas Turbine Intake, American Air Filter Co.

Pankhurts, R. C. (1952), Wind-Tunnel Technique. An account of experimental methods in low and high speed tunnels, Sir Isaac Pitman & Sons, UK.

Peltier, R. and Swanekamp, R. (1995), LM2500 recoverable and non-recoverable power loss, American Society of Mechanical Engineers, 95-CTP-104, pp. 6.

Quibel, A. (1996), Performance and Deterioration Diagnostics of a 25 MW Turbine Plant at an Oil Refinery (MSc Thesis), Cranfield University, UK.

Ramsden, K. (2002), Axial Compressor Design and Performance Notes, Cranfield University, UK

Ramson, W. (2004), Adiabatic Effectiveness Measurements of Leakage Flows near the Hub Region of Gas Turbine Engines (MSc Thesis), Virginia Polithecnique Institute and State University, 2004.

Raykowski, A., Hader, M., Maragno, B., and Spelt, J. (2001), Blast cleaning of gas turbine components deposit removal and substrate deformation, Wear, Vol. 249, No. 1-2, pp. 127-132.

Razak, A. M. Y. and Dosanjh, M. S. (2002), Application of an advanced performance monitoring system to detect an implanted fault on a twin spool aero derived gas turbine, Gas Path Analysis Ltd., R. M. E. T. U. UK, Vol. 2 A at Amsterdam, The Netherlands; American Society of Mechanical Engineers, The Netherlands, pp. 29-36.

Rubini, P. (2006), Computational Fluid Dynamics Notes, Cranfield University, UK.

Saravanamuttoo, H., Cohen, H., and Rogers, G. (1996), Gas Turbine Theory (4 edition), Longman, UK.

Saravanamuttoo, I. and Lakshminarasimha, A. (1985), Preliminary assessment of compressor fouling, Turbomachinery International, Vol. 26, No. 7, pp. 14-18.

Scala Sinclaire, Konrad, M., and Mason, R. (2003), Predicting the Performance of a Gas Turbine Engine Undergoing Compressor Blade Erosion (AIAA 39th edition), Joint Propulsion Conference and Exhibition.

Scheper, G. W., Mayoral, A. J., and Hipp E.J. (1978), Maintining gas turbine compressors for high efficiency, Power Engineering.

Schlichting, H. (1979), Boundary Layer Theory, Mc Graw Hill, USA.

Scott, J. N. (1979), Axial compressor monitoring by measuring depression (In N.R.C. of Canada edition), 3rd Symposium of Gas Turbine Operations and Maintenance, Canada.

Seddigh, F. and Saravanamuttoo, H. (1990), Proposed method for assessing the susceptibility of axial compressors to fouling, International Gas Turbine and Aeroengine Congress and Exposition, Jun 11-14 1990, Brussels, Belg, pp. 8.

Siemens (2005), available at: www.siemens.com

Singh, D. (1996), Simulation of Performance Deterioration in Eroded Compressor, American Society of Mechanical Engineering.*

Singh, R. (2002), Gas Turbine Applications Notes, Cranfield University, UK.

Sorli, A., Langes, K., Laagland, G., and Hastings, M. (2002), Performance monitoring on the ASGARD "A" FPSO as part of an integrated monitoring strategy, ASME TURBO EXPO 2002, Vol. 2, No. A, pp. 37-44.

Stalder, J.-P. and Sire, J. (2001), Salt percolation through gas turbine air filtration systems and its contribution to total contaminant level, Proceedings of the International Joint Power Generation Conference, Vol. 2, pp. 445-446.

Stalder, J.-P. and Van Oosten, P. (1994), Compressor washing maintains plant performance and reduces cost of energy production, American Society of Mechanical Engineers, pp. 1-16.

Syverud, E. and Bakken, L. (2005), Online water wash tests of GE J85-13, ASME Turbo Expo 2005.*

Syverud, E., Bakken, L. W., Langnes, K., and Bjornas, F. (2003), Gas turbine operation offshore; on-line compressor wash at peak load, Norwegian University of Science and Technology , Vol. 4 at Atlanta, Georgia, USA; American Society of Mechanical Engineers, USA, pp. 17-27.

Syverud, E., Brekke O., and Bakken L. (2005), Axial compressor deterioration caused by saltwater ingestion, ASME Turbo Expo 2005.*

Tabakoff, W. (1986), Compressor Erosion and Performance Deterioration, AIAA/ASME 4th Joint Fluid Mechanics, Plasma Dynamics, and Laser Conference May 12-14, Atlanta.

Tabakoff, W. and Balan, C. (1983), A Study of Surface Deterioration due to Erosion, Journal of Engineering for Power, Vol. 112, No.1, ASME.

Tabakoff, W., Lakshminarasimha, A. N., and Pasin, M. (1990), Simulation of Compressor Performance

Deterioration Due to Erosion, Journal of Engineering for Power, Vol. 112, No.1, ASME.

Tarabrin, A., Bodrov, A., Schurovsky, V., and Stalder, J.-P. (1996), Analysis of axial compressors fouling and a cleaning method of their blading, American Society of Mechanical Engineers, 96-GT-363, pp. 7.

Tarabrin, A., Schurovsky, V., Bodrov, A., Stalder, J.-P., and Bodrov, A. (1998), Influence of axial compressor fouling on gas turbine unit performance based on different schemes and with different initial parameters, American Society of Mechanical Engineers, n GT, 98-GT-416, pp. 6.

Taylor Hobson Ltd (2001), User Guide, Surtronic 25, Taylor Hobson Ltd, UK.

Thames, J., Stegmaier, J., and Ford, J. J. J. (1989), On-line compressor washing practices and benefits, American Society of Mechanical Engineers, Jun 4-8 1989, Toronto, Ontario, Canada , pp. 6.

Tsuchiya, T. (1982), Aerodynamics of Axial-Flow Compressors with Water Ingestion, Purdue University, USA.

Upton A.W.J. (1974), Axial Compressor and Turbine Blade Fouling Some Causes, Effects and Cleaning Methods (Gas Turbine Operations and Maintenance Symposium edition), National Research Council Canada, Canada.

Valenti, M. (1998), Drier way to clean turbines, Mechanical Engineering, Vol. 120, No. 3, pp. 98-100.

Vigueras Zuniga, M. O. (2003a), Intake Systems for Industrial Gas Turbines, Cranfield Gas Turbine Symposium 2003, Cranfield University, pp. 3-18.

Vigueras Zuniga, M. O. (2003b), Technoeconomic Analysis of Compressor Washing (MSc Thesis), Cranfield University, UK.

Walsh, P. P. and Fletcher, P. (1999), Gas Turbine Performance Blackwell Science.

Weisman, J. and Eckart, L. E. (1985), Modern Power Plant Engineering, Prentice-Hall, USA.

Wilkinson, P. and Shark, L.-K. (2004), Automatic monitoring of gas turbine air intakes using colour imaging techniques, Insight: Non-Destructive Testing and Condition Monitoring, Vol. 46, No. 2, pp. 94-97.

Williams, L. J. (1981), The optimisation of time between overhauls for gas turbine compressor units (4th Symposium of Gas Turbine Operations and Maintenance edition), In N.R.C of Canada, Canada.

Woodson, J. B., Cooper, L. A., White, H. M., and Fischer, G. C. (1989), Cleaning gas turbine compressors, US Patent 4808235, USA.

Yee, R. and Myers, L. (2003), Enhanced tf40b gas turbine engine design changes to improve resistance to the Landing Craft Air Cushion (LCAC) operational environment, Naval Surface Warfare Center Carderock Division, C. S. C. A. M. C. USA, Vol. 3 at Atlanta Georgia USA; American Society of Mechanical Engineers, USA, pp. 495-499.

Zaba, T. L. P. (1984), Experience in the Operation of Air Filters in Gas Turbine Installations (29th International Gas Turbine Conference Exhibition edition), ASME.

Zwebek, A. (1993), One giga watt single shaft Industrial Gas Turbine Design (MSc Thesis), Cranfield University, UK.

Zwebek, A. (2002), Combined Cycle Performance Deterioration Analysis (PhD Thesis), Cranfield

University, UK.

Zwebek, A. and Pilidis, P. (2003), Degradation effects on combined cycle power plant performance - Part II: steam turbine cycle component degradation effects, Journal of Engineering for Gas Turbines and Power, Vol. 125, pp. 658-663.

Zwebek, A. and Pilidis, P. (2004), Degradation Effects on combined cycle power plant performance - Part III: gas and steam turbine component degradation effects, Journal of Engineering for Gas Turbines and Power, Vol. 126, pp. 306-315.

Zwebek, A. P. P. (2003), Degradation Effects on Combined Cycle Power Plant Performance - Part I: gas turbine cycle component degradation effects, Journal of Engineering for Gas Turbines and Power, Vol. 125, pp. 651-657.

* The complete reference source of this document was not available.

APPENDICES

A. Engines specifications

GAS TURBINE SOLAR MODEL SATURN 20

Specifications:

Production 1.2 MW with a
Gross efficiency of 24.7%
Two-Shaft
Axial Compressor
- 8 stages
- Compression Ratio: 6.2:1,
- Inlet Airflow of 6.4 kg/sec,
- Max. Speed: 22,850 rpm),

Combustion Chamber
- Annular-Type
- 12 Fuel Injectors
- Torch Ignitor System

Gas Producer Turbine
- 2 stages Reaction
- Max. Speed: 22,850 rpm)

Power Turbine
- 1 stage
- Reaction, Max
- Speed: 22,300 rpm

Bearings
- Journal: Multi-Ramp Sleeve
- Thrust: Fixed Tapered Land

Coatings
- Compressor: Inorganic Aluminium
- Turbine and Nozzle Blades: Precious Metal Diffusion Aluminide

Vibration Transducer Type Velocity.

Photo-1 Gas Turbine model Saturn 20

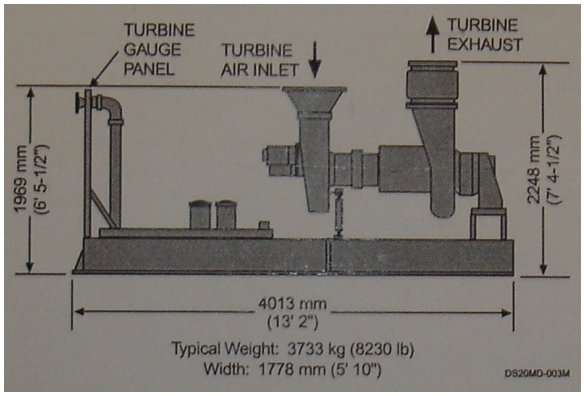

Photo-2 Gas Turbine model Saturn 20

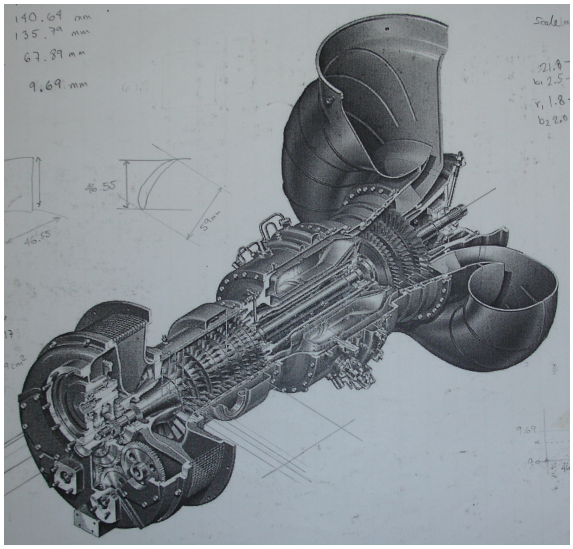

Photo-3 Gas Turbine model Saturn 20 (Caterpillar (2005))

GAS TURBINE SIEMENS MODEL V94.3A (SGT5-4000)

Specifications:

Production 260 MW
Gross efficiency of 38.5%
Single-Shaft
Axial Compressor
- 15 stages
- Compression Ratio: 16:1
- Inlet Airflow of 630 kg/s
- Controlled diffusion airfoils

Combustion Chamber
- Annular-Type
- 24 hybrid burners
- Ceramic combustion chamber tiles)

Turbine Section
- 1 stage
- Reaction-Power

Coatings
- Compressor: Inorganic Aluminium
- Turbine and Nozzle Blades Single-crystal and thermal barrier coating

Gas Turbine model SIEMENS V94.3A (Siemens (2005)).

GENERAL ELECTRIC MODEL FRAME 6B (LM6000)

Specifications:

Production 42.3 MW
Gross efficiency of 42%
Two-Shaft
Axial Compressor
- 5 stages LPC @ 3600rpm
- 14 stages HPC
- 6 variable geometry stages
- Compression Ratio 29:1
- Inlet Airflow of 120 kg/sec

Combustion Chamber
- Annular-Type
- 30 individually replaceable fuel nozzles
- Dual fuel

Turbine Section
- 2 stages HPT (air-cooled)
- 5 stages LPT Stage
- Reaction-Power

Coatings
- Compressor: Inorganic Aluminium
- Turbine and Nozzle Blades Single-crystal and thermal barrier coating film cooling

Dual-rotor gas turbine, derived from the CF6-80C2, high bypass, turbofan aircraft engine.

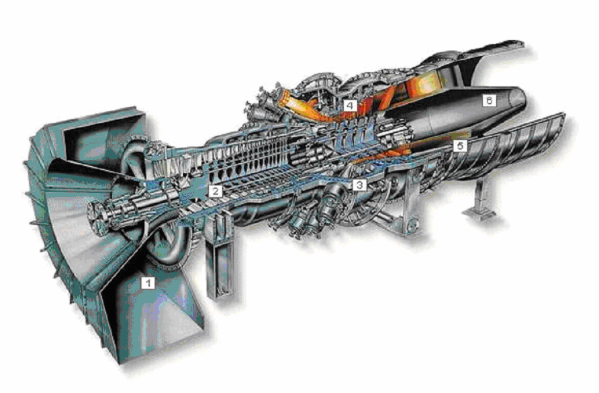

Gas Turbine model G&E Frame 6 (G&E (2005)).

B. Preliminary axial compressor design

GENERAL CHARACTERISTICS

TYPE	GAS TURBINE 1.185 mw
MODEL	SATURN 20
MANUFACTURER	SOLAR (CATERPILLAR)
TWIN SHAFT	COMPRESSOR & TURBINE DRIVE
	TURBINE POWER

COMPRESSOR

MASS FLOW	23410 kg/h = 6.4 kg/s
STAGES	8
SPPED MAX	22850 rpm
COMPRESSOR RATIO	6.2:1
GAS TURBINE POWER (FULL LOAD)	
STAGES	2
MAX. SPEED	22850 rpm
OUT POWER	1.4MW
EXHAUST TEMPERATURE	525 C
FUEL FLOW	4.75 MW (MM BTU/h)
EXHAUST FLOW	23410 kg/h
THERMAL EFFICIENCY	0.245

ISA CONDITIONS	
AMBIENT TEMPERATURE	15 C
AMBIENT PRESSURE (SEA LEVEL)	101000 Pa
HUMIDITY	0.6
FUEL	NATURAL GAS LHV=31.5~43.3 MJ/nm^3 (800~1100 BTU/scf)

1.0. SPECIFICATION

1. Overall Pressure Ratio (Solar=S)	Rc=	data	6.2
Target Efficiency Polytropic (Ken Ramsden=KR)	np=	goal	0.88
Mass Flow (S)	W=	data	6.4
Inlet Pressure (S)	P1=	data	101000
Inlet Temperature (S)	T1=	data	288
Ratio of Specific Heats (KR)	g=	assump	1.4
Blockage factor (KR)	kb1=	assump	0.99
Shaft Speed [rpm] (S)	N=	data	22850
Diameter Tip 1st rotor, it is cte=annulus config (S)	Dt=	data	0.281
Blade Height 1st rotor (S)	B1=	data	0.07
Gap (www.sulzermetco.com)	gap=	assump	0.000127
Ideal Gas Constant (KR)	R=	data	273
Diameter Hub 1st rotor	Dhr1=	Dt1-2(B1+gap)	0.140746
Diameter Medium 1st rotor	Dmr1=	(Dt1-Dh1)/2+Dh1	0.210873

2.0. INITIAL CHOSEN VARIABLE

No.Stages (S)	stages=	data	8
Mean Blade Speed 1st rotor inlet	Umr1=	N*3.1415*Dm1/60	252.285909
Mean Absolute Air Angle at Inlet to 1st Stage IGV (S)	alfa0=	assumpt&variable	30
Mean Axial absoluty Velocity	Vo1=	assumpt&variable	140
Mean Axial Velocity at Inlet	Va1=	cos(alfa0)*Vo	121.246256

Inlet Hub/Tip Ratio	Dhr1/Dt=	Dhr1/Dt1	0.50087544
Stage Temperature Rise Distribution (KR)	S, ¬T=	assumpt	Constant
Annulus Configuration (S)	AC=	data	cte. Diam
3.0. DESIGN PROCEDURE			
3.1 Overall Efficiency	nc=	(Rc^((g-1)/g)-1)/(Rc^((g-1)/(g*np))-1)	0.84648888
3.2	¬Tc=	T1/nc*(Rc^((g-1)/g)-1)	232.789856
3.3	¬Tstage=	¬Tc/stages	29.0987321
3.4	Va/$T1=	Va/$T1	7.14450416
	> Qo=	tables	0.023285
ROTOR INLET ABSOLUTE MACH NUMBER	Mo=	tables	0.36
CROSS AREA INLET 1ST ROTOR	A1=	W*$T1/kb1*P1*Qo	0.04664911
I don't use this equation, because I want Dt=cte=data	Dt=	A1*4/(3.1415*(1-(Dh1/Dt)^2)	0.281
Dhr1 has to give us the Area calculated	Dhr1=	Dhr1/Dt*Dt && ((Dt-4*A/3.1415))^0.5	0.13987048
	Dmr1=	(Dhr1+Dt)/2	0.21043524
3.5. ROTATIONAL SPEED	N=	Um*60/(3.1415*Dm)	22897.5341
3.6.	T2=	T1+¬Tstages	317.098732
	Rstage1=	(nc*(¬Tstages/T1)+1)^(g/(g-1))	1.3473358
	P2=	Rstage*P1	136080.916
	Va1/$T2=	Va1/$T2	6.80880795
	> Qo=	tables	0.022454
(KR)	kb2=	assumption	0.95
ANNULUS AREA AT FIRST STAGE EXIT	A2=	W*$T2/kb2*P2*Qo	0.03926112
	Dhr2=	$((Dt^2-((A2*4)/3.1415))	0.17020786
DIAMETER MEDIUM AT 1ST STATOR OUTLET	Dmr2=	(Dt+Dh2)/2	0.22560393
3.7. DIAMETER MEDIUM AT 1ST STATOR	Dms1=	(Dmr2+Dmr1)/2	0.21801958
MEAN ROTOR BLADE SPEED	U2mr1=	3.1415*Dms1*N/60	261.378605
	Dhs1=	(Dh1+Dh2)/2	0.15503917
3.8.	tan alfa1=	Umr1/Va1	2.08077278
	alfa1=	angtan(alfa1)	64.3362333
	Cp=	g*R/(g-1)	1004.5
	Vw3m=	Cp*(¬Tc/stages)/U2mr1	111.828879
1st Iteration	Va2=	Va1	121.246256
	V3=	(Va1^2+w3m^2)^0.5	164.943484
	V3/$T2=	V3/$T2=	9.26270665
	>Q2=	tables	0.028833
ANNULUS AREA AT OUTLET 1ST ROTOR	Ar2=	(3.1415/4)*(Dt^2-Dhs1^2)	0.04313582
	Q2cos alfa3=	(W*T2^0.5)/(kb1*P2*Ar2)	0.01961131
	cos alfa3=	Q2cos alfa3/Q2	0.68016908
	alfa3=	angcos(alfa3)	47.1466159
	tan alfa3=	tan(alfa3)	1.07775448
	Va'2=	Vw3m/tan(alfa3)	103.760997
2nd	Va2=	(Va1+Va'2)/2	112.503626
	V3=	(Va1^2+w3m^2)^0.5	158.627753

	V3/$T2=	V3/$T2=	8.90803513
	>Q2'=	tables	0.028137
	Ar2=	(3.1415/4)*(Dt^2-Dhs1^2)	0.04313582
	Q2'cos alfa3=	(W*T2^0.5)/(kb1*P2*Ar2)	0.01961131
	cos alfa3=	Q2cos alfa3/Q2	0.69699382
	alfa3=	angcos(alfa3)	45.8170624
	tan alfa3=	tan(alfa3)	1.0288142
	Va2'=	Vw3m/tan(alfa3)	108.696865
3rd	Va2=	(Va1+Va'2)/2	114.971561
	V3=	(Va1^2+w3m^2)^0.5	160.387524
	V3/$T2=	V3/$T2=	9.00685832
	>Q2'=	tables	0.028371
	Ar2=	(3.1415/4)*(Dt^2-Dhs1^2)	0.04313582
	Q2'cos alfa3=	(W*T2^0.5)/(kb1*P2*Ar2)	0.01961131
	cos alfa3=	Q2cos alfa3/Q2	0.69124511
	alfa3=	angcos(alfa3)	46.2746574
	tan alfa3=	tan(alfa3)	1.04538949
	Va2'=	Vw3m/tan(alfa3)	106.973411
4th	Va2=	(Va1+Va'2)/2	114.109833
	V3=	(Va1^2+w3m^2)^0.5	159.770937
	V3/$T2=	V3/$T2=	8.97223271
	>Q2'=	tables	0.028371
	Ar2=	(3.1415/4)*(Dt^2-Dhs1^2)	0.04313582
	Q2'cos alfa3=	(W*T2^0.5)/(kb1*P2*Ar2)	0.01961131
	cos alfa3=	Q2cos alfa3/Q2	0.69124511
	alfa3=	angcos(alfa3)	46.2746574
	tan alfa3=	tan(alfa3)	1.04538949
	Va2'=	Vw3m/tan(alfa3)	106.973411
5th	Va2=	(Va1+Va'2)/2	114.109833
	V3=	(Va1^2+w3m^2)^0.5	159.770937
	V3/$T2=	V3/$T2=	8.97223271
	>Q2'=	tables	0.028371
	Ar2=	(3.1415/4)*(Dt^2-Dhs1^2)	0.04313582
	Q2'cos alfa3=	(W*T2^0.5)/(kb1*P2*Ar2)	0.01961131
	cos alfa3=	Q2cos alfa3/Q2	0.69124511
	alfa3=	angcos(alfa3)	46.2746574
	tan alfa3=	tan(alfa3)	1.04538949
	Va2'=	Vw3m/tan(alfa3)	106.973411
6th	Va2=	(Va1+Va'2)/2	114.109833
	V3=	(Va1^2+w3m^2)^0.5	159.770937
	V3/$T2=	V3/$T2=	8.97223271
	>Q2'=	tables	0.028371
	Ar2=	(3.1415/4)*(Dt^2-Dhs1^2)	0.04313582
	Q2'cos alfa3=	(W*T2^0.5)/(kb1*P2*Ar2)	0.01961131
	cos alfa3=	Q2cos alfa3/Q2	0.69124511
	alfa3=	angcos(alfa3)	46.2746574
	tan alfa3=	tan(alfa3)	1.04538949
	Va2'=	Vw3m/tan(alfa3)	106.973411

	tan alfa2=	(U2mr1-Vw3m)/Va2'	1.39800839
	alfa2=	angtan (alfa2)	54.4277438
	cos alfa2=	Cos(alfa2)	0.58178609
	cos alfa1=	cos(alfa1)	0.43316371
3.9. DE HALLER NUMBER MEDIUM ROTOR	DDmr1=	(Va2'*cos(alfa1))/ (Va1*cos(alfa2))	0.65689543
DE HALLER NUMBER MEDIUM STATOR	DDms1=	(Va1*cos (alfa3))/(Va2')	0.78347396
3.10. ROTOR EXIT ABSOLUTE MACH NUMBER	M3=	tables	0.46
3.11. ROTOR RELATIVE INLET MACH NUMBER	M1=	Mo*cos(alfa0)/cos(alfa1)	0.71976502
TRIANGLE OF VELOCITIES INLET MEDIUM 1st ROTOR	Umr1=		252.285909
	Vo1=		140
	alfa0=		30
	Va1=		121.246256
	MVa1=	Tables (Va1/$T1)	0.36
	Vw0=	Vo1/cos(alfa 0)	69.995324
	V1=	$((Um1- Vwo)^2+Va1^2)	218.930382
	alfa1=	angcos (Va1/V1)	56.3752303
	V1/$T1=	V1/$T1	12.9005965
	M1=	Tables (V1/$T1)	0.675
TRIANGLE OF VELOCITIES OUTLET MEDIUM 1st ROTOR	U2m1r=		261.378605
	Vw3m=		111.828879
	V3=		159.770937
	M3=		0.46
	alfa3=		46.2746574
	Va2=		106.973411
	alfa2=		54.4277438
	MVa2=	Tables (Va2/$T2)	0.305
	V2=	Va2/cos(alfa 2)	183.870691
	M2=	Tables (V2/$T2)	0.53

SUMMARY

alfa0=	30
Vo=	140
Mo=	0.36
Va=	121.24
Ma=	0.361
V1=	218.93
M1=	0.7197
Va2=	106.97
V2=	183.8706911
M2=	0.53

C. Computational simulation of gas turbine performance

EXAMPLE OF DESIGN POINT CALCULATION BY THE ENGINE PERFORMANCNE CODE (TURBOMATCH)

```
TURBOMATCH SCHEME - Windows NT version (October 1999)

 LIMITS:100 Codewords, 800 Brick Data Items, 50 Station Vector
 15 BD Items printable by any call of:-
 OUTPUT, OUTPBD, OUTPSV, PLOTIT, PLOTBD or PLOTSV

  Input "Program" follows

 SIEMENS AG PG (V94.3A) SINGLE SHAFT INDUSTRIAL GAS TURBINE ENGINE
 DP SI KE CT FP
  -1
  -1
 INTAKE S1-2     D1-4        R100
 COMPRE S2-3     D5-10       R101    V5      V6
 PREMAS S3,10,4  D11-14
 BURNER S4-5     D15-17      R102
 MIXEES S5,10,6
 TURBIN S6-7     D18-25,101          V19
 DUCTER S7-8     D26-29      R103
 NOZCON S8-9,1   D30         R104
 PERFOR S1,0,0   D18,31-33,104,100,102,0,0,103,0,0,0
 CODEND

 BRICK DATA ITEMS

 ! INTAKE
 1  0.0              ! ALTITUDE
 2  0.0              ! I. S. A. DEVIATION, DEV FROM STABDART TEMP
 3  0.0              ! MACH NUMBER
 4  0.9951           ! EXP / USAF
 !COMPRESSOR
 5  -1.0             ! SURGE MARGIN (Z)
 6   1.0             ! PCN (ROTATIONAL SPEED N)
 7   16.6            ! DEASIGN PRESSURE RATIO
 8   0.88            ! ISENTROPIC EFFICIENCY
 9   0.0             ! ERROR
 10  3.0             ! COMPRESSOR MAP NUMBER
 ! PREMAS
 11  0.148           ! EXTRACTED AIR PERCENTAGE
 12  0.00            ! MASS FLOW LOSS
 13  1.00            ! PRESSURE RECOVERY
 14  0.00            ! PRESSURE DROP
 ! BURNER
 15  0.05            ! DP/P (PRESSURE LOSS IN THE BURNER)
 16  0.9995          ! COMBUSTION EFFEICNIECY
 17 -1.0             ! FUEL FLOW
 ! TURBINE
 18 240000000.0      ! AUXILIARY WORK (OTHER THAN FOR COMPRESSOR)
 19 -1.00            ! TURBINE MASS FLOW
 20 -1.00            ! CN
 21  0.90            ! ISENTROPIC EFFICIENCY
 22 -1.0             ! PCN
 23  1.00            ! COMPRESSOR NUMBER
 24  3.00            ! TURBINE MAP NUMBER
 25  1000.0             ! POWER INDEX
 ! DUCTER
 26  0.0             ! SWITCH (NO REHEATING AT ALL)
 27  0.0             ! TOTAL PRESSURE LOSS/INLET TOTAL PRESSURE
 28  0.0             ! COMBUSTION EFFICIENCY
 29  1000000.0       ! LIMITING VALUE OF FEUL FLOW
 ! NOZCON
 30 -1.0             ! THROAT AREA
 ! PERFOR
 31  1.00            ! SHAFT EFFICIENCY
 32  0.0             ! SCALE INDEX
 33  0.0             ! DESIGN NET THRUST
```

```
-1
1 2 640.0           ! INLET MASS FLOW
5 6 1583.0          ! TURBINE ENTRY TEMPERATURE (TET)
-1
                                                  Time Now 16:15:57
*********************************************
                The Units for this Run are as follows:-
Temperature = K   Pressure = Atmospheres   Length = metres
Area = sq metres  Mass Flow = kg/sec       Velocity = metres/sec
Force = Newtons   s.f.c.(Thrust) =  mg/N sec   s.f.c.(Power) = mug/J
Sp. Thrust =    N/kg/sec     Power =   Watts
1

     ***** DESIGN POINT ENGINE CALCULATIONS *****

***** AMBIENT AND INLET PARAMETERS *****
Alt. =      0.0      I.S.A. Dev. =    0.000       Mach No. =  0.00
Etar = 0.9951        Momentum Drag =      0.00

***** COMPRESSOR  1 PARAMETERS *****
PRSF =  0.21351E+01     ETASF =  0.10484E+01     WASF =  0.64453E+01
Z = 0.85000             PR =  16.600             ETA = 0.88000
PCN =   1.0000          CN = 1.00000             COMWK =  0.25820E+09

***** COMBUSTION CHAMBER PARAMETERS *****
ETASF =  0.99950E+00
ETA = 0.99950           DLP = 0.8259             WFB =  14.6367

***** TURBINE  1 PARAMETERS *****
CNSF =  0.10521E+03     ETASF =  0.10039E+01     TFSF =  0.27002E+00
DHSF =  0.15404E+05
TF =  430.924            ETA = 0.90000            CN =  2.750
AUXWK =  0.24000E+09

***** CONVERGENT NOZZLE  1 PARAMETERS *****
NCOSF =  0.10000E+01
Area = 14.1124          Exit Velocity =  108.92  Gross Thrust =  69270.55
Nozzle Coeff. =  0.97145E+00

Scale Factor on above Mass Flows, Areas, Thrusts & Powers =     1.0000

Station  F.A.R. Mass Flow   Pstatic    Ptotal Tstatic  Ttotal     Vel    Area
    1   0.00000   640.000   1.00000   1.00000  288.15  288.15     0.0  ******
    2   0.00000   640.000    ******   0.99510  ******  288.15  ******  ******
    3   0.00000   640.000    ******  16.51867  ******  679.96  ******  ******
    4   0.00000   545.280    ******  16.51867  ******  679.96  ******  ******
    5   0.02684   559.917    ******  15.69274  ****** 1583.00  ******  ******
    6   0.02287   654.637    ******  15.69274  ****** 1463.58  ******  ******
    7   0.02287   654.637    ******   1.02551  ******  834.20  ******  ******
    8   0.02287   654.637    ******   1.02551  ******  834.20  ******  ******
    9   0.02287   654.637   1.00000   1.02551  829.01  834.20   108.9 14.1124
   10   0.00000    94.720    ******  16.51867  ******  679.96  ******  ******


  Shaft Power = 240000000.00
   Net Thrust = 69270.55
 Equiv. Power = 244466352.00
    Fuel Flow =  14.6367
       S.F.C. =  60.9861
    E.S.F.C. =  59.8719
Sp. Sh. Power =    375000.00
Sp. Eq. Power =    381978.69
Sh. Th. Effy. =   0.3802
         Time Now 16:15:58

*********************************************
-3
```

EXAMPLE OF PARAMETERS CORRELATION BY GAS PATH ANALYSIS (GOTRESS)

Input File

```
GENERAL GAS PATH ANALYSIS OF GAS TURBINE
Different Number of Dependent and Independent Parameters////
NR                        ! LR - Linear GPA; NR - Non-Linear GPA.
3                         ! Number of Dependent, NROW (Measurable) Parameters
ie. (P, T, MW)
2                         ! Number of Independent, NCOL (Non-Measurable) Parameters
ie.(Effic,Airflow)
-0.01                     ! Perturbetion value. Default value, suggestion dont move
0.001                     ! Implanted Fault (1st Independent parameter)
ie. (Effic=-0.1%)
0.002                     ! Implanted Fault (2nd Independent parameter)
ie. (Airflow=0.2%)
15                        ! Clean value for 1st Dependent parameters
ie. Pressure Ratio P [bar]
600                       ! Clean value for 2nd Dependent parameters
ie. T  [Kelvines]
250                       ! Clean value for 3rd Dependent parameters.
ie. UW, MW [megawatt]
14.994                    ! 1st Dependent parameter for 1st perturbed Independent
parameter ie. Turbom P=f(Effi)
14.992                    ! 1st Dependent parameter for 2nd perturbed Independent
parameter ie. Turbom P=f(Airflow)
599.994                   ! 2nd Dependent parameter for 1st perturbed Independent
parameter ie. Turbom T=f(Effi)
599.990                   ! 2nd Dependent parameter for 2nd perturbed Independent
parameter ie. Turbom T=f(Airflow)
249.994                   ! 3rd Dependent parameter for 1st perturbed Independent
parameter ie. Turbom MW=f(Effi)
249.989                   ! 3rd Dependent parameter for 2nd perturbed Independent
parameter ie. Turbom MW=f(Airflow)
14.990                    ! Deteriorated value for 1st Dependent parameters
ie. P=f(Effi,Airflow)
599.987                   ! Deteriorated value for 2nd Dependent parameters
ie. T=f(Effi,Airflow)
249.982                   ! Deteriorated value for 3rd Dependent parameters
ie. MW=f(Effi.Airflow)
```

Results

```
################################################################################
#                                                                              #
#                               G O T R E S S                                  #
#                                                                              #
################################################################################
              GOTRESS, A GENERAL GAS PATH ANALYSIS SIMULATION CODE.
                           Version 1.0a, December 2001.
             CRANFIELD UNIVERSITY - SME/PEP : 7/10/1997 - 7/10/2001.

 Input File Name is:
 GENERAL GAS PATH ANALYSIS OF GAS TURBINE
 Different Number of Dependent and Independent Parameters

        ******** Input conditions for this run are ********

 NR                        ! LR - Linear GPA; NR - Non-Linear GPA.
 LINEAR & NON-LINEAR GPA ANALYSIS
 ------------------------------------------------------------------------------
       ********      Linear Gas Path Analysis      ********
   ---------------------------------------------------------------------------
 ******************************************************************************
 * Time Now is 16:48:34.49  ==============  and Today's Date is  19/05/2006 *
 ******************************************************************************
 Number of Dependent Parameters     :  3
 Number of Independent Parameters   :  2
```

```
 Clean Engine "Measurable" Parameter Values are:
      0.0001      0.0040      0.0025
  Fault Generation MATRIX is:
     14.9940     14.9920
    599.9940    599.9900
    249.9940    249.9890
 The Deteriorated Values are:
     14.9900    599.9870    249.9820
 The ICM MATRIX is:
9995900.00009994566.6667
9999750.00009999650.0000
9999660.00009999460.0000
 The FCM MATRIX is:
      0.0008     -0.0005     -0.0004
     -0.0008      0.0005      0.0004
 The Implanted Faults are:
      0.0010      0.0020
 The Detected Faults are:
      0.9825     -1.9825
 The RMS Error of the above approach is:
      1.5655
 ------------------------------------------------------------------------------
        ********    Non-Linear Gas Path Analysis    ********
 ------------------------------------------------------------------------------
 Non-Linear Gas Path Analysis Converged After:   1 Loops.
 ------------------------------------------------------------------------------
 ******************************************************************************
 * Time Now is 16:48:34.49  ==============  and Today's Date is  19/05/2006 *
 ******************************************************************************
 Number of Dependent Parameters     :  3
 Number of Independent Parameters   :  2
 Clean Engine "Measurable" Parameter Values are:
      0.0001      0.0040      0.0025
 Fault Generation MATRIX is:
     14.9940     14.9920
    599.9940    599.9900
    249.9940    249.9890
 The Deteriorated Values are:
     14.9900    599.9870    249.9820
 The ICM MATRIX is:
************5041429.9594
************5043994.0794
************5043898.2402
 The FCM MATRIX is:
     -0.0008      0.0005      0.0004
     -0.0017      0.0009      0.0007
 The Implanted Faults are:
      0.0010      0.0020
 The Detected Faults are:
      0.0098     -0.0198
 The RMS Error of the above approach is:
      0.0166
```

EXAMPLE OF MULTIPLE DETERIORATION CALCULATION BY THE ENGINE PERFORMANCE CODE (TURBOMATCH)

```
TURBOMATCH SCHEME - Windows NT version (October 1999)

 LIMITS:100 Codewords, 800 Brick Data Items, 50 Station Vector
 15 BD Items printable by any call of:-
 OUTPUT, OUTPBD, OUTPSV, PLOTIT, PLOTBD or PLOTSV

  Input "Program" follows

 SIEMENS AG PG (V94.3A) SINGLE SHAFT INDUSTRIAL GAS TURBINE ENGINE
 OD SI KE CT FP
  -1
  -1
 INTAKE S1-2     D1-4        R100
 ARITHY          D300-307
 ARITHY          D310-317
 ARITHY          D320-327
 COMPRE S2-3     D5-10       R101    V5      V6
 PREMAS S3,10,4  D11-14
 ARITHY          D330-337
 BURNER S4-5     D15-17      R102
 MIXEES S5,10,6
 ARITHY          D340-347
 ARITHY          D350-357
 ARITHY          D360-367
 TURBIN S6-7     D18-25,101          V19
 DUCTER S7-8     D26-29      R103
 NOZCON S8-9,1   D30         R104
 PERFOR S1,0,0   D18,31-33,104,100,102,0,0,103,0,0,0
 CODEND

 BRICK DATA ITEMS

 ! INTAKE
 1  0.0              ! ALTITUDE
 2  0.0              ! I. S. A. DEVIATION
 3  0.0              ! MACH NUMBER
 4  0.9951           ! EXP / USAF
 !COMPRESSOR
 5  -1.0             ! SURGE MARGIN (Z)
 6   1.0             ! PCN (ROTATIONAL SPEED N)
 7   16.6            ! DEASIGN PRESSURE RATIO
 8   0.88            ! ISENTROPIC EFFICIENCY
 9   0.0             ! ERROR
 10  3.0             ! COMPRESSOR MAP NUMBER
 ! PREMAS
 11  0.148           ! EXTRACTED AIR PERCENTAGE
 12  0.00            ! MASS FLOW LOSS
 13  1.00            ! PRESSURE RECOVERY
 14  0.00            ! PRESSURE DROP
 ! BURNER
 15  0.05            ! DP/P (PRESSURE LOSS IN THE BURNER)
 16  0.9995          ! COMBUSTION EFFEICNIECY
 17 -1.0             ! FUEL FLOW
 ! TURBINE
 18 240000000.0      ! AUXILIARY WORK (OTHER THAN FOR COMPRESSOR)
 19 -1.00            ! TURBINE MASS FLOW
 20 -1.00            ! CN
 21  0.90            ! ISENTROPIC EFFICIENCY
 22 -1.0             ! PCN
 23  1.00            ! COMPRESSOR NUMBER
 24  3.00            ! TURBINE MAP NUMBER
 25  1000.0             ! POWER INDEX
 ! DUCTER
 26  0.0             ! SWITCH (NO REHEATING AT ALL)
 27  0.0             ! TOTAL PRESSURE LOSS/INLET TOTAL PRESSURE
 28  0.0             ! COMBUSTION EFFICIENCY
 29  1000000.0       ! LIMITING VALUE OF FEUL FLOW
 ! NOZCON
 30 -1.0             ! THROAT AREA
```

```
! PERFOR
31  1.00            ! SHAFT EFFICIENCY
32  0.0             ! SCALE INDEX
33  0.0             ! DESIGN NET THRUST

!COMPRESSOR PRESSURE (PRSF) DETERIORATION
300  3.0            !COMPRESSOR, BD(810)=BD(810)*BD(307)
301  -1.0
302  810.0          !PRSF FOR COMPRESSOR
303  -1.0
304  810.0
305  -1
306  307.0
307  1.0            !COMPRESSOR DETERIORATION OF 0% IN PRESSURE RATIO

!COMPRESSOR EFFICIENCY (ETASF) DETERIORATION
310  3.0            !COMPRESSOR, BD(820)=BD(820)*BD(317)
311  -1.0
312  820.0          !ETASF FOR COMPRESSOR
313  -1.0
314  820.0
315  -1
316  317.0
317  1.0            !COMPRESSOR DETERIORATION OF 0% IN EFFIENCY

!COMPRESSOR NON-DIMENSIONAL MASS FLOW (WASF) DETERIORATION
320  3.0            !COMPRESSOR, BD(830)=BD(830)*BD(327)
321  -1.0
322  830.0          !WASF FOR COMPRESSOR
323  -1.0
324  830.0
325  -1
326  327.0
327  1.0            !COMPRESSOR DETERIORATION OF 0% IN NON-DIMENSIONAL MASS FLOW

!BURNER EFFICIENCY (ETASF) DETERIORATION
330  3.0            !BURNER, BD(870)=BD(820)*BD(337)
331  -1.0
332  870.0          !ETASF FOR COMPRESSOR
333  -1.0
334  870.0
335  -1
336  337.0
337  1.0            !BURNER DETERIORATION OF 0% IN EFFIENCY

!TURBINE NON-DIMENSIONAL MASS FLOW DETERIORATION
340  3.0            !TURBINE, BD(840)=BD(840)*BD(347)
341  -1.0
342  840.0          !TFSF FOR TURBINE (NON-DIMENSIONAL MASS FLOW)
343  -1.0
344  840.0
345  -1
346  347.0
347  1.0            !TURBINE DETERIORATION OF 0% IN NON-DIMENSIONAL MASS FLOW

!TURBINE EFFICIENCY (ETASF) DETERIORATION
350  3.0            !TURBINE, BD(850)=BD(850)*BD(357)
351  -1.0
352  850.0          !ETASF FOR TURBINE
353  -1.0
354  850.0
355  -1
356  357.0
357  1.0            !TURBINE DETERIORATION OF 0% IN EFFIENCY

!TURBINE DH/T ENTHALPIA DETERIORATION
360  3.0            !COMPRESSOR, BD(860)=BD(860)*BD(367)
361  -1.0
362  860.0          !DH/T FOR TURBINE
363  -1.0
364  860.0
365  -1
366  367.0
367  1.0            !TURBINE DETERIORATION OF 0% IN DH/T ENTHALPIA
```

```
 -1
 1 2 640.0           ! INLET MASS FLOW
 5 6 1583.0          ! TURBINE ENTRY TEMPERATURE (TET)

 -1
                                                  Time Now 01:44:49
 ************************************************
                 The Units for this Run are as follows:-

 Temperature = K   Pressure = Atmospheres   Length = metres
 Area = sq metres  Mass Flow = kg/sec       Velocity = metres/sec
 Force = Newtons   s.f.c.(Thrust) =  mg/N sec   s.f.c.(Power) = mug/J
 Sp. Thrust =    N/kg/sec     Power =   Watts
1

     ***** DESIGN POINT ENGINE CALCULATIONS *****
 ***** AMBIENT AND INLET PARAMETERS *****
 Alt. =      0.0      I.S.A. Dev. =    0.000       Mach No. =  0.00
 Etar = 0.9951        Momentum Drag =      0.00

 ***** COMPRESSOR  1 PARAMETERS *****
 PRSF =  0.21351E+01     ETASF =  0.10484E+01     WASF =  0.64453E+01
 Z = 0.85000             PR =  16.600             ETA = 0.88000
 PCN =   1.0000          CN = 1.00000             COMWK =  0.25820E+09

 ***** COMBUSTION CHAMBER PARAMETERS *****
 ETASF =  0.99950E+00
 ETA = 0.99950           DLP = 0.8259             WFB =  14.6367

 ***** TURBINE  1 PARAMETERS *****
 CNSF =  0.10521E+03     ETASF =  0.10039E+01     TFSF =  0.27002E+00
 DHSF =  0.15404E+05
 TF =  430.924            ETA = 0.90000            CN =  2.750
 AUXWK =  0.24000E+09

 ***** CONVERGENT NOZZLE  1 PARAMETERS *****
 NCOSF =  0.10000E+01
 Area = 14.1124          Exit Velocity =  108.92  Gross Thrust =  69270.55
 Nozzle Coeff. =  0.97145E+00

 Scale Factor on above Mass Flows, Areas, Thrusts & Powers =     1.0000

 Station  F.A.R. Mass Flow   Pstatic    Ptotal Tstatic  Ttotal     Vel    Area
     1   0.00000   640.000   1.00000   1.00000  288.15  288.15     0.0  ******
     2   0.00000   640.000    ******   0.99510  ******  288.15  ******  ******
     3   0.00000   640.000    ******  16.51867  ******  679.96  ******  ******
     4   0.00000   545.280    ******  16.51867  ******  679.96  ******  ******
     5   0.02684   559.917    ******  15.69274  ****** 1583.00  ******  ******
     6   0.02287   654.637    ******  15.69274  ****** 1463.58  ******  ******
     7   0.02287   654.637    ******   1.02551  ******  834.20  ******  ******
     8   0.02287   654.637    ******   1.02551  ******  834.20  ******  ******
     9   0.02287   654.637   1.00000   1.02551  829.01  834.20   108.9 14.1124
    10   0.00000    94.720    ******  16.51867  ******  679.96  ******  ******

   Shaft Power = 240000000.00
    Net Thrust = 69270.55
  Equiv. Power = 244466352.00
     Fuel Flow =  14.6367
        S.F.C. =  60.9861
     E.S.F.C. =  59.8719
 Sp. Sh. Power =    375000.00
 Sp. Eq. Power =    381978.69
 Sh. Th. Effy. =   0.3802
           Time Now 01:44:49

 ************************************************
 307 0.9999          !COMPRESSOR DETERIORATION IN PRESSURE RATIO
 317 0.9999          !COMPRESSOR DETERIORATION IN EFFICIENCY
 327 0.9999          !COMPRESSOR DETERIORATION IN NON-DIMENSIONAL FLOW
 337 0.9999          !BURNER DETERIORATION IN COMBUSTION EFFICIENCY
 347 0.9999          !TURBINE DETERIORATION IN NON-DIMENSIONAL FLOW
 357 0.9999          !TURBINE DETERIORATION IN EFFICIENCY
 367 0.9999          !TURBINE DETERIORATION IN DH/T ENTHALPY DROP
```

```
 -1
 -1
                                                    Time Now 01:44:49

 ***********************************************
 BERR( 1) =    0.10339E-03
 BERR( 2) =   -0.16628E-03
 BERR( 3) =   -0.93228E-03
1

      ***** OFF DESIGN ENGINE CALCULATIONS. Converged after   0 Loops *****

 ***** AMBIENT AND INLET PARAMETERS *****
 Alt. =      0.0      I.S.A. Dev. =    0.000       Mach No. =  0.00
 Etar = 0.9951        Momentum Drag =      0.00

 ***** COMPRESSOR  1 PARAMETERS *****
 PRSF =  0.21346E+01     ETASF =  0.10482E+01     WASF =  0.64440E+01
 Z = 0.85000             PR =  16.597             ETA = 0.87982
 PCN =   1.0000          CN = 1.00000             COMWK =  0.25817E+09

 ***** COMBUSTION CHAMBER PARAMETERS *****
 ETASF =  0.99930E+00
 ETA = 0.99930           DLP = 0.8258             WFB =  14.6361

 ***** TURBINE  1 PARAMETERS *****
 CNSF =  0.10521E+03     ETASF =  0.10037E+01     TFSF =  0.26996E+00
 DHSF =  0.15401E+05
 TF =  430.924            ETA = 0.89982            CN =  2.750
 AUXWK =  0.24000E+09

 ***** CONVERGENT NOZZLE  1 PARAMETERS *****
 NCOSF =  0.10000E+01
 Area = 14.1124          Exit Velocity =  108.88  Gross Thrust =  69225.24
 Nozzle Coeff. =  0.97143E+00

 Scale Factor on above Mass Flows, Areas, Thrusts & Powers =     1.0000

 Station  F.A.R. Mass Flow   Pstatic    Ptotal Tstatic  Ttotal     Vel    Area
     1   0.00000   639.936   1.00000   1.00000  288.15  288.15     0.0  ******
     2   0.00000   639.872    ******   0.99510  ******  288.15  ******  ******
     3   0.00000   639.872    ******  16.51557  ******  680.00  ******  ******
     4   0.00000   545.171    ******  16.51557  ******  680.00  ******  ******
     5   0.02685   559.807    ******  15.68976  ****** 1583.00  ******  ******
     6   0.02287   654.508    ******  15.68976  ****** 1463.58  ******  ******
     7   0.02287   654.508    ******   1.02396  ******  834.11  ******  ******
     8   0.02287   654.508    ******   1.02396  ******  834.11  ******  ******
     9   0.02287   654.508   1.00000   1.02396  828.82  834.11   108.9 14.1124
    10   0.00000    94.701    ******  16.51557  ******  680.00  ******  ******

   Shaft Power = 240000000.00
    Net Thrust = 69225.24
  Equiv. Power = 244463440.00
     Fuel Flow =  14.6361
        S.F.C. =  60.9836
      E.S.F.C. =  59.8702
 Sp. Sh. Power =    375037.50
 Sp. Eq. Power =    382012.31
 Sh. Th. Effy. =   0.3802
           Time Now 01:44:49

 ***********************************************
 307 0.9990          !COMPRESSOR DETERIORATION IN PRESSURE RATIO
 317 0.9990          !COMPRESSOR DETERIORATION IN EFFICIENCY
 327 0.9990          !COMPRESSOR DETERIORATION IN NON-DIMENSIONAL FLOW
 337 0.9995          !BURNER DETERIORATION IN COMBUSTION EFFICIENCY
 347 0.9990          !TURBINE DETERIORATION IN NON-DIMENSIONAL FLOW
 357 0.9990          !TURBINE DETERIORATION IN EFFICIENCY
 367 0.9990          !TURBINE DETERIORATION IN DH/T ENTHALPY DROP
 -1
 -1
                                                    Time Now 01:44:49

 ***********************************************
```

```
 BERR( 1) =    0.12427E-02
 BERR( 2) =   -0.20762E-02
 BERR( 3) =   -0.92155E-02

 Loop   1
 BERR( 1) =   -0.39589E-06
 BERR( 2) =    0.21192E-03
 BERR( 3) =    0.27909E-03
1

      ***** OFF DESIGN ENGINE CALCULATIONS. Converged after   1 Loops *****

 ***** AMBIENT AND INLET PARAMETERS *****
 Alt. =      0.0      I.S.A. Dev. =    0.000       Mach No. =  0.00
 Etar = 0.9951        Momentum Drag =      0.00

 ***** COMPRESSOR  1 PARAMETERS *****
 PRSF =  0.21325E+01     ETASF =  0.10472E+01     WASF =  0.64376E+01
 Z = 0.84910             PR =  16.565             ETA = 0.87894
 PCN =   1.0000          CN = 0.99999             COMWK =  0.25793E+09

 ***** COMBUSTION CHAMBER PARAMETERS *****
 ETASF =  0.99880E+00
 ETA = 0.99880           DLP = 0.8259             WFB =  14.6299

 ***** TURBINE  1 PARAMETERS *****
 CNSF =  0.10521E+03     ETASF =  0.10027E+01     TFSF =  0.26969E+00
 DHSF =  0.15386E+05
 TF =  430.897            ETA = 0.89897            CN =  2.750
 AUXWK =  0.23880E+09

 ***** CONVERGENT NOZZLE  1 PARAMETERS *****
 NCOSF =  0.10000E+01
 Area = 14.1124          Exit Velocity =  108.95  Gross Thrust =  69211.77
 Nozzle Coeff. =  0.97146E+00

 Scale Factor on above Mass Flows, Areas, Thrusts & Powers =     1.0000

 Station  F.A.R. Mass Flow   Pstatic    Ptotal Tstatic  Ttotal     Vel    Area
     1   0.00000   639.281   1.00000   1.00000  288.15  288.15     0.0  ******
     2   0.00000   639.281    ******   0.99510  ******  288.15  ******  ******
     3   0.00000   639.281    ******  16.48345  ******  680.01  ******  ******
     4   0.00000   544.668    ******  16.48345  ******  680.01  ******  ******
     5   0.02686   559.297    ******  15.65756  ****** 1583.00  ******  ******
     6   0.02288   653.911    ******  15.65756  ****** 1463.59  ******  ******
     7   0.02288   653.911    ******   1.02596  ******  835.44  ******  ******
     8   0.02288   653.911    ******   1.02596  ******  835.44  ******  ******
     9   0.02288   653.911   1.00000   1.02596  830.14  835.44   109.0 14.1124
    10   0.00000    94.614    ******  16.48345  ******  680.01  ******  ******

   Shaft Power = 238801376.00
    Net Thrust = 69211.77
  Equiv. Power = 243263936.00
     Fuel Flow =  14.6299
        S.F.C. =  61.2637
      E.S.F.C. =  60.1398
 Sp. Sh. Power =    373546.69
 Sp. Eq. Power =    380527.31
 Sh. Th. Effy. =   0.3785
           Time Now 01:44:49

 ********************************************
 307 0.9987          !COMPRESSOR DETERIORATION IN PRESSURE RATIO
 317 0.9987          !COMPRESSOR DETERIORATION IN EFFICIENCY
 327 0.9669          !COMPRESSOR DETERIORATION IN NON-DIMENSIONAL FLOW
 337 0.9990          !BURNER DETERIORATION IN COMBUSTION EFFICIENCY
 347 0.9987          !TURBINE DETERIORATION IN NON-DIMENSIONAL FLOW
 357 0.9987          !TURBINE DETERIORATION IN EFFICIENCY
 367 0.9987          !TURBINE DETERIORATION IN DH/T ENTHALPY DROP
 -1
 -1
                                                  Time Now 01:44:49

 ********************************************
```

```
 BERR( 1) =    0.37692E-01
 BERR( 2) =   -0.17574E-01
 BERR( 3) =   -0.64193E-01

 Loop   1
 BERR( 1) =    0.73982E-04
 BERR( 2) =    0.15062E-02
 BERR( 3) =    0.32316E-03
1

      ***** OFF DESIGN ENGINE CALCULATIONS. Converged after   1 Loops *****

 ***** AMBIENT AND INLET PARAMETERS *****
 Alt. =      0.0      I.S.A. Dev. =    0.000       Mach No. =  0.00
 Etar = 0.9951        Momentum Drag =      0.00

 ***** COMPRESSOR  1 PARAMETERS *****
 PRSF =  0.21297E+01     ETASF =  0.10458E+01     WASF =  0.62245E+01
 Z = 0.82186             PR =  16.045             ETA = 0.87779
 PCN =   1.0000          CN = 0.99996             COMWK =  0.24628E+09

 ***** COMBUSTION CHAMBER PARAMETERS *****
 ETASF =  0.99780E+00
 ETA = 0.99780           DLP = 0.7945             WFB =  14.2777

 ***** TURBINE  1 PARAMETERS *****
 CNSF =  0.10521E+03     ETASF =  0.10014E+01     TFSF =  0.26934E+00
 DHSF =  0.15366E+05
 TF =  430.504            ETA = 0.89844            CN =  2.750
 AUXWK =  0.23107E+09

 ***** CONVERGENT NOZZLE  1 PARAMETERS *****
 NCOSF =  0.10000E+01
 Area = 14.1124          Exit Velocity =  106.33  Gross Thrust =  65485.01
 Nozzle Coeff. =  0.97144E+00

 Scale Factor on above Mass Flows, Areas, Thrusts & Powers =     1.0000

 Station  F.A.R. Mass Flow   Pstatic    Ptotal Tstatic  Ttotal     Vel    Area
     1   0.00000   619.680   1.00000   1.00000  288.15  288.15     0.0  ******
     2   0.00000   619.680    ******   0.99510  ******  288.15  ******  ******
     3   0.00000   619.680    ******  15.96616  ******  674.34  ******  ******
     4   0.00000   527.967    ******  15.96616  ******  674.34  ******  ******
     5   0.02704   542.245    ******  15.17166  ****** 1583.00  ******  ******
     6   0.02304   633.957    ******  15.17166  ****** 1462.94  ******  ******
     7   0.02304   633.957    ******   1.02460  ******  840.72  ******  ******
     8   0.02304   633.957    ******   1.02460  ******  840.72  ******  ******
     9   0.02304   633.957   1.00000   1.02460  835.69  840.72   106.3 14.1124
    10   0.00000    91.713    ******  15.96616  ******  674.34  ******  ******

   Shaft Power = 231072064.00
    Net Thrust = 65485.01
  Equiv. Power = 235294336.00
     Fuel Flow =  14.2777
        S.F.C. =  61.7889
      E.S.F.C. =  60.6801
 Sp. Sh. Power =    372889.50
 Sp. Eq. Power =    379703.12
 Sh. Th. Effy. =   0.3753
           Time Now 01:44:49

 *******************************************
 -3
```